PHARMACEUTICALS AND PHYSICS: DRUGS AND MEMBRANES

PHARMACEUTICALS AND PHYSICS: STUDIES OF DRUG-MEMBRANE INTERACTIONS USING ADVANCED X-RAY AND NEUTRON SCATTERING TECHNIQUES

By

RICHARD J. ALSOP, H.B.Sc.

A Thesis
Submitted to the School of Graduate Studies
in Partial Fulfillment of the Requirements
for the Degree
Doctor of Philosophy

McMaster University

DOCTOR OF PHILOSOPHY (2017)
(Biophysics)

McMaster University
Hamilton, Ontario

TITLE: Pharmaceuticals and Physics: Studies of Drug-Membrane Interactions Using Advanced X-ray and Neutron Scattering Techniques

AUTHOR: Richard J. Alsop, H.B.Sc.(McMaster University)

SUPERVISOR: Dr. Maikel C. Rheinstädter

NUMBER OF PAGES: vi, 138

Abstract

Active pharmaceutical ingredients (APIs) are usually designed to stick to some target in the body. This target is typically a protein, and the drug is supposed to change how that protein functions. However, side-effects are an inevitable consequence of introducing foreign molecules, such as drugs, into the body, since drug molecules are more than likely to interact non-specifically with other cellular structures, such as lipid membranes. The membrane is a highly relevant structure, as it is a ubiquitous biological interface, that defines the surface of cells and also internal cell components. The membrane is more than just a wall, as it plays an important role in controlling processes on the cell surface. Drug molecules have been shown to interact with membranes by non-specific Van-der-Waals interactions. However, not enough is known regarding how drugs influence the membrane structure, or how to design drugs that minimize membrane related side-effects.

X-ray and neutron scattering techniques, as well as Molecular Dynamics simulations, are capable of providing the molecular details. Synthetic membranes may be prepared with any lipid or drug composition and are tools for modelling interactions. In this thesis, I used scattering experiments on synthetic systems to study drug-membrane interactions on the atomic and molecular scales, in order to understand how the drugs influence membrane properties. I optimized the use of scattering techniques for determining drug effects on membranes.

From my research, there are two main insights.

1. Drug-membrane interactions disrupt local membrane structure. This is based on a case study of aspirin where, over three studies, I presented evidence that the aspirin disrupts cholesterol in the lipid membrane. X-ray and neutron scattering techniques, in combination with Molecular Dynamics simulations were used to determine that aspirin's impacts are the result of locallized disruptions to the lipid structure.

2. I also present three case studies for how the properties of the membrane itself play a role in shaping the drug interaction. Biophysical properties, such as hydration and stiffness, tune how the drug interacts with the membrane. X-ray and neutron scattering are required to generate the molecular picture for why the specific biophysical membrane properties are relevant.

The set of interactions discovered here are not, by any means, exhaustive. However, the work demonstrates that molecular level details reveal unique insights on drug-membrane interactions, details that may be useful when designing drugs and mitigating their side effects.

Acknowledgements

First and foremost, I need to express my gratiude to Maikel Rheinstädter, who is a superb supervisor. His unwavering support, encouragement, and most of all, his endless *enthiusiasm* made the PhD process seem painless. He always pushed me to go above and beyond, and to dream big with every project. His open-door policy, tireless work ethic, and creative approach enables the success of everyone in the lab. The lessons I've learned from working with him, personal and professional, will forever enhance my career.

I've worked with other amazing people in the lab. Matt, Laura, Fei-Chi, Asfia, Adree, Sebastian, and Alex have been great colleagues and, perhaps most importantly, were great people to travel with. A special thanks to Dr. Todd Hoare and his research group (Emilia, Trevor, Eva *et al.*) for providing a unique opportunity to try science outside my comfort zone. I've had great support outside the university as well. Special mention goes to Sam, Tyler, Ali, Anna, Elise, Ashley, Calvin, Christina, Brendan, and Kelly for always making me sound like a superhero.

My family, John & Donna, and Rob, were all deeply supportive. They constant reminded me that I could overcome any obstacle. I also feel it necessary to thank the canines in my life. There was no better escape from the stresses of graduate life than a walk in the fields with my temporary shadow, Nike. As a day-to-day substitute, the wolf-howl of Chiquita was good comic relief.

I am deeply grateful to the Wong family for bringing me in on countless occasionss, feeding me, and letting me hijack their dining room table with my laptop. This leads me to the biggest hero in my life: my partner, Summer. I really, truly, could not have done it without your love and care.

Contents

1 Preface **1**

1.1 Thesis Overview 2

1.2 Scientific Contributions 3

2 Introduction **9**

2.1 Biological Membranes 9

2.1.1 Lipids and Model Lipid Bilayers 10

2.1.2 Lipid Phases 13

2.1.3 Cholesterol and Lipid Rafts 14

2.2 Scattering Theory of X-rays and Neutrons 17

2.2.1 General Scattering Principles 17

2.2.2 Neutron Scattering 19

2.3 Molecular Dynamics Simulations 23

2.4 A Review of Drug Membrane Interactions 25

3 Experimental Methods **27**

3.1 Sample Preparation 27

3.1.1 Chemicals and Materials 27

3.1.2 Preparation of solid-supported, stacked lipid membranes 29

3.2 Protocols for Scattering Experiments 30

3.2.1 X-ray Experiments 30

3.2.2 Neutron Scattering Experiments 32

3.2.3 Hydration Chambers for Scattering Experiments 33

3.3 Molecular Dynamics Simulations 34

4 Aspirin Impacts Local Membrane Structure and Function: Publications I, II, & III **37**

4.1 Paper I: Acetylsalicylic Acid (ASA) Increases the Solubility of Cholesterol When Incorporated in Lipid Membranes 38
4.1.1 Preface to Paper I 38
4.2 Paper II: Aspirin Inhibits Formation of Cholesterol Rafts in Fluid Lipid Membranes 52
4.2.1 Preface to Paper II 52
4.3 Paper III: Aspirin Locally Disrupts the Liquid Ordered Phaser 62
4.3.1 Preface to Paper III 62

5 Membranes Influence the Molecular Effects of Drugs: Publications IV, V, & VI 77
5.1 Paper IV: Cholesterol Expels Ibuprofen from the Hydrophobic Membrane Core and Stabilizes Lamellar Phases in Lipid Membranes Containing Ibuprofen 78
5.1.1 Preface to Paper IV 78
5.2 Paper V: The Lipid Bilayer Provides a Site for Cortisone Crystallization at High Cortisone Concentrations 92
5.2.1 Preface to Paper V 92
5.3 Paper VI: Curcumin Protects Membranes Through Carpet or Insertion Model Depending on Hydration 108
5.3.1 Preface to Paper VI 108

6 Outlook & Conclusions 125

A Copyright Information for Publications 129
A.1 Soft Matter Publications 129
A.2 BBA-Biomembranes Publication 129
A.3 Scientific Reports 129
A.4 Langmuir 130

Chapter 1

Preface

Western medicine relies heavily on specialized chemicals intended to specifically alter the human body. These active pharmaceutical ingredients (APIs) are typically designed to bind some target, typically a protein, and change the function of that target, thereby providing therapeutic effect. However, the set of organs, tissues, cells, and molecules that compose the human body are not a set of unique "locks" for the APIs to interact with, like a "key". Side-effects are an inevitable consequence of introducing foreign molecules such as drugs into the body, as drug molecules are more than likely to interact non-specifically with various cellular structures. Observing and measuring these interactions is a unique experimental challenge in drug design.

Understanding the interaction with lipid membranes is especially challenging. The membrane is a ubiquitous biological interface, that defines the surface of cells and also most internal organelles. It is not an inert structure and plays a important role in the regulation of membrane bound proteins, as well as controlling passive diffusion [1]. Drug molecules have been shown to disrupt membrane structure by simple, non-specific Van-der-Waals interactions [2]. However, many membrane phenomena occur on nanosecond timescales and nanometre length scales that are well outside the realm of standard biological techniques, making a comprehensive understanding of these interactions difficult. Understanding these interactions is necessary, in order to design drugs that optimize or minimize them.

X-ray and neutron scattering techniques, as well as Molecular Dynamics simulations, are able to access the necessary length and time scales. These techniques measure structure and dynamics on nanometre and nanosecond scales. Native biological systems are generally too disordered for these techniques to be useful, so model systems have been developed. Oriented membranes stacks on solid support can be prepared with any lipid or drug composition, and provide exquisite resolution of drug-membrane effects.

In this thesis, I studied how drugs interact non-specifically with lipid bilayers on the nanometre length scales. This is a sandwich thesis, where six individual case studies of drug membrane interactions are synthesized. I took common drugs, introduced them into model lipid bilayer systems, and measured their effects primarily using scattering techniques. I optimized the use of scattering

experiments, and the analysis of scattering experiments, for drug-membrane research. The studies I conducted yielded two main insights.

For one, drugs can disrupt the local structure and function of lipid membranes. In this thesis, I present a case study of aspirin disrupting cholesterol rafts in lipid bilayers. Cholesterol is an important component of eukaryotic membranes as it stiffens the structure and gives it integrity. Cholesterol also creates highly ordered patches in membranes, commonly known as rafts, that are important for sorting membrane proteins. At high concentration, cholesterol even forms cholesterol crystals in the bilayer that contribute to atheroslerosis. We observe that aspirin, by making the membrane more fluid, mitigates the effect of cholesterol and homogenizes the membrane, dissolving rafts and plaques. The specificity of neutron scattering provided support that aspirin locally disrupts the raft structure.

Secondly, the membrane itself plays a role in the drug interaction. For example, the common analgesic ibuprofen creates pores in lipid membranes at high concentrations, but not in bilayers containing cholesterol. The Indian spice curcumin embeds in fluid membranes and increases fluidity, but does not do so in dehydrated bilayers. Our studies conclude that the biophysical properties of the membrane influence the interaction.

1.1 Thesis Overview

This thesis is written such that a scientist, who is not an expert in this field, can understand and appreciate the major findings of my PhD work. It is sandwich style, combining the six most important first-author papers in my portfolio into a coherent package. See Section 1.2 for a full list of my contributions.

Chapter 2 will give the reader a background understanding of the necessary scientific concepts. The material properties of lipid membranes and lipids are discussed, with an emphasis on the lipids used in the experiments I conducted. In addition, the importance of cholesterol is discussed and a review of the controversial topic of lipid rafts is conducted. The most important parts of X-ray and neutron scattering theory are presented, followed by Molecular Dynamics simulations.

Chapter 3 then presents a tutorial on the systems used for investigation. As alluded to above, model systems need to be used with scattering technqiues and I primarily used stacked membranes on solid support. Preparation of these stacks is not trivial, and the optimized procedures are outlined. I then give the reader a walk-through of how measurements are made, both using our in-house X-ray diffractometer and using triple-axis neutron spectrometers. Finally, I explain how we use MacSim for computer simulations!

This takes us into the scientific findings of the thesis. Chapter 4 presents, over three papers, a case study of aspirin aleviating the effect of cholesterol. *Acetylsalicylic Acid (ASA) Increases the Solubility of Cholesterol When Incorporated in Lipid Membranes* illustrates, using X-ray diffraction, how aspirin increase area per lipid, permitting more cholesterol in the membrane and eliminating plaques. *Aspirin Inhibits Formation of Cholesterol Rafts in Fluid Lipid Membranes* using neutron

diffraction to present evidence that aspirin also eliminates ordered cholesterol structures, and finally, *Aspirin Locally Disrupts the Liquid Ordered Phase* uses inelastic neutron scattering to show aspirin locally disrupts cholesterol rafts causing changes to the material properties of the structure.

The second results Chapter, Chapter 5, contains three papers where the effect of drug membrane interaction was influenced by the membrane itself. *Cholesterol Expels Ibuprofen from the Hydrophobic Membrane Core and Stabilizes Lamellar Phases in Lipid Membranes Containing Ibuprofen* demonstrates how ibuprofen creates pores in membranes, but not when cholesterol is present. *Curcumin Protects Membranes Through Carpet or Insertion Model Depending on Hydration* presents evidence that curcumin embeds in fluid membranes, but also rests on the surface of gel membranes. Finally *The Lipid Bilayer Provides a Site for Cortisone Crystallization at High Cortisone Concentrations* demonstrates that cortisone uses the bilayer as a substrate for crystallization.

A concluding section then wraps up the thesis by synthesizing the findings and provide outlook.

1.2 Scientific Contributions

First Author Publications

- **Alsop, R.J.**, Himbert, S., Schmalzl, K., and Rheinstädter, M.C. *Aspirin Locally Disrupts the Liquid Ordered Phase.* Submitted.
- **Alsop, R.J.**, Dhaliwal, A., Rheinstädter, M.C. *Curcumin Protects Membranes Through Carpet or Insertion Model Depending on Hydration.* Langmuir, 33(34), 8516-8524.
- **Alsop, R.J.**, Khondker, A., Hub, J.S., Rheinstädter, M.C. (2016). *The Lipid Bilayer Provides a Site for Cortisone Crystallization at High Cortisone Concentrations.* Scientific Reports, 6, 22425.
- **Alsop, R.J.**, Soomro, A., Zhang, Y., Pieterse, M., Fatona, A., Dej, K., Rheinstädter, M.C. (2016). *Structural Abnormalities in the Hair of a Patient with a Novel Ribosomopathy.* PLoS ONE, 11(3), e0149610.
- **Alsop, R.J.**, Rheinstädter, M.C. (2016) *Lipid Rafts in Binary Lipid/Cholesterol Bilayers* in "Membrane Organization and Lipid Rafts in the Cell and Artificial Membranes". Pages 17-42, ISBN 978-1-63484-589-2.
- **Alsop, R.J.**, Schober, R., Rheinstädter, M.C. (2016). *Swelling of Phospholipid Membranes by Divalent Metal Ions Depends on the Location of the Ions in the Bilayers.* Soft Matter, 12, 6737-6748.
- **Alsop, R.J.**, Armstrong, C.L., Maqbool, A., Toppozini, L., Rheinstädter, M.C. (2015). *Cholesterol Expels Ibuprofen from the Hydrophobic Membrane Core and Stabilizes Lamellar Phases in Lipid Membranes Containing Ibuprofen.* Soft Matter, 11(24) 4756-4767.

- **Alsop, R.J.**, Toppozini, L., Marquardt, D., Kucerka, N., Harroun, T.A., Rheinstädter, M.C. (2015). *Aspirin Inhibits Formation of Cholesterol Rafts in Fluid Lipid Membranes.* BBA-Biomembranes, 1848, 805-812.

- **Alsop, R.J.**, Barrett, M.A., Zheng, S., Dies, H., Rheinstädter, M.C. (2014). *Acetylsalicylic Acid (ASA) Increases the Solubility of Cholesterol When Incorporated in Lipid Membranes.* Soft Matter, 10(24), 4275-4286.

Other Publications

- Mueller, A., **Alsop, R.J.**, Scotti, A., Bluel, M., Rheinstädter, M.C., Hoare, T. *Dynamically-Crosslinked Self-Assembled Thermoresponsive Microgels with Homogeneous Internal Structures.* Submitted.

- Dhaliwal, A., **Alsop, R.J.**, Khondker, A., Rheinstädter, M.C. *Glucose Vitrifies the Membrane Core in Dehydrated Lipid Membranes.* Submitted.

- Gilbert, T., **Alsop, R.J.**, Babi, M., Rheinstädter, M.C., Moran-Mirabal, J.M., Hoare, T. *Nanostructure of Fully Injectable Hydrazone-Thiosuccinimide Interpenetrating Polymer Network Hydrogels Assessed by Small-Angle Neutron Scattering and dSTORM Single-Molecule Fluorescence Microscopy.* Submitted.

- Schmidt, A., **Alsop, R.J.**, Lenzig, R.P., Gervasi, N.N., Grunder, S., Rheinstädter, M.C., Wiemuth, D. *Amphiphilic Substances Modulate DEG/ENACS by Modifying Membrane Structure and Density.* Submitted.

- Khondker, A., Dhaliwal, A.K., **Alsop, R.J.**, Tang, J., Backholm, M., Shi, A-C., Rheinstädter, M.C. *Caffeine in Drug Cocktails: The Formation of "Water Pockets" in Membranes.* Physics in Canada, in-press.

- Khondker, A., **Alsop, R.J.**, Rheinstädter, M.C. (2017) *Membrane-Accelerated Amyloid-β Aggregation and Formation of Cross-β Sheets.* Membranes, 7(3), 49.

- Bakaic, E., Smeets, N., Barrigar, O., **Alsop, R.J.**, Rheinstädter, M.C., Hoare, T. (2017). *pH-Ionizable In situ-Gelling Poly(Oligo ethylene glycol methacrylate)-Based Hydrogels: The Role of Internal Network Structures in Controlling Macroscopic Properties.* Macromolecules, 50(19), 7687-7698.

- Khondker, A., **Alsop, R.J.**, Dhaliwal, A., Saem, S., Moran-Mirabal, J.M., Rheinstädter, M.C. (2017) *Membrane Cholesterol Protects Against Polymyxin B Nephrotoxicity in Renal Membrane Analogues.* Biophysical Journal, DOI: 10.1016/j.bpj.2017.09.013.

- Soomro, A., **Alsop, R.J.**, Negishi, A., Kreplak, L., Fudge, D., Kuczmarski, E., Goldman, R., Rheinstädter M.C. (2017). *Giant Axonal Neuropathy alters the structure of keratin intermediate filaments in human hair.* Journal of the Royal Society Interface, 19, 7101-7111.

- Khondker, A., Dhaliwal, A., **Alsop, R.J.**, Tang, J., Backholm, M., Rheinstädter, M.C. (2017). *Partitioning of Caffeine in Lipid Bilayers Reduces Membrane Fluidity and Increases Membrane Thickness.* Physical Chemistry Chemical Physics. 19, 7101-7111.

- Himbert, S., **Alsop, R.J.**, Rose, M., Hertz, L., Dhaliwal, L., Moran-Mirabal, J.M., Verschoor, C.P., Bowdish, D.M.E., Kaestner, L., Wagner, C., Rheinstädter, M.C. (2017). *The Molecular Structure of Human Red Blood Cell Membranes frRheinstädter, M.C.om Highly Oriented, Solid Supported Multi Lamellar Membranes.* Scientific Reports. 7, 39661.

- Rheinstädter, M.C., Himbert, S., **Alsop, R.J.**, Moran-Mirabal, J.M., Saem, S., Bowdish, D.M.E. *Biological Membrane Based Sensor.* U.S. Provisional Patent, Serial N. 62/413,652, filed, October 27 2016.

- Urosev, I., Bakaic, E., **Alsop, R.J.**, Rheinstädter, M.C., Hoare, T. (2016). *Tuning the Properties of Injectable Poly(Oligoethylene Glycol Methacrylate) Hydrogels by Controlling Precursor Polymer Molecular Weight.* Journal of Materials Chemistry B. 4, 6541-6551.

- Schmidt, A., Löhrer, D., **Alsop, R.J.**, Lenzig, P., Osslender-Bujotzek, A., Wirtz, M., Rheinstädter, M.C., Gründer, S., Wiemuth, D. (2016). *A Cytoslic Amphiphilic Alpha Helix controls the Activity of the Bile Acid-Sensitive Ion Channel BASIC.* The Journal of Biological Chemistry. 291, 24551-24565.

- Shao, S., Do, T.N., Razi, A., Chitgupi, U., Geng, J., **Alsop, R.J.**, Dzikovski, B.G., Rheinstädter, M.C., Ortega, J., Karttunen, M., Spernyak, J.A., Lovell, J.F. (2016). *Design of Hydrated Porphyrin-phospholipid Bilayers with Enhanced Magnetic Resonance Contrast.* Small. 13, 1602505.

- Tang, J. **Alsop, R.J.**, Backholm, M., Dies, H., Shi, A-C., Rheinstädter, M.C. (2016). *Amyloid-β_{25-35} Peptides Aggregate Into Cross-b Sheets in Unsaturated Anionic Lipid Membranes at High Peptide Concentrations.* Soft Matter. 12, 3165-3176.

- Barrett, M.A., *Alsop, R.J.*, Hauss, T., Rheinstädter, M.C. (2016). *The position of $A\beta_{22-40}$ and $A\beta_{1-42}$ in anionic lipid membranes containing cholesterol.* Membranes. 5(4), 824-843.

- Tang, J., **Alsop, R.J.**, Backholm, M., Dies, H., Rheinstädter, M.C. (2015). *The Formation of Alzheimer's Plaques in Synthetic Membranes.* Physics in Canada. 71(3), 141-143.

- Tang, J., **Alsop, R.J.**, Schmalzl, K., Epand, R.M., Rheinstädter, M.C. (2015). *Strong Static Magnetic Fields Increase the Gel Signal in Partially Hydrated DPPC/DMPC Membranes.* Membranes. 5, 532-552.

- Zhang, Y., **Alsop, R.J.**, Soomro, A., Yang, F-C., Rheinstädter, M.C. (2015). *Effect of Shampoo, Conditioner and Permanent Waving on the Molecular Structure of Human Hair.* PeerJ. 3:e1296.

- Marquardt, D., **Alsop, R.J.**, Rheinstädter, M.C., Harroun, T.A. (2015). *Neutron Scattering at the Intersection of Heart Health Science and Biophysics.* Journal of Cardiovascular Disease and Development. 2(2), 125-140.

- Barrett, M.A., Zheng, S., Toppozini, L., **Alsop, R.J.**, Dies, H., Wang, A., Jago, N., Moore, M., Rheinstädter, M.C. (2013). *Solubility of Cholesterol in Lipid Membranes and the Formation of Immiscible Cholesterol Plaques at High Cholesterol Concentrations.* Soft Matter. 9(39), 9342-9351.

- Barrett, M.A., Zheng, S., Roshankar, G., **Alsop, R.J.**, Belanger, R.K.R., Huyhn, C., Kucerka, N.,Rheinstädter, M.C. (2012). *Interaction of Aspirin (acetylsalicylic acid) with lipid membranes.* PLoS One. 7(4): e34357.

Contributed Talks

- **Alsop, R.J.**, Dhaliwal, A., Rheinstädter, M.C. *Curcumin Protects Lipid Membranes.* Canadian Association of Physics Congress, Kingston, Ontario, 05/2017.

- **Alsop, R.J.**, Tang, J., Dies, H. Rheinstädter, M.C. *Creating Alzheimer's On A Chip, Then Curing It.* Chemical Biophysics Symposium, Toronto, Ontario, 05/2017.

- **Alsop, R.J.**, Rheinstädter, M.C. *Aspirin Reorganizes the Lipid Membrane.* American Conference on Neutron Scattering, Long Beach, California, 07/2016.

- **Alsop, R.J.**, Rheinstädter, M.C. *Ibuprofen Increases the Solubility of Cholesterol in Lipid Membranes.* Canadian Association of Physics Congress, Ottawa, Ontario, 06/2016.

- **Alsop, R.J.** *Breaking the Wall of Anti-Alzheimers Medication.* Falling Walls, Berlin, Germany, 11/2015.

- **Alsop, R.J.**, Toppozini, L., Marquardt, D., Kucerka, N., Harroun, T.A., Rheinstädter, M.C. *Aspirin inhibits the formation of cholesterol rafts in fluid lipidmembranes.* Chemical Biophysics Symposium, Toronto, Ontario, 04/2015.

- **Alsop, R.J.**, Toppozini, L., Kucerka, N., Rheinstädter, M.C. *Aspirin Reorganizes the Lipid Membrane.* Canadian Association of Physics Congress, Sudbury, Ontario, 06/2014.

- **Alsop, R.J.**, Toppozini, L., Kucerka, N., Rheinstädter, M.C. *Aspirin Reorganizes the Lipid Membrane.* American Conference on Neutron Scattering, Knoxville, Tennessee, 06/2014.

- **Alsop, R.J.**, Barrett, M.A., Zheng, S., Dies, H., Rheinstädter, M.C. *Aspirin Increases the Solubility of Cholesterol in DMPC Membranes.* APS March Meeting, Denver, Colorado, 03/2014.

Poster Presentations

- **Alsop, R.J.**, Rheinstädter, M.C. *Structural Abnormalities in the Hair of A Patient with a Novel Ribosomopathy.* Chemical Biophysics Symposium, Toronto, Ontario, 05/2016.
- **Alsop, R.J.**, Rheinstädter, M.C. *Non-specific drug interactions mediated by the lipid membrane.* EBSA Congress, Dresden, Germany, 07/2015.
- **Alsop, R.J.**, Rheinstädter, M.C. *The Interaction of Common Drugs with Lipid Membranes.* NBIA Workshop on ESS Science, Copenhagen, Denmark, 11/2014.
- **Alsop, R.J.**, Barrett, M.A., Zheng, S., Dies, H., Rheinstädter, M.C. *Aspirin Increases the Solubility of Cholesterol in DMPC Membranes.* Chemical Biophysics Symposium, Toronto, Ontaro, 04/2014.

Chapter 2

Introduction

2.1 Biological Membranes

Biological lipid membranes play a number of vital roles in the cell. In a particularly important role, they define the surface of the cell and provide the barrier which encapsulates all cell contents. In that sense, membranes are fundamental building blocks and a necessary requirement for even the earliest forms of life [4]. In eukaryotes, they also define the surface of many organelles, which are structures that further sub-encapsulate the cell and permit cell complexity and differentiation.

The membrane is a bilayer structure of surfactant molecules known as lipids. The bilayer structure allows for the passive diffusion of small molecules such oxygen and carbon dioxide, but blocks larger items, such as proteins, from crossing into the cell [1]. . Large molecules such as these often must be transported across the membrane by active processes that require energy.

However, biological membranes are much more than passive barriers. In addition to lipids, proteins are a major membrane component. In fact, 20-30% of all proteins are membrane proteins, and as proteins are work-horses of the cell, they convey great importance to membrane structure

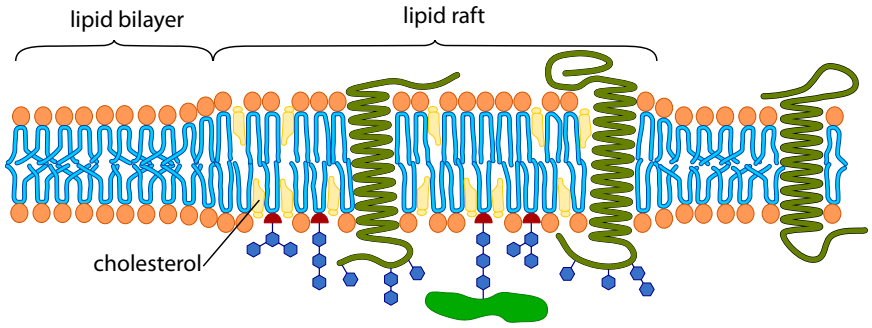

Figure 2.1: A schematic representation of the plasma membrane. The membrane contains lipids, cholesterol, integral and peripheral proteins, carbohydrates, and water. Modified from a public domain figure [3].

and function [1]. Peripheral membrane proteins bind to the surface of the membrane, and often chaperone other proteins to the membrane. Integral membrane proteins imbed directly into the membrane, and act as channels for ions, other proteins, and for cell adhesion [5].

Shortly after membrane-associated proteins were discovered, the first accepted model for their interaction with the lipid bilayer was devised by Singer and Nicholson and called the fluid mosaic model [6]. In this model, proteins embed within the lipid bilayer and diffuse randomly in the plane of the bilayer, effectively "swimming" in the fluid 2-dimensional matrix that is the bilayer. This model does not convey importance to specific lipids, despite the fact that there is great diversity in lipid composition within and between different cell membrane types. Over 100 different lipid species may be present in a single membrane [1].

A landmark discovery was lipid rafts, which are lipid structures that have a distinct functional purpose [7, 8, 9]. Rafts are regions of the membrane rich in saturated lipids and cholesterol and proteins may choose to embed in the raft or non-raft region. Proteins may even be transported and sorted using rafts as platforms [10, 11]. Therefore, in contrast to the model by Singer and Nicholson, the current view is that the structure, dynamics, and composition of the *lipids* as well as the proteins is important to the health of the cell. The membrane is also susceptible to perturbation by external agents [2]. The modern image of a lipid membrane, with lipid rafts and membrane-embedded proteins, is depicted in Fig. 2.1.

Understanding lipid structure and dynamics is therefore important for understanding proper cell function. Perhaps more importantly, theories are needed for how lipid structure and function can be disturbed, for example by a drug molecule. However, the complexity of the biological membrane makes studying many of these relevant processes almost intractable. Many processes are too small and too fast to be studied by, for example, an optical microscope. The relevant lipid structural parameters are ∼Ångstroms in size and lipid dyamics occur on ∼nanosecond timescales, as will be discussed below.

For these reasons, model lipid bilayers are a common and accepted tool for isolating and studying membrane phenomena. The lipid composition, as well as the phase of the lipids, can all be varied. Using X-ray and neutron scattering techniques, the relevant parameters can be measured. Model lipid membranes were the predominant tool of study in this thesis. In this Chapter, I will discuss the biophysics of lipids and lipid membranes.

2.1.1 Lipids and Model Lipid Bilayers

Lipids are surfactant molecules, and have a hydrophilic head group and a hydrophobic tail group. Due to their amphiphilic nature, lipid molecules spontaneously aggregate in aqueous environments, into bilayer structures. There are many classes of lipids, such as glycerophospholipids, sphingolipids, and cholesterol. Cholesterol will be discussed in the next section. Here, we focus on glycerophospholipids, aka phospholipids, as they are the dominant lipid in biological membranes and also the only lipid used in this thesis [12]. A conceptual overview of lipids is given in Fig. 2.2a).

Phospholipids vary in the chemistry of the heads as well as the number of carbons on the lipid

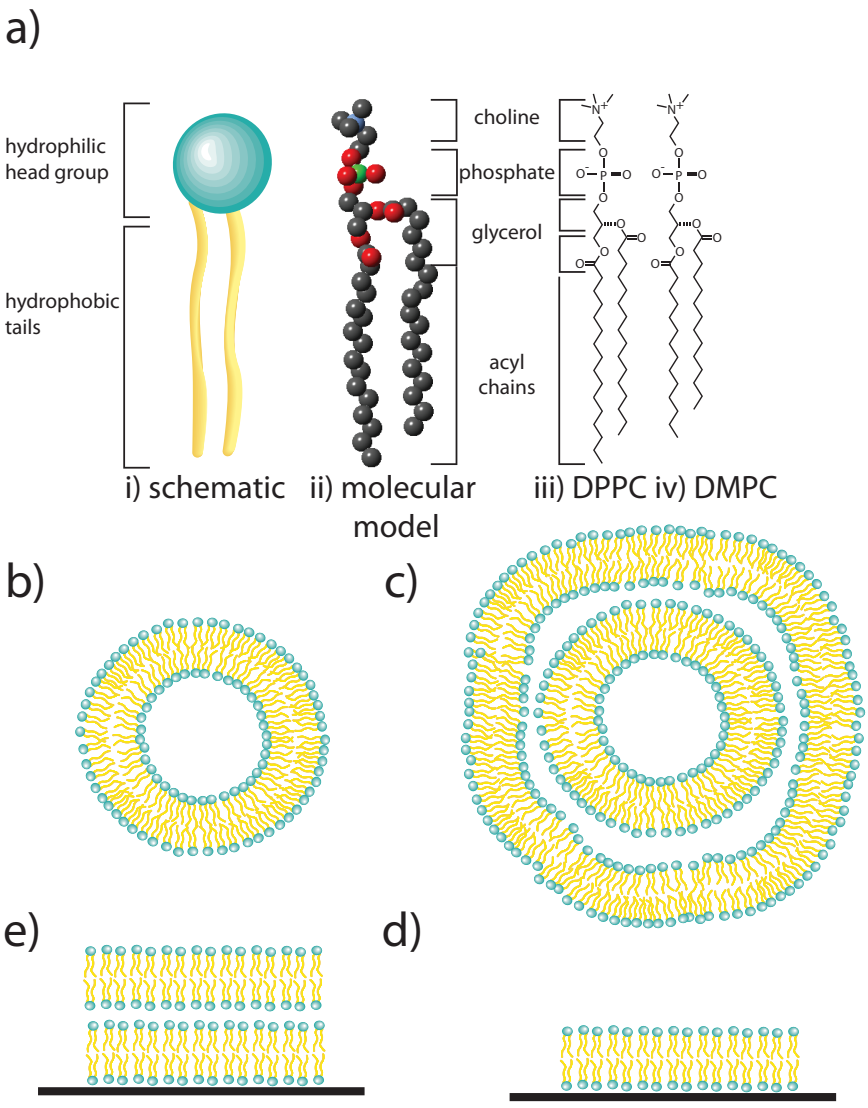

Figure 2.2: a) Schematics illustrating the relevant properties of lipids. i) A cartoon representation of a lipid, highlighting the lipid head groups and tail groups. ii) A molecular image, where each atom is represented by beads. iii) Chemical image of a DPPC (1,2-dipalmitoyl-sn-glycero-3-phosphocholine) molecule next to iv) a DMPC (1,2-dimyristoyl-sn-glycero-3-phosphocholine) molecule, showing the similarity in head group structure of the two molecules combined with the difference in chain length. b) A vesicle model membrane system. c) A multi-lamellar vesicle. d) A single, oriented bilayer on solid substrate. e) Multi-lamellar, oriented membranes.

chains, and the saturation of the lipid tail groups. Saturation refers to the number of double bonds on the tails: fully saturated chains have no double bonds (are "saturated" with hydrogen), and unsaturated chains have one or more double bonds. The chemistry in the head group is slightly more complex. For phospholipids, the head group contains a gycerol group, a phosphate group, and a choline group. The head group can be neutral, positive or negatively charged, or zwitterionic (net neutral charge, but possessing physically separated charges), thereby making it hydrophilic.

Common lipids used in this study are 1,2-dimyristoyl-sn-glycero-3-phosphocholine (DMPC), 1,2-dipalmitoyl-sn-glycero-3-phosphocholine (DPPC), and 1-palmitoyl-2-oleoyl-sn-glycero-3-phosphocholine (POPC). DMPC is a zwitterionic phospholipid with the glycerol, phosphate, and choline groups, and two fully saturated, 14-carbon long tails. DPPC is the similar to DMPC, with longer, 16-saturated-carbon tails. POPC has the same head group as DPPC and DMPC, but is an unsaturated lipid. One tail is 18-carbons long with an unsaturated bond, the other is 16-carbons long and is saturated.

The typical image of a bilayer is depicted in Fig. 2.1, where lipids form a symmetric, two-leaflet system, and the bilayer forms a surface encapsulating the cell and its contents. However, model bilayers can be arranged in a number of different geometries, and a few of these are illustrated in Fig 2.2 b) - e). Vesicles are single bilayers with spherical geometry similar to plasma membranes. Bilayers in a spherical geometry can also be stacked radially outward, forming multi-lamellar vesicles. A flat geometry is also possible, in the presence of solid support. The supported lipids may exist as a single bilayer, or as stacked bilayers.

Each model system has its own advantages, depending on the experimental question. Vesicles and multi-lamellar vesicles are useful in studies of bulk bilayer properties, such as mechanical and thermodynamic properties in solution. Oriented systems are useful for isolating and studying nano-scale bilayer properties using atomic force microscopy or scattering experiements, as will be discussed below.

It is the nano-scale properties that are the focus of this thesis. There are two main length scales important to describing lipid bilayers, and are related to the volume occupied by the lipids. The bilayer thickness is typically determined based on the head group-head group distance across the bilayer and is denoted d_{HH}. Secondly, the in-plane lateral area occupied, on average, by a lipid in the bilayer is called the area per lipid (A_L). For a POPC bilayer d_{HH} ~40 Å, and A_L ~65 Å^2 [13]. However, these properties vary significantly depending on the chemistry of the lipid species [14]. DPPC is thicker (has higher d_{HH} and has a smaller A_L) compared to POPC [14]. This is because DPPC is a saturated lipid, and the hydrocarbon tails of DPPC molecules pack tightly together by adopting an all-trans configuration in the tails. The double-bond of the POPC prevents tight packing by introducing a gauche defect, increasing the area per lipid and minimizing the membrane thickness.

2.1.2 Lipid Phases

The properties of the lipid also depend on thermodynamic phase. Lipid bilayers undergo phase transitions depending on temperature and hydration. At low temperature and humidity, lipids enter

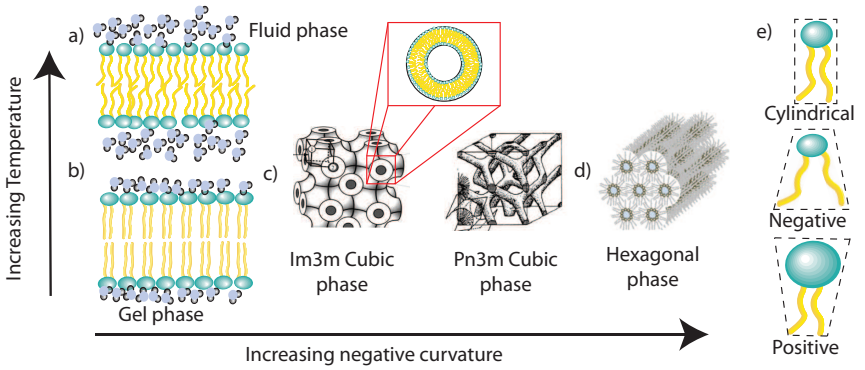

Figure 2.3: Phases observed for single lipid bilayers. a) A lamellar fluid phase, with low chain order and high hydration. b) The gel phase, with high chain order and low hydration. c) With increasing lipid curvature, lipids in the lamellar phase transition to a cubic phase, with three-dimensional symmetry. d) At even higher curvatures, the hexagonal phase is formed. e) Diagrams illustrating the physical origin of positive and negative curvature. Images are adapted from [15, 16].

a "gel" phase, denoted by the L_β symbol. In the gel phase, Van-der-Waals forces dominate over entropic forces causing lipid tails to pack tightly together. Consequently, lipid diffusion is slow, the bilayer thickness is maximum, and A_L is small. With increasing temperature and humidity, entropic forces become stronger and lipid tails fluctuate more. The bilayer melts from the gel to the liquid phase (symbolized by L_α), causing increased A_L and decreased d_{HH}, and resulting in rapid diffusion. The temperature at which the chains melt from L_β to L_α is known as the main transition, and varies depending on the head group size, chain length, and chain saturation [17]. POPC melts at 271 K. In comparison, DPPC melts at 313 K as more thermal energy is necessary to melt the longer, saturated tails. The fluid and gel phases are visualized in Fig. 2.3 a) and b).

Head group hydration also plays an important role in determining bilayer phase and properties [18]. At low hydration, the number of water molecules in the head groups is small, and head groups pack closer together, decreasing the area per lipid. Increasing hydration causes the tails to melt (if the tempearture is above the main transition), as water molecules cause the head groups to increase in area. For bilayers exposed to air, the hydration is controlled by the relative humidity of the atmosphere. In aqueous systems, bilayer hydration is controlled by the osmotic pressure, which in turn is tuned by the concentration of solutes near the bilayer [19]. Solutes may include salt and proteins. In conditions of high osmotic pressure, the bilayer becomes dehydrated.

The L_β and L_α refer to lipid phases where all the head groups exist in the same plane and have one-dimensional symmetry. These are the phases most relevant to physiological bilayers. However, there are structures where lipids are curved into phases with higher-symmetry, due to the physical properties of the bilayer system. For example, lipids can pack in so-called hexagonal phases, where lipids curve into cylinders, and the cylinders pack into a two dimensional cylindrical lattice [20]. These phases occur when the lipids have negative intrinsic curvature, which is a property of lipids that have greater volume in the tails than heads. Cubic phases are also caused by negative curvature

lipids, but at curvatures less than the hexagonal phase. Cubic phases have 3-dimensional symmetry and repeating distances on the order of 120 Å. [21]. See Fig. 2.3 c)-e) for images of inverse phases and curved lipids. Bilayers initially in a planar lipid phase can be transitioned to a curved phase by introducing a curved lipid or by embedding surfactants causing curvature [22]. Positive curvature lipids may also exist, where the volume of the heads is greater than the tails, and these lipids produce micellar structures [21].

The area per lipid, bilayer width, bilayer curvature, and bilayer phase of biological membranes are all relevant to physiological function. For example, increased A_L provides greater diffusion for small molecules [23]. Also, intrinsic membrane proteins will only embed in membranes where the tail thickness, d_c, matches the hydrophobic thickness of the protein. Alternatively, the protein may cause the membrane to deform around the peptide. The lipid composition of the membrane is important to tuning this thickness [24]. Proteins may also have intrinsic curvature, and curved lipids have been observed assembling around curved proteins to stabilize the lipid-protein structure [25]. However, if lipids in a plasma membrane possess enough curvature to transition from a lamellar to curved phase, the integrity of the bilayer and of the cell will be compromised. This emphasizes the importance of lipid composition to cell function. In mammalian cells, cholesterol, in addition to phospholipids, is a membrane component that plays a very particular and profound role.

2.1.3 Cholesterol and Lipid Rafts

Cholesterol is a sterol molecule highly abundant in eukaryotic plasma membranes, present in concentrations of 20-50% [27]. It is characterized by a stiff, hydrophobic ring structure that encourages it to embed into lipid bilayers and position upright with the bilayer normal. This is known as the umbrella molecule [28]. Cholesterol then causes the lipid tails to straighten and the bilayer to become stiffer [29]. The area per lipid decreases, and the bilayer width increases. For this reason, cholesterol prefers to interact with more ordered saturated lipid tails [30]. Cholesterol is essential to eukaryotic membranes, and provides vital integrity to the structure. In fact, at high concentration, a distinct lipid phase emerges, known as the liquid-ordered phase, ℓ_o [1]. This phase has properties intermediated between the fluid and gel phases. See Fig. 2.4 for illustration. The ℓ_o phase known to be stiff, like the gel phase, but softer than the fluid phase [31]. While the phase has integrity, it also permits lipid diffusion [31]. Cholesterol is most abundant in the plasma membrane, which allows the plasma membrane to hold the cell shape [28].

An extremely common observation, in both real and model systems, is that membranes with cholesterol are not homogeneous in structure [28]. Patches, that are nm to μm in size, exist in these membranes that are enriched in cholesterol and often saturated lipids, and are more ordered. These structures float in a surround of less ordered lipids. These are known as lipid "rafts". In physiological systems, protein molecules may embed in the raft region or the non-raft region, depending, for instance, on their hydrophobic thicknesses [7]. In this way, rafts can "sort" integral membrane proteins [10, 11].

However, little is known about the properties of lipid rafts. This is largely because experimental

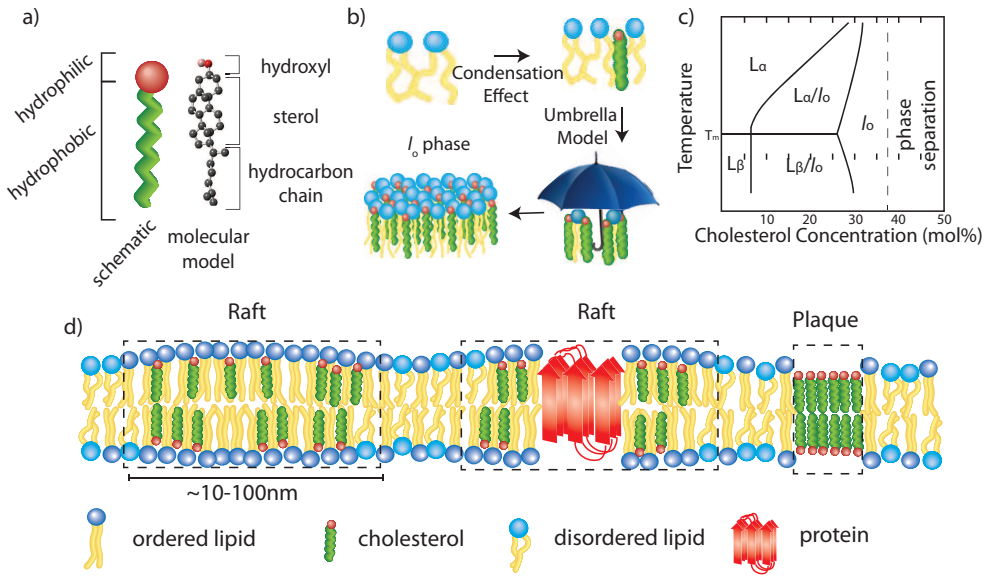

Figure 2.4: Cholesterol has a profound effect on the lipid membrane. a) Cholesterol is a largely hydrophobic molecule with a stiff sterol ring. b) Cholesterol inserts into the bilayer and condenses fluid tails. The main model for this interaction is the "umbrella model" which suggests that cholesterol interacts with the tail to avoid water contact. High concentrations of cholesterol create the ℓ_o phase, an entirely unique phase. c) At concentrations above ~30 mol%, the ℓ_o phase is formed at all temperatures [26]. d) A cartoon of a membrane with lipid rafts and cholesterol plaques. Rafts are modelled as regions enriched in cholesterol and ordered lipid that host proteins. Plaques are cholesterol-only crystals that co-exist with the lipid bilayer and occur at cholesterol concentrations 37.5 mol%.

measurement is difficult, and evidence for rafts is often indirect [32]. Initial theories of rafts were built from the observation that proteins clustered on plasma membrane, and that the clustering could be eliminated by removing cholesterol and saturated lipids. Then, rafts were associated with detergent-resistant plasma membrane fractions, despite the fact that detergents distort membrane structure [33]. Fluorescent microscopy of tagged proteins has identified protein clusters that are small (∼nm in size) and transiently short-lived (∼ μs to ms lifetimes) [34, 8]. All these studies confirm that cholesterol and saturated lipids are necessary for rafts, but probing the underlying lipid structure has been an experimental challenge. Experiments focussed on proteins do not answer why rafts form, or shed light on the forces determining raft size and lifetime.

Attempts have been made, using model lipid systems, to understand raft phenomena. So-called "raft-mixtures" are used that contain saturated lipids, unsaturated lipids, and cholesterol [35]. At particular temperatures, these systems form relatively larg,e μm sized domains that are stable [36]. These systems suggest that the driving force for domain formation is coalescence of ordered lipids with larger hydrophobic thickness to minimize mis-match with disordered lipids. This mis-match produces a line-tension that can be minimized by forming domains [36]. The mechanisms preventing complete coalescence (*i.e.* all thick lipids in one structure) of domains are not known, although popular theories suggest that dielectric repulsion or curvature effects play a role [35, 37].

However, the lipid structure of rafts in real membranes has not been directly observed [38]. The likely reason is that they are smaller than the phase separated domains observed with fluorescence in model membranes. This has led to speculation that rafts are not separate phases, but instead non-equilibrium structures caused by critical-point fluctuations or microemulsions [39, 40, 41]. These theories still do not provide complete theories for the size, lifetime, and composition of rafts. However rafts are ubiquitous: even in binary lipid/cholesterol bilayers they are observed [28]. What is common among the different systems is that cholesterol drives domain formation by sharply increasing local lipid organization.

At abnormally high concentrations of cholesterol (>40 mol%), cholesterol domains of a different form are observed. Cholesterol becomes no longer miscible in the bilayer and forms two-dimensional, cholesterol-only crystals that coexist with the lipid bilayer [42, 43]. In biological systems, these plaques have been known to leave the bilayer and deposit on arterial walls, thereby causing arterial blockage and the disease known as atherosclerosis [44]. The homeostasis of membrane cholesterol is therefore essential to the health of the cell and the organism. It is crucial to not only have cholesterol, but also to maintain healthy levels within the membrane.

2.2 Scattering Theory of X-rays and Neutrons

Section 2.1 illustrated that understanding membranes is an exercise in studying the small. Lipids exist on Å length scales and many of the relevant structures and processes (such as rafts) occur on nanosecond timescales. A full structural understanding of membranes is challenging with optical microscopy, fluorescence microscopy, or even super-resolution microscopy, because of their spatial

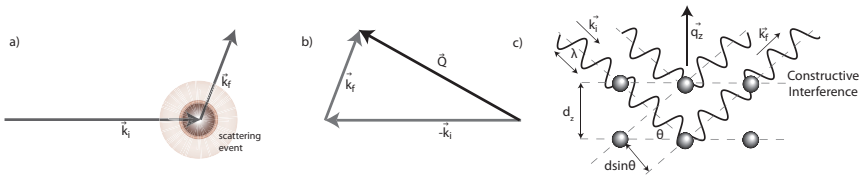

Figure 2.5: Vector diagrams illustrating the physics of a scattering experiment. a) Neutrons with incident wave-vector $\vec{k_i}$ on an atom scatter with wavevector $\vec{k_f}$. b) Scattering vector $\vec{Q} = \vec{k_f} - \vec{k_i}$. c) An illustration of scattering using wave mechanics, and highlighting Bragg's law. The condition for constructive interference occurs at $\lambda = 2d \sin\theta$.

resolution. Precision techniques such as X-ray or electron microscopy require frozen samples and only measure small regions at a time. Therefore, they often struggle to capture the complexity of biologically relevant membranes.

X-ray and neutron scattering are robust and popular techniques for probing the molecular structure of both hard and soft matter. The techniques exploit the quantum mechanical wave-particle duality intrinsic to matter, especially subatomic particles. The De Broglie wavelength of X-rays and neutrons is on the order of 1-8 Å, which is ideal for studying structures 1-500 Å in size, so perfect for studying lipid membranes. Inelastic neutron scattering techniques probe processes from picoseconds up to microseconds in timescale. With the use of temperature and humidity controlled chambers, membranes can be studied in various phases. In this section, I will outline the physics of scattering (in particular, diffraction) to highlight how scattering is useful for studying membrane phenomena.

2.2.1 General Scattering Principles

To understand how to study the molecular structure using scattering, consider first a particle (X-ray or neutron) with wave vector $\vec{k_i}$. The momentum of the wave is related to the wavelengh, λ:

$$|\vec{k_i}| = \frac{2\pi}{\lambda}. \tag{2.1}$$

Then, consider that the incoming particle is incident on an atom, and scatters with new $\vec{k_f}$. The resultant vector, $\vec{Q}$, is determined by:

$$\vec{Q} = \vec{k_f} - \vec{k_i}. \tag{2.2}$$

This scattering condition is visualized in Fig. 2.5a) and b). Now lets consider the condition where $|\vec{k_i}| = |\vec{k_f}|$, or where elastic scattering occurs. From Fig. 2.5b), we see that $Q = 2k_i \sin\theta$. By combining with Eq. 2.1:

$$|\vec{Q}| = \frac{4\pi}{\lambda} \sin\theta, \tag{2.3}$$

where θ is the scattering angle. Diffraction of regular structures, such as atomic or molecular lattices, is depicted in Fig. 2.5c). In this real-space view, plane waves are incident on a regular lattice of atoms at some angle to the lattice plane, and are reflected from different layers of the lattice. In

this example, $\vec{k_i}$, $\vec{k_f}$, and $\vec{Q}$ are always in the same plane and $\vec{Q} = \vec{q_z}$ always points along the z-axis. At specific angles from the scattering plane, θ, waves scattered from adjacent lattice planes will constructively interfere. This condition occurs at:

$$n\lambda = 2d_z \sin\theta, \tag{2.4}$$

where d_z is the lattice spacing. This is the well known Bragg's law for constructive interference. Combinining equations Eq. 2.3 and Eq. 2.4:

$$q_z = \frac{2\pi n}{d_z}, \tag{2.5}$$

which illustrates that based on the q_z-position of high-intensity, the lattice spacing of atoms in the material, d_z is determined. A typical diffraction experiment is the methodical scanning of $\vec{Q}$ to identify regions of with high intensity due to constructive interference. Eq. 2.5 is then used to determine the length scale associated with the constructive interference. From a bilayer, for example, constructive interference may occur at $q_z \sim 0.11$ Å^{-1}, or $d_z \sim 60$ Å, related to the distance between two stacked membranes in the stack..

However as noted in Eq. 2.4, constructive interference occurs at more than one angle for a given d_z-spacing. Many peaks can occur at higher angles for different n, and these are known as overtones. These peaks will occur at q_n, where q_{n+1} - $q_n = \Delta q_z$. The relative intensity of the different overtones is related to the structure of the material. The intensity of the scattered wave is proportional to the Fourier transform of the density, $\rho(z)$ of the material along the z-axis:

$$\rho(z) \sim \int I(q_z) e^{-iq_z \cdot z} dq_z. \tag{2.6}$$

When the intensity is sampled at discrete Bragg peaks, the continuous Fourier transform becomes discrete [45]:

$$\rho(z) = \frac{2}{d_z} \sum_n \sqrt{I_n q_n} \nu_n \cos(\Delta q_z z), \tag{2.7}$$

where I_n are the integrated intensities of the Bragg peaks at positions q_n. $\nu_n = \pm 1$ are the phases, and the method for determining these is outlined in Chapter 3. Using this treatment for a membrane system, the density of the bilayer along the axis perpendicular to the bilayer plane is determined. Changes in density are used to determine the position of peptides or molecules in the membrane, as will be discussed in the next chapter.

With oriented membranes, the scattering vector, $\vec{Q}$, can be directed into the membrane plane (it is "in-plane"), such that it measures the in-plane structure and $\vec{Q} = \vec{q_{||}}$. In-plane structure yields information such as the A_L, and the molecular structure within lipid rafts.

The discussion so far has been general and applicable to both X-ray and neutron scattering. However, there are important differences between the two techniques. X-rays scatter off the electron shell of atoms, whereas neutrons scatter off of the nucleus. While both techniques involve the analysis

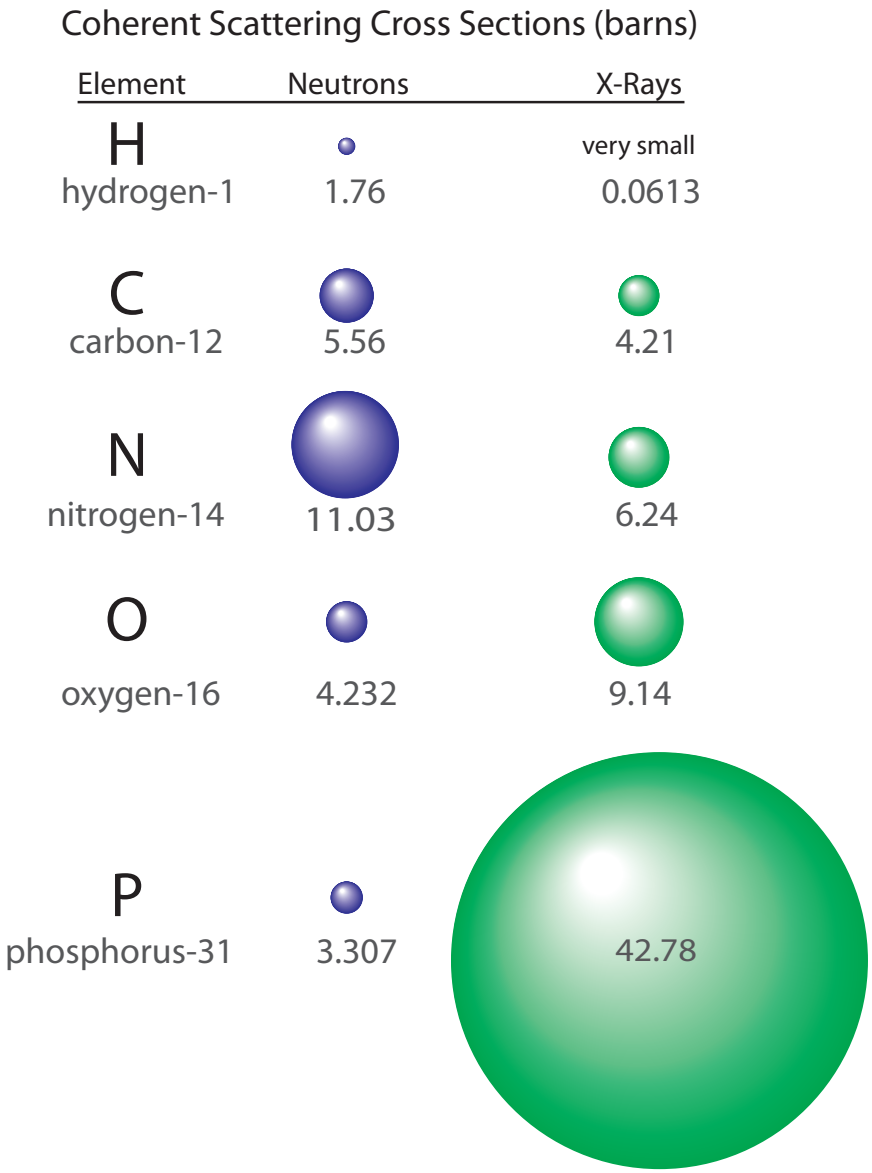

Figure 2.6: An illustration in the scattering cross sections of various atoms in neutron and X-ray scattering experiments (in barns) [46]. While scattering cross section directly scales with atomic number for X-rays, neutron cross section is almost randomly distributed. This creates functional differences between X-ray and neutron scattering results.

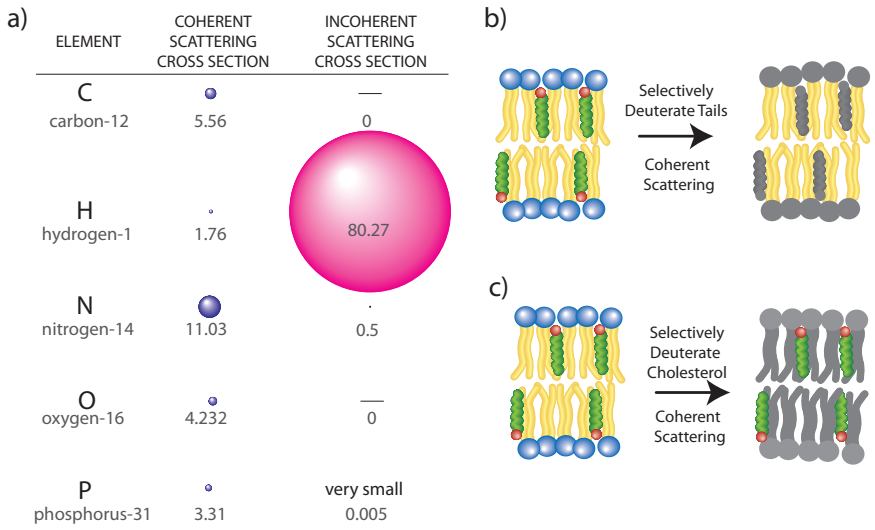

Figure 2.7: Selective deuteration enables special contrast conditions for neutron scattering experiments. a) Coherent and incoherent cross sections for various atoms. Note that the incoherent cross section for hydrogen is very large, while the coherent cross section is very small (compared to deuterium). b) Selective deuteration enhances the coherent signal from lipid tails. c) In contrast, selective deuteration of the cholesterol molecules would instead enhance the coherent scattering from cholesterol molecules.

of scattered wave intensity, the distinction creates a clear separation between the two techniques based on contrast. Contrast in a material is necessary for the X-rays or neutrons to distinguish between atoms. Differences in scattering power create contrast. X-rays scatter more strongly off of atoms that have more electrons, whereas neutrons scatter more strongly off of atoms which have a larger nuclear scattering length. Electron number scales directly with atomic number, but the nuclear scattering length is an effectively random function of atomic number, as highlighted in Fig. 2.6. In addition, isotopes of an atom may have entirely different nuclear scattering lengths. For example, while hydrogen scatters X-rays extremely weakly, hydrogen and deuterium strongly scatter neutrons. Fig. 2.6 illustrates the difference in scattering power for different, membrane-relevant atoms. Next, I will discuss neutron scattering in more detail and highlight other key differences between neutron and X-ray scattering.

2.2.2 Neutron Scattering

In the previous section, we discussed the elastic scattering scenario where $|\vec{k_i}| = |\vec{k_f}|$. However, in general, $|\vec{k_i}| \neq |\vec{k_f}|$ due to energy transfer between the system and the scatterer. In this case the intensity is now a function of energy $I(\vec{Q}) \rightarrow I(\vec{Q}, E)$. For neutron scattering, $I(\vec{Q}, E)$ is proportional to the scattering function $S(\vec{Q}, E)$, convoluted with an instrumental resolution, $R(\vec{Q}, E)$ [47]:

$$I(\vec{Q}, E) = \int S(\vec{Q}, E) R(\vec{Q}, E) d\vec{Q} dE. \tag{2.8}$$

$S(\vec{Q}, E)$ is explicitly derived by considering each atomic scatterer in the sample in both space and time. By assigning the jth scatterer a nuclear scattering length $b_j$and position $\vec{R}_j$:

$$S(\vec{Q}, E) = \frac{k_f}{k_i} \frac{1}{2\pi\hbar} \sum_{j'j} \langle b_{j'} b_j \rangle \int \langle e^{i\vec{Q}\cdot(\vec{R}_j(t) - \vec{R}_{j'}(0))} \rangle e^{-iEt/\hbar}\, dt. \tag{2.9}$$

Expanding the sum over b_j:

$$\sum_{jj'} \langle b_j b_{j'} \rangle = \langle b^2 \rangle + \langle b \rangle^2, \tag{2.10}$$

Gives:

$$\begin{aligned} S(\vec{Q}, E) &= \frac{k_f}{k_i} \langle b \rangle^2 \frac{1}{2\pi\hbar} \sum_{j'j(j' \neq j)} \int \langle e^{i\vec{Q}\cdot(\vec{R}_j(t) - \vec{R}_{j'}(0))} \rangle e^{-i\omega t}\, dt \qquad (2.11) \\ &\quad + \frac{k_f}{k_i} \langle b^2 \rangle \frac{1}{2\pi\hbar} \sum_j \int \langle e^{i\vec{Q}\cdot(\vec{R}_j(t) - \vec{R}_j(0))} \rangle e^{-i\omega t}\, dt \\ &= S_{coh}(\vec{Q}, E) + S_{inc}(\vec{Q}, E). \qquad (2.12) \end{aligned}$$

Eq. 2.12 demonstrates that neutron scattering signals are in fact a superposition of two contributions: $S_{coh}(\vec{Q}, E)$ is from coherent neutron scattering, and $S_{inc}(\vec{Q}, E)$ is from incoherent scattering. The coherent scattering arises from correlations between different atoms over time, whereas the incoherent scattering comes from self-correlated motions. The term $\langle b^2 \rangle$ is called the coherent cross-section, or b_{coh}, whereas the incoherent cross-section is $b_{inc} = \sqrt{\langle b^2 \rangle - \langle b \rangle^2}$.

The coherent scattering arises from collective structure and motions of atoms. This corresponds to the lattice structure and collective motion of atoms within the lattice, known as phonons [48]. Phonons are excited at specific energies, and therefore produce peaks at those exact energy transfers. Incoherent scattering describes the motion of individual atoms over time, and is therefore related to diffusion processes. Diffusion processes are continuous, and produce broad peaks centred at zero energy transfer.

Each isotope of an atom has a different coherent and incoherent cross section, as shown in Fig. 2.7a). For example, hydrogen has a very large b_{inc} but a small (even negative) b_{coh}, while deuterium has large b_{coh} but small b_{inc}. The signal from a sample with large hydrogen content will be dominated by the incoherent term, whereas the signal from a deuterium-rich (or simply low-hydrogen) sample will be dominated by coherent scattering. This fact introduces a powerful degree of freedom into neutron scattering experiments: by substituting hydrogen and deuterium, the incoherent or coherent signal for the sample, or even a specified component of the sample, can be turned on or off. For example, when performing an experiment with lipids, the static structure of the tails can be enhanced by deuterating the tails, as depicted in Fig. 2.7.

A generic energy scan is shown in Fg. 2.8. Energy scans are conducted at some fixed $\vec{Q}$, with varying E. The image shows the main three components of an inelastic neutron scan: A sharp peak at $E = 0$ resulting from elastic scattering; a broad peak also centred at E=0 which is a result of incoherent scattering; and peaks at $|E| > 0$ that result from phonon scattering. Since the frequency,

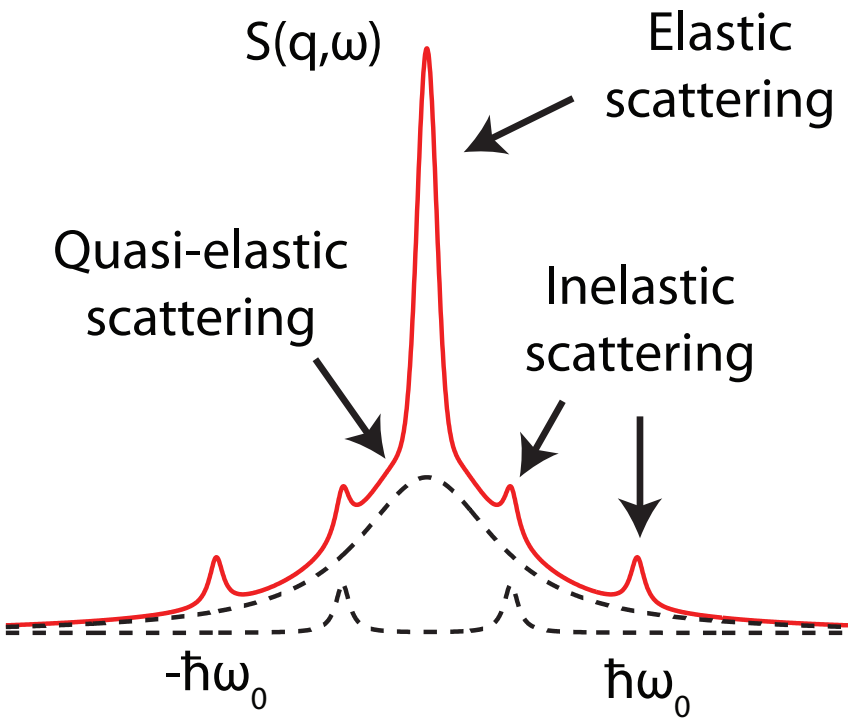

Figure 2.8: A sample graph illustrating the three components of an inelastic neutron scattering experiment. 1) Elastic scattering appears at $\hbar\omega = 0$ due to instrument resolution effects. 2) Quasi-elastic scattering occurs due to relaxation dynamics in the sample (incoherent scattering). 3) Peaks occur at $\hbar\omega > 0$ due to collective motions in the sample (coherent scattering).

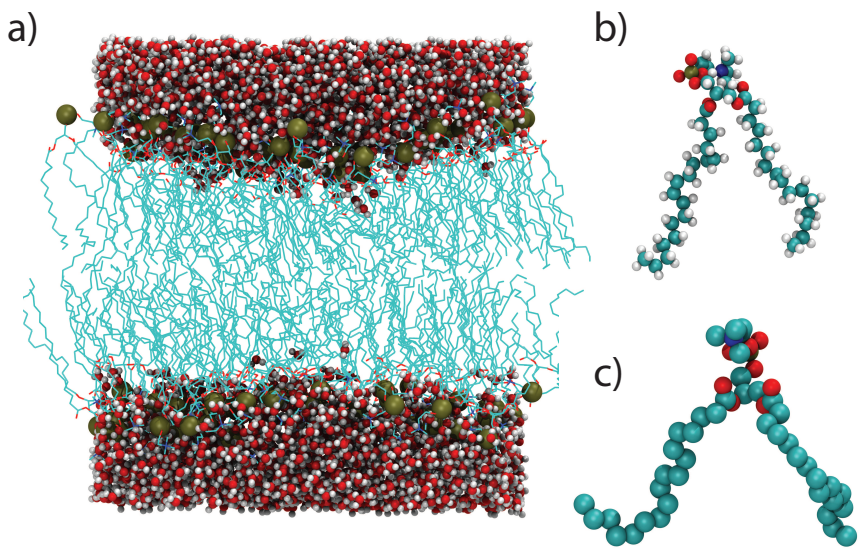

Figure 2.9: Images from Molecular Dynamics simulations. a) A snapshot of a 128-lipid POPC bilayer simulated with 25 water molecules per lipid. The phosphorous atom in the head groups is emphasized using the gold spheres. b) A representation of a single, all-atom POPC molecule. c) A single POPC in a united-atom configuration.

ω, of the neutron wave-packet is related to the energy by $E = \hbar\omega$, energy is often represented by $\hbar\omega$.

From Heisenberg's Uncertainty Principle, the energy resolution of a molecular process is inversely proportional to the time scale of the process by $\Delta E \Delta t \sim \hbar$. Neutron scattering achieves resolutions of $\Delta E \sim$ 10-100 μev or $\sim$meV. Therefore, it can resolve processes on picosecond to nanosecond timescales, making it ideal for the study of structure and dynamics in membranes.

2.3 Molecular Dynamics Simulations

Scattering experiments of model lipid system provide molecular level detail into membrane processes. The techniques provide an ensemble measurement of the bilayer. While these properties represent a strength of the scattering technique, they also pose weaknesses. Scattering does not provide access to atomic level membrane detail, nor does it provide information on the motions of individual molecules or atoms. A technique highly complementary to scattering is Molecular Dynamics (MD) simulation, as it can provide the atomistic and individualistic detail.

MD simulations are designed to generate an atomic resolution image of bilayer phenomena using a computation representation of the membrane. The exact composition of the membrane system is explicitly controlled. MD simulations are performed on bilayers with $\sim$128 total lipids, more than 30 waters per lipid, and with protein or other molecules included. Simulations are performed on freely available software, such as GROMACS [49]. Processing power is provided by supercomputers

or GPU accelerated workstations. Molecules used in the simulations are derived from PDB files, or calculated using tools such as the Automated Topology Builder [50]. An image of a simulated bilayer is in Fig. 2.9a).

To perform a MD simulation, all atoms in the system are assigned positions, velocities, and the appropriate bonds are identified. In addition, the energies required to deform (bend, twist, extend) are obtained. Next, the force on each atom is determined by summing interactions with all neighbouring atoms, and the equations of motion are solved for each atom to find new positions and velocities [51]. This constitutes one simulation step. To start another simulation step, the potential on each atom is re-calculated based on the new positions. A simulation step occurs on the timescale of femptoseconds, and a typical simulation time is 100-200 ns.

To solve the potential on each atom using an exact many-body quantum-mechanical solution would require many variables. Therefore, quantum potentials are approximated to reduce the calculations to a set of two-body problems that are solved using Newton's equations. These "force-fields" describe the potentials between each atom type, and the appropriate bond lengths and angles. Different force fields have been developed and are freely available. They must reproduce known physical quantities to be considered a reasonable approximation for real potentials [52]. For example, a key test for lipid force-fields is to generate areas per lipid that match experiment.

For bilayer systems, further approximations may be made to increase efficiency. For example, the hydrogen atoms on lipid tails may not be explicitly simulated, but instead the masses and interactions are incorporated into the associated carbon atoms, as in Fig. 2.9b). This "united-atom" representation of the lipid still reproduces bilayer properties. In situations where greater accuracy is needed, "all-atom" representations are used (Fig. 2.9c)) [53].

A simulation may be run to test a structural hypothesis, such as how lipid tail conformation or head group hydration are impacted by a temperature change or a drug. Alternatively, since the postion of atoms and molecules are traced over time, dynamic information is available. One could test the insertion time of a drug in the membrane, or the diffusion of water across the bilayer.

Simulations provide atomistic detail, but are limited in the accessible length and timescales, due to limits on computational resources. Bilayer patches beyond 250 nm^3 are not often used in all-atom simulations, which means that long length-scale phenomena such as bilayer undulations are not measured in all-atom. In addition, it is costly to simulate beyond a few hundred nanoseconds, which means that processes beyond $\sim \mu$s are not easily accessible. An event such as protein insertion can often not be observed. For these reasons, MD simulations can provide complementary information to scattering experiments.

2.4 A Review of Drug Membrane Interactions

Drug-membrane interactions have been a topic of research since the Mayer-Overton experiment. The experiment found a correlation between the potency of anesthetic drugs and their partitioning coefficient in olive oil [54]. The more potent the anesthetic, the more it partitioned into olive oil. This

experiment suggests a link between the hydrophobicity of the drug and its anesthetic action. As the lipid membranes is a ubiquitous hydrophobic interface, this led to speculation that the anesthetics exerted their effect through membrane interactions.

Early molecular hypothesis for this membrane effect suggested that the drug partitioned into the membrane and physically altered the structure. For example, the drug would enter the hydrophobic region and swell the tail volume, and influencing the structure of the membrane and membrane bound ion channels [55]. This theory has largely been discredited, as subtle changes to the drug structure can have large influence on anesthetic effect, suggesting a simple volume effect is not the source [56].

However, modern theories of anesthetic action are reintroducing the membrane as a factor. Anesthetic action is believed to be caused by altered function of membrane bound ion channels. New hypotheses suggest that the drug influences the dynamics of the membrane, as opposed to the structure. Drugs may influence the lateral pressure profile of the membrane: drugs may increase the pressure in the tail and exert pressures on the channel, forcing them closed [57]. Awareness of the potential membrane-effect of anesthetics has created a general interest in studying drug-membrane interactions.

Understanding drug membrane interactions is particularly important for phamacokinetics and pharmacodynamics [2]. Pharmacokinetics is concerned with the movement of drugs within the body. When quantifying kinetics, it is important to understand retention by membranes, as it could influence passage of the drug into the cell. Pharmacodynamics is the "mechanism of action" of a drug. This subject is concerned with how to design drugs that have the intended effect on the body, and minimize potential side effects. When optimizing pharmacokinetics and dynamics, understanding of membrane interactions, and how they correlate with the chemistry and molecular structure of the drug, is necessary during design.

Common techniques are differential scanning calorimetry (DSC) and Langmuir troughs. DSC studies how a drug influences the phase behaviour of a membrane system [17]. To perform this experiment, multilamellar lipid vesicles are prepared in water. They are then slowly heated and the instrument measures the heat necessary to raise the water temperature. Specifically, it measures the differential heat: by recording the slope of the heat *vs* temperature plot. If a first order phase transition occurs, a peak is registered. For example, for DMPC bilayers, a sharp peak is measured at $T = 24°\mathrm{C}$, related to the gel to fluid phase transition (the main transition). Drugs can influence the appearance of this peak by broadening or shifting it. Aspirin is known to broaden and shift the main transition peak in DSC thermograms, as is iron and several other drugs [58, 59, 60]. Broadening the main transition implies reduced collective lipid motion during the transition, whereas shifting it implies reduced energy needed to melt the chains.

Another common drug-membrane probe is a Langmuir trough [2]. This is typically a monolayer experiment: lipids are spread over a bath of highly pure water. Only enough lipid is deposited to create a single layer, where the heads are in the water phase and the tails stick in the air. Next, a physical barrier moves across the surface and reduces the accessible area to the lipids, and a Wilhemy

plate measures the surface pressure of the lipid film. A drug may be dissolved into the lipid film, or it may be dissolved in the water subphase and permitted to interact with the lipids from the subphase. Changes in lipid pressure or compressibility are associated with drug interactions. For example, cholesterol will decrease the pressure at a given area due to its condensing effect, and will also decrease compressibility.

It is difficult to ascertain, based on experiments such as these, the molecular details of the lipid interaction. For example, in a DSC thermogram, lipids partitioning into the heads or tails could disrupt tail ordering and broaden the main transition. Therefore, more nano-scale information is necessary. There are several groups performing Molecular Dynamics simulations of drugs in membranes, and determining the molecular partitioning of the drug [61]. Nuclear magnetic resonance measurements can also give insight on the drug location in the membrane, and relate it to membrane perturbations [2].

Scattering experiments of oriented membranes provide a unique innovation to the field of drug-membrane research. Since the stacked membranes create a repeating unit cell, they permit greater structural resolution, by Fourier reconstruction, yielding a better model for where the molecule partitions into the membrane. Since the membranes are oriented, the in-plane ($q_{||}$) and out-of-plane (q_z) structures scatter along different axis. The two structures can therefore be decoupled. Information on the effect of drugs on membrane bending, phase, area per lipid, lamellar spacing, lipid tilt, and orientational order are all accessible from a single measurement. When combined with MD simulations, as well as bulk experiments such as DSC or Langmuir, the oriented membrane systems can provide rich information into the pharmacokinetic properties of drugs. At the same time, they can provide insight into the mechanism of action for how the drug creates both intended effects and side effects.

Chapter 3

Experimental Methods

3.1 Sample Preparation

The system of choice for the majority of the experiments in this work was oriented, solid-supported bilayers. These bilayers are built bottom-up, such that the composition of the bilayer is easily tuned, adding cholesterol, saturated lipids, etc. Solid-supported bilayers are useful in scattering experiments, as the in-plane and out-of-plane structure of the membranes are decoupled from the scattering signal. All samples are prepared by depositing lipids, that are dissolved in a solvent, onto a silicon wafer. The materials & methods required to prepare the wafers, the lipid solutions, and prepare the oriented membranes will be described below.

3.1.1 Chemicals and Materials

Si substrates

The silicon wafers used for X-ray (and some neutron) scattering were obtained from Silchem

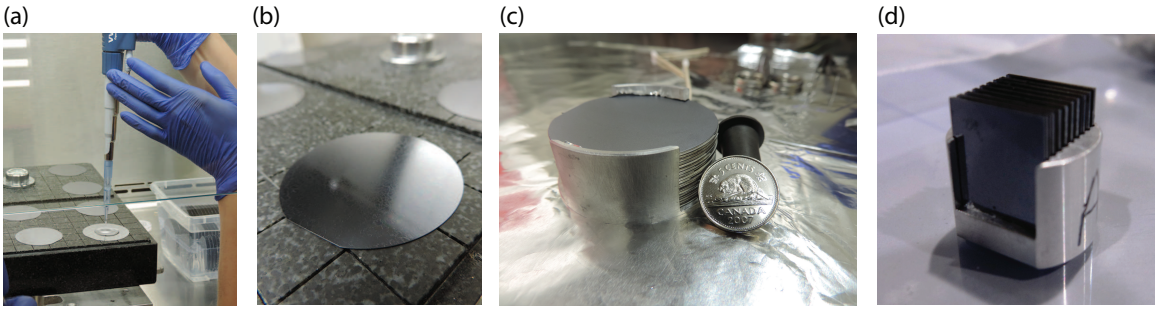

Figure 3.1: Images of preparing oriented lipid membrane samples. a) Depositing lipid solution on 2 inch diameter wafers. b) the solution dried, leaving the lipid film. c) Stacked 2 inch wafers before measurement, in Paper III. d) 1×1 cm^2 wafers in the sample holder designed for experiments on IN12.

and pre-cut into 1 cm × 1 cm or 2 cm × 2 cm chips. In addition, round 2-inch diameter wafers were obtained from WRS Materials and used for some neutron scattering experiments. All wafers used were single-side polished, and cut along the [100] crystal face. The thickness of the wafers was ∼250 μm.

Solvents

A number of organic solvents were used in the process of making oriented bilayers:

- Methanol (CH_3OH): general equipment cleaning as part of the wafer cleaning protocol.
- Dichloromethane (DCM, CH_2Cl_2): used for deep cleaning of the wafers to produce a hydrophobic surface.
- Chloroform ($CHCl_3$): one part of the solution used to dissolve and deposit lipids on the wafers.
- 2,2,2-trifluoroethanol (TFE, $C_2H_3F_3O$): the second part of the wafer solution.
- Ultra-pure water: produced by the Cascade LS Water System with a resistivity of 18.2 MΩ·cm.

All organic solvents Organic solvents were obtained from Sigma Aldrich in HPCL grade..

Molecules

The the molecules in this study can all be classified into phospholipids, cholesterol, and drug molecules.

- *Lipids*: Three types of lipids were used in this thesis. All lipids were acquired from Avanti Polar Lipids and used without further purification. The lipids were packed and shipped with dry-ice and, upon arrival to the lab, were stored in the freezer at -20°C until use. 1,2-dimyristoyl-sn-glycero-3-phosphocholine (DMPC, CAS 18194-24-6) is a 14-carbon saturated phospholipid. 1,2-dipalmitoyl-sn-glycero-3-phosphocholine (DPPC, CAS 63-89-8) is a 16-carbon saturated phospholipid. 1-palmitoyl-2-oleoyl-sn-glycero-3-phosphocholine (POPC, CAS 26853-31-6) is a lipid with a 16-carbon long saturated chain and an 18-carbon monounsaturated chain. Chain-deuterated lipids were also used in the thesis. DMPC-d54 (CAS 78415-49-3) is chemically identical to DMPC, but with every hydrogen on the carbon chains replaced with deuterium. Similarly, DPPC-d62 (CAS 25582-63-2) is chemically identical to DPPC with the chain-hydrogen atoms replaced.
- *Cholesterol*: Cholesterol($C_{27}H_{46}O$, CAS 57-88-5)) was also acquired from Avanti Polar Lipids, transported and stored at -20°C.
- *Molecules*: Four different drug molecules were studied in this thesis. All molecules studied were acquired in powder form
    1. Aspirin (acetylsalicylic acid, ASA, CAS 50-78-2). Chemical formula $C_9H_8O_4$. Acquired from Sigma in powder form and stored at room temperature.
    2. Ibuprofen (chemical formula $C_{13}H_{18}O_2$, CAS 15687-27-1) was acquired from Sigma and stored at room temperature.

3. Cortisone (chemical formula $C_{21}H_{28}O_5$, CAS 53-06-5) was acquired from Sigma and stored at room temperature.
4. Curcumin (trade name turmuric, formula $C_{21}H_{20}O_5$, CAS 458-37-7) was acquired from Sigma and stored at -20°.

3.1.2 Preparation of solid-supported, stacked lipid membranes

Single side polished silicon wafers were first cleaned to prepare the surface for lipid deposition. There were two protocols used to clean wafers that were used for X-ray and neutron scattering experiments, respectively.

1. Preparation of wafters using dichloromethane (DCM). This procedure was used to prepare 1 cm × 1 cm or 2 cm × 2 cm wafers. Wafers were placed in a glass dish and covered with DCM. The dish was sealed with a glass top (and secured with parafilm) and placed in a bath sonicator (Branson 2510) that was filled with ultra-pure water heated to 37°C. The wafers were sonicated for 25 minutes. Following sonication, the wafers were removed from DCM and rinsed three times with ∼50 mL ultra-pure water and methanol. The wafers were then dried and lipid solution was deposited, or the wafers were stored in fresh methanol for use later that day.

2. Preparation of wafers using water and methanol. This procedure was used for the circular, 5 inch diameter wafers. Initially, the wafers were placed in a plastic container and filled with ultrapure water. The container was then placed in the sonicator (also filled with ultrapure water) and allowed to equilibrate to 37°C, then sonicated for 12 min. The process was repeated with methanol, then repeated again each for water and methanol. Following the final methanol cleaning, the wafers were dried under N_2 and lipid solution was deposited.

Lipid were weighted with a micro-balance (Ohause Discovery) and mixed with a 1:1 solution of chloroform and trifluoroethanol (TFE). Cholesterol and drug molecules were also weighed and dissolved in chloroform:TFE mixtures. The different solutions were then combined to achieve the desired molecular concentrations, to a total mass concentration of 20 mg/mL.

Dried wafers were then placed on a level granite block. To ensure that the lipids are deposited in their fluid phase, the granite block and wafers are heated well above the transition temperature of the lipid. For example, when DPPC is deposited the wafers are heated to 50°C (10°C above the main transition). The lipid solution is then deposited. Depending on the size of the wafers, slightly different procedures are followed:

1. For square wafers, 80 μL of lipid solution is placed on the wafer. The wafers and granite block are on a rotating platform (VWR Rotating Wave) to ensure even coverage of lipid solution.

2. For the circular, 5 inch diameter wafers, 1.2 mL are deposited. The granite block is then lifted and gently rocked until the solution is evaporated.

After the lipid solution has evaporated, the samples are placed in vacuum overnight.

Next, the samples are hydrated. Hydration is required to anneal the lipids on the wafer into bilayers. They are placed in a sealed vial with a beaker of pure water. The sealed container is placed in an incubater at a temperature high enough to put the lipids in the fluid phase. The membranes are hydrated for at least 24 hours.

For X-ray analysis, the wafers are now ready for measurement as a single prepared wafer was sufficient. Neutron flux at reactor sources is significantly lower than even laboratory X-ray sources, so several wafers were required for neutron scattering and the wafers must be packed into sample cans specially designed for the specific neutron instrument. In the paper *Aspirin Inhibits Formation of Cholesterol Rafts in Fluid Lipid Membranes*, 20 prepared 5 inch wafers were stacked into an aluminum can. Each wafer was separated by 100 μm thick aluminum spacers (Fig. 3.1c)). For the paper *Aspirin Locally Disrupts the Liquid Ordered Phase*, 20 1×1 cm^2 wafers were placed vertically into a container (Fig. 3.1d)).

3.2 Protocols for Scattering Experiments

3.2.1 X-ray Experiments

All X-ray scattering data were obtained using the Rigaku SmartLab X-ray diffractometer within the Laboratory for Membrane and Protein Dynamics at McMaster University. This diffractometer is referred to as the Biological Large Angle Diffraction Experiment (BLADE), see Fig. 3.2. X-rays are generated using a rotating anode that uses a 9 kW (45 kV, 200 mA) of power to generate X-rays peaked at a 1.5418 Å wavelength (CuKα). The rotating anode X-ray generator is a vacuum sealed enclosure in which electrons are ejected from a high-voltage filament, by thermionic emission, and travel toward a copper target. The target is rotating and also water-cooled in order to dissipate heat over a large area, thus ensuring a consistent X-ray flux.

When electrons from the filament strike the copper target, they cause electrons in the K-shell to be ejected. Electrons in outer shells then relax to fill the inner shell, releasing radiation in the process. The copper $K\alpha$ emission is selected and guided to the sample by the Rigaku optics [62]. BLADE's beam geometry provides intensities of up to 10^{10} counts/(mm^2·s), this high-intensity illumination of the samples ensures a high scattering signal. The sample is stationary on a flat sample stage, and the source and detector move. The source and detector move along an angle perpindicular the normal of the stage, θ. The detector is also capable of swinging into the sample plane and measuring scattering at an angle θ_χ. BLADE samples θ and θ_χ to form a 2-dimensional scattering image, Fig. 3.2b).

Information from the measurement of the out-of-plane Bragg peaks from the membrane stacks allows the determination of a density profile perpendicular to the plane of the membranes. With X-ray scattering we determine the electron density profile, whereas for neutron scattering we determine a scattering length density profile. The Fourier transform in this case is discrete due to the convolution with the lamellar structure factor. The integrated intensities of the out-of-plane Bragg

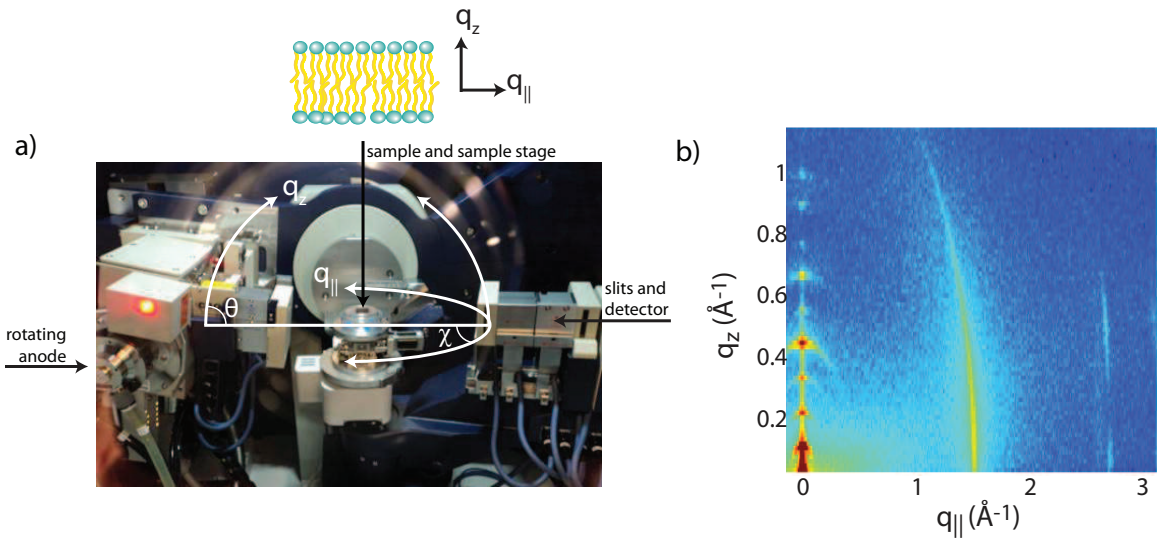

Figure 3.2: Image of the X-ray diffraction setup. a) A photograph of inside BLADE, with arrows indicating the relevant axis. b) A 2-dimensional X-ray diffraction image of oriented membrane stacks acquired by BLADE. A single lipid peak is observed in-plane ($q_{||}$) and a set of Bragg peaks are observed in the out-of-plane axis (q_z).

peaks are simply the Fourier components. We use one-dimensional Fourier analysis to approximate the electron density, $\rho(z)$,

$$\begin{aligned}\rho(z) &= \rho_W + \frac{F(0)}{d_z} + \frac{2}{d_z}\sum_{n=1}^{N} F(q_n)\nu_n \cos(q_n z) \\ &= \rho_W + \frac{F(0)}{d_z} + \frac{2}{d_z}\sum_{n=1}^{N} \sqrt{I_n q_n}\nu_n \cos\left(\frac{2\pi n z}{d_z}\right),\end{aligned} \tag{3.1}$$

where N is the highest order of observed Bragg peaks and ρ_W the electron density of water (or other solvent) [45]. I_n are the integrated peak intensities, which are combined with the q_z value at which the peak occurs, q_n, to obtain the form factors, $F(q_n)$. The membrane form factor $F(q_z)$, is in general a complex quantity, however, in this case it is real-valued due to centro-symmetry. Therefore, the phase problem of crystallography simplifies to the sign problem: $F(q_z) = \nu_n|F(q_z)|$. A given phase can only take on two values, $\nu_n = \pm 1$. By measuring the bilayer form factor F(q_z) at several q_z values, we can construct a related, continuous function, T(q_z),

$$T(q_z) = \sum_n \sqrt{I_n q_n} sinc\left(\frac{1}{2} d_z q_z - \pi n\right), \tag{3.2}$$

which can be fit using the data [63]. Fitting the Bragg peak intensities from the data allows for an analytical expression of $T(q_z)$, from which the phases, ν_n can be assessed. Electron density profiles are calculated and used in Papers I, IV, V, VI.

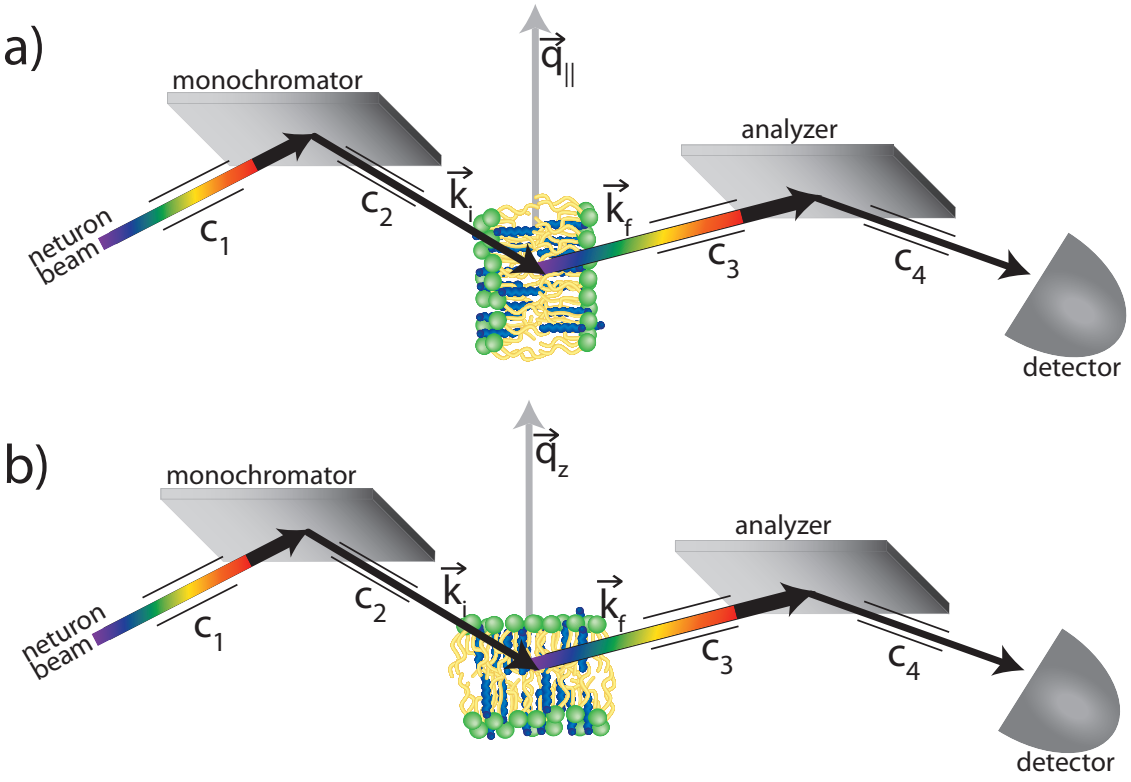

Figure 3.3: A diagram illustrating the operation of a triple axis spectrometer measuring a) in-plane ($q_{||}$) and b) out-of-plane (q_z) scattering.

3.2.2 Neutron Scattering Experiments

Two of the papers included in this these contain neutron data. Both of these experiments were performed using triple-axis spectrometers (TAS) at reactor sources. Paper II used the N5 spectrometer at the Canadian Neutron Beam Centre and Paper III used the IN12 spectrometer at the Institut Laue-Langevin (ILL). Neutrons arrive from the core of the reactor with a distribution of wavelengths. The neutrons are incident on a polylytic graphite (PG). Using Bragg's law (Eq. 2.4), a monochromatic beam with momentum $\vec{k_i}$ is scattered from the crystal and incident on the sample. After scattering from the sample, the neutrons are incident on a second PG crystal to select neutrons with momentum $\vec{k_f}$ that are then guided to a detector (Fig. 3.3).

$\vec{k_i}$ and $\vec{k_f}$ can therefore be independently varied, and $\hbar\omega = \frac{\hbar^2}{2m_n}(k_i - k_f)^2$. The angle between $\vec{k_i}$ and $\vec{k_f}$ is the scattering angle θ. The triple-axis measures $S(\vec{Q}, \hbar\omega)$ by either holding $\vec{Q}$ constant and varying $\hbar\omega$ (constant-Q scans) or by holding $\hbar\omega$ fixed and varying $\vec{Q}$ (constant-energy).

The third axis of the spectrometer is the sample axis. Membranes are mounted vertically on the spectrometer, such that the scattering vector can be rotated from in-plane ($q_{||}$) to out-of-plane (q_z) by rotating the sample by 90° as illustrated in Fig. 3.3.

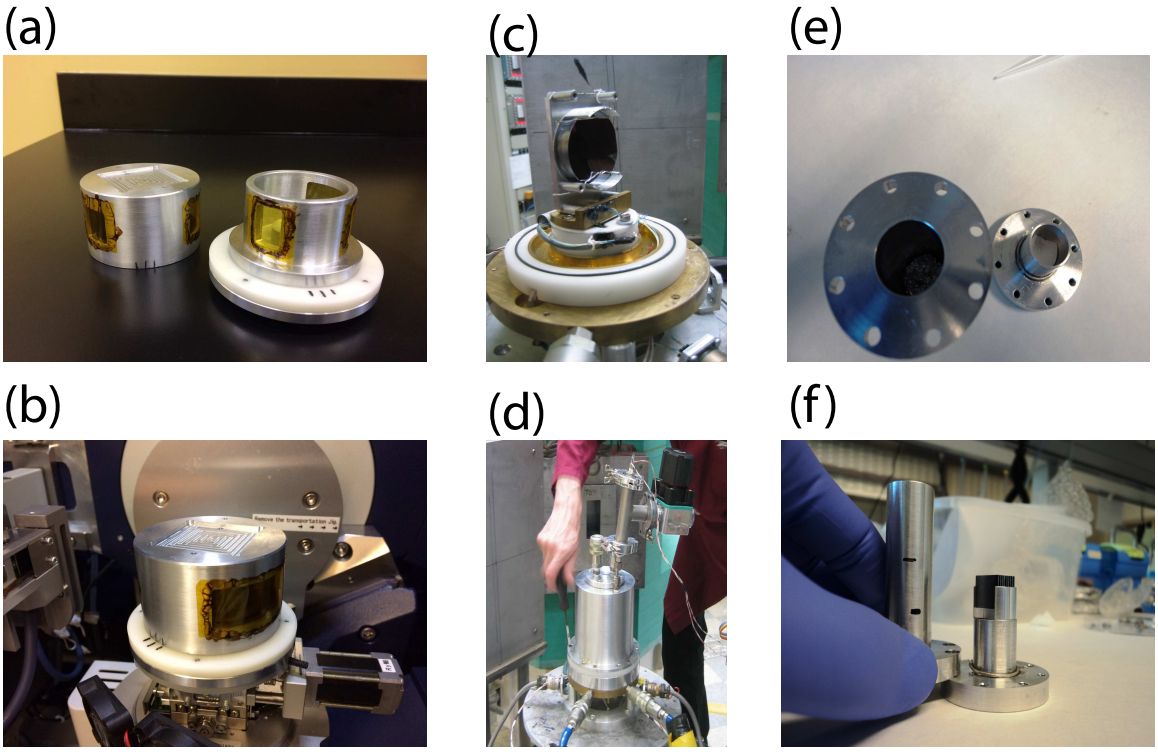

Figure 3.4: Pictures of the various hydration chambers used for the scattering experiments. a) The double-walled chamber, with yellow kapton windows, used on BLADE. b) The X-ray chamber assembled and placed on BLADE. c) The windowless chamber used at N5 for Paper II. The wafers are mounted vertically and suspended. d) Securing the lid of the chamber on N5. e) An overhead view of the sample chamber for IN12, showing the presence of filter paper at the bottom that is designed to capture D_2O. f) The wafers placed on the chamber (filter paper is below the wafers), and the lid about to be placed on top.

3.2.3 Hydration Chambers for Scattering Experiments

Temperature and humidity controlled chambers are required to perform scattering experiments on supported membranes under different conditions. Typically, the goal of these chambers is to achieve 100% relative humidity in the atmosphere of the chamber. In order to maintain this humidity, temperature gradients inside the chamber need to be eliminated, otherwise rapid loss of humidity will be caused by condensation. Thermoelectric heating at multiple locations in the chamber is necessary to set the temperature evenly over the chamber. The design principles associated with chambers for X-ray and neutron scattering are significantly different.

The primary material used for the chambers is aluminum. X-rays cannot penetrate aluminum, so windows are required to permit X-rays to enter into and scatter out of the chamber and to the detector. The material used for the window is kapton, a polymeric material that is fabricated into sheets 13 μm thick, in order to minimize X-ray attenuation. The chamber used inside BLADE contains a trough for water at the base. The sample is placed on the central stage and a lid with

the windows is placed on top, creating a tight seal. Temperature control is not used in BLADE, as the ambient temperature in the machine is 28°C which is above the melting temperature for both DMPC and POPC: the lipids measured on BLADE for this thesis. Images of the chamber are shown in Fig. 3.4a)-b).

Neutrons are in fact able to penetrate even cm thick aluminum walls, which means that humidity chambers for neutron scattering do not require special windows, as can be seen in Fig. 3.4c)-d). For *Aspirin Locally Disrupts the Liquid Ordered Phase*, the wafers were suspended above a trough of water. The water trough was heated by an external water bath, and the chamber walls and roof are heated by separate Peliter elements, to remove gradients. However, a different setup is used for the *Aspirin Locally Disrupts the Liquid Ordered Phase* experiment. The 1×1 cm^2 wafers are placed in a sealed vessel (Fig. 3.4e)-f)) with a damp filter paper prepared with enough water to achieve full hydration. Temperature is then controlled with an orange crystat.

3.3 Molecular Dynamics Simulations

Simulations were mostly run in-house on MacSim, a GPU accelerated workstation with 20 physical Intel XeonCPU cores and two GeForce GTX 1080 high power graphics cards resulting in 5120 CUDA Cores. This system produces 50-180 ns of MD simulations in standard 128 lipid membrane patches in GROMACS per day (B24 h), depending on the system in question. The exception is *Paper V: The Lipid Bilayer Provides a Site for Cortisone Crystallization at High Cortisone Concentrations*, where simulations were performed by Jochen Hub.

The GROMACS (GROningen Machine for Chemical Simulations) software was used [49]. Forcefields are downloaded and used un-altered. Two force fields were used in this thesis: the SLipids forcefields was used for the Paper V [64], while GROMOS 54a7 forcefield was used for the other works [65]. Simulations are generally run with 128 lipids in a bilayer patch (64 per leaflet), and a variable number of water molecules per lipid.

The forcefield parameters identify the interactions between atoms that are bonded, non-bonded, the interaction parameters for torsional bond rotation, etc. However, to use a molecule in the simulation, the forcefield needs to be able to identify atomic groups to assign interaction parameters to. These "topology" files are typically built by leading groups such as the Tieleman group and made freely available for download. All-atom POPC molecules were used with the SLipids forcefield in Paper V, while united atom DMPC molecules were used for the others. Drug molecules, such as aspirin, cortisone, and curcumin, also require topology files. These are built either using the Generalized Amber Force Field, or downloaded from online repositories such as the Automatic Topology Builder [50].

Before performing simulations for analysis (denoted production runs), a three stage equilibration protocol is performed. . First of all, an energy minimization step is run that removes extreme forces within the system. This is performed by conducting simulations at zero temperature, and minimizing the total force on all atoms. Secondly, a simulation is run at constant volume to ensure the system

achieves the designed temperature. After the equilibration, the thermodynamic parameters of the system, such as temperature and pressure, should no longer depend on simulation time. This typically requires 500 ps of simulation. Lastly, a simulation is run at constant pressure to ensure that the pressure is stabilized, typically taking 1 ns. Finally, production runs typically ran for 200 ns.

Chapter 4

Aspirin Impacts Local Membrane Structure and Function: Publications I, II, & III

Many drug molecules, similar to lipid membranes, are amphiphilic. They will embed in the membrane to satisfy both hydrophilic and hydrophobic interactions. In addition, charge or hydrogen bonding interactions will attract drugs to the bilayer [2]. There are a variety of possible responses to the drug binding the membrane: it could increase the lipid fluidity, it could tighten the lipid much like cholesterol, or it could cause increased curvature. This information is available from various experimental techniques, including fluorescence techniques, and NMR [2]. However, as outlined in Section 2, key events for the membrane happen on small length and timescales. How could a drug influence ephemeral phenomena such as raft formation and structure, for example? Molecular level techniques are required to ellucidate these effects.

In this thesis, to start answering those questions, a case study of aspirin was performed. Aspirin (chemical name acetylsalicylic acid, ASA) is a common analgesic that has been on the market for over 100 years. Salicylic acid, from which Aspirin is derived, is found in willow trees, and extract or tea made from these trees had been used to cure pain or fever [66]. Bayer trademarked Aspirin in 1899 but the rights to name expired and aspirin is now a trade name. It is still widely used for treating pain or fever. The main mechanism for curing pain was discovered in 1962: aspirin binds to cyclo-oxygenase (COX) and inhibits the production of prostaglandins [67].

In recent decades, aspirin has also been used as a secondary measure in the prevention of heart attacks for patients with high cholesterol [68]. Some evidence suggests the COX inhibition is the reason for a benefit for high cholesterol [69]. However, this is not the whole story, as, for example, patients who are "aspirin resistant" (they don't see any benefit from aspirin therapy) experience COX inhibition [70]. Our hypothesis was that aspirin in fact influenced cholesterol by interacting with lipids membranes.

We therefore prepared oriented membranes with high cholesterol, as well as aspirin, and studied the systems using X-ray and neutron scattering. Over three papers, we determined that aspirin has a clear effect on membranes with cholesterol. In particular we learned that aspirin creates local distortions in the membrane, local changes in the area per lipid, and frustrates cholesterol organization. This effect appears to eliminate plaques, and also causes increased solubility for cholesterol in membranes. At high concentrations, cholesterol leaves the membrane and forms immiscible cholesterol crystals. These "plaques" then aggregate outside the membrane and cause blocked arteries [44]. Our conclusion that aspirin homogenizes membranes, increasing cholesterol solubility, may explain the so-called Low Dose Aspirin Therapy.

A key insight from these experiments is that the effect of aspirin on the ℓ_o phase is distinctly local. This means that aspirin does not require a critical threshold to produce effect. Even though the experiments discussed sometimes use physiologically unrealistic drug concentrations, small concentrations of the drug influence the membrane structure.

4.1 Paper I: Acetylsalicylic Acid (ASA) Increases the Solubility of Cholesterol When Incorporated in Lipid Membranes

Richard J. Alsop, Matthew A. Barrett, Songbo Zheng, Hannah Dies, Maikel C. Rheinstädter. (2014). *Acetylsalicylic Acid (ASA) Increases the Solubility of Cholesterol When Incorporated in Lipid Membranes.* Soft Matter. 10(24), 4275-4286.

4.1.1 Preface to Paper I

This was the first test of both aspirin and high cholesterol in the same membrane. Our choice of experimental system is DMPC in the gel phase. While the gel phase is not generally considered the most physiologically relevant phase, by suppressing fluctuations associated with the fluid phase, a greater number of Bragg peaks are available for structure refinement.

We prepared membranes with cholesterol concentrations of up to 40 mol%. Cholesterol concentrations in human plasma membranes vary from 30-50%, but in our gel-phase DMPC systems, 40 mol% is already above the the solubility threshold, causing cholesterol to leave the membrane and form cholesterol plaques [44].

The evidence for plaques is present in both measurements along q_z and along $q_{||}$. Along q_z, a homogenous lamellar membrane diffracts evenly spaced Bragg peaks. At high cholesterol concentrations, however, extra peaks exist between the lamaller peaks. Indexing these peaks reveals a spacing of $\sim$34 Å, which is the thickness of two cholesterol molecules stacked. Along $q_{||}$, peaks appear that are indexed to a unit cell in agreement with crystalline cholesterol. The high cholesterol data, therefore, point to cholesterol crystals that coexist with the lamellar membrane. We then added aspirin

to the membranes. We used an electron density analysis to show that aspirin sits in the lipid head groups, at $|z| \sim 20$ Å from the membrane core. Aspirin also decreases d_z and increases A_L.

The most relevant result, however, is that it causes the volume fraction of the cholesterol plaques to decrease. This was measured by integrating the in-plane cholesterol peaks and normalizing by the lipid peaks. At 10 mol% aspirin, there is zero evidence for plaques and that is also true at 12.5 mol%. This result is best explained by increased lipid area, allowing more cholesterol to incorporate into the membrane. The experiment provided the first piece of evidence that aspirin, by increasing the area per lipid, actually influences the formation of cholesterol structures. The position of the plaque peaks did not change, meaning the structure was not affected. Instead, we related the intensity of the peaks to the volume of the plaques.

Author Contributions:

- *Experimental Concept:* Maikel Rheinstädter
- *Sample Preparation:* Richard Alsop, Matthew Barrett, Songbo Zheng
- *X-ray diffraction Experiments:* Richard Alsop, Songbo Zheng, Maikel Rheinstädter
- *Data Analysis:* Richard Alsop, Hannah Dies, Maikel Rheinstädter
- *Manuscript Preparation:* Richard Alsop, Maikel Rheinstädter

Soft Matter

PAPER

Acetylsalicylic acid (ASA) increases the solubility of cholesterol when incorporated in lipid membranes

Cite this: *Soft Matter*, 2014, **10**, 4275

Richard J. Alsop,[a] Matthew A. Barrett,[a] Songbo Zheng,[a] Hannah Dies[a] and Maikel C. Rheinstädter*[ab]

Received 16th February 2014
Accepted 8th April 2014

DOI: 10.1039/c4sm00372a

www.rsc.org/softmatter

Cholesterol has been well established as a mediator of cell membrane fluidity. By interacting with lipid tails, cholesterol causes the membrane tails to be constrained thereby reducing membrane fluidity, well known as the condensation effect. Acetylsalicylic acid (ASA), the main ingredient in aspirin, has recently been shown to increase fluidity in lipid bilayers by primarily interacting with lipid head groups. We used high-resolution X-ray diffraction to study both ASA and cholesterol coexisting in model membranes of dimyristoylphosphatidylcholine (DMPC). While a high cholesterol concentration of 40 mol% cholesterol leads to the formation of immiscible cholesterol bilayers, as was reported previously, increasing the amount of ASA in the membranes between 0 to 12.5 mol% was found to significantly increase the fluidity of the bilayers and dissolve the cholesterol plaques. We, therefore, present experimental evidence for an interaction between cholesterol and ASA on the level of the cell membrane at elevated levels of cholesterol and ASA.

1. Introduction

The biological membrane is a complex structure, composed of various lipid species, sterols, proteins, and other small molecules. An important consequence arising from the complexity of the structure is fluidity.[1–3] By being fluid, the structure allows for fast diffusion of small molecules and lateral diffusion of membrane proteins.[4] The fluidity of a membrane also determines its bending modulus, and ability to form pores.[5,6] Cholesterol, with its stiff hydrocarbon ring structure, is known to increase membrane rigidity acting as a physiological mediator of membrane fluidity. The liquid-ordered (l_o) phase, which is observed at high concentrations of cholesterol,[7] was reported to combine the properties of gel and fluid phases, in other words, it is as well ordered as the gel phase, but 'softer' than the fluid phase,[8,9] with smaller viscosity and restoring forces. In addition, cholesterol is speculated to be un-evenly distributed in the membrane. Regions with high cholesterol among a larger membrane are labeled lipid rafts,[10] which are often implicated in cell signalling and neuro-transmission, among other roles.[10–21]

However, a high concentration of cholesterol causes a disadvantageous decrease in fluidity and a change in homeostasis, leading to reduced health of the individual. Possible effects of high cholesterol include high blood pressure and hypertension. As well, high cholesterol serves as a risk factor for myocardial infarctions. Biochemical and physiological studies have allowed for the discovery of many pharmaceuticals to specifically lower cholesterol levels, along with medications to reduce the symptoms and effects of high cholesterol. A common treatment for the primary and secondary prevention of myocardial events, in patients with high cholesterol, is the daily intake of the analgesic aspirin (acetylsalicylic acid, ASA) as part of a regimen known as low-dose aspirin therapy.[22–24]

Despite progress in the treatment of high cholesterol, explaining and mitigating the adverse effects of cholesterol is still a rich area. In particular, the field of membrane biophysics has proven effective in explaining and quantifying the effects of cholesterol in the context of model membrane systems. X-Ray and neutron scattering experiments have been able to probe the position of cholesterol within the membrane and quantify and understand the effects of cholesterol.[3,8,9,25–35] The hydrophobic cholesterol molecule partitions itself in the hydrophobic membrane core. In saturated lipid bilayers, the cholesterol molecules are known to align parallel to the lipid acyl chains, well known as the umbrella model.[34,36] In the umbrella model each lipid molecule is associated with two cholesterol molecules, which cause the membrane tails to be constrained, suppress lipid tail fluctuations thereby increasing membrane thickness and reducing membrane fluidity. The lipid head group is thought to act as an 'umbrella', which protects the hydrophobic part of the cholesterol molecules from the aqueous environment. In highly unsaturated membranes, cholesterol was found to reside also in the centre of the membranes.[28,37] Small, transient cholesterol domains at physiological cholesterol levels were recently reported from computer simulations[38] and experiments.[35] At high

[a]*Department of Physics and Astronomy, McMaster University, Hamilton, ON, Canada*
[b]*Canadian Neutron Beam Centre, National Research Council Canada, Chalk River, ON, Canada. E-mail: rheinstadter@mcmaster.ca*

concentrations of cholesterol, above ~40 mol%, immiscible cholesterol bilayers may form spontaneously.[39–45]

Aspirin and other non-steroidal anti-inflammatory drugs (NSAID's) are able to interact with lipid membranes leading to increased bending ability and pore formation in real and model membranes.[47–49] ASA was found to incorporate in lipid membranes and to primarily interact with the head groups, increasing lipid fluidity.[46] However, given the opposing effects of ASA and cholesterol in the membrane, a direct interaction has never been investigated.

We investigated DMPC membranes containing varied amounts of cholesterol and ASA using high-resolution X-ray diffraction. Lamellar stacks of bilayers containing ASA, cholesterol, and the saturated phospholipid dimyristoylphosphocholine (DMPC) were prepared. Samples contained up to 12.5 mol% ASA and 40 mol% cholesterol. We used 2-dimensional X-ray diffraction, covering large areas of reciprocal space, to probe the in-plane and out-of-plane structure of the membranes in their liquid-ordered phase. We find experimental evidence for an interaction between cholesterol and ASA in model membranes.

2. Materials and methods

2.1. Preparation of the highly-oriented multi-lamellar membrane samples

Highly oriented multi lamellar membranes were prepared on single-side polished silicon wafers. 100 mm diameter, 300 μm thick silicon (100) wafers were pre-cut into 2 × 2 cm^2 chips. 1,2-dimyristoyl-*sn-glycero*-3-phosphocholine (DMPC, $C_{36}H_{72}NO_8P$), acetylsalicylic acid (ASA, $C_9H_8O_4$) and cholesterol ($C_{27}H_{46}O$), as depicted in Fig. 1a, were mixed in different ratios and dissolved in a 1 : 1 chloroform–2,2,2-trifluoroethanol (TFE) solution at a concentration of 15 mg mL^{-1}.

The lipid solution did not spread well on ultrasonic-cleaned wafers and de-wetted during drying. The silicon substrates were, therefore, cleaned in a piranha acid solution made of 98% concentrated H_2SO_4 and 30% concentrated H_2O_2 at a ratio of 3 : 1 by volume. Wafers were placed in this solution, covered with parafilm and kept at 298 K for 30 minutes. This treatment removes all organic contamination and leaves the substrates in a hydrophilic state. The 1 : 1 mix of chloroform–TFE, which was used to dissolve lipids and chloroform, is a non-polar solvent. In order for the solvent to spread well and cover the substrate uniformly, the silicon wafers were made hydrophobic to match the solvent properties. We used silanization to cover the silicon surface through self-assembly with organo-functional alkoxysilane molecules (APTES). The organic part of the APTES molecules was found to provide a perfect hydrophobic interface for the formation of the biological tissue.[39,46]

A 1% (by volume) solution of APTES and 99% ethanol was prepared. A 1 mL syringe was filled with 0.2 mL of dry nitrogen. This nitrogen was ejected into 99% APTES, and 0.2 mL of APTES was drawn into the syringe. This syringe is then submerged in 19.8 mL of ethanol before ejecting the APTES. The wafers were immersed in the APTES solution and covered with parafilm, kept at 298 K and placed on a tilting incubator (20 speed, 3 tilt) for 12 hours. The tilting incubator creates a circular flow in the beaker to ensure an even APTES distribution and prevent buildup on the surface of the wafers. The wafers were then placed in a clean Pyrex dish and annealed in vacuum at 388 K for 3 hours to create a uniform coverage of the APTES molecules on the surface.[50]

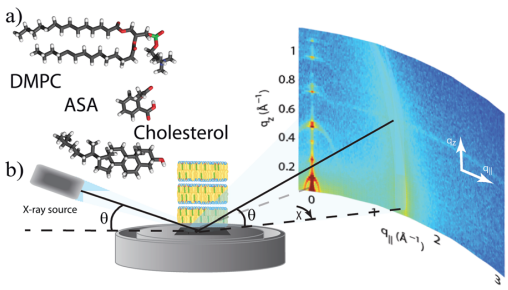

Fig. 1 (a) Lipid, ASA and cholesterol molecule. (b) Schematic diagram of the X-ray scattering experiment. The in-plane and out-of-plane structure of the membranes was determined from 2-dimensional intensity maps. Highly oriented multi lamellar membranes were prepared. 2θ and $2\theta_x$ are the out-of-plane respective in-plane diffraction angles.

Each wafer was thoroughly rinsed three times by alternating with ~50 mL of ultra pure water and methanol. The methanol was cleaned using a 0.2 μm filter before use to avoid surface contamination. The tilting incubator was heated to 313 K and the lipid solution was placed inside to equilibrate. The wafers were rinsed in methanol, dried with nitrogen gas and placed in the incubator. 200 μL of lipid solution was applied on each wafer and the wafers were covered with a Petri dish to let the solvent evaporate slowly during a period of ~15 minutes. The slow drying allows time for the lamellar membranes to form on the substrate. Wafers were tilted during the drying process for 30 minutes (speed 15, tilt 1) such that the lipid solution spread evenly on the wafers.

After drying, the samples were placed in vacuum at 313 K for 12 hours to remove all traces of the solvent. The bilayers were annealed and rehydrated before use in a saturated K_2SO_4 solution which provides ~98% relative humidity (RH). The hydration container was allowed to equilibrate at 293 K in an incubator. The temperature of the incubator was then increased gradually from 293 K to 303 K over a period of ~5 hours to slowly anneal the multi lamellar structure.

This procedure results in highly oriented multi lamellar membrane stacks and a uniform coverage of the silicon substrates. About 3000 highly oriented stacked membranes with a total thickness of ~10 μm are produced using this protocol. The samples were stored in a refrigerator at 5 °C and heated to 55 °C for 1 h before scanning to erase a possible thermal history. This procedure in particular destroys possible crystalline L_C or sub-gel phases that may form during storage at low temperatures and low hydration.[51]

The high sample quality and high degree of order is a prerequisite to determine the in-plane structure of the membranes and the arrangement of cholesterol and ASA molecules. Table 1 lists all samples prepared for this study.

2.2. X-ray scattering experiment

X-ray diffraction data was obtained using the Biological Large Angle Diffraction Experiment (BLADE) in the Laboratory for Membrane and Protein Dynamics at McMaster University. BLADE uses a 9 kW (45 kV, 200 mA) CuKα rotating anode at a wavelength of 1.5418 Å. Both source and detector are mounted on movable arms such that the membranes stay horizontal during the measurements. Focussing multi-layer optics provides a high intensity parallel beam with monochromatic X-ray intensities up to 10^{10} counts per (s × mm^2). This beam geometry provides optimal illumination of the solid supported membrane samples to maximize the scattering signal.

A sketch of the scattering geometry is shown in Fig. 1b). By using highly oriented membrane stacks, the lateral in-plane ($q_\parallel$) and out-of-plane (q_z) structure of the membranes could be determined with sub-nanometer resolution. A point detector was used in combination with slits and collimators in front and after the samples to optimize the signal-to-noise-ratio. The detector was moved along a spherical surface around the sample, as defined by the two angles 2θ and $2\theta_\chi$. The result of such an X-ray experiment is a 2-dimensional intensity map of a large area ($0.03\ \text{Å}^{-1} < q_z < 1.1\ \text{Å}^{-1}$ and $0\ \text{Å}^{-1} < q_\parallel < 3.1\ \text{Å}^{-1}$) of the reciprocal space, as sketched in Fig. 1b. This information was used to develop the molecular structure of the membrane samples.

All scans were measured at 20 °C and 50% RH, in the gel phase of the bilayers.[52,53] Fully hydrated liquid-crystalline samples are generally assumed to best mimic physiologically relevant conditions.[54,31] However, these disordered bilayers do not diffract well (*i.e.* give rise to a limited number of quasi-Bragg peaks), and as such do not lend themselves ideally to traditional crystallographic analysis. In order to obtain high resolution diffraction data, the membranes in this study were measured below the gel–fluid transition temperature of $T = 296.6$ K in multi-lamellar DMPC systems[55,56] and at a reduced hydration. As high resolution structural data are needed to determine the location of the different molecular components, this protocol permits the measurement of high order Bragg peaks, and thereby achieve a high spatial resolution, as demonstrated by Hristova and White.[57] Consequently, the membranes were in their gel (L_β) phase.[33,52,53] All conclusions drawn, therefore, refer to this phase state of the system.

2.3. The calculation of electron densities

The out-of-plane structure of the membranes was determined using specular reflectivity, see, for instance ref. 31 and 54 for recent reviews. The electron density, $\rho(z)$, is approximated by a 1-dimensional Fourier analysis:[58]

$$\rho(z) = \rho_W + \frac{F(0)}{d_z} + \frac{2}{d_z}\sum_{n=1}^{N} F(q_n)\nu_n \cos(q_n z)$$
$$= \rho_W + \frac{F(0)}{d_z} + \frac{2}{d_z}\sum_{n=1}^{N} \sqrt{I_n q_n}\nu_n \cos\left(\frac{2\pi n z}{d_z}\right). \quad (1)$$

Table 1 List of all the samples prepared for this study and their molecular composition. Unit cell dimensions, area per lipid and cholesterol molecules and the lamellar spacings for lipid and cholesterol bilayers (d_z^{lipid} and d_z^{chol}) are given. See text for details

Sample	DMPC (mol%)	cholesterol (mol%)	ASA (mol%)	Unit cell	Area per lipid (Å^2)	d_z^{lipid} (Å)	Area per cholesterol (Å^2)	d_z^{chol} (Å)
1	100	0	0	Head groups: $a_H = 8.77$ Å, $b_H = 9.31$ Å, $\gamma_H = 90°$; Lipid tails: $a_T = 4.97$ Å, $b_T = 8.25$ Å, $\gamma_T = 94.18°$	40.84 ± 0.1	52.6 ± 0.1	—	—
2	80	20	0	$a_T = 5.03$ Å, $\gamma_H = 120°$	44 ± 1	50.1 ± 0.1	—	—
3	70	30	0	$a_T = 5.12$ Å, $\gamma_H = 120°$	45.2 ± 2	50.5 ± 0.1	—	—
4	60	40	0	Lipid tails: $a_T = 4.48$ Å, $\gamma_T = 120°$; Chol monoclinic: $a = 10.70$ Å, $b = 8.60$ Å, $\gamma = 103.0°$	34.8 ± 0.1	50.9 ± 0.1	44.83 ± 0.1	32.5 ± 0.3
5	95	0	5	$a_T = 4.86$ Å, $\gamma_H = 120°$	41 ± 1	55.3	—	—
6	80	15	5	$a_T = 4.90$ Å, $\gamma_H = 120°$	41.6 ± 1	49.1	—	—
7	65	30	5	$a_T = 5.10$ Å, $\gamma_H = 120°$	45.2 ± 1.5	48.89	—	—
8	55	40	5	Lipid tails: $a_T = 4.45$ Å, $\gamma_T = 120°$; Chol monoclinic: $a = 10.37$ Å, $b = 8.4$ Å, $\gamma = 103.0°$	34.2 ± 0.5	43.8 ± 0.3	42.44 ± 0.1	34.3 ± 0.1
9	90	0	10	$a_T = 4.86$ Å, $\gamma_H = 120°$	41 ± 1	53	—	—
10	75	15	10	$a_T = 4.91$ Å, $\gamma_H = 120°$	42 ± 1.5	51.55	—	—
11	60	30	10	$a_T = 5.06$ Å, $\gamma_H = 120°$	45.2 ± 2	44.5	—	—
12	50	40	10	Lipid tails: $a_T = 4.58$ Å, $\gamma_T = 120°$; Chol monoclinic: $a = 10.4$ Å, $b = 8.27$ Å, $\gamma = 103.0°$	36.3 ± 0.1	44.4 ± 0.1	42.0 ± 0.1	34.4 ± 1.7
13	62.5	30	7.5	$a_T = 5.15$ Å, $\gamma_H = 120°$	45.9 ± 1.5	50	—	—
14	57.5	30	12.5	$a_T = 5.18$ Å, $\gamma_H = 120°$	46.5 ± 1.5	50	—	—
15	52.5	40	7.5	Lipid tails: $a_T = 4.62$ Å, $\gamma_T = 120°$; Chol monoclinic: $a = 10.64$ Å, $b = 8.4$ Å, $\gamma = 103.0°$	37.0 ± 0.1	43.1 ± 0.1	43.5 ± 0.1	34.2 ± 0.1
16	47.5	40	12.5	Lipid tails: $a_T = 4.83$ Å, $\gamma_T = 120°$	40.5 ± 0.1	41.8 ± 0.5	—	34.11 ± 0.1

N is the highest order of the Bragg peaks observed in the experiment and ρ_W the electron density of bulk water. The integrated peak intensities, I_n, are multiplied by q_n to receive the form factors, $F(q_n)$.[59,60] The bilayer form factor F(q_z), which is in general a complex quantity, is real-valued in the case of centrosymmetry. The phase problem of crystallography, therefore, simplifies to the sign problem $F(q_z) = \pm |F(q_z)|$ and the phases, ν_n, can only take the values ± 1. The phases ν_n are needed to reconstruct the electron density profile from the scattering data following eqn (1). When the membrane form factor $F(q_z)$ is measured at several q_z values, a continuous function, $T(q_z)$, which is proportional to $F(q_z)$, can be fitted to the data:[59–62]

$$T(q_z) = \sum_n \sqrt{I_n q_n}\, \mathrm{sinc}\left(\frac{1}{2} d_z q_z - \pi n\right). \quad (2)$$

Once an analytical expression for $T(q_z)$ has been determined from fitting the experimental peak intensities, the phases ν_n can be assessed from $T(q_z)$.

In order to put ρ_z on an absolute scale, the electron densities were scaled to fulfil the condition $\rho(0) = 0.22$ e Å^{-3} (the electron density of a CH_3 group) in the centre of the bilayer, and $\rho(d_z/2) = 0.33$ e Å^{-3} (the electron density of water, ρ_W) outside the bilayers. All samples were well fit by the phase array $[\bar{1}\bar{1}1\bar{1}1\bar{1}1\bar{1}1\bar{1}]$. Up to 11 pronounced Bragg peaks were observed resulting in a high spatial resolution.

The d_z-spacing between two neighbouring membranes in the stack was determined from the distance between the well developed Bragg reflections ($d_z = 2\pi/\Delta q_z$). The reflectivity peaks were well fit by Gaussian peak profiles. To assign the peaks to different phases, Bragg's law can be re-written as $\sin(\theta) = \lambda/(2d_z) \times n$. By plotting the sine of the Bragg angles *versus* the order of the different Bragg reflections, $\sin(\theta(n))$ *vs.* n, peaks which belong to the same d_z-spacing fall on a straight line through the origin, whose slope is proportional to $1/d_z$. Note that not all diffraction orders are necessarily observed for the different d_z-spacings as their scattering intensity depends on the form factor of the bilayers and oscillates between zero and maximum intensity as a function of q_z.

3. Results

Sixteen different samples were created containing varied amounts of DMPC, ASA and cholesterol. Samples with up to 12.5 mol% ASA and 40 mol% cholesterol were prepared, as listed in Table 1. Two-dimensional X-ray intensity maps were gathered for all samples, with select samples displayed in Fig. 2.

Some qualitative conclusions can be drawn from the 2-dimensional maps. As shown in Fig. 2a, a number of Bragg peaks are scattered for pure DMPC along $q_\parallel$, caused by long range order of lipid tails and lipid head groups in the plane of the membrane, as discussed for instance in ref. 46, 63 and 64. However, as shown in Fig. 2b at 30 mol% cholesterol, long range lateral order is suppressed and a single broad Bragg peak is observed along $q_\parallel$, indicative of a disordered system with a range of nearest-neighbour distances due to the inclusion of cholesterol.[30,46,65]

At 40 mol% cholesterol in Fig. 2c, additional Bragg peaks were observed along the out-of-plane and in-plane axes, related to the formation of immiscible cholesterol plaques, *i.e.*, cholesterol bilayers coexisting with the lamellar membrane structure, as reported previously by Barrett *et al.*[39] The intensity of these peaks was found to increase in the presence of 5 mol% ASA in Fig. 2d. Addition of 10 mol% ASA in part (e) led to a decrease of the intensity of the cholesterol Bragg peaks indicating a shrinking fraction of cholesterol plaques.

For a quantitative analysis of the diffracted intensity, the 2-dimensional data were cut along the out-of-plane and in-plane

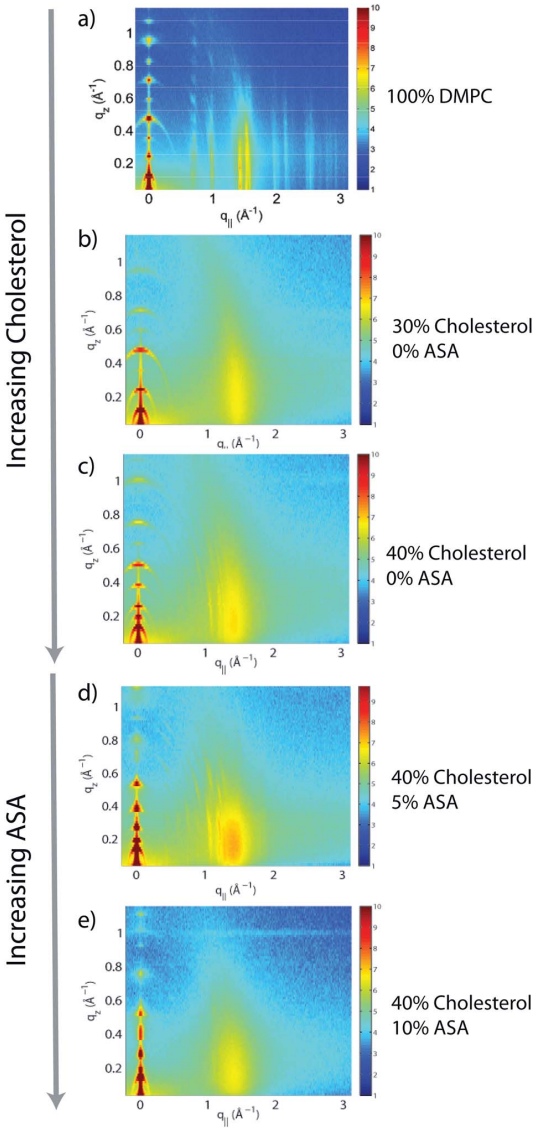

Fig. 2 Two-dimensional X-ray intensity maps of: (a) 100 mol% DMPC, (b) 30 mol% cholesterol, (c) 40 mol% cholesterol, (d) 5 mol% ASA + 40 mol% cholesterol, (e) 10 mol% ASA + 40 mol% cholesterol in DMPC.

axes. As in-plane features are usually orders of magnitude weaker than the pronounced out-of-plane reflections, slices 0.03 Å < q_z < 0.3 Å were integrated to enhance the data quality.

3.1. Out-of-plane structure and electron densities

The position of ASA and cholesterol molecules along the membrane normal, and the bilayer spacing, d_z, were determined from the out-of-plane scans. Reflectivities for samples 1, 3 and 11 are shown in Fig. 3a–c. The peaks are pronounced and equally spaced, indicative of a well-organized lamellar membrane structure. The assembled electron density profiles are shown in Fig. 3d and e, along with cartoons suggesting approximate positions for the molecules along the membrane normal.

Fig. 3d displays the electron density profiles for a pure DMPC membrane as well as for a membrane prepared with 30 mol% cholesterol. The profile for pure DMPC corresponds to a DMPC molecule in the well ordered gel state with both chains in all-*trans* configuration, as has been reported previously by the Nagle group.[46,58] The electron rich phosphorous group in the head group region can easily be identified by the peak in the electron density at ~22 Å. ρ_z monotonically decreases towards the bilayer centre at $z = 0$ to $\rho(0) = 0.22$ e Å^{-3}, the electron density of a CH_3 group.[46,66]

The electron density in the central region of the lipid tails was found to increase in the presence of cholesterol, as shown in Fig. 3d. As depicted in the figure, a cholesterol molecule can be fitted at z values of 2 Å < z < 19 Å, with the hydrophilic, electron-rich oxygen groups at a z position of ~18 Å. This orientation is compatible with the umbrella model[34,36] and "protects" the hydrophobic part of the cholesterol molecule from the aqueous environment, as reported previously for cholesterol in saturated phospholipid bilayers made of DMPC and DPPC.[8,39,67] The umbrella model suggests[68,69] that cholesterol molecules associate strongly with ordered hydrocarbon chains (usually ones that are fully saturated) in such a manner that they are shielded from contact with the aqueous environment by the lipid head group. The electron density in Fig. 3d also demonstrates that the cholesterol molecules are not lying flat between the two leaflets, as was reported recently for highly unsaturated lipid bilayers.[28,37]

Fig. 3e shows the profile of the 30 mol% cholesterol sample, along with a sample prepared with 30 mol% and 10 mol% ASA. This mixture was found to still form homogenous, multi lamellar structures. The sample prepared with ASA shows an overall reduced electron density because more electron rich lipid molecules were replaced by smaller ASA molecules. A pronounced loss of electron density is observed near the head group region at z values of ~21 Å, as was shown previously by Barrett *et al.*[46] As depicted in the figure, an ASA molecule can be fitted at z values of 16 Å < z < 21 Å, with the hydrophilic, electron-richer oxygen groups at a z position of ~21 Å, pointing towards the hydration water. This orientation "protects" the hydrophobic part of the ASA molecule from the aqueous environment. Fig. 3e also demonstrates that ASA and cholesterol molecules coexist in lipid membranes, in particular at high concentrations of cholesterol and ASA. While the cholesterol molecules take an upright position in the hydrophobic membrane core parallel to the lipid acyl chains, the ASA molecules reside preferably in the lipid head group region.

The lamellar spacing, the distance between two bilayers in the membrane stack, was determined from the position of the out-of-plane peaks. When the data is presented as sin(θ), the Bragg angle of the lamellar peaks *versus* the order of the reflection, n, the slope of the fitted line is a function of the

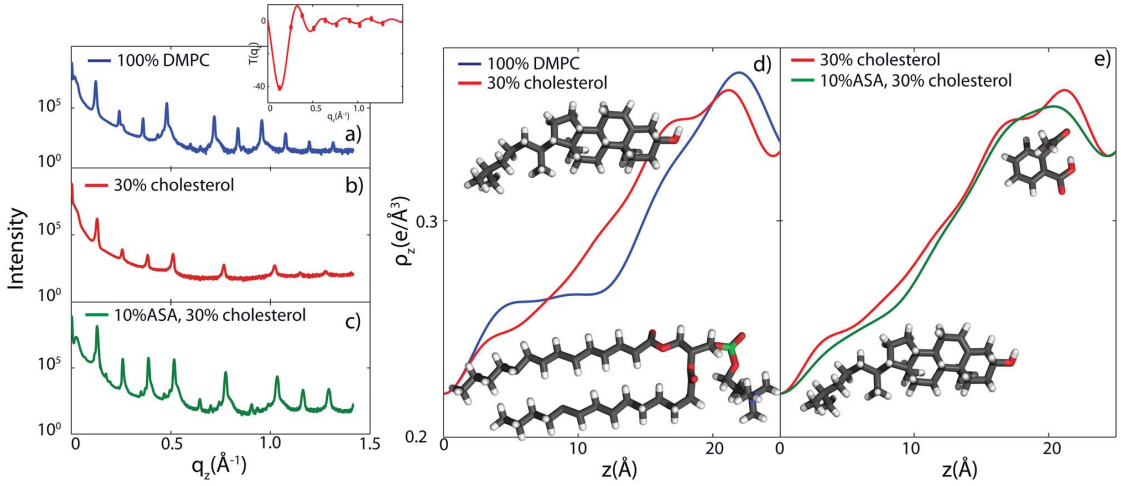

Fig. 3 Reflectivities and corresponding electron density profiles. (a) Reflectivity for a sample with 100 mol% DMPC, (b) 30 mol% cholesterol, (c) 30 mol% cholesterol and 10 mol% ASA. $T(q_z)$ is shown exemplarily for 30 mol% cholesterol as inset to part (a). (d) Electron density profiles for samples with 100% DMPC (blue) and 70 mol% DMPC with 30 mol% cholesterol (red). (e) Electron profiles for a samples with 30 mol% cholesterol (red) and 30 mol% cholesterol with 10 mol% ASA (green). Approximate positions of the molecules are shown.

lamellar spacing, d_z. The corresponding data for samples 4, 8, 12, 15 and 16 for DMPC/40 mol% and ASA concentrations from 0 mol% to 12.5 mol% are shown in Fig. 4.

As was reported previously, two lamellar spacings are observed at 40 mol% cholesterol due to the presence of immiscible cholesterol plaques. As described by Barrett *et al.*,[39] these extra peaks are due to a coexisting, immiscible cholesterol bilayer within the larger lipid structure.[39] The data in Fig. 4 were all well fit by two lines through the origin corresponding to two distinct d_z-spacings. Three lines could be assigned to the 12.5 mol% sample in Fig. 4e, as will be discussed below. The different d_z-spacing, labeled as d_z, d_z' and d_z'', were determined from the slopes and are given in the figures as well as in Table 1.

3 2. Lateral membrane structure

Molecular order of lipids, cholesterol, and ASA molecules in the plane of the membrane was determined from scattering patterns observed along $q_{||}$, as shown in Fig. 5. As discussed in ref. 46, 63 and 64, Bragg peaks of a pure DMPC sample are indexed by an orthorhombic head group lattice, while the tails form a monoclinic unit cell.

Only one peak was observed for samples up to 30 mol% cholesterol, and up to 12.5 mol% ASA (for samples with 30 mol% cholesterol or less). The presence of small amounts of ASA or cholesterol inhibits long range order, as evidenced by the absence of Bragg peaks as described previously.[39,46] This is likely due to a stochastic distribution of ASA and cholesterol molecules in the plane of the membrane. The lipid tails form a densely packed

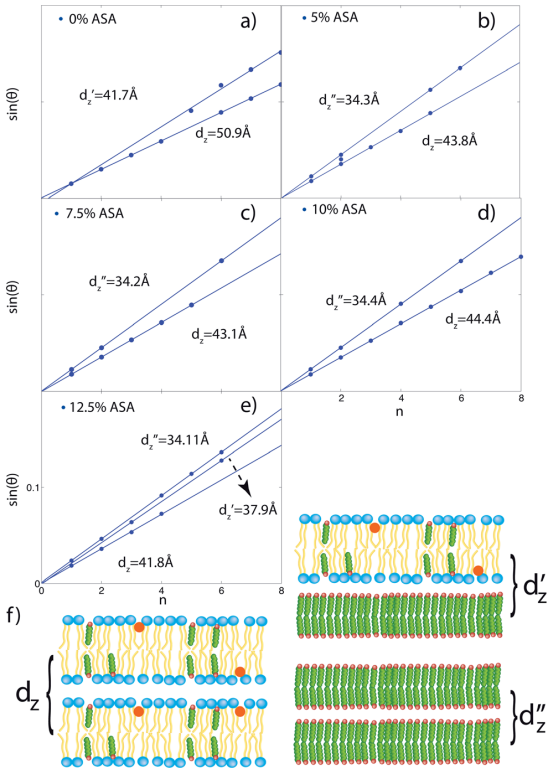

Fig. 4 Position of out-of-plane peaks, sin(θ) *vs.* Bragg order n for (a) 40 mol% cholesterol, (b) 40 mol% cholesterol and 5 mol% ASA, (c) 40 mol% cholesterol and 7.5 mol% ASA, (d) 40 mol% cholesterol and 10 mol% ASA, (e) 40 mol% cholesterol and 12.5 mol% ASA. The slope of the line is proportional to the lamellar spacing, d_z. The corresponding bilayer distances are indicated next to the slopes. (f) Cartoons depict two adjacent lipid bilayers, a lipid bilayer adjacent to a cholesterol bilayer and two stacked cholesterol bilayers.

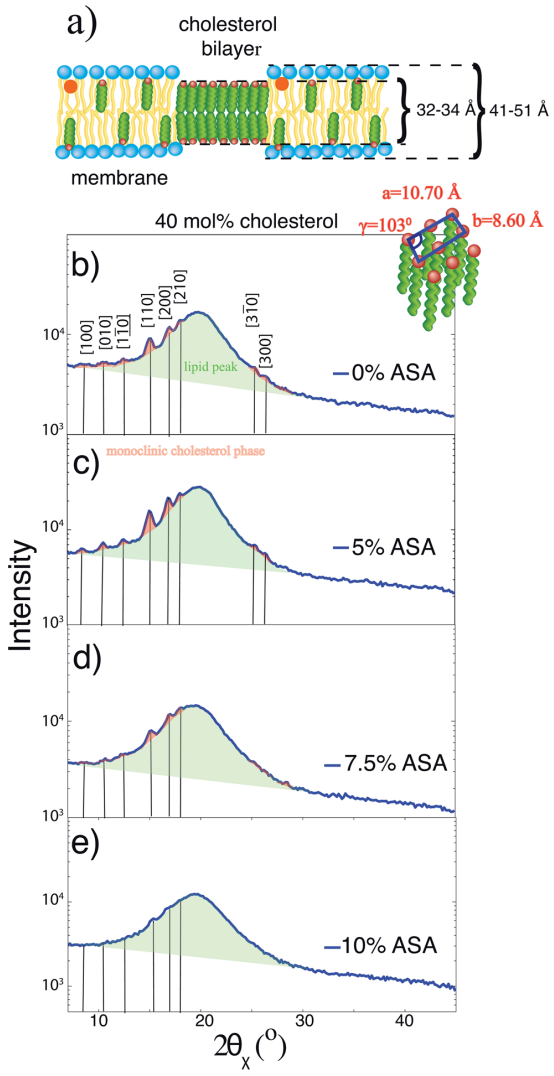

Fig. 5 (a) Cartoon depicting a cholesterol bilayer coexisting with a DMPC bilayer. (b)–(e): In-plane scans for samples with 0 mol% ASA, 5 mol% ASA, 7.5 mol% ASA, and 10 mol% ASA all with 40 mol% cholesterol. The vertical lines indicate the positions of the monoclinic Bragg peaks associated with cholesterol molecules in the cholesterol bilayer, with the appropriate Miller indices indicated in (b).

structure with hexagonal symmetry.[35] In the absence of fluctuations, the area per lipid molecule can be determined from the position of the Bragg peak scattered in-plane at a $q_{\|}$ position of q_T. The area per lipid is calculated using $A_L = 16\pi^2/(\sqrt{3}q_T{}^2)$. The distance between two acyl tails is determined to be $a_T = 4\pi/(\sqrt{3}q_T)$, with the area per lipid simplifies of $A_L = \sqrt{3}a_T{}^2$. The area per lipid for all samples are listed in Table 1.

Additional in-plane Bragg peaks were observed at 40 mol% cholesterol and were assigned to the structure of cholesterol molecules in coexisting cholesterol bilayer plaques. A cartoon depicting one of these plaques is shown in Fig. 5a. In-plane intensity from the sample prepared with 40 mol% cholesterol is shown in Fig. 5b, plotted as function of the in-plane scattering angle $2\theta_\chi$. The data show a broad Bragg peak at $\approx 20^\circ$, and a number of additional, narrow peaks. The structure of the cholesterol bilayers could be determined from the additional narrow peaks. As detailed in ref. 39, for a sample with 40 mol% cholesterol the additional in-plane Bragg peaks can be assigned to a monoclinic unit cell, with parameters $a = 10.7$ Å, $b = 8.6$ Å, $\alpha = \beta = 90^\circ$ and $\gamma = 103^\circ$. Based on this model, the additional Bragg peaks are labelled with their corresponding Miller indices in Fig. 5.

In-plane peaks from Samples containing 40 mol% cholesterol and between 5 mol% and 10 mol% ASA are depicted in Fig. 5c–e. These samples also show additional, narrow Bragg peaks along with the broad lipid tail peak. Additional Bragg peaks are located at nearly identical positions along $2\theta_\chi$, suggesting that the structure of the cholesterol plaques is unchanged by the addition of ASA. However, the intensity of these peaks was found to drastically decrease with increasing ASA.

4. Discussion

4.1. Effect of aspirin

The impact of aspirin and its metabolites on the body are usually studied with regards to their effects on the cyclo-oxygenase (COX) pathway. The COX pathway contributes to platelet aggregation. The inhibition of COX-1 and COX-2 by higher dose aspirin is understood to cause analgesic and anti-inflammatory effects, whereas lower doses, enough to inhibit COX-1 activity, are sufficient for anti-platelet activity.[70,71] The anti platelet activity leads to reduced blood clot formation and hence reduced blockage of arteries and increased blood flow. However, there is growing evidence for the influence of aspirin beyond the COX pathway, and for an influence of aspirin and other NSAID's on the lipid membrane.[72–74] Aspirin has been shown to have a high affinity for phospholipids,[47] and to perturb lipid bilayers in a concentration dependent manner.[75] Suwalsky *et al.*[75] found that ASA strongly perturbed model membranes made of DMPC and DMPE, predominantly found in the outer and inner monolayers of the human erythrocyte membrane and observed that aspirin affects the human erythrocyte shape. In addition, non-steroidal anti-inflammatory drugs such as aspirin and ibuprofen have been shown to increase membrane fluidity and the incidence of pores, decrease the hydrophobic surface barrier, leading to diffusion of acid and cellular injury.[47,49,76]

There is also growing evidence for the effect of lipid organization on platelet function. Increased platelet aggregation has been associated with decreased platelet membrane fludity,[77–79] and platelet aggregation has been associated with lipid rafts. In addition, β-carbolines were found to inhibit platelet activity by modifying platelet membrane fluidity.[80] Our results add to the growing evidence for aspirin's effect on the lipid membrane, and highlight the ability of aspirin to re-organize the membrane.

4.2. The interaction of aspirin with membranes

Membranes containing ASA were previously studied using X-ray diffraction.[46,75,81] While cholesterol is known to reside in the hydrophobic membrane core and to align parallel to the saturated lipid tails (see, *e.g.*, ref. 8 and 67), in agreement with the umbrella model, ASA is located among the head groups of the lipid molecules. The formation of cholesterol plaques in model membranes at high cholesterol levels was reported recently[39] and a model for initiation of atherosclerosis from cholesterol crystal nuclei formed at the cell membrane interface has been proposed.[82]

As reviewed recently by Pereira-Leite, Nunes and Reis,[74] studies are typically performed with NSAID concentration in the range of μM, which is close to the plasma concentration of NSAIDs, but also in the range of mM.[75]

K_p values of up to $K_p \sim 3200$ were reported for different NSAIDs in DMPC suspensions[83] (see the Appendix for a conversion between K_p and molar concentrations). These coefficients correspond to molar concentrations on the order of ~10 mol%, *i.e.*, concentrations of 1 ASA molecule per about 10 lipid molecules in the bilayers. The ASA concentrations in Table 1 are certainly elevated as compared to plasma concentrations of less than 1 mol%, however comparable to ASA concentrations typically used in the literature. We note that the measurements in this study were conducted in synthetic model membranes at very high ASA concentrations. Despite the fact that our findings are very conclusive, we can, at this point, not comment on their physiological relevance.

The formation of cholesterol plaques depends on the solubility limit of cholesterol in membranes, which is strongly dependent on the lipid composition of the corresponding bilayers. The solubility limits for model membranes made of saturated DMPC and DPPC were recently reported to be 40 mol % (ref. 39) and 37.5 mol% (ref. 35) cholesterol, respectively. Plaques were observed already at physiological concentrations of 30 mol% cholesterol in anionic lipid model membranes consisting of 97 mol% DMPC/3 mol% DMPS[84] such that the observed effect of ASA should be even more pronounced in charged membranes. We can, at this point, not comment on the relevance of the effect in unsaturated or poly-unsaturated lipid membranes, which more closely mimic the composition of plasma membranes, as the corresponding solubility limits have not yet been reported in the literature. However,

dimyristoylphosphatidylcholine represents phospholipid classes in the human erythrocyte membranes.[75]

4.3. Structure of the membranes containing cholesterol and ASA

The lamellar spacings of the membrane complexes together with the areas per membrane molecule were determined from the analysis of the out-of-plane and in-plane diffraction data, as listed in Table 1. The corresponding data are plotted in Fig. 6. The area per lipid was found to increase from ~41 Å^2 to ~45 Å^2 with increasing cholesterol content until immiscible cholesterol plaques formed at ~40 mol% cholesterol, in agreement with Barrett *et al.*[39] We then studied the effect of ASA on the cholesterol plaques at a cholesterol concentration of 40 mol%, close to the solubility limit of cholesterol in DMPC model membranes. The area per lipid was found to increase with the addition of ASA. Up to 12.5 mol% ASA were added to the DMPC/40 mol% cholesterol membranes. The lamellar d_z-spacing was approximately constant with increasing cholesterol and dropped from ~52 Å to ~43 Å when ASA was added. Increasing the amount of ASA did not change the d_z-spacing within the resolution of this experiment. The increase in the lipid area at constant d_z in Fig. 6 is indicative of an increase in lipid volume by ~20%, from ~1400 Å^3 to 1700 Å^3. This increase in volume is indicative of an increase in fluidity of the bilayers in the presence of ASA.

Given the high lipid : cholesterol ratio of about 1 : 1, where precipitation was observed, different scenarios can be envisioned. A given membrane in the stack can be adjacent to (1) another membrane, (2) a cholesterol bilayer or (3) two cholesterol plaques stack, as pictured in Fig. 4f.

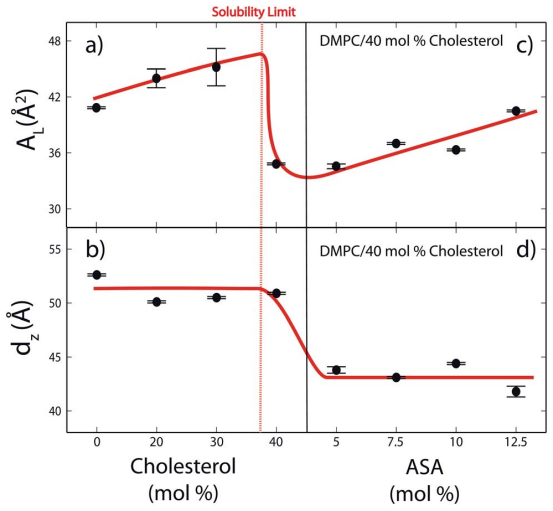

Fig. 6 (a) Area per lipid, A_L, and (b) d_z-spacing as function of increasing cholesterol concentration in the DMPC bilayers. The red line indicates the solubility limit of cholesterol in model DMPC membranes of ~37.5 mol%.[39] Parts (c) and (d) show the effect of addition of ASA to a DMPC/40 mol% cholesterol membrane, where cholesterol plaques formed. Addition of ASA leads to an increase in lipid area, while the lamellar spacing did not change within the resolution of the present experiment.

Three d_z-spacings, d_z, d_z' and d_z'' were observed in the data in Fig. 4e for the highest concentration of ASA of 12.5 mol%. The larger d_z-spacing agrees well with the distance between two membranes in the stack. This d_z-spacing is equivalent to the thickness of a bilayer including the water layer that separates neighbouring bilayers in the stack. The second, smaller d_z (d_z' in Fig. 4f and in Table 1) spacing was indicative of a coexisting, smaller repeat distance. d_z'-spacing involved a bilayer and an adjacent cholesterol bilayer such that $d_z' = \frac{1}{2}d_{\mathrm{lipid}} + \frac{1}{2}d_{\mathrm{chol}}$, which gives $d_{\mathrm{chol}} = 2 \times d_z' - d_{\mathrm{bilayer}}$. The corresponding values for d_{chol} vary between 32.5 Å and 34.2 Å and are listed in Table 1. Given the length of a cholesterol molecule of ~17 Å, these values are in excellent agreement with a cholesterol bilayer, where the cholesterol molecules are oriented along the perpendicular z direction, as sketched in Fig. 5a. The smallest lamellar spacing, d_z'', was directly equivalent to the thickness of a cholesterol bilayer, d_{chol}, as depicted in Fig. 4f. We note that d_{chol} determined from d_z' and d_z'', are in excellent agreement, which strongly supports the model in Fig. 4f.

Additional in-plane Bragg reflections were observed in Fig. 5a when the immiscible cholesterol plaques formed. As reported previously,[39–42,45] the cholesterol molecules in the cholesterol bilayer organize laterally in a monoclinic unit cell at this concentration.

4.4. Effect of ASA on cholesterol plaques

The intensity of the corresponding Bragg peaks in Fig. 5 is directly proportional to the volume fraction of the cholesterol molecules participating in plaques. The corresponding area of the monoclinic peaks was determined by fitting the peaks to Lorentzian peak profiles and normalized to the total intensity scattered into monoclinic and lipid peaks. The normalized area is plotted in Fig. 7.

The fraction of cholesterol plaques initially increased when 5 mol% ASA molecules were included. The ratio between lipid and cholesterol molecules increased from 40 mol% to ~42 mol % as lipid and cholesterol molecules made only 95% of the bilayers. However, despite the fact that the ratio between lipid and cholesterol kept decreasing when increasing the amount of ASA molecules, the volume fraction of cholesterol plaques drastically decreased until no peaks could be detected at an ASA concentration of 12.5 mol%.

From the data in Fig. 6 and 7, the inclusion of ASA molecules in membranes containing cholesterol led to a re-fluidification of the bilayers and to a decomposition of immiscible cholesterol plaques. We note that signs of cholesterol plaques were still detected in the out-of-plane scans in Fig. 4e while no in-plane signals could be detected within the resolution of this experiment. The lamellar Bragg peaks are usually orders of magnitude stronger in highly-aligned stacked membrane systems than the in-plane scattering. We can, therefore, not exclude that small cholesterol plaques were still present at 40 mol% cholesterol and 12.5 mol% ASA. We note that the cholesterol : lipid ratio

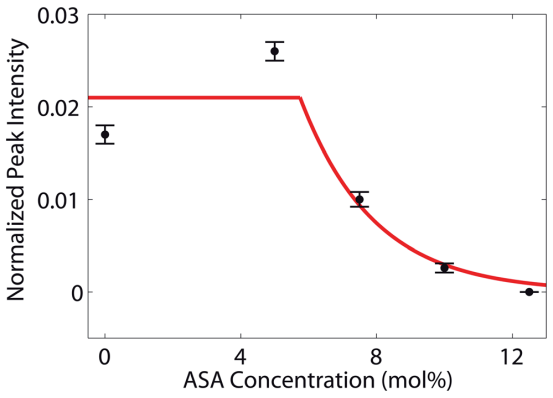

Fig. 7 Normalized integrated area of the monoclinic cholesterol Bragg peaks as function of ASA concentration. The volume fraction of the immiscible cholesterol plaques shows an initial increase before decreasing at higher ASA concentrations. No immiscible domains were observed in the in-plane scans at 12.5 mol% ASA.

was increased to 46 mol% in this sample. However the volume fraction of plaques was drastically reduced as compared to a DMPC/40 mol% cholesterol system.

5. Conclusion

The molecular out-of-plane and in-plane structures of highly oriented, solid supported membranes containing up to 12.5 mol% ASA and 40 mol% cholesterol were studied using high-resolution X-ray diffraction. ASA and cholesterol were found to coexist within saturated lipid membranes made from DMPC, even at high levels of cholesterol and ASA of up to 40 mol% cholesterol and 12.5 mol% ASA. The cholesterol molecules partitioned in the hydrophobic membrane aligning parallel to the lipid acyl chains, in agreement with the umbrella model, while the ASA molecules were found to reside in the lipid head group region.

High cholesterol concentrations above 40 mol% lead to the formation of immiscible cholesterol plaques, in agreement with previous studies. Increasing the amount of ASA in the membranes resulted in a significant increase in fluidity of the bilayers and dissolved the cholesterol plaques. These results add to the growing evidence for aspirin's effect on the lipid membrane and present experimental evidence for a potential interaction between cholesterol and ASA on the level of the cell membrane. Further investigations will clarify if the observed effect is the result of a direct ASA–cholesterol interaction or a general effect of the increased fluidity of the membranes due to the presence of ASA.

6. Appendix: calculation of partitioning coefficients

The molar coefficient of ASA partitioning into lipid bilayers, K_p, is defined as $K_p = X^{ASA}_{lipid}/X^{ASA}_{water}$, where X^{ASA}_{lipid} and X^{ASA}_{water} are the mole fractions of ASA in lipid and water phases, respectively. K_p can also be expressed using molar ratios $K_p = \frac{677.933}{18.015} \times \text{molar ratio}^{ASA}_{lipid}/\text{molar ratio}^{ASA}_{water}$, with $M_{lipid} = 677.933$ g mol^{-1} the molar weight of a DMPC molecule and $M_{water} = 18.015$ g mol^{-1} the molar mass of water.

Acknowledgements

This research was funded by the Natural Sciences and Engineering Research Council (NSERC) of Canada, the National Research Council (NRC), the Canada Foundation for Innovation (CFI), and the Ontario Ministry of Economic Development and Innovation. H.D. is the recipients of NSERC Undergraduate Research Awards (USRA). M.C.R. is the recipient of an Early Researcher Award from the Province of Ontario.

References

1 S. J. Singer and G. L. Nicolson, The fluid mosaic model of the structure of cell membranes, *Science*, 1972, **175**, 720–731.
2 O. G. Mouritsen, *Life-as a matter of fat: the emerging science of lipidomics*, Springer, 2005.
3 M. C. Rheinstädter and O. G. Mouritsen, Small-scale structure in fluid cholesterol-lipid bilayers, *Curr. Opin. Colloid Interface Sci.*, 2013, **18**, 440–447.
4 G. Vereb, J. Szöllősi, J. Matko, P. Nagy, T. Farkas, *et al.*, Dynamic, yet structured: the cell membrane three decades after the singer–nicolson model, *Proc. Natl. Acad. Sci. U. S. A.*, 2003, **100**, 8053–8058.
5 K. E. Bloch, Sterol, structure and membrane function, *Crit. Rev. Biochem. Mol. Biol.*, 1983, **14**, 47–92.
6 P. L. Yeagle, Lanosterol and cholesterol have different effects on phospholipid acyl chain ordering, *Biomembranes*, 1985, **815**, 33–36.
7 M. R. Vist and J. H. Davis, Phase equilibria of cholesterol/dipalmitoylphosphatidylcholine mixtures: deuterium nuclear magnetic resonance and differential scanning calorimetry, *Biochemistry*, 1990, **29**, 451–464.
8 C. L. Armstrong, M. A. Barrett, A. Hiess, T. Salditt, J. Katsaras, *et al.*, Effect of cholesterol on the lateral nanoscale dynamics of fluid membranes, *Eur. Biophys. J.*, 2012, **41**, 901–913.
9 C. L. Armstrong, W. Häußler, T. Seydel, J. Katsaras and M. C. Rheinstädter, Nanosecond lipid dynamics in membranes containing cholesterol, *Soft Matter*, 2014, **10**, 2600–2611.
10 K. Simons and E. Ikonen, Functional rafts in cell membranes, *Nature*, 1997, **387**, 569572.
11 K. Simons and E. Ikonen, How cells handle cholesterol, *Science*, 2000, **290**, 1721–1726.
12 D. M. Engelman, Membranes are more mosaic than fluid, *Nature*, 2005, **438**, 578–580.
13 P. S. Niemelä, S. Ollila, M. T. Hyvnen, M. Karttunen and I. Vattulainen, Assessing the nature of lipid raft membranes, *PLoS Comput. Biol.*, 2007, **3**, e34.
14 L. J. Pike, The challenge of lipid rafts, *J. Lipid Res.*, 2009, **50**, S323–S328.

15 D. Lingwood and K. Simons, Lipid rafts as a membrane organizing principle, *Science*, 2009, **327**, 4650.
16 C. Eggeling, C. Ringemann, R. Medda, G. Schwarzmann, K. Sandhoff, *et al.*, Direc observation of the nanoscale dynamics of membrane lipids in a living cell, *Nature*, 2009, **457**, 1159–1162.
17 F. G. van der Goot and T. Harder, Raft membrane domains: from a liquid-ordered membrane phase to a site of pathogen attack, *Semin. Immunol.*, 2001, **13**, 89–97.
18 P. F. Lenne and A. Nicolas, Physics puzzles on membrane domains posed by cell biology, *Soft Matter*, 2009, **5**, 2841–2848.
19 T. Apajalahti, P. Niemelä, P. N. Govindan, M. S. Miettinen, E. Salonen, *et al.*, Concerted diffusion of lipids in raft-like membranes, *Faraday Discuss.*, 2010, **144**, 411–430.
20 A. Hall, T. Róg, M. Karttunen and I. Vattulainen, Role of glycolipids in lipid rafts: A view through atomistic molecular dynamics simulations with galactosylceramide, *J. Phys. Chem. B*, 2010, **114**, 7797–7807.
21 K. Simons and M. J. Gerl, Revitalizing membrane rafts: new tools and insights, *Nat. Rev. Mol. Cell Biol.*, 2010, **11**, 688–699.
22 L. Hansson, A. Zanchetti, S. G. Carruthers, B. Dahlöf, D. Elmfeldt, *et al.*, Effects of intensive blood-pressure lowering and low-dose aspirin in patients with hypertension: principal results of the hypertension optimal treatment (hot) randomised trial, *Lancet*, 1998, **351**, 1755–1762.
23 S. M. Weisman and D. Y. Graham, Evaluation of the benefits and risks of low-dose aspirin in the secondary prevention of cardiovascular and cerebrovascular events, *Arch. Intern. Med.*, 2002, **162**, 2197.
24 P. M. Ridker, J. E. Manson, J. M. Gaziano, J. E. Buring and C. H. Hennekens, Low-dose aspirin therapy for chronic stable anginaa randomized, placebo-controlled clinical trial, *Ann. Intern. Med.*, 1991, **114**, 835–839.
25 T. J. McIntosh, The effect of cholesterol on the structure of phosphatidylcholine bilayers, *Biochim. Biophys. Acta, Biomembr.*, 1978, **513**, 43–58.
26 D. E. Vance and H. Van den Bosch, Cholesterol in the year 2000, *Biochim. Biophys. Acta, Mol. Cell Biol. Lipids*, 2000, **1529**, 1–8.
27 J. Pan, T. T. Mills, S. Tristram-Nagle and J. F. Nagle, Cholesterol perturbs lipid bilayers nonuniversally, *Phys. Rev. Lett.*, 2008, **100**, 198103.
28 N. Kučerka, D. Marquardt, T. Harroun, M. P. Nieh, S. Wassall, *et al.*, The functional significance of lipid diversity: Orientation of cholesterol in bilayers is determined by lipid species, *J. Am. Chem. Soc.*, 2009, **131**, 16358.
29 J. Pan, S. Tristram-Nagle and J. F. Nagle, Effect of cholesterol on structural and mechanical properties of membranes depends on lipid chain saturation, *Phys. Rev. E: Stat., Nonlinear, Soft Matter Phys.*, 2009, **80**, 021931.
30 T. Mills, J. Huang, G. Feigenson and J. Nagle, Effects of cholesterol and unsaturated dopc lipid on chain packing of saturated gel-phase dppc bilayers, *Gen. Physiol. Biophys.*, 2009, **28**, 126–139.
31 G. Pabst, N. Kučerka, M. P. Nieh, M. Rheinstädter and J. Katsaras, Applications of neutron and X-ray scattering to the study of biologically relevant model membranes, *Chem. Phys. Lipids*, 2010, **163**, 460–479.
32 O. G. Mouritsen, The liquid-ordered state comes of age, *Biomembranes*, 2010, **1798**, 1286–1288.
33 D. Marsh, Liquid-ordered phases induced by cholesterol: A compendium of binary phase diagrams, *Biomembranes*, 2010, **1798**, 688–699.
34 J. Dai, M. Alwarawrah and J. Huang, Instability of cholesterol clusters in lipid bilayers and the cholesterol?s umbrella effect, *J. Phys. Chem. B*, 2010, **114**, 840–848.
35 C. L. Armstrong, D. Marquardt, H. Dies, N. Kučerka, Z. Yamani, *et al.*, The observation of highly ordered domains in membranes with cholesterol, *PLoS One*, 2013, **8**, e66162.
36 J. Huang and G. W. Feigenson, A microscopic interaction model of maximum solubility of cholesterol in lipid bilayers, *Biophys. J.*, 1999, **76**, 2142–2157.
37 N. Kučerka, D. Marquardt, T. Harroun, M. P. Nieh, S. Wassall, *et al.*, Cholesterol in bilayers with pufa chains: Doping with dmpc or popc results in sterol reorientation and membrane-domain formation, *Biochemistry*, 2010, **49**, 7485.
38 S. Meinhardt, R. L. C. Vink and F. Schmid, Monolayer curvature stabilizes nanoscale raft domains in mixed lipid bilayers, *Proc. Natl. Acad. Sci. U. S. A.*, 2013, **110**, 4476–4481.
39 M. Barrett, S. Zheng, L. Toppozini, R. Alsop, H. Dies, *et al.*, Solubility of cholesterol in lipid membranes and the formation of immiscible cholesterol plaques at high cholesterol concentrations, *Soft Matter*, 2013, **9**, 9342–9351.
40 H. Rapaport, I. Kuzmenko, S. Lafont, K. Kjaer, P. B. Howes, *et al.*, Cholesterol monohydrate nucleation in ultrathin films on water, *Biophys. J.*, 2001, **81**, 2729–2736.
41 I. Solomonov, M. J. Weygand, K. Kjaer, H. Rapaport and L. Leiserowitz, Trapping crystal nucleation of cholesterol monohydrate: Relevance to pathological crystallization, *Biophys. J.*, 2005, **88**, 1809–1817.
42 I. Solomonov, J. Daillant, G. Fragneto, K. Kjaer, J. Micha, *et al.*, Hydrated cholesterol: Phospholipid domains probed by synchrotron radiation, *Eur. Phys. J. A*, 2009, **30**, 215–221.
43 R. Ziblat, L. Leiserowitz and L. Addadi, Crystalline domain structure and cholesterol crystal nucleation in single hydrated dppc:cholesterol:popc bilayers, *J. Am. Chem. Soc.*, 2010, **132**, 9920–9927.
44 R. Ziblat, L. Leiserowitz and L. Addadi, Crystalline lipid domains: Characterization by X-ray diffraction and their relation to biology, *Angew. Chem., Int. Ed.*, 2011, **50**, 3620–3629.
45 R. Ziblat, I. Fargion, L. Leiserowitz and L. Addadi, Spontaneous formation of two-dimensional and three-dimensional cholesterol crystals in single hydrated lipid bilayers, *Biophys. J.*, 2012, **103**, 255–264.
46 M. Barrett, S. Zheng, G. Roshankar, R. Alsop, R. Belanger, *et al.*, Interaction of aspirin (acetylsalicylic acid) with lipid membranes, *PLoS One*, 2012, **7**, e34357.
47 L. M. Lichtenberger, Y. Zhou, V. Jayaraman, J. R. Doyen, R. G. O'Neil, *et al.*, Insight into nsaid-induced membrane alterations, pathogenesis and therapeutics: characterization of interaction of nsaids with

phosphatidylcholine, *Biochim. Biophys. Acta, Mol. Cell Biol. Lipids*, 2012, **1821**, 994–1002.
48 Y. Zhou and R. M. Raphael, Effect of salicylate on the elasticity, bending stiffness, and strength of sopc membranes, *Biophys. J.*, 2005, **89**, 1789–1801.
49 L. M. Lichtenberger, Y. Zhou, E. J. Dial and R. M. Raphael, Nsaid injury to the gastrointestinal tract: evidence that nsaids interact with phospholipids to weaken the hydrophobic surface barrier and induce the formation of unstable pores in membranes, *J. Pharm. Pharmacol.*, 2006, **58**, 1421–1428.
50 E. T. Vandenberg, L. Bertilsson, B. Liedberg, K. Uvdal, R. Erlandsson, *et al.*, Structure of 3-aminopropyl triethoxy silane on silicon oxide, *J. Colloid Interface Sci.*, 1991, **147**, 103–118.
51 H. W. Meyer, K. Semmler, W. Rettig, W. Pohle, A. S. Ulrich, *et al.*, Hydration of DMPC and DPPC at 4oc produces a novel subgel phase with convex-concave bilayer curvatures, *Chem. Phys. Lipids*, 2000, **105**, 149–166.
52 K. Nomura, M. Lintuluoto and K. Morigaki, Hydration and temperature dependence of 13c and 1h nmr spectra of the dmpc phospholipid membrane and complete resonance assignment of its crystalline state, *J. Phys. Chem. B*, 2011, **115**, 14991–15001.
53 F. J. M. de Meyer, A. Benjamini, J. M. Rodgers, Y. Misteli and B. Smit, Molecular simulation of the dmpc-cholesterol phase diagram, *J. Phys. Chem. B*, 2010, **114**, 10451–10461.
54 G. Fragneto and M. Rheinstädter, Structural and dynamical studies from bio-mimetic systems: an overview, *C. R. Phys.*, 2007, **8**, 865–883.
55 M. C. Rheinstädter, T. Seydel, F. Demmel and T. Salditt, Molecular motions in lipid bilayers studied by the neutron backscattering technique, *Phys. Rev. E: Stat., Nonlinear, Soft Matter Phys.*, 2005, **71**, 061908.
56 M. Weik, U. Lehnert and G. Zaccai, Liquid-like water confined in stacks of biological membranes at 200 K and its relation to protein dynamics, *Biophys. J.*, 2005, **89**, 3639–3646.
57 K. Hristova and S. H. White, Determination of the hydrocarbon core structure of fluid dioleoylphosphocholine (dopc) bilayers by x-ray diffraction using specific bromination of the double-bonds: Effect of hydration, *Biophys. J.*, 1998, **74**, 2419–2433.
58 S. Tristram-Nagle, Y. Liu, J. Legleiter and J. F. Nagle, Structure of gel phase dmpc determined by X-ray diffraction, *Biophys. J.*, 2002, **83**, 3324–3335.
59 J. F. Nagle and M. C. Wiener, Relations for lipid bilayers, *Biophys. J.*, 1989, **55**, 309–313.
60 J. Nagle, R. Zhang, S. Tristram-Nagle, W. Sun, H. Petrache, *et al.*, X-ray structure determination of fully hydrated lα phase dipalmitoylphosphatidylcholine bilayers, *Biophys. J.*, 1996, **70**, 1419–1431.
61 G. I. King and C. R. Worthington, Analytic continuation as a method of phase determination, *Phys. Lett.*, 1971, **35A**, 259–260.
62 T. Adachi, A new method for determining the phase in the x-ray diffraction structure analysis of phosphatidylcholine/alcohol, *Chem. Phys. Lipids*, 2000, **107**, 93–97.
63 J. Katsaras, V. A. Raghunathan, E. J. Dufourc and J. Dufourcq, Evidence for a two-dimensional molecular lattice in subgel phase dppc bilayers, *Biochemistry*, 1995, **34**, 4684–4688.
64 V. A. Raghunathan and J. Katsaras, Structure of the l_c' phase in a hydrated lipid multilamellar system, *Phys. Rev. Lett.*, 1995, **74**, 4456–4459.
65 T. T. Mills, G. E. S. Toombes, S. Tristram-Nagle, D. M. Smilgies, G. W. Feigenson, *et al.*, Order parameters and areas in fluid-phase oriented lipid membranes using wide angle x-ray scattering, *Biophys. J.*, 2008, **95**, 669–681.
66 L. Toppozini, C. L. Armstrong, M. A. Barrett, S. Zheng, L. Luo, *et al.*, Partitioning of ethanol into lipid membranes and its effect on fluidity and permeability as seen by x-ray and neutron scattering, *Soft Matter*, 2012, **8**, 11839–11849.
67 A. Léonard, C. Escrive, M. Laguerre, E. Pebay-Peyroula, W. Néri, *et al.*, Location of cholesterol in dmpc membranes. A comparative study by neutron diffraction and molecular mechanics simulation, *Langmuir*, 2001, **17**, 2019–2030.
68 R. J. Petrie, P. P. Schnetkamp, K. D. Patel, M. Awasthi-Kalia and J. P. Deans, Transient translocation of the b cell receptor and src homology 2 domain-containing inositol phosphatase to lipid rafts: evidence toward a role in calcium regulation, *J. Immunol.*, 2000, **165**, 1220–1227.
69 A. Papanikolaou, A. Papafotika, C. Murphy, T. Papamarcaki, O. Tsolas, *et al.*, Cholesterol-dependent lipid assemblies regulate the activity of the ecto-nucleotidase cd39, *J. Biol. Chem.*, 2005, **280**, 26406–26414.
70 G. J. Roth, N. Stanford and P. W. Majerus, Acetylation of prostaglandin synthase by aspirin, *Proc. Natl. Acad. Sci. U. S. A.*, 1975, **72**, 3073–3076.
71 C. Patrono, L. A. García Rodríguez, R. Landolfi and C. Baigent, Low-dose aspirin for the prevention of atherothrombosis, *N. Engl. J. Med.*, 2005, **353**, 2373–2383.
72 A. Assadian, J. Lax, U. Meixner-Loicht, G. W. Hagmüller, P. M. Bayer, *et al.*, Aspirin resistance among long-term aspirin users after carotid endarterectomy and controls: flow cytometric measurement of aspirin-induced platelet inhibition, *J. Cardiovasc. Surg.*, 2007, **45**, 1142–1147.
73 J. N. G. Frydman, F. AdSd, R. VCd, M. O. Benarroz, R. GdS, *et al.*, Acetylsalicylic acid and morphology of red blood cells, *Braz. Arch. Biol. Technol.*, 2010, **53**, 575–582.
74 C. Pereira-Leite, C. Nunes and S. Reis, Interaction of nonsteroidal anti-inflammatory drugs with membranes: *In vitro* assessment and relevance for their biological actions, *Prog. Lipid Res.*, 2013, **52**, 571–584.
75 M. Suwalsky, J. Belmar, F. Villena, M. J. Gallardo, M. Jemiola-Rzeminska, *et al.*, Acetylsalicylic acid (aspirin) and salicylic acid interaction with the human erythrocyte membrane bilayer induce in vitro changes in the morphology of erythrocytes, *Arch. Biochem. Biophys.*, 2013, **539**, 9–19.
76 C. Sousa, C. Nunes, M. Lúcio, H. Ferreira, J. L. Lima, *et al.*, Effect of nonsteroidal anti-inflammatory drugs on the cellular membrane fluidity, *J. Pharm. Sci.*, 2008, **97**, 3195–3206.

77 S. J. Shattil and R. A. Cooper, Membrane microviscosity and human platelet function, *Biochemistry*, 1976, **15**, 4832–4837.
78 K. Gousset, W. F. Wolkers, N. M. Tsvetkova, A. E. Oliver, C. L. Field, *et al.*, Evidence for a physiological role for membrane rafts in human platelets, *J. Cell. Physiol.*, 2002, **190**, 117–128.
79 P. Padmavathi, V. D. Reddy, P. Maturu and N. Varadacharyulu, Smoking-induced alterations in platelet membrane fluidity and na+/k+-atpase activity in chronic cigarette smokers, *J. Atheroscler. Thromb.*, 2010, **17**, 619–627.
80 H. Tsuchiya and S. Ohmoto, Comparative effects of b-carbolines on platelet aggregation and lipid membranes, *Pharmacol. Rep.*, 2010, **62**, 689–695.
81 A. Nasedkin, J. Davidsson and M. Kumpugdee-Vollrath, Determination of nanostructure of liposomes containing two model drugs by x-ray scattering from a synchrotron source, *J. Synchrotron Radiat.*, 2013, **20**, 721–728.
82 D. S. Ong, J. J. Anzinger, F. J. Leyva, N. Rubin, L. Addadi, *et al.*, Extracellular cholesterol-rich microdomains generated by human macrophages and their potential function in reverse cholesterol transport, *J. Lipid Res.*, 2010, **51**, 2303–2313.
83 M. Lúcio, C. Nunes, D. Gaspar, K. Golebska, M. Wisniewski, *et al.*, Effect of anti-inflammatory drugs in phosphatidylcholine membranes: A fluorescence and calorimetric study, *Chem. Phys. Lett.*, 2009, **471**, 300–309.
84 H. Dies, L. Toppozini and M. C. Rheinstädter, The interaction between amyloid-β peptides and anionic lipid membranes containing cholesterol and melatonin, *PLoS One*, 2014, in press.

4.2 Paper II: Aspirin Inhibits Formation of Cholesterol Rafts in Fluid Lipid Membranes

Richard J. Alsop, Laura Toppozini, Drew Marquardt, Norbert Kucerka, Thad A. Harroun, and Maikel C. Rheinstädter. (2015). *Aspirin Inhibits Formation of Cholesterol Rafts in Fluid Lipid Membranes.* BBA-Biomembranes. 1848, 805-812

4.2.1 Preface to Paper II

Paper I observed cholesterol plaques using X-ray diffraction in gel phase membranes. Plaques are relevant cholesterol structures, that contribute to atherosclerosis. However, they are believed to nucleate from cholesterol rafts [44]. Therefore, we theorized that aspirin may impact rafts as well. As alluded to in the introduction, rafts are functionally important domains in membranes that are enriched in cholesterol and high in molecular order [7, 8]. To observe an effect on cholesterol raft structure, we needed to use neutron diffraction.

The reason X-ray diffraction is inadequate is the long coherence length of X-rays. Understanding the importance of coherence length requires a return to scattering theory. The picture of an X-ray or neutron impinging on a material is as a wavefront, as in Fig. 2.5. However, the particle wave-packet is not an infinitely coherent wavefront. The packet only scatters from an area proportional to the neutron coherence length [71].

If the structure the particle scatters from contains domains that are much smaller than the particle coherence length, then the domain will be coherently averaged with the surround. X-rays typically have coherence lengths of ∼1000 nm, so raft structures that are ∼10 nm are not distinguishable. If the coherence length is smaller than domain size, then the measured neutron signal is an incoherent sum of coherent averages over both domain and non-domain structure, thereby granting representation to the raft structure. Neutrons have coherence lengths of ∼1-10 nm, which span the speculated size of lipid rafts [72].

Armstrong *et al.* measured the in-plane structure of fluid phase DPPC bilayers with 32.5 mol% cholesterol using neutrons with different coherence lengths [72]. At low coherence length, and only at low coherence, peaks appeared that were indexed by a monoclinic lipid lattice. These peaks are associated with domain structures in the membranes. In this experiment, the tails were deuterated such that the lipid structure was most pronounced. The result was verified by Toppozini *et al.* using deuterated cholesterol [73].

Therefore, we knew that deuterated DPPC bilayers with cholesterol/DPPC ratio of 32.5 mol% contained ordered domains measurable with neutrons. We therefore prepared this system and added 10 mol% aspirin, hypothesizing that it would diminish or alter the domain structure. We performed a neutron diffraction experiment using the N5 Triple Axis Spectrometer at the Canadian Neutron Beam Centre, Chalk River, Ontario, with the help of instrument scientist Dr. Norbert Kucerka. The membranes were hydrated using a customized humidity chamber as detailed in Chapter 3. In the triple-axis setup, the coherence length (ξ) is a function of the wavelength resolution ($\Delta\lambda$) as

well as the wavelength of the neutrons (λ), by $\xi=\frac{\lambda^2}{\Delta\lambda}$. λ is determined by the monochromating crystal, while $\Delta\lambda$ is a function of the instrument properties and the columnation used. Therefore, coherence length could be varied by simply changing λ (rotating the monochromating crystal), without changing anything on the sample stage.

As expected, at low neutron coherence, sharp peaks appeared that were not present at high coherence. The peaks, based on their position in $q_{||}$, indicated lipid organization into a repeating unit with structure on length scales of $\sim$20 Å or a lipid superlattice.

Such a structure had never been observed before. To gain additional insight, we performed additional experiments in collaboration with Drew Marquardt and Dr. Thad Harroun at Brock University. First, Langmuir trough experiments were conducted using lipid monolayers on a water surface. The isotherm measurements measure surface tension of the lipid monolayer. Aspirin was dissolved in the lipid subphase and, as predicted, decreased the surface pressure. In addition, differential scanning calorimetry (DSC) measurements on multi-lamellar vesicles observed changes in the lipid phase behaviour. Membranes with 32.5 mol% cholesterol show no temperature transition [72]. However, when aspirin is present, peaks do appear in the thermogram that change with time. This indicates that new, transient structures form when aspirin is present [17].

There was one other unique feature observed in neutron scattering. A broad peak was found at $q_{||}$ $\sim$1.26 Å^{-1}, implying lipid-lipid correlations 10% larger than without cholesterol, likely caused by interactions with aspirin. We combined the neutron, Langmuir, and DSC results to form a picture of how aspirin fluidifies the ℓ_o phase. We proposed that aspirin creates hyperfluid patches that spontaneously organize. Similar results have been reported in simulations with melatonin and cholesterol. These hyper-fluid patches frustrate cholesterol organization and therefore eliminate rafts, and in turn, the plaques. This is in agreement with Paper I, which saw a global increase in A_L with aspirin. The experiment confirms that, in addition to plaques, aspirin dissolves cholesterol rafts.

Author Contributions:

- *Experimental Concept:* Richard Alsop, Maikel Rheinstädter
- *Sample Preparation:* Richard Alsop, Laura Toppozini, Drew Marquardt
- *Neutron Experiments:* Richard Alsop, Laura Toppozini, Norbert Kucerka, Maikel Rheinstädter
- *Non-neutron experiments:* Richard Alsop, Drew Marquardt, Thad Harroun
- *Data Analysis:* Richard Alsop, Drew Marquardt, Norbert Kucerka, Maikel Rheinstädter
- *Manuscript Preparation:* Richard Alsop, Maikel Rheinstädter

Biochimica et Biophysica Acta 1848 (2015) 805–812

Contents lists available at ScienceDirect

Biochimica et Biophysica Acta

journal homepage: www.elsevier.com/locate/bbamem

Aspirin inhibits formation of cholesterol rafts in fluid lipid membranes

Richard J. Alsop [a], Laura Toppozini [a], Drew Marquardt [b], Norbert Kučerka [c,d,e], Thad A. Harroun [b], Maikel C. Rheinstädter [a,c,*]

[a] Department of Physics and Astronomy, McMaster University, Hamilton, ON, Canada
[b] Department of Physics, Brock University, St. Catharines, ON, Canada
[c] Canadian Neutron Beam Centre, Chalk River, ON, Canada
[d] Department of Physical Chemistry of Drugs, Comenius University, Bratislava, Slovakia
[e] Frank Laboratory of Neutron Physics, Joint Institute for Nuclear Research, Dubna, Russia

ARTICLE INFO

Article history:
Received 21 August 2014
Received in revised form 18 November 2014
Accepted 19 November 2014
Available online 2 December 2014

Keywords:
Lipid membranes
Cholesterol
Aspirin
Cholesterol rafts
Aspirin–cholesterol interaction

ABSTRACT

Aspirin and other non-steroidal anti-inflammatory drugs have a high affinity for phospholipid membranes, altering their structure and biophysical properties. Aspirin has been shown to partition into the lipid head groups, thereby increasing membrane fluidity. Cholesterol is another well known mediator of membrane fluidity, in turn increasing membrane stiffness. As well, cholesterol is believed to distribute unevenly within lipid membranes leading to the formation of lipid rafts or plaques. In many studies, aspirin has increased positive outcomes for patients with high cholesterol. We are interested if these effects may be, at least partially, the result of a non-specific interaction between aspirin and cholesterol in lipid membranes.

We have studied the effect of aspirin on the organization of 1,2-dipalmitoyl-*sn*-*glycero*-3-phosphatidylcholine (DPPC) membranes containing cholesterol. Through Langmuir–Blodgett experiments we show that aspirin increases the area per lipid and decreases compressibility at 32.5 mol% cholesterol, leading to a significant increase of fluidity of the membranes. Differential scanning calorimetry provides evidence for the formation of metastable structures in the presence of aspirin. The molecular organization of lipids, cholesterol and aspirin was studied using neutron diffraction. While the formation of rafts has been reported in binary DPPC/cholesterol membranes, aspirin was found to locally disrupt membrane organization and lead to the frustration of raft formation. Our results suggest that aspirin is able to directly oppose the formation of cholesterol structures through non-specific interactions with lipid membranes.

1. Introduction

Lateral heterogeneity in lipid composition in membranes permits the existence of so-called lipid rafts: regions of the membrane believed to contain elevated cholesterol composition and increased molecular order [1–4]. Domains serve a functional purpose as they are thought to take part in membrane-associated events such as lipid/protein sorting and signal transduction, among other roles [5–10]. Experimental observation of rafts has been challenging as they are believed to be both small and short lived [11–14].

Cholesterol is suggested to drive domain formation through lipid interactions with cholesterol's stiff ring structure leading to the so-called liquid ordered (l_o) phase [15–18]. Small, transient cholesterol domains in binary lipid bilayers at physiological levels of cholesterol were recently reported from computer simulations and experiments [18–23]. At high concentrations of cholesterol, above ~40 mol%, immiscible cholesterol bilayers were reported to form spontaneously in model lipid bilayers [24–28].

There is growing evidence for an influence of various pharmaceuticals on lipid membrane organization and stability [29]. In particular, non-steroidal anti-inflammatory drugs (NSAID's) have been shown to disturb bilayer structures in real and model membranes [30,31]. Aspirin (acetylsalicylic acid, ASA) is the most common NSAID and has been shown to have strong interactions with bilayer structures [30,32]. Aspirin strongly perturbs model membrane structures in a concentration dependent manner and influences human erythrocyte shape [33]. As well, aspirin decreases the hydrophobic surface barrier in mucosal membranes, leading to a diffusion of acid and gastrointestinal injury [34] and has an effect on protein sorting [35]. Recently, a direct interaction between aspirin and cholesterol was reported as aspirin was observed to reduce the volume of cholesterol plaques in model membranes with elevated cholesterol concentrations of 40 mol% [36].

Abbreviations: DPPC, dipalmitolyphosphatidylcholine; ASA, acetylsalicylic acid; DSC, differential scanning calorimetry; L-B, Langmuir–Blodgett; PG, pyrolytic graphite; TFE, trifluoroethanol; RH, relative humidity; COX, cyclooxygenase

* Corresponding author at: Department of Physics and Astronomy, McMaster University, ABB-241, 1280 Main Street West, Hamilton, Ontario L8S 4M1, Canada. Tel.: +1 905 525 9140 23134; fax: +1 905 546 1252.
E-mail address: rheinstadter@mcmaster.ca (M.C. Rheinstädter).

http://dx.doi.org/10.1016/j.bbamem.2014.11.023
0005-2736/

However, an influence of aspirin on membranes with physiological levels of cholesterol has not been explored.

We examined the effect of aspirin on membranes composed of DPPC and physiological levels of cholesterol. The molecules are depicted in Fig. 1. By combining Langmuir–Blodgett isotherms, calorimetric measurements and neutron diffraction, we present evidence that the presence of 10 mol% ASA leads to a significant re-fluidification of DPPC/32.5 mol% cholesterol bilayers. The neutron diffraction patterns are indicative of ASA super-structures in the fluid bilayers, which seem to frustrate the formation of cholesterol rafts.

2. Results

2.1. Langmuir–Blodgett monolayer compression isotherms

Pressure versus area isotherms were recorded for DPPC monolayers with and without cholesterol in order to determine molecular areas and compressibility. ASA was dissolved in the aqueous sub-phase at concentrations of 0 mM and 3 mM. All experiments were performed with a sub-phase temperature of 50 °C. Fig. 2a) shows the compression isotherms for all experiments. The addition of 32.5 mol% cholesterol to the monolayer shifts the isotherm towards lower pressures and lower area per lipid compared to a monolayer composed of pure DPPC. However, with the addition of 3 mM ASA into the water sub-phase, the compression isotherm shifted to higher pressures and higher area per lipid, for both pure DPPC monolayers and monolayers containing 32.5 mol% cholesterol. To best capture trends observed in the compression isotherms, a pressure of 27 mN/m was chosen to compare the changes in the monolayer area per molecule as well as in the compressibility modulus due to the incorporation of cholesterol and ASA.

The mean molecular area for all isotherms at a pressure of 27 mN/m is plotted in Fig. 2b). At this pressure, a DPPC monolayer has a mean area of $A_L = 71.9 \pm 0.5$ Å^2. The addition of 32.5 mol% cholesterol to the DPPC monolayers decreases A_L significantly to 38.6 ± 0.2 Å^2. Inclusion of 3 mM ASA in the sub-phase leads to an increase of the area per lipid to 74.4 ± 0.7 Å^2. The same effect is observed in the presence of cholesterol: the addition of 3 mM ASA in the sub phase leads to a significant increase of the area per lipid in DPPC/32.5 mol% cholesterol from 38.6 ± 0.2 Å^2 to 44.3 ± 0.3 Å^2.

The compressibility of the monolayers is determined by the slope of the isotherms (as detailed in the Materials and methods section, Section 4). The addition of ASA to the water sub-phase decreases the elastic compressibility modulus, C_S^{-1}, from 84 ± 1 mN/M for pure DPPC to 63 ± 1 mN/M for DPPC/3 mM ASA as depicted in Fig. 2c), at a pressure of 27 mN/m. This is in strong contrast to cholesterol, which increases the compressibility modulus when added to the monolayer from 84 ± 1 mN/M to 89.8 ± 0.3 mN/M, as reported previously [37,38]. Addition of ASA to the DPPC/32.5 mol% cholesterol monolayers reduces the compressibility from 89.8 ± 0.3 mN/M to 80.6 ± 0.5 mN/M.

A decreased compressibility modulus is indicative of membranes, which are softer and more compressible. The increase in molecular area and decrease in compressibility for a pure DPPC bilayer in the presence of aspirin points to a general increase in fluidity of the membranes. The increase in molecular area and decrease in compressibility for DPPC/32.5 mol% cholesterol bilayers is strong evidence for a re-fluidification of the bilayers at a physiological cholesterol concentration with ASA.

2.2. Differential scanning calorimetry

The effect of ASA on the phase behavior of membranes was examined using differential scanning calorimetry. Multi-lamellar vesicles (MLVs) of different composition were prepared for these experiments. Heating thermograms are plotted in Fig. 3a). A thermogram taken from a pure DPPC sample shows two endothermic transitions. There is a pre-transition from the gel to ripple phase ($L_\beta \rightarrow P_{\beta'}$) at T ~ 308 K. The main transition to the fluid phase (L_α) occurs at 314 K, in agreement with literature values [39]. Addition of ASA resulted in a decrease in the main transition temperature and broadened the main transition peak (and eliminated the pre-transition). Similar results have been reported when ASA is added to DMPC liposomes [33]. A reduction or suppression in transition temperatures and transition enthalpy is evidence that ASA reduces the cooperativity of the main and pre-transitions, indicative of a more fluid structure.

As expected, thermograms of samples composed of DPPC with 32.5 mol% cholesterol in Fig. 3b) show no transitions, as was reported previously for the l_o phase [20,40]. The absence of a transition proves that a cholesterol concentration of 32.5 mol% is high enough to induce the l_o phase in DPPC bilayers. No change was observed after addition of 1 mM ASA (data not shown). However, as shown in Fig. 3b), addition of 6 mM ASA led to the appearance of an exothermic transition at $T = 313.6$ K.

The bilayers were then cooled and the heating thermogram was repeated. After this second cycling the transition peak shifted to $T = 308$ K and significantly broadened. The temperature cycling was repeated, and a third thermogram shows no transition peak. We note that no peak was observed upon cooling, regardless of cycle number. The dependence of the thermogram upon temperature cycling indicates the presence of inhomogeneities and kinetically trapped states existing on

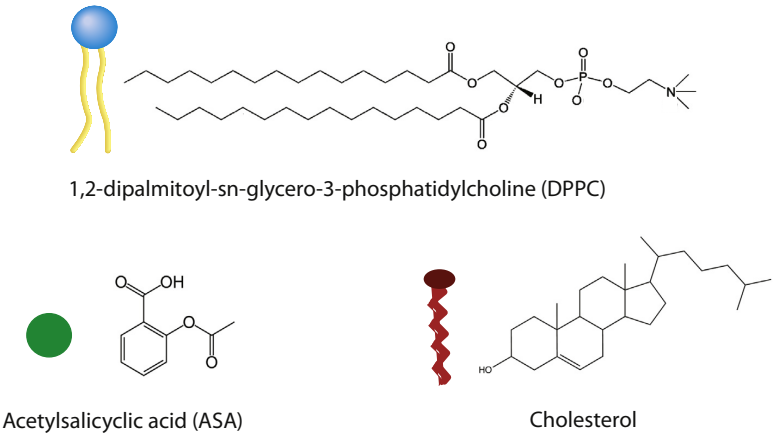

Fig. 1. Schematic representations of the 1,2-dipalmitoyl-*sn-glycero*-3-phosphatidylcholine (DPPC), cholesterol, and acetylsalicylic acid (ASA, aspirin) molecules used in this study.

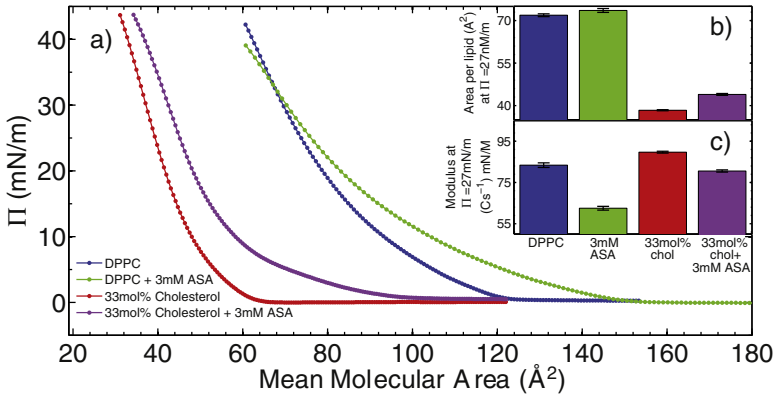

Fig. 2. Langmuir–Blodgett experiments were performed on DPPC monolayers with and without cholesterol. a) Compression isotherms of monolayers of DPPC (blue), DPPC with 3 mM ASA in the subphase (green), DPPC/32.5 mol% cholesterol (red) and DPPC/32.5 mol% cholesterol and 3 mM ASA in the subphase (purple). b) Area per lipid molecule for isotherms at $\Pi = 27$ mN/m for all samples. c) Compressibility modulus (C_S^{-1}) for all samples, measured at $\Pi = 27$ mN/m.

timescales comparable to the rate of cycling [41–43]. The caloric data point, therefore, to the existence of meta-stable structures in cholesterol bilayers in the presence of ASA, as will be discussed below.

2.3. Neutron diffraction

Lateral molecular order of chain perdeuterated DPPC bilayers containing 32.5 mol% cholesterol and 10 mol% ASA was studied using in-plane neutron diffraction. Rafts have been reported at this concentration of cholesterol in DPPC bilayers from computer simulations and experiments [18–23]. Highly oriented, solid supported membranes were prepared and placed in a humidity chamber at $T = 50$ °C and a D_2O relative humidity of ~100%, ensuring full hydration of bilayers. Bilayers made of DPPC/32.5 mol% cholesterol were previously studied using this setup by Armstrong et al. [20] and d_z-spacings of 64 Å were observed, in good agreement with lamellar spacings reported by Gallová et al. [53] in multi-lamellar DPPC liposomes with 33.3 mol% cholesterol. This proves that fully hydrated bilayers can be prepared using our technique.

Two different neutron scattering setups were used: (1) a conventional high energy and momentum resolution setup and (2) a low energy and momentum resolution setup, which permits greater spatial resolution for detecting small structures and weak signals, as reported previously [20,23,44,45]. The two setups were achieved by changing the incoming neutron wavelength, λ, without any need to re-align the sample or change the hydration state of the bilayers. By using chain perdeuterated DPPC-d62, our experiment was predominantly sensitive to molecular structure and arrangement of the lipid acyl chains. The sample was aligned in the neutron beam such that the scattering vector, $\vec{Q}$, was always in the plane of the membranes. This in-plane component of the scattering vector is referred to as $q_{||}$.

Data taken using the conventional setup is shown in Fig. 4a). Sharp peaks occur at $q_{||} = 1.1$ Å^{-1} and 1.65 Å^{-1}, which are assigned to scattering from silicon (in higher orders) and are highlighted in gray. The

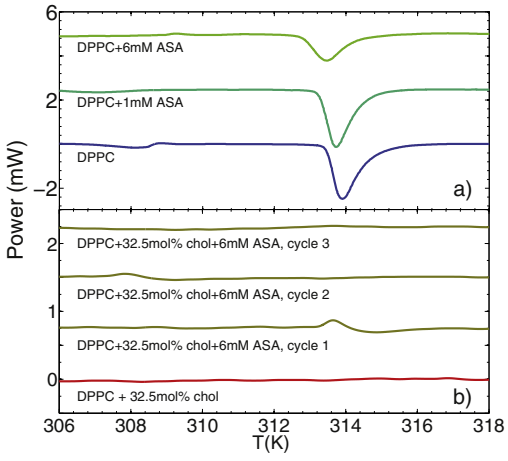

Fig. 3. Differential scanning calorimetry studies of multi-lamellar vesicles with cholesterol and ASA. a) Heating scans of pure DPPC membranes with different ASA concentrations in the aqueous phase. b) Heating scans of DPPC membranes with 32.5 mol% cholesterol. With no ASA in the sub-phase, a heating scan shows no feature indicating membranes with 32.5 mol% cholesterol are in the l_o phase. However, addition of 6 mM ASA leads to the appearance of an additional feature, which is unstable upon repeated heating scans.

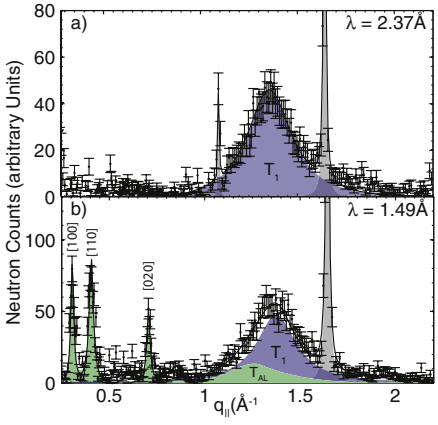

Fig. 4. In-plane neutron diffraction profiles of DPPC-d62 membranes containing 32.5 mol% cholesterol and 10 mol% ASA. a) An in-plane profile recorded with a typical low spatial resolution setup. The sharp gray peaks at $q_{||} = 1.1$ Å^{-1} and 1.65 Å^{-1} originate, respectively, from 3rd and 2nd order scattering of silicon. The single feature, typically observed in diffraction patterns, is a broad correlation peak due to the packing of the lipid tails in the hydrophobic membrane core. b) An in-plane profile recorded with a high spatial resolution setup. Additional, narrow and pronounced features appear with change in resolution, as explained in the text.

diffraction pattern shows a single broad peak centered at $q_{||} \sim 1.36$ Å^{-1}, indicated in blue. The broad correlation peak was well described by a Lorentzian peak profile, and was previously assigned to a hexagonal packing of the lipid acyl chains in the hydrophobic membrane core with parameters $a_{lipid-l_o} = b_{lipid-l_o} = 5.58$ Å and $\gamma = 120°$ [20,23]. The data in Fig. 4a) show a diffraction pattern typical of a fluid, liquid-ordered (l_o) membrane.

The diffraction pattern obtained using a high spatial resolution is shown in Fig. 4b). In addition to a broad correlation peak and sharp peaks originating from silicon, three narrow and pronounced correlation peaks are visible, indicating a coexisting and well-ordered lateral structure. The broad correlation peak at $q_{||} \sim 1.36$ Å^{-1} is no longer well described by a single distribution. Rather, two Lorentzian profiles were required to fit the observed scattering: (1) a peak located at $q_{||} \sim 1.37$ Å^{-1} (in agreement with part a)); and (2) a weaker peak at $q_{||} \sim 1.28$ Å^{-1}. The latter is highlighted by the green profile in Fig. 4b). The observation of two peak profiles suggests the presence of two environments for the lipid tails in the presence of ASA. The integrated area of the green Lorentzian at smaller $q_{||}$-values in Fig. 4b) is ~1/3 the integrated area of the blue profile. The concentration of ASA and DPPC in the bilayers is 10 mol% and 60.75 mol% respectively, resulting in a ratio between ASA and lipid molecules of ~1/6. The ratio between the integrated intensities is then indicative that one ASA molecule interacts with two lipid molecules leading to a lipid environment with a larger tail spacing.

The position of the sharp peaks ($q_{||} = 0.305$ Å^{-1}, $q_{||} = 0.41$ Å^{-1}, $q_{||} = 0.705$ Å^{-1}) are best indexed by the [100], [110] and [020] reflections, respectively, of a monoclinic unit cell with parameters $a_{superlattice} = 21.2$ Å, $b_{superlattice} = 18.2$ Å, $\gamma = 104°$. The dimensions of the unit cell suggest the formation of a super-lattice-type structure, containing several lipid and cholesterol molecules. The corresponding molecular structure is depicted in Fig. 5. We note that the diffraction pattern in Fig. 4b) does not show evidence for the highly ordered, monoclinic lipid raft structure, which was observed previously by Armstrong et al. in DPPC/32.5 mol% cholesterol bilayers through neutron diffraction.

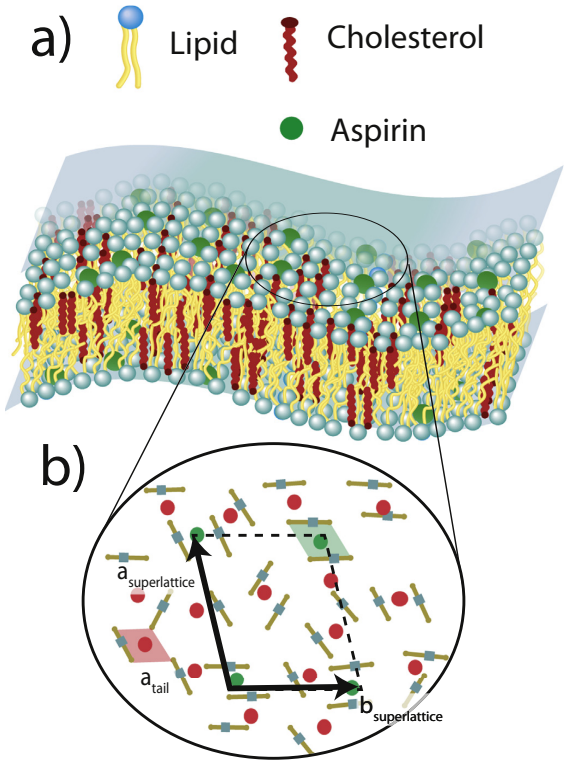

Fig. 5. Cartoon of a DPPC membrane containing 32.5 mol% cholesterol and 10 mol% ASA, as deduced from the neutron diffraction data in Fig. 4a). A depiction of a bilayer containing cholesterol and ASA. b) A cartoon of the super-lattice as imaged by the high spatial resolution setup. The black arrows highlight a super-lattice cell, determined from the diffraction pattern in Fig. 4b). The different lipid environments are highlighted by the green and red parallelograms.

3. Discussion and conclusions

When introduced into the body, aspirin and its metabolites are understood to interact through specific biochemical reactions. Aspirin is known to interact with the cyclo-oxygenase (COX) pathway. The inhibition of both COX isoforms, COX-1 and COX-2, by higher dose aspirin is believed to lead to analgesic and anti-inflammatory effects, while lower doses, sufficient to inhibit COX-1 activity, leads to anti-platelet activity [46,47]. However, there is evidence for the role of platelet membrane composition and fluidity in determining platelet cell function [48–50]. Platelet aggregation has also been associated with lipid rafts [51]. As discussed in the Introduction, there is growing evidence for an interaction of aspirin with lipid membranes through non-specific effects.

As a prerequisite for such non-specific interactions, aspirin was reported to partition into lipid bilayers and position itself in the lipid head group region [32,36]. Our experiments suggest that aspirin is able to directly interact with model lipid membranes and oppose the molecular level organization induced by cholesterol.

We studied the interaction between DPPC bilayers containing 32.5 mol% cholesterol and ASA using three different techniques, namely Langmuir–Blodgett experiments, differential scanning calorimetry and neutron diffraction. At this physiological cholesterol concentration, the DPPC bilayers are in their liquid-ordered phase. The l_o phase in binary DPPC/cholesterol bilayers was recently reported to form rafts [18–23] from experiments and simulations.

In order to use the different experimental techniques, different systems were prepared: monolayers were used in the Langmuir–Blodgett experiments, fully hydrated multilamellar vesicles in the calorimetric experiments and highly oriented solid supported multilamellar bilayers hydrated through the vapor phase in the neutron diffraction experiments. We note that the area per molecule in the lipid monolayers of ~72 Å^2 is larger than the area per lipid reported for multilamellar DPPC bilayers of ~64 Å^2 [52]. The lamellar spacing that we determine at ~57 Å is significantly lower than the d_z-spacing of ~65 Å reported for fully DPPC/32.5 mol% cholesterol bilayers [20,53]. While we attribute the reduction in d_z-spacing mainly to the presence of ASA in the bilayers, we cannot exclude that the bilayers in our study did not achieve full hydration, as no reference values are published in the literature. Nevertheless, qualitatively similar results were observed when ASA was added to each of the systems: the bilayers showed an increase in fluidity and the effects of cholesterol are countered. We, therefore, can argue that the conclusions we draw below are robust and supported by the experiments.

10 mol% ASA was added to the membranes, i.e., 1 ASA molecule per 10 lipid molecules. This ASA concentration is elevated as compared to plasma concentrations of less than 1 mol%, however, comparable to ASA concentrations typically used in the literature [54]. Floating monolayers were used to determine the area per molecule and compressibility in the presence of ASA. Multi-lamellar vesicles were studied in the calorimetric experiments to determine the effect of ASA on the phase behavior. Finally, solid supported bilayers were used for neutron diffraction experiments to study arrangement of the molecules in the plane of the membranes.

Several conclusions can be drawn from this combination of techniques and systems. ASA interacts with monolayers, vesicles and

supported bilayers, independent of whether membranes were formed first and ASA was added to the aqueous phase (monolayers and vesicles) or included in the membranes at the time of the bilayer formation (solid supported bilayers). From the trough experiments, ASA leads to an increase in the area per molecule and a decrease in compressibility in pure DPPC and in DPPC/32.5 mol% cholesterol systems, indicative of a significant fluidification of the membranes. We note that ASA was reported previously by Alsop et al. [36] to dissolve cholesterol plaques, which form at higher cholesterol concentrations above ~40 mol%.

This increase in fluidity is also seen as a loss of cooperativity in the calorimetric experiments as broadening of the endothermic main transition in DPPC bilayers [41]. As a fingerprint of the l_o-phase, the main transition is suppressed in DPPC/32.5 mol% cholesterol bilayers. However, addition of 6 mM ASA to the aqueous phase led to the formation of a meta-stable phase in DPPC/cholesterol bilayers, as evidenced by an exothermic peak in the thermogram upon heating, which was shifted and eventually disappeared upon temperature cycling. Similar results were found when a quinoline antibiotic was studied with DPPC membranes [55], and it was suggested that the inclusion interaction of the drug with membranes led to the formation of meta-stable structures in the bilayers. Similar behavior can be observed in orientational glasses caused by a dynamic domain pattern and often related to aging and memory effects [56,57].

Neutron diffraction of oriented bilayers, using deuterium labeled lipid molecules, was used to study potential lateral structures in the presence of aspirin. Neutron measurements were taken at a constant temperature of 323 K, as continuous temperature cycling was not possible given the long counting times required for data collection. At low spatial resolution, the in-plane neutron diffraction pattern is indicative of a membrane in a uniform, disordered fluid state as reported previously [20,58,59]. The broad correlation peak in Fig. 4a) is the result of the hexagonal packing of the lipid acyl chains in the hydrophobic membrane core (planar group p6), as reported from, e.g., neutron diffraction [20].

With an increase in spatial resolution the lipid correlation peak is best described by two Lorentzian peak profiles, suggestive of two short-ranged lipid correlations and corresponding environments. A small, broad peak at $q_{||} \sim 1.28$ Å^{-1}, equivalent of an increased tail spacing, is associated with lipids interacting with aspirin molecules. The additional narrow and pronounced monoclinic super-lattice peaks are also driven by the presence of aspirin in the membrane. The corresponding molecular structure is depicted in Fig. 5. The ASA molecules, and the interacting lipid molecules, organize in a regular pattern throughout the membrane. Based on the ratio between the lipid chain peaks in the neutron data, each ASA molecule associates with two lipid molecules. This structure was observed with a neutron setup, which measured $q_{||}$ with $q_z = 0$. We can, therefore, not comment on whether the observed in-plane superlattice is possibly correlated across bilayers in the membrane stack.

This structure is different from the structure typically observed in binary DPPC/cholesterol membranes. While rafts were reported from computer simulations [19,21,22] and experiments [20,23], the presence of the ASA molecules in the bilayers seems to frustrate the formation of locally ordered cholesterol domains. While correlation peaks corresponding to raft structures were reported from neutron diffraction by Armstrong et al. [20] and Toppozini et al. [23] in DPPC/32.5 mol% cholesterol, these peaks were not observed in the diffraction data in Fig. 4, indicative that raft formation is inhibited in the presence of ASA.

In summary, the effect of aspirin (acetylsalicylic acid, ASA) on the structure of fluid lipid membranes made of DPPC containing 32.5 mol% cholesterol was studied at a concentration of 10 mol% ASA. Langmuir–Blodgett experiments suggest that ASA interacts with DPPC monolayers from the aqueous phase and leads to a fluidification of DPPC and DPPC/cholesterol membranes. Signatures of meta-stable patterns were observed in differential scanning calorimetry experiments. The corresponding molecular structure was determined from neutron diffraction. The observed diffraction pattern indicates that the presence of ASA leads to the formation of a super-lattice and the frustration of highly ordered cholesterol domains that were reported in binary DPPC/cholesterol membranes previously.

Although an interaction between aspirin and cholesterol was studied using three different membrane systems, the results in all systems suggest that ASA is able to counteract the effects of cholesterol when interacting with fluid lipid membranes. ASA induces changes to both the domain structure and the mechanical properties of DPPC membranes. These results add to the growing evidence for the potential of ASA to have a profound influence on the properties of membranes through non-specific interactions.

4. Materials and methods

Lipids and cholesterol were purchased from Avanti Polar Lipids (Alabaster, AL) and used without further purification. Acetylsalicylic acid (>99% crystalline) was purchased from Sigma Aldrich (Mississauga, ON).

4.1. Preparation of Langmuir monolayers and measurement of isotherms

Langmuir isotherms were performed on a KSV NIMA Minitrough (50 mm × 155 mm) and delrin barriers. Barrier control and data acquisition were achieved using the LB measurement system provided by KSV NIMA (Biolin Scientific, Linthicum Heights, Maryland USA). The balance was calibrated using a 264.9 mg calibration standard provided by the manufacturer prior to the commencement of the experiments.

Surface pressures were measured using pre-wetted paper Wilhemy plates at temperatures of 50 °C. Ultrapure (18.2 MΩ cm) water performed the role of the sub-phase. The sub-phase pressure was kept below 0.1 mN/m prior to spreading the lipid. If the pressure exceeded 0.1 mN/m, the surface was re-cleaned and the procedure repeated. Phospolipid films were spread by careful deposition of 2 μL volumes of chloroform solution containing 3 mg/mL lipid solution. After deposition, 10 min was allotted for solvent evaporation. The compression rate was 5 cm^2/min. Two lipid solutions were prepared: a pure DPPC solution, and a solution composed of DPPC/32.5 mol% cholesterol, both with concentrations at 3 mg/mL. Sub-phase solutions with two different concentrations of ASA were prepared: 0 mM ASA and 3 mM ASA.

The elastic compressibility can be determined from the pressure versus area isotherm, by calculating the corresponding slope:

$$C_s^{-1} = -A\left(\frac{d\pi}{dA}\right), \tag{1}$$

with C_S^{-1} being the compression modulus, A the area in the trough and π the pressure.

4.2. Differential scanning calorimetry

Solutions of DPPC and DPPC with 32.5 mol% cholesterol were prepared in chloroform, then dried. Mixtures were placed under vacuum for ~6 h to ensure that all residual solvent was removed. Samples were then hydrated with ultrapure water (18.2 MΩ cm), with ASA concentrations of 0 mM, 1 mM and 6 mM to final DPPC concentrations of 125 mg/mL. Samples were put through 5 freeze/thaw cycles with vortexing, ensuring during the thaw step the solutions reached 50 °C. 25 μL of solution was loaded into Shimadzu Aluminum Hermetic Pans and crimp sealed. Thermograms were collected at 1 °C/min and a sampling rate of 1 s using a Shimadzu DSC-60 and a TA-60WS Thermal Analyzer.

4.3. Supported bilayer preparation

Highly oriented bilayers of 1,2-dipalmitoyl-sn-glycero-3-phosocholine (DPPC) containing cholesterol and acetylsalicylic acid

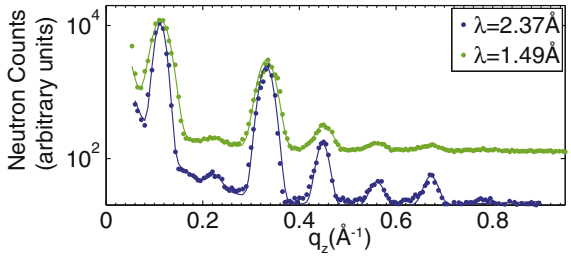

Fig. 6. Neutron reflectivities measured simultaneously with the in-plane data. Results from the typical setup are shown in blue, and results from the high spatial resolution setup are shown in green. The reflectivity shows a series of equally spaced and pronounced reflections, indicative of a well-ordered multi-lamellar membrane structure.

(ASA) were prepared by lipid deposition onto silicon wafers. The coherent scattering of lipid hydrocarbon chains was enhanced using chain perdeuterated lipids, DPPC-d62. A solution of 16.67 mg/mL of DPPC-d62 with 32.5 mol% cholesterol and 10 mol% ASA in 1:1 chloroform and 2,2,2-trifluoroethanol was prepared. 2 inch circular silicon wafers with a thickness of ~300 μm were cleaned with 12 min alternate sonications in methanol and ultrapure water (18.2 MΩ cm) at 310 K. This process was repeated twice. Clean, dry wafers were individually placed on a 4 in. × 4 in. marble block. The marble block was heated to 323 K, well above the main transition temperature of DPPC, ensuring that lipids were well in the fluid state during deposition. 1.2 mL of the lipid solution was deposited on the silicon wafer. Immediately after deposition, the marble block was manually lifted and gently rocked while the bulk of the solution evaporated (~1–2 min), to ensure even coverage of material.

The wafers were kept under vacuum overnight at 310 K to remove all traces of solvent. Nineteen such wafers were then stacked with 0.6 mm alumium spacers placed in between each wafer, to ensure proper hydration control. This "sandwich" sample was then placed inside a sealed container with a beaker of heavy water and placed in an incubator. The temperature of the incubator was increased in discrete steps from 300 K to 323 K over a period of 24 h, then held at 323 K and incubated for additional 24 h. Following this procedure, each wafer contained ~3000 highly oriented stacked membranes with a total thickness of ~10 μm.

During the neutron experiment, the sample was sealed in a temperature controlled aluminium chamber (CNBC, Chalk River, Canada). Hydration of the membranes from the vapor phase was achieved by separately controlling the temperature of a heavy water bath, the sample, and the walls of the chamber. Temperature sensors were installed close to the sample. A circulating water bath was used to control the temperature of the reservoirs and peltier elements were used to control the temperature of the sample and chamber. The sample was mounted vertically in the neutron beam such that the scattering vector, $\vec{Q}$, could

Table 1
Peak parameters of the correlation peaks observed in Fig. 4a) and b) and the association with the observed structures, such as the l_o phase, lipids associated with ASA molecules and the super-lattice driven by the presence of ASA molecules. T_1 denotes the unit cell of the lipid tails in the l_o regions of the membrane. T_{AL} denotes the peak assigned to correlations between lipid molecules when influenced by ASA. Peaks were fitted using Lorentzian peak profiles and the corresponding widths are listed as Lorentzian widths (HWHM), γ_L.

	Amplitude (counts)	Center (Å^{-1})	γ_L (Å^{-1})	l_o	ASA bound lipids	Super-lattice phase
Fig. 4a)	48	1.36	0.14	T_1		
Fig. 4b)	85	0.306	0.01			[1 0 0]
	89	0.406	0.014			[1 1 0]
	50	0.705	0.011			[0 2 0]
	14	1.26	0.14		T_{AL}	

Table 2
Instrumental parameters of the triple-axis spectrometer.

λ (Å)	E (meV)	ΔE (meV)	ΔQ (Å^{-1})
2.37	14.6	0.757	0.020
1.49	37.3	3.239	0.032

either be placed in the plane of the membrane ($q_{||}$) or perpendicular to it (q_z). The out-of-plane and in-plane structures could be measured simply by rotating the sample by 90°.

The lamellar spacing, i.e., the distance between membranes in the stack, d_z, was determined from reflectivity scans. The corresponding out-of-plane or reflectivity scans are shown in Fig. 6, and show a series of pronounced and evenly spaced Bragg peaks indicative of uniform and well developed membrane stacks. Scans were performed with different wavelengths and over the duration of the experiment of two weeks. During the experiment, the bilayer spacing stayed within the range 55.8 Å and 57.9 Å. This setup has been used before to produce fluid DPPC bilayers [20,44] with d_z-spacings in agreement with literature values for fully hydrated bilayers of ~64 Å [20,58]. The observed decrease in lamellar spacing is most likely the effect of the incorporation of ASA in the bilayers, in agreement with the increased fluidification found in the trough and calorimetric experiments. The main transition of DPPC-d62 is reported as 313 K [60,61]. All scans were done with a sample temperature of 323 K, well above the main transition, in the fluid phase of the bilayers.

4.4. Neutron experiment

Experiments were conducted using the N5 triple axis spectrometer at the Canadian Neutron Beam Centre (Chalk River, Canada). The three axis of the spectrometer refer to the axis of rotation of the monochromator, the sample and the analyzer. The incident and final wavelengths were defined by Bragg reflections from pyrolytic graphite (PG) crystals. The divergence of the beam was controlled by Soller collimators. The energy and momentum (Q) resolution, ΔE and ΔQ, of a neutron triple axis spectrometer are determined by: (1) the incident energy of the neutron beam; (2) the divergence of the neutron beam; (3) the wavelength resolution of the monochromator and analyzer crystal. Collimation of the beam was held constant during the experiment and set to ($c1$-$c2$-$c3$-$c4$): 30-18-28-60 (in minutes). Small and large ΔE setups were achieved by varying the incident energy and corresponding neutron wavelength selected by the monochromator.

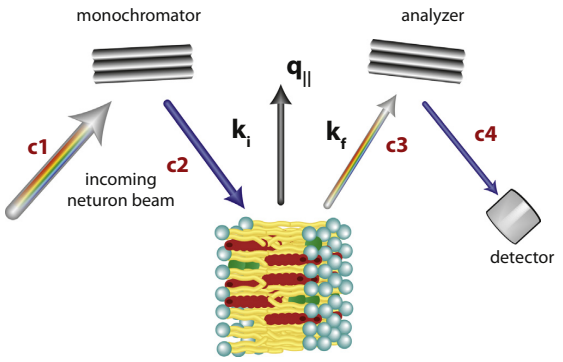

Fig. 7. A diagram of the setup used for the neutron scattering experiment. The orientation of the sample was chosen such that the scattering vector, $\vec{Q}$, lies in the plane of the membrane and is designated $q_{||}$. k_i and k_f are the incident and final neutron wave vectors. The c's indicate the collimation of the neutron beam at various stages. The resolution of the experiment is changed by rotating the monochromating crystal and selecting a different neutron wavelength.

The instrumental parameters for the two setups used in this experiment are listed in Table 2. Energy and Q-resolution (given as FWHM) were calculated using the ResLib software package by A. Zheludev [62] adapted to the N5 spectrometer. The longitudinal coherence length of the neutron beam, ξ, is defined by $\xi = \lambda^2/\Delta\lambda$.

While small collimation was used, the beam size was set to 2 in. by 2 in. to optimally illuminate the silicon wafers, leading to a significant scattering contribution at small Q-values, close to the direct beam. This background was accounted for by a Lorentzian peak centered at $q_{||} = 0$ Å^{-1} including a constant. In contrast to coherent scattering, incoherent scattering is isotropic, *Q*-independent and well accounted for by a constant background at larger *Q*-values of $Q \gtrsim 0.45$ Å^{-1}. After background subtraction, the observed peaks were fit with Lorentzian profiles using a least squares method, and the results plotted in Fig. 4, with the fitting parameters presented in Table 1.

Switching between the high and low energy resolution setups was done by simply changing λ. A smaller neutron wavelength leads to strongly relaxed Δ*Q* and Δ*E*. In addition, the longitudinal coherence length of the neutron beam decreases. The most significant changes between the high and low energy resolution setups are: (1) a more efficient integration over larger $q_{||}$ ranges to enhance small signals; and (2) a reduction of the coherently added scattering volume. A diagram of the scattering geometry for the in-plane measurements is depicted in Fig. 7.

Acknowledgments

This research was funded by the Natural Sciences and Engineering Research Council (NSERC) of Canada, the National Research Council (NRC), the Canada Foundation for Innovation (CFI), and the Ontario Ministry of Economic Development and Innovation. R.J.A. is the recipient of an Ontario Graduate Scholarship, L.T. is the recipient of an NSERC Canada Graduate Scholarship, M.C.R. is the recipient of an Early Researcher Award from the Province of Ontario. D.M. is the recipient of an NSERC Vanier Canada Graduate Scholarship.

References

[1] K. Simons, E. Ikonen, Functional rafts in cell membranes, Nature 387 (1997) 569572.
[2] K. Simons, E. Ikonen, How cells handle cholesterol, Science 290 (2000) 1721–1726.
[3] D.M. Engelman, Membranes are more mosaic than fluid, Nature 438 (2005) 578–580.
[4] L.J. Pike, The challenge of lipid rafts, J. Lipid Res. 50 (2009) S323–S328.
[5] D. Lingwood, K. Simons, Lipid rafts as a membrane-organizing principle, Science 327 (2010) 46–50.
[6] C. Eggeling, C. Ringemann, R. Medda, G. Schwarzmann, K. Sandhoff, et al., Direct observation of the nanoscale dynamics of membrane lipids in a living cell, Nature 457 (2009) 1159–1162.
[7] F.G. van der Goot, T. Harder, Raft membrane domains: from a liquid-ordered membrane phase to a site of pathogen attack, Semin. Immunol. 13 (2001) 89–97.
[8] T. Apajalahti, P. Niemelä, P.N. Govindan, M.S. Miettinen, E. Salonen, et al., Concerted diffusion of lipids in raft-like membranes, Faraday Discuss. 144 (2010) 411–430.
[9] A. Hall, T. Róg, M. Karttunen, I. Vattulainen, Role of glycolipids in lipid rafts: a view through atomistic molecular dynamics simulations with galactosylceramide, J. Phys. Chem. B 114 (2010) 7797–7807.
[10] K. Simons, M.J. Gerl, Revitalizing membrane rafts: new tools and insights, Nat. Rev. Mol. Cell Biol. 11 (2010) 688–699.
[11] J. Ehrig, E.P. Petrov, P. Schwille, Phase separation and near-critical fluctuations in two-component lipid membranes: Monte Carlo simulations on experimentally relevant scales, New J. Phys. 13 (2011) 045019.
[12] T. Murtola, T. Róg, E. Falck, M. Karttunen, I. Vattulainen, Transient ordered domains in single-component phospholipid bilayers, Phys. Rev. Lett. 97 (2006) 238102.
[13] B. Brüning, E. Wald, W. Schrader, R. Behrends, U. Kaatze, Slowing down in lipid bilayers: domain structure fluctuations and axial diffusion, Soft Matter 5 (2009) 3340–3346.
[14] M.C. Rheinstädter, O.G. Mouritsen, Small-scale structure in fluid cholesterol-lipid bilayers, Curr. Opin. Colloid Interface Sci. 18 (2013) 440–447.
[15] J.H. Ipsen, O.G. Mouritsen, M.J. Zuckermann, Theory of thermal anomalies in the specific heat of lipid bilayers containing cholesterol, Biophys. J. 56 (1989) 661–667.
[16] M.R. Vist, J.H. Davis, Phase equilibria of cholesterol/dipalmitoylphosphatidylcholine mixtures: deuterium nuclear magnetic resonance and differential scanning calorimetry, Biochemistry 29 (1990) 451–464.
[17] C.L. Armstrong, M.A. Barrett, A. Hiess, T. Salditt, J. Katsaras, et al., Effect of cholesterol on the lateral nanoscale dynamics of fluid membranes, Eur. Biophys. J. 41 (2012) 901–913.
[18] C.L. Armstrong, W. Häußler, T. Seydel, J. Katsaras, M.C. Rheinstädter, Nanosecond lipid dynamics in membranes containing cholesterol, Soft Matter 10 (2014) 2600–2611.
[19] S. Meinhardt, R.L.C. Vink, F. Schmid, Monolayer curvature stabilizes nanoscale raft domains in mixed lipid bilayers, Proc. Natl. Acad. Sci. U. S. A. 110 (2013) 4476–4481.
[20] C.L. Armstrong, D. Marquardt, H. Dies, N. Kučerka, Z. Yamani, et al., The observation of highly ordered domains in membranes with cholesterol, PLoS ONE 8 (2013) e66162.
[21] A.J. Sodt, M.L. Sandar, K. Gawrisch, R.W. Pastor, E. Lyman, The molecular structure of the liquid-ordered phase of lipid bilayers, J. Am. Chem. Soc. 136 (2014) 725–732.
[22] Y. Zhang, A. Lervik, J. Seddon, F. Bresme, A coarse-grained molecular dynamics investigation of the phase behavior of dppc/cholesterol mixtures, Chem. Phys. Lipids (2014), http://dx.doi.org/10.1016/j.chemphyslip.2014.07.011.
[23] L. Toppozini, S. Meinhardt, C. Armstrong, Z. Yamani, N. Kučerka, et al., The structure of cholesterol in lipid rafts, Phys. Rev. Lett. 113 (2014) 228101.
[24] M. Barrett, S. Zheng, L. Toppozini, R. Alsop, H. Dies, et al., Solubility of cholesterol in lipid membranes and the formation of immiscible cholesterol plaques at high cholesterol concentrations, Soft Matter 9 (2013) 9342–9351.
[25] R. Ziblat, L. Leiserowitz, L. Addadi, Crystalline domain structure and cholesterol crystal nucleation in single hydrated DPPC:cholesterol:POPC bilayers, J. Am. Chem. Soc. 132 (2010) 9920–9927.
[26] R. Ziblat, L. Leiserowitz, L. Addadi, Crystalline lipid domains: characterization by X-ray diffraction and their relation to biology, Angew. Chem. Int. Ed. 50 (2011) 3620–3629.
[27] R. Ziblat, I. Fargion, L. Leiserowitz, L. Addadi, Spontaneous formation of two-dimensional and three-dimensional cholesterol crystals in single hydrated lipid bilayers, Biophys. J. 103 (2012) 255–264.
[28] I. Solomonov, J. Daillant, G. Fragneto, K. Kjaer, J. Micha, et al., Hydrated cholesterol: phospholipid domains probed by synchrotron radiation, Eur. Phys. J. A. 30 (2009) 215–221.
[29] M. Lucio, J. Lima, S. Reis, Drug-membrane interactions: significance for medicinal chemistry, Curr. Med. Chem. 17 (2010) 1795–1809.
[30] L.M. Lichtenberger, Y. Zhou, V. Jayaraman, J.R. Doyen, R.G. O'Neil, et al., Insight into nsaid-induced membrane alterations, pathogenesis and therapeutics: characterization of interaction of nsaids with phosphatidylcholine, Biochim. Biophys. Acta Mol. Cell Biol. Lipids 1821 (2012) 994–1002.
[31] C. Pereira-Leite, C. Nunes, S. Reis, Interaction of nonsteroidal anti-inflammatory drugs with membranes: *in vitro* assessment and relevance for their biological actions, Prog. Lipid Res. 52 (2013) 571–584.
[32] M. Barrett, S. Zheng, G. Roshankar, R. Alsop, R. Belanger, et al., Interaction of aspirin (acetylsalicylic acid) with lipid membranes, PLoS ONE 7 (2012) e34357.
[33] M. Suwalsky, J. Belmar, F. Villena, M.J. Gallardo, M. Jemiola-Rzeminska, et al., Acetylsalicylic acid (aspirin) and salicylic acid interaction with the human erythrocyte membrane bilayer induce *in vitro* changes in the morphology of erythrocytes, Arch. Biochem. Biophys. 539 (2013) 9–19.
[34] L.M. Lichtenberger, Y. Zhou, E.J. Dial, R.M. Raphael, Nsaid injury to the gastrointestinal tract: evidence that nsaids interact with phospholipids to weaken the hydrophobic surface barrier and induce the formation of unstable pores in membranes, J. Pharm. Pharmacol. 58 (2006) 1421–1428.
[35] Y. Zhou, K.J. Cho, S.J. Plowman, J.F. Hancock, Nonsteroidal anti-inflammatory drugs alter the spatiotemporal organization of ras proteins on the plasma membrane, J. Biol. Chem. 287 (2012) 16586–16595.
[36] R.J. Alsop, M.A. Barrett, S. Zheng, H. Dies, M.C. Rheinstädter, Acetylsalicylic acid (asa) increases the solubility of cholesterol when incorporated in lipid membranes, Soft Matter 10 (2014) 4275–4286.
[37] Y. Choi, S.J. Attwood, M.I. Hoopes, E. Drolle, M. Karttunen, et al., Melatonin directly interacts with cholesterol and alleviates cholesterol effects in dipalmitoylphosphatidylcholine monolayers, Soft Matter 10 (2014) 206–213.
[38] P. Wydro, K. Hac-Wydro, Thermodynamic description of the interactions between lipids in ternary Langmuir monolayers: the study of cholesterol distribution in membranes, J. Phys. Chem. B 111 (2007) 2495–2502.
[39] J. Katsaras, K.R. Jeffrey, Evidence of the hydration force in gel phase lipid multibilayers, Europhys. Lett. 38 (1997) 43–48.
[40] D. Marsh, Liquid-ordered phases induced by cholesterol: a compendium of binary phase diagrams, Biochim. Biophys. Acta Biomembr. 1798 (2010) 688–699.
[41] T. Heimburg, Thermal biophysics of membranes, John Wiley & Sons., 2008
[42] J. Jones, L. Lue, A. Saiani, G. Tiddy, Density, DSC, X-ray and NMR measurements through the gel and lamellar phase transitions of 1-myristoyl-2-stearoyl-sn-glycero-3-phosphatidylcholine (MSPC) and 1-stearoyl-2-myristoyl-sn-glycero-3-phosphatidylcholine (SMPC): observation of slow relaxation processes and mechanisms of phase transitions, Phys. Chem. Chem. Phys. 14 (2012) 5452–5469.
[43] A.M. Alaouie, A.I. Smirnov, Formation of a ripple phase in nanotubular dimyristoylphosphatidylcholine bilayers confined inside nanoporous aluminum oxide substrates observed by DSC, Langmuir 22 (2006) 5563–5565.
[44] C.L. Armstrong, M.A. Barrett, L. Toppozini, N. Kučerka, Z. Yamani, et al., Co-existence of gel and fluid domains in single-component phospholipid membranes, Soft Matter 8 (2012) 4687–4694.
[45] C.F. Majkrzak, C. Metting, B.B. Maranville, J.A. Dura, S. Satija, et al., Determination of the effective transverse coherence of the neutron wave packet as employed in reflectivity investigations of condensed-matter structures. I. Measurements, Phys. Rev. A 89 (2014) 033851.
[46] G.J. Roth, N. Stanford, P.W. Majerus, Acetylation of prostaglandin synthase by aspirin, Proc. Natl. Acad. Sci. U. S. A. 72 (1975) 3073–3076.

[47] C. Patrono, L.A. Garca Rodrguez, R. Landolfi, C. Baigent, Low-dose aspirin for the prevention of atherothrombosis, N. Engl. J. Med. 353 (2005) 2373–2383.
[48] V.B. O'Donnell, R.C. Murphy, S.P. Watson, Platelet lipidomics modern day perspective on lipid discovery and characterization in platelets, Circ. Res. 114 (2014) 1185–1203.
[49] S.J. Shattil, R.A. Cooper, Membrane microviscosity and human platelet function, Biochemistry (Mosc) 15 (1976) 4832–4837.
[50] P. Padmavathi, V.D. Reddy, P. Maturu, N. Varadacharyulu, Smoking-induced alterations in platelet membrane fluidity and na+/k+-ATPpase activity in chronic cigarette smokers, J. Atheroscler. Thromb. 17 (2010) 619–627.
[51] K. Gousset, W.F. Wolkers, N.M. Tsvetkova, A.E. Oliver, C.L. Field, et al., Evidence for a physiological role for membrane rafts in human platelets, J. Cell. Physiol. 190 (2002) 117–128.
[52] N. Kučerka, S. Tristram-Nagle, J.F. Nagle, Closer look at structure of fully hydrated fluid phase DPPC bilayers, Biophys. J. 90 (2006) L83–L85.
[53] J. Gallová, D. Uhrková, N. Kučerka, S. Doktorovová, S.S. Funari, et al., The effects of cholesterol and β-sitosterol on the structure of saturated diacylphosphatidylcholine bilayers, Eur. Biophys. J. 40 (2011) 153–163.
[54] M. Lúcio, C. Nunes, D. Gaspar, K. Golebska, M. Wisniewski, et al., Effect of anti-inflammatory drugs in phosphatidylcholine membranes: a fluorescence and calorimetric study, Chem. Phys. Lett. 471 (2009) 300–309.
[55] K. Nag, K. Keough, M. Montero, J. Trias, M. Pons, et al., Evidence of segregation of a quinolone antibiotic in dipalmitoylphosphatidylcholine environment, J. Liposome Res. 6 (1996) 713–736.
[56] A.V. Kityk, M.C. Rheinstädter, K. Knorr, H. Rieger, Aging and memory effects in β-hydroquinone-clathrate, Phys. Rev. B 65 (2002) 144415.
[57] M.C. Rheinstädter, K. Knorr, H. Rieger, Aging and scaling laws in β-hydroquinone-clathrate, Phys. Rev. B 69 (2004) 144427.
[58] T.T. Mills, G.E.S. Toombes, S. Tristram-Nagle, D.M. Smilgies, G.W. Feigenson, et al., Order parameters and areas in fluid-phase oriented lipid membranes using wide angle X-ray scattering, Biophys. J. 95 (2008) 669–681.
[59] M.C. Rheinstädter, C. Ollinger, G. Fragneto, T. Salditt, Collective dynamics in phospholipid bilayers investigated by inelastic neutron scattering: exploring the dynamics of biological membranes with neutrons, Physica B 350 (2004) 136–139.
[60] J. Katsaras, R. Epand, R. Epand, Absence of chiral domains in mixtures of dipalmitoylphosphatidylcholine molecules of opposite chirality, Phys. Rev. E. 55 (1997) 3751.
[61] S. Mabrey, J.M. Sturtevant, Investigation of phase transitions of lipids and lipid mixtures by sensitivity differential scanning calorimetry, Proc. Natl. Acad. Sci. 73 (1976) 3862–3866.
[62] A. Zheludev, Reslib, http://www.neutron.ethz.ch/research/resources/reslib 2009.

4.3 Paper III: Aspirin Locally Disrupts the Liquid Ordered Phaser

Richard J. Alsop, Sebastian Himbert, Karin Schmalzl, and Maikel C. Rheinstädter. *Aspirin Locally Disrupts the Liquid Ordered Phase.* Submitted.

4.3.1 Preface to Paper III

Papers I & II demonstrated that aspirin eliminates structural evidence for cholesterol plaques and rafts, homogenizing membranes with cholesterol. Neutron diffraction suggested that aspirin creates highly localized disorder that frustrates cholesterol organization. Our own Langmuir and DSC experiments, in combination with literature reports, provided evidence that the drug influences bulk dynamical properties. However, what is not clear is if the local structural distortions influence nanoscale collective lipid motions.

Collective motions in lipid membranes are believed to be important for the various membrane functions [74]. Collective fluctuations in membranes encourage passive diffusion of small molecules. Collective motions of proteins and lipids are likely relevant for protein organization and raft formation [75].

Inelastic scattering experiments are required to measure collective motions. Neutrons interact with the phonon-like collective fluctuations of the lipid tails and scatter with a change in energy that can be measured by, *e.g.* a triple axis spectrometer. Neutrons used for inelastic scattering experiments can be tuned to have low coherence length (∼30 Å), and are therefore sensitive to small-scale structure. Our group has measured phonons in membranes with raft concentrations of cholesterol using inelastic neutron scattering [76]. Phonons measured by a set of constant-$q_{||}$ and constant-$\hbar\omega$ scans are placed on a $\hbar\omega$ *vs* $q_{||}$, plot known as a dispersion. A membrane has a characteristic dispersion, as detailed in the paper and *e.g.* [77, 78]. When Armstrong *et al.* measured phonons in membranes with cholesterol, they found that not all observed excitations could be placed on a single dispersion [77]. Three dispersions were necessary, two of which were characteristic of gel and fluid phases, and the third represented the ℓ_o phase. The ℓ_o phase was more ordered than the fluid phase, but softer than the gel phase.

We prepared an analagous system with deuterated DMPC, 29 mol% cholesterol, and 10 mol% aspirin, and measured the corresponding dispersion relation. A membrane with only DMPC-d54 and 32.5 mol% cholesterol was also prepared and measured. Experiments were conducted on the IN12 triple-axis spectrometer at the Institut Laue Langevin, with assistance from instrument scientist Dr. Karin Schmalzl and masters student Sebastian Himbert. Three dispersions were measured that were fit to gel, fluid, and ℓ_o phases. No change to the dynamic properties was observed in gel and fluid phases within the resolution of our experiment. However, two significant changes were detected for the ℓ_o phase: the phonons were seen to be more damped, and required more energy to excite. This indicates the aspirin is suppressing collective motions, but in the ℓ_o phase only.

Molecular Dynamics (MD) simulations were performed to gain an atomistic picture of what

aspirin is doing to the ℓ_o phase. All-atom simulations were performed in-house using MacSim on a united-atom DMPC membrane. Aspirin, in the simulated system caused increased lipid disorder, as expected. It also caused very local increases to A_L, in agreement with the the neutron scattering experiments in Paper II. Interestingly, MD also provided support for the in-plane, superlattice-like ordering of the aspirin in the membrane also observed in Paper II. Finally, there was a hydrogen bonding interaction between aspirin and cholesterol, which presents a truly unexpected finding.

To summarize papers I-III, aspirin has an affinity for the ℓ_o phase and causes local disruptions to the structure that frustrate collective motions. These disruptions alleviate the segregation of cholesterol into dense ordered phases, and this increases cholesterol solubility. The evidence for local disruptions comes from scattering of neutrons with $\sim$20 Å coherence lengths. This case study presents a testimony for how molecules can influence the functional purpose of a membrane. In a phyisological system, eliminating rafts would theoretically impact protein function.

Paper III observed an affinity for the ℓ_o phase specifically. This demonstrates that membrane composition matters for what effects are observed for aspirin. The drug would have different consequences for membranes with cholesterol than without. The membrane therefore tunes the drug's effect. This topic is explored in more detail in the next chapter.

Author Contributions:

- *Experimental Concept:* Richard Alsop, Maikel Rheinstädter
- *Sample Preparation:* Richard Alsop, Maikel Rheinstädter
- *Neutron Experiments:* Richard Alsop, Sebastian Himbert, Karin Schmalzl, Maikel Rheinstädter
- *MD Simulations:* Richard Alsop
- *Data Analysis:* Richard Alsop, Maikel Rheinstädter
- *Manuscript Preparation:* Richard Alsop, Maikel Rheinstädter

Aspirin Locally Disrupts the Liquid Ordered Phase

Richard J. Alsop,[1] Sebastian Himbert,[1] Karin Schmalzl,[2] and Maikel C. Rheinstädter[1,*]

[1] *Department of Physics and Astronomy, McMaster University, Hamilton, Ontario, Canada*
[2] *JCNS, Forschungszentrum Jülich GmbH, Outstation at Institut Laue-Langevin, Grenoble, France*

(Dated: October 23, 2017)

Local structure and dynamics of lipid membranes play an important role in membrane function. The diffusion of small molecules, the curvature of lipids around a protein, and the existence of cholesterol-rich lipid domains (rafts) are important examples for the membrane to serve as a functional interface. The collective fluctuations of lipid tails, in particular, are relevant for diffusion of membrane constituents and small molecules in and across membranes, and for structure and formation of membrane domains. We studied the effect of aspirin (acetylsalicylic acid, ASA) on local structure and dynamics of membranes composed of dimyristoylphosphocholine (DMPC) and cholesterol. Aspirin is a common analgesic, but is also used in the treatment of cholesterol. Using coherent inelastic neutron scattering experiments and Molecular Dynamics simulations, we present evidence that ASA binds to liquid ordered, raft-like domains and disturbs domain organization and dampens collective fluctuations. By hydrogen bonding to lipid molecules, ASA forms 'superfluid' complexes with lipid molecules that can organize laterally in superlattices and suppress cholesterol's ordering effect.

Keywords: Lipid Membranes, Cholesterol, Aspirin, Liquid Ordered Phase, Membrane-Drug Interactions

1. INTRODUCTION

Membrane research progresses with ever-increasing levels of granularity. Initial models of the membrane as an inert, physical barrier were revised with the discovery of membrane-embedded proteins. Singer and Nicholson devised their famous "fluid mosaic" model to describe a system where proteins float in a featureless soup of various lipid types [1]. Most-recently, membrane research has focussed on membrane details on the level of individual lipids and proteins. The lipid environment in the specific region around a protein, such as the hydrophobic thickness or spontaneous curvature of the lipid tails, is now believed to be crucial to proper protein function [2]. Lateral diffusion of membrane constituents [3–7] and transmembrane diffusion of small molecules are believed to involve the local, collective motion of lipid tails [8–11].

Lipid rafts are an example of function arising from nano-scale structure. Rafts are small lipid heterogeneities in plasma membranes [12, 13]. Rafts are typically described as structures that are enriched in cholesterol and exist to chaperone proteins from the golgi apparatus to the plasma membrane surface [14]. Although their existence in biological membranes is still a matter of debate [15], various raft-like structures have been observed in model membranes, and from studies on model membranes, plasma membrane rafts are believed to be manifestations of the so-called liquid-ordered (l_o) phase [12, 16–27]. The l_o phase is unique in that it is characterized by elevated cholesterol concentrations as well as high lipid positional and chain order, however, at the same time low viscosity [28] and high surface tension. It is soft and stiff at the same time by being more rigid than a gel-state membrane, but less viscous than a fluid membrane.

The effect of drug molecules on lipid membranes is typically characterized by their effect on bulk membrane properties, such as mechanical properties and area per lipid head group [29–31], which affect for instance permeability. Drug-membrane interactions can also indirectly influence the function of membrane proteins through their membrane effects, and they also effect membrane heterogeneities [30, 32, 33]. For example, there are numerous reports that the common analgesic aspirin (acetylsalicylic acid, ASA) interacts with the lipid membrane and makes it softer and more fluid, and also impacts the formation of lipid raft structures [34–39]. Neutron scattering experiments recently presented evidence that aspirin creates local structural distortions in the l_o phase in model membranes [30], suppressing the formation of cholesterol clustering.

In this paper, we performed inelastic neutron scattering experiments and molecular dynamics (MD) simulations on membranes containing cholesterol and aspirin. The cholesterol concentration was chosen such that cholesterol rafts form, but well below the solubility limit of cholesterol [40]. We observed that aspirin creates local increases in area per lipid, causing a decrease in positional order and a damping of collective lipid tail fluctuations. We find evidence for 'superfluid' ASA-lipid complexes that organize in the membranes and impact cholesterol's effect on the bilayers. We also present evidence for a direct ASA-cholesterol interaction in membranes through hydrogen bonding of ASA to cholesterol molecules.

* rheinstadter@mcmaster.ca

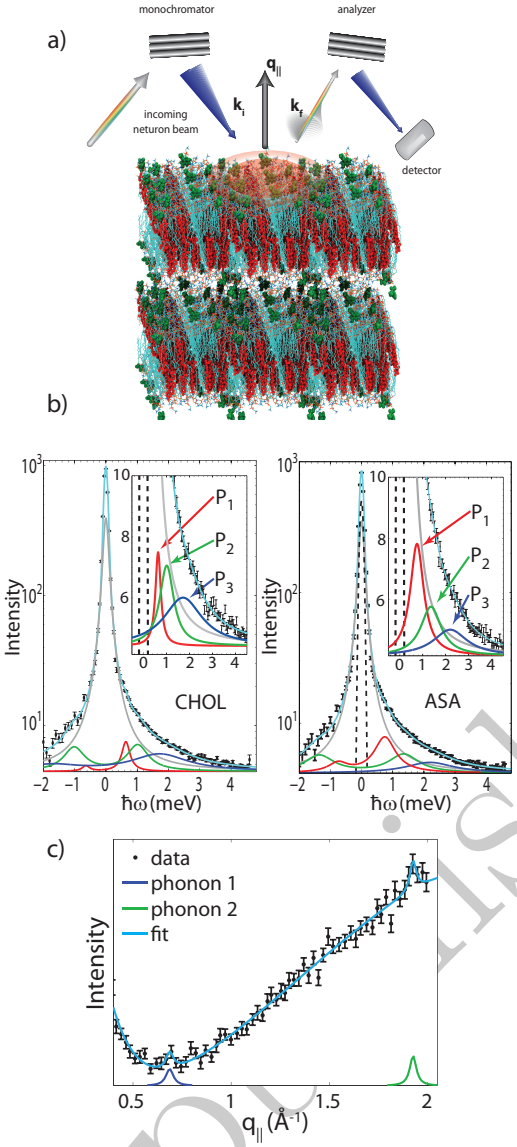

FIG. 1. a) Sketch of the scattering geometry. b) Sample constant-$q_{||}$ scans for the CHOL sample at $q_{||}$=1.37 Å^{-1}. Data was fit using a Gaussian instrumental resolution, a Lorentzian peak centred at $q_{||} = 0$ to capture incoherent scattering contributions, and three phonon excitations. The Gaussian instrumental resolution was fixed to values based on resolutions calculated using the ResLib package. The position of the incoherent peak was fixed at $\hbar\omega = 0$ meV; all other parameters are free. The inset shows that three phonon excitations (P_1, P_2 and P_3) in more detail. c) Constant-energy scan for the ASA sample at an energy of $\hbar\omega$=2.5 meV. All parameters are free in the constant-energy scans.

2. RESULTS

2.1. Inelastic Neutron Scattering

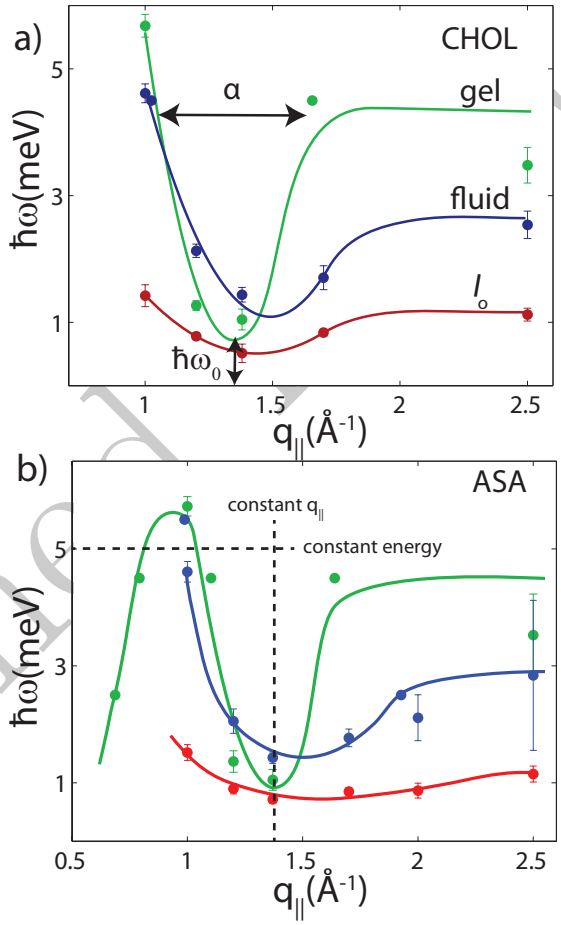

FIG. 2. Dispersion relations for (a) the CHOL sample and (b) the ASA sample, as determined from constand $q_{||}$ and energy scans in Fig. 1. Three dispersion branches were observed, related to lipid molecules in gel (P_β), fluid (L_α) and liquid ordered (l_o) patches. The CHOL dispersion in part a) is in good agreement with previous reports on the collective short-wavelength dynamics in cholesterol-rich lipid membranes [41]. The meaning of the parameters α and $\hbar\omega$ in Eq. (2) are displayed in part a). The direction of constant-$q_{||}$ and constant energy scans is shown in part b).

Coherent, inelastic neutron scattering experiments were performed on oriented DMPC-d54 (1,2-dimyristoyl-sn-glycero-3-phosphocholine) bilayers containing cholesterol and ASA. The lipid chains were selectively deuterated, enhancing the contribution of collective tail dynamics to the signal. In addition, the bilayers were

hydrated with D_2O to reduce incoherent contributions. Two membrane systems were prepared: bilayers with 32.5 mol% cholesterol (CHOL sample), and bilayers with 29 mol% cholesterol and 10 mol% ASA (ASA sample). This cholesterol concentration has been shown to form rafts before and is well below the solubility limit of cholesterol in DMPC of ∼40 mol% [40]. Membranes were prepared by dissolving DMPC, cholesterol, and aspirin in a 1:1 solution of trifluoroethanol/chloroform, at the appropriate molar ratios, and depositing the solution on 1×1 cm^2 silicon wafers. Following drying in vacuum and incubation at 100% relative humidity for 48 hours, highly oriented bilayers are formed [30, 34, 36, 42]. 20 such wafers were prepared and aligned with respect to each other to create a "sandwich sample" with a total mosaicity of $<0.5°$ and a total mass (lipids, cholesterol, aspirin) of 34 mg.

Neutron measurements were performed on the IN12 cold triple-axis spectrometer at the high flux reactor of the Institut Laue-Langevin (ILL) in Grenoble, France. All experiments were conducted at a temperature of 30°C, in the fluid phase of the membranes. The scattering vector $\boldsymbol{Q}$ was placed in the plane of the membranes ($q_{||}$) to measure the static ($S(q_{||})$) and dynamic structure factors ($S(q_{||}, \omega)$). A sketch of the scattering geometry is shown in Fig. 1a).

We note that IN12 was recently upgraded and was used in focussing mode, which significantly increases the neutron intensity at the sample position, however, at the cost of Q and energy resolution. When comparing our results to previous experiments in similar systems by Armstrong *et al.* [41] using a parallel beam configuration on IN12, signals in Q and energy appear slightly broader. In previous experiments, however, 400 mg of material was needed to conduct inelastic experiments while only 34 mg was sufficient to see a clear signal in this paper.

Typical constant-$q_{||}$ scans, taken from the ASA and CHOL samples at $q_{||} = 1.37$ Å^{-1} are shown in Fig. 1b). The constant-$q_{||}$ scans were well fit by analytical functions described by three contributions: the energy resolution of the spectrometer described by a Gaussian peak centred at $\hbar\omega = 0$ meV. The corresponding Gaussian width was calculated using the ResLib software using the geometry of the IN12 spectrometer [**?**]. Secondly, a Lorentzian peak, arising from incoherent molecular motions in the sample, centred at $\hbar\omega = 0$ meV. The remaining scattering contributions were fit by three phonon peaks, positioned at $\hbar\omega \neq 0$. The width of these peaks is proportional to the damping experienced by the collective motions. The overall fitted analytic function also includes a linear background and can be written as:

$$I(q_{||}) = A_{el}\exp(-(q_{||})^2/(2\sigma_{el}^2)) + mq_{||} + b + \sum_{i=1}^{3} \frac{A_{+,i}}{(1+(q_{||}-\mu_i)^2/\sigma_i^2)} + \frac{A_{-,i}}{(1+(q_{||}+\mu_i)^2/\sigma_i^2)} + \frac{A_{incoherent}}{(1+(q_{||})^2/\sigma_{inel}^2)}. \quad (1)$$

Fixed values were used for the position and width of the experimental resolution. The position of the incoherent peak was fixed to $\hbar\omega = 0$ meV. The ration of the amplitudes A_+ and A_- was determined by detailed balance.

A constant-energy scan at an energy of 2.5 meV is shown in Fig. 1c) as an example. Constant-E scans were fit with an empirical exponential background, as well as a broad background Lorentzian peak at $q_{||} \sim 2.5$ Å^{-1}. The background peak arises from convolution of dynamics at higher $q_{||}$ values (see Fig. 9 in the Materials and Methods Section). The position of the phonon branches are determined by the positions of the Lorentzian signals. The positions of phonons observed in both constant-$q_{||}$ and constant-E scans were combined to determine entire dispersion relations, shown in Fig. 2.

Lipid dispersions have been measured previously in inelastic X-ray and neutron scattering experiments [9–11, 41, 43–47] and using MD simulations [46, 48, 49]. All dispersions show similar features: at low-$q_{||}$, the dispersion increases linearly with the slope related to the speed of sound. After reaching a maximum, the dispersion descends into a minimum at $q_{||} = q_T$, where q_T typically agrees well with the position of the chain correlation peak (the maximum in the static structure factor). Finally, the dispersion increases with increasing $q_{||}$ to form a plateau.

The dispersion in the region of the minima can empirically be described by a quadratic function [41]:

$$\hbar\omega = \alpha(q_{||} - q_{||0})^2 + \hbar\omega_0, \quad (2)$$

where $\hbar\omega_0$ is the minimum energy in the dispersion, and α is the width of the dispersion. $\hbar\omega_0$ is related to lipid order, as a lower value indicates better ordered, more "crystal-like" bilayer. α is an empirical measure of the "softness" of the bilayer [41].

As previously observed by Armstrong *et al.*, DMPC membranes containing cholesterol generate collective excitations belonging to three dispersions [41], related to coexisting gel, fluid, and l_o phases. Evidence for this phase coexistence was also observed in the long wavelength fluctuations from neutron spin-echo measurements [28]. Armstrong *et al.* and Toppozini *et al.* later used neutron diffraction and demonstrated that l_o phases coexist in DMPC and DPPC bilayers with cholesterol [26, 27, 41, 50, 51].

Phonons were, therefore, assigned to three different phases. In the CHOL membranes shown in Fig. 2a), the gel phase (green) reaches $\hbar\omega > 5$ meV at $q_{||} = 1$ Å^{-1}, then decreases to an energy minimum of $\hbar\omega \sim 1.2$ meV at $q_{||} \sim 1.4$ Å^{-1}. A second of the phases is observed, with a wider minimum at $\hbar\omega \sim 1.5$ meV (blue), and is assigned to the fluid phase. Finally, a third dispersion is recorded at lower energies, with a minimum $\hbar\omega \sim 0.6$ meV. Armstrong *et al.* assigned the dispersion at low-energy, that is only observed in the presence of cholesterol, to the l_o phase (red).

With the phonons assigned to specific phases, the effect of ASA on the collective motions of each phase is examined. First of all, the damping of the phonons can

	α (meV/$q_{||}^2$)			$\hbar\omega_0$ (meV)		
Dispersion	Armstrong *et al.* (40 mol% chol)	Cholesterol 30 mol%	ASA 10 mol%	Armstrong *et al.* (40 mol% chol)	Cholesterol 30 mol%	ASA 10 mol%
Gel	30.3	41±9	41.6±10	1.80	1.34±0.1	1.35±0.1
Fluid	10.7	14.9±3	17.1±5	2.63	1.49±0.1	1.47±0.1
l_o	6.6	4.8±0.3	3.7±0.9	1.09	0.51±0.02	0.66±0.07

TABLE 1. Results of the fits to Eq. (2). α is a metric of the "stiffness" of the tails on nano-scale distances. ω_0 can be related to the order in the bilayer. Results are compared to Armstrong *et al* [41] for DMPC membranes containing 40 mol% cholesterol. Parameters for the CHOL and ASA samples are also graphed in Fig. 3.

be ascertained from the width of the phonon peak. As described in the Materials and Methods Section, measurements along $q_{||}$=1.37 Å^{-1} represent the truest representation of the phonon widths. An increase in peak width, from ∼0.14 meV to ∼0.31 meV, in the l_o phase is observed in the ASA sample. However, no statistically significant changes to the damping of the fluid or gel phases were observed, as displayed in Fig. 3a).

Eq. (2) was fit to the phonon branches in the region 1.0 Å^{-1} < $q_{||}$ <2.0 Å^{-1}, around the minimum. The fitting parameters are summarized in Table 1 and also plotted in Figs. 3b) and c). When comparing the dispersions from the ASA sample to the CHOL sample, two distinct points become important. First of all, for all structures, there is no statistically significant difference in bilayer softness, α. Secondly, we observe an increase in $\hbar\omega_0$ in the l_o phase for the ASA sample, indicating a decrease in lipid order.

The increase in phonon damping and the decrease in lipid order are compatible with the occurrence of defects in the structure and a fluidification of the l_o phase, as will be discussed below.

2.2. Molecular Dynamics Simulation

To gain an atomistic view of aspirin's effect on the l_o phase, MD simulations of membranes with 30 mol% cholesterol were performed. Simulations were performed on MacSim, a GPU accelerated workstation, using parametrics described previously [52] and also in the Materials and Methods Section. A united-atom DMPC + 30 mol% cholesterol bilayer with 142 lipid + cholesterol molecules, was obtained from Hub *et al.* [53]. The number of water molecules per lipid was adjusted to 25, to mimic typical full-hydration conditions in agreement with the experiment, and the system was simulated for 200 ns. The membranes equilibrated to an area per lipid (DMPC and cholesterol) of A_L=41.1 Å^2, which agrees closely with simulations by Hub *et al.* [53] and the experimentally determined area from Armstrong *et al.* [50]. In addition, the area per DMPC was determined using the GridMAT protocol, and was determined to be 48.6±1 Å^2 [54], slightly smaller than the experimentally determined partial lipid area in membranes containing 32.5 mol% cholesterol [50].

Afterwards, the water in the system was removed and the aspirin was added to the now-dehydrated aqueous phase. Next, all water molecules (25 water molecules per lipid) were replaced and the system was equilibrated using the identical procedure as the pure bilayer. The equilibrated bilayer +aspirin system was then simulated for 200 ns. A snapshot of the simulation is shown in Fig. 4a). The molecules spontaneously embedded in the membrane within 10 ns. The density decomposition of the bilayer with ASA in Fig. 4b) revealed that the molecules partitioned into the lipid head groups at z values of $|z|$ ∼20 Å, in excellent agreement with past experiments [34, 36]. In order to compare the MD simulations with the experiment, Fig. 4c) shows mass density profiles of the bilayers with and without ASA, which take into account the lipid acyl tails and the hydration water molecules, only. As MD simulations are typically conducted in protonated systems, the simulated membranes do no reflect the deuteration labelling of the membranes prepared for the experiment, such that the calculated neutron scattering length density can not directly be compared to the data. The mass density of lipid tails and water molecules shows an at least qualitative agreement with the experimental neutron scattering length density (in Fig. 8c)).

A local change in the area per lipid near ASA molecules was observed. As depicted in Fig. 5a), DMPC molecules within a ∼5 Å radius around an ASA molecule have an area per lipid of >50 Å^2, a 5% increase. As the area per lipid is a common proxy for membrane fluidity [55], these results suggest a local increase in fluidity due to ASA. The proportion of gauche defects in the lipid chains was calculated in Fig. 5b). The presence of ASA did not result in a statistically significant change in the number of tail gauche defects. So while ASA was found to increase *positional disorder*, the proportion of Gauche defects in the lipid tails was found to be unchanged, indicating that ASA did not influence *chain segmental order* [56].

To probe the positional order of the different membrane constituents, radial distribution functions (RDFs) were calculated for DMPC-DMPC correlations. The RDF in Fig. 5c) is proportional to the probability of finding a DMPC tail a distance r from another DMPC tail. A peak at r ∼4.8 Å indicates a lipid tail separation of 4.8 Å, in agreement with diffraction experiments in bilayer systems [41]. The RDF oscillates and decays at increasing r. By fitting an exponential decay to the maxima in the oscillations, a decay constant was extracted from the RDF. This decay constant serves as a proxy for the positional

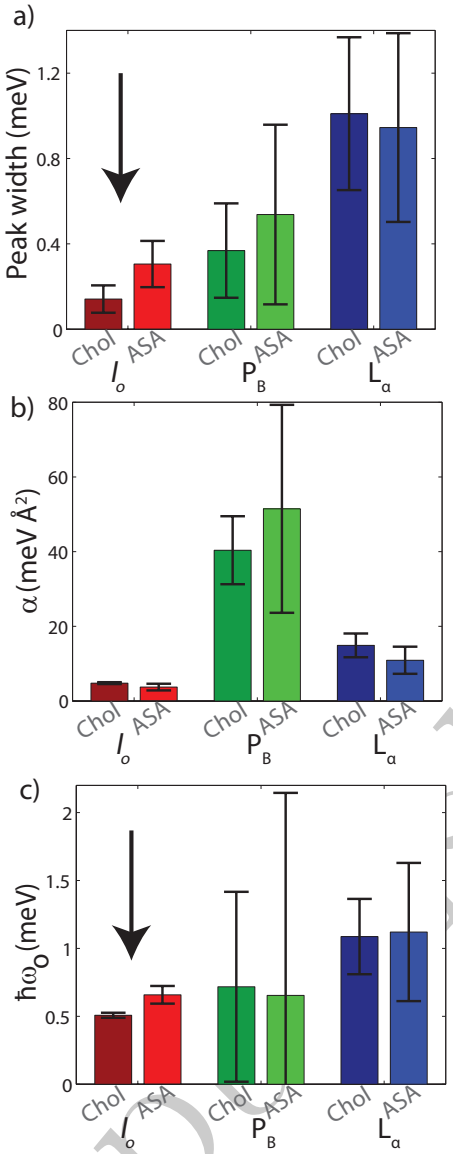

FIG. 3. a) Phonon widths for gel, fluid and l_o phase in Fig. 2 from phonon lines measured at $q_{||} = 1.37$ Å^{-1}. b) Parameters α and $\hbar\omega$ from Eq. (2) from fits to the dispersion curves. Statistically significant differences between CHOL and ASA samples were observed in the phonon width (a) and energy value of the minimum (c) in the l_o phase, only. Statistically significant results are indicated by the arrow.

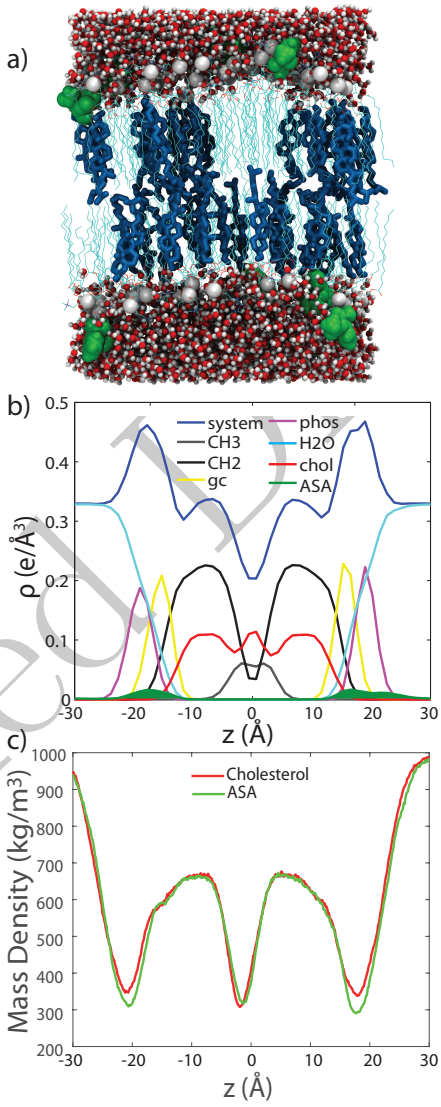

FIG. 4. Results of the Molecular Dynamics (MD) simulations. Simulations were performed for 30 mol% cholesterol in DMPC (CHOL), and the same system with 10 mol% ASA (ASA). a) A snapshot of the ASA simulation. b) An electron density breakdown for the components of the bilayer, indicating the position of ASA (green) is in the head groups at $|z| \sim 20$ Å. c) Mass density profile including lipid acyl tails and hydration water, only. This density can be compared to and is in qualitative agreement with the experimentally determined neutron scattering length density shown Fig. 8c).

order in the system. DMPC correlations were found to decay on a scale of 5 Å. While the lipid-lipid distance appears to be unchanged in the presence of ASA, the correlation length was found to be slightly reduced in the ASA sample, to 4.5 Å. This agrees with a visual inspection of Fig.5c), where the RDF for the ASA sample is observed to decay quicker than the CHOL sample.The

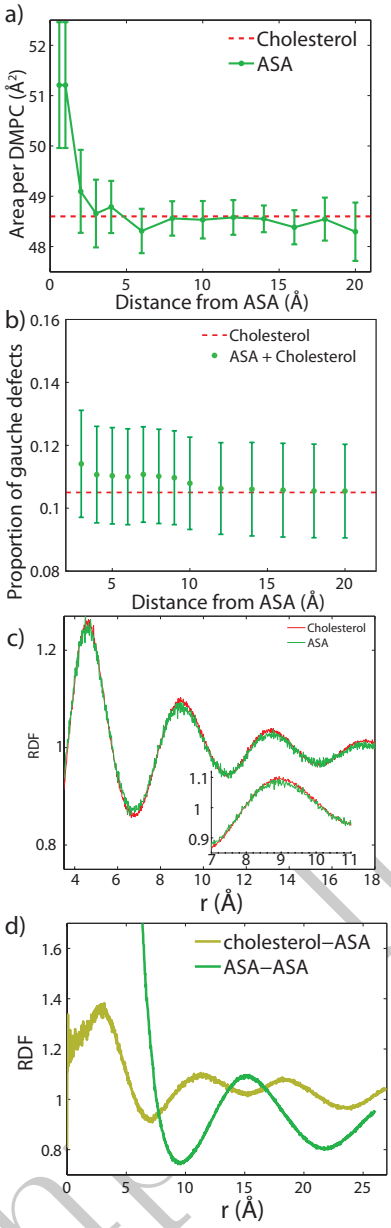

FIG. 5. A) Area per DMPC molecule at increasing distance from an ASA molecule. b) Proportion of gauche defects in the DMPC molecules at increasing distance from ASA. c) Radial distribution function (RDF) for DMPC-DMPC correlations, taken from both CHOL and ASA simulations. d) RDF for cholesterol-ASA and ASA-ASA interactions.

simulations, therefore, record increased positional disorder with ASA.

The simulations can in particular be used to search for correlations between cholesterol and ASA and ASA-ASA molecules. The cholesterol-ASA RDF is plotted in Fig. 5d). This function probes potential organization between cholesterol and ASA molecules in the bilayers. Peaks appear at r ∼11.5 Å and 19 Å, indicating a preferred separation between ASA and cholesterol. Peaks are observed at length scales larger than a lipid-lipid distance, suggesting superlattice ordering, as it has been suggested previously [30]. This ordering is further supported by the ASA-ASA RDF, also plotted in Fig. 5d). A maximum is observed at 15 Å as is a second peak is just outside the measurement frame at 25 Å. Both peaks are compatible with a superlattice of lipid-ASA complexes, as will be discussed in the next section.

We note that an additional peak in the choesterol-ASA RDF at $|r|$ ∼3 Å was observed. This was an important finding as on visual inspection of the simulation results, ASA molecules were found to transiently hydrogen bond with cholesterol molecules, without embedding in the bilayer.

3. DISCUSSION

Much literature exists showing that ASA has a disordering effect on membranes [30, 34, 37, 57]. This disordering effect is for instance used to explain how aspirin disrupts proteins embedded in lipid rafts [58]. So far, studies of drug-membrane interactions have mainly focussed on bulk, global changes in membrane properties due to drugs, such as changes in phase behaviour (a decrease or broadening in the gel-fluid transition), or an overall change in bilayer thickness. However, physiological membranes are dynamic and heterogeneous, and their nano-scale properties, such as lipid curvature near a protein or the presence of domains, matter to the membrane's function. In this paper, we used neutron scattering and MD simulations to demonstrate that ASA preferably interacts with the cholesterol rich l_o phase and leads to local changes in the lipid arrangement and collective fluctuations.

ASA is known to partition into the lipid head groups and decrease lamellar spacing and widen the main transition in calorimetry experiments. Dispersion curves of the collective short-wavelength dynamics were measured in DMPC bilayers containing cholesterol and cholesterol and ASA. As was reported previously, the inelastic spectra present evidence for three dispersion branches, corresponding to lipids in their gel, fluid and liquid ordered phase. By fitting an empirical function to the dispersion minimum, the degree of order and the softness of the corresponding phases were estimated from the depth of the minimum ($\hbar\omega_0$) and the width of the dispersion in the minimum (α). The only statistically significant difference was observed in the energy value of the minimum. The increase in $\hbar\omega_0$ in the presence of ASA was assigned to a decrease in lipid order when ASA was present in the membranes. The decrease in order was accompanied

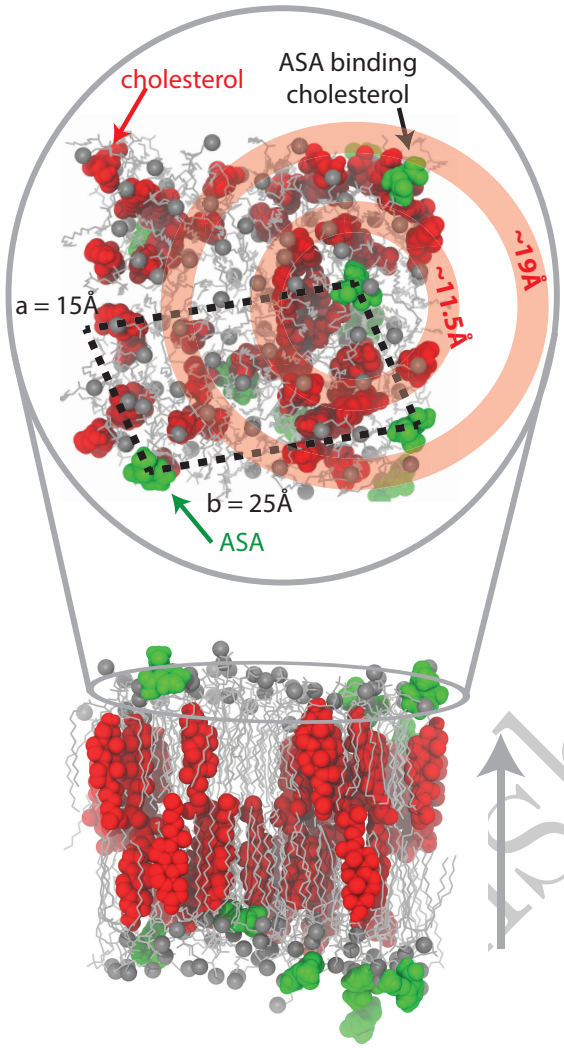

FIG. 6. A simulation snapshot that captures the main points of the paper. The upper panel is an overhead view (along q_z). The black dashed lines indicate the lateral separation of ASA into a lattice-like structure. The concentric red circles, centred on ASA, illustrate that cholesterol molecules prefer to be at regular distances from ASA.

by an increase in phonon line width, indicative of an increased phonon damping, likely related to the formation of defects.

Our experiments, therefore, present evidence that aspirin has the largest effect on l_o phases, where it reduces the size of coherently coupled patches [4] and makes the l_o phase overall more fluid. These observations are compatible with the idea that ASA forms superfluid complexes with lipid molecules, that act as defects in the otherwise well ordered l_o phase, as has been proposed by Alsop *et al.* using neutron diffraction [30]. It has been suggested that these complexes can organize throughout the l_o and form a superlattice-type structure in membranes with cholesterol and aspirin. The lattice spacing of this 2-dimensional structure was reported as a =21.2 Å, b =18 Å, $\gamma = 103°$. In addition, lipid-aspirin complexes were observed where aspirin caused local increases in the area-per-lipid. The authors proposed that ASA interacted with the l_o phase to create fluid patches and that these patches organize in the membranes and suppress cholesterol raft formation.

In experiments using highly monochromatic beams, such as synchrotron X-rays, local structure much smaller than the coherence length will be averaged with the surrounding membrane [27, 50, 51, 59]. In a membrane at high coherence length, non-raft regions dominate in a diffraction measurement. By shrinking the coherence length of the X-ray or neutron probe, the scattering signal becomes an incoherent sum of many smaller coherent averages, giving more weight to the smaller scale structure. The longitudinal coherence length of a neutron beam, ξ, is defined by $\xi = \lambda^2/\Delta\lambda$ [60]. ξ has been estimated to $\xi = \sqrt{E}/\Delta E$ [50], where E is the energy of the neutron beam, and ΔE the energy distribution. In a typically monochromatic diffraction experiment, ΔE is small, making ξ large. Alsop *et al.* used a setup with a low beam monochromaticity in their diffraction experiments to observe small, local structures in membranes with ASA and cholesterol with a coherence length, ξ, in the order of ∼30 Å. The coherence length in our *inelastic* experiments is estimated to $\xi = 18\sqrt{5}/1.5$ ∼30 Å (with the energy of the incident neutrons of ∼5 meV measuring an excitation at ∼1.5 meV). This value is comparable to the above diffraction experiments and also other inelastic neutron experiments in membranes [4]. We, therefore, argue that inelastic neutron scattering experiments can provide information about local structures in membranes.

Details of the molecular structure is assessed using our MD simulations. Lipid molecules in close proximity to ASA molecules were found to be more fluid, showing an increasing area per lipid and decreased positional order. ASA and cholesterol molecules are surprisingly well organized, with well defined nearest neighbour distances. A snapshot of the structure of the membranes containing cholesterol and ASA from MD simulations is shown in Fig. 6. Here, the ASA/lipid complexes indeed form superlattices in the membrane plane with dimensions of 15 Å × 25 Å, in very good agreement with the experimentally determined dimensions. The peaks in the cholesterol-ASA RDF at 11.5 Å and 19 Å are roughly positioned at the minima in the ASA-ASA RDF, indicating that the cholesterol prefers to be in the lattice at positions not occupied by ASA.

An interesting question is why aspirin seems to be preferably attracted to l_o phases. It has been shown that ASA increases the solubility of cholesterol in lipid membranes [36] and has an effect on cholesterol rich lipid

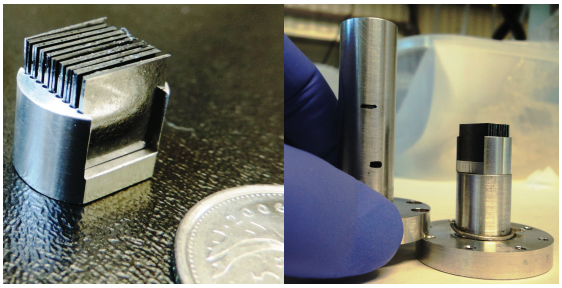

FIG. 7. Photographs of the silicon wafers with highly oriented membranes. Wafers were mounted in the sample holder, custom manufactured for the IN12 cryostat. The water reservoir in the bottom of the can was filled with D_2O to ensure hydration of the membranes during the elastic and inelastic scans. Sample can was sealed and mounted in an orange cryostat for temperature control (±0.01°C).

rafts [30]. Aspirin's affinity to l_o phases has recently also been demonstrated in human red blood cell plasma membranes [38]. This affinity could be entropy driven, as ASA increases the fluidity of membranes and enhances lipid tail fluctuations. However, our results point to a free energy argument as the MD simulations also show evidence for ASA molecules hydrogen bonding to cholesterol molecules. To the best of our knowledge, this is the first report of a direct interaction between ASA and cholesterol molecules in lipid bilayers.

4. CONCLUSION

By combining coherent, inelastic neutron scattering experiments and Molecular Dynamics simulations, we investigated the effect of ASA on the liquid ordered phase in phospholipid membranes. ASA was found to preferably bind to the liquid ordered, raft-like domains. The dynamical experiments present evidence that ASA makes the l_o phase more fluid by creating local defects. From MD simulations there is evidence that the ASA molecules form superfluid complexes by hydrogen bonding to lipid molecules, which organize laterally in superlattices and suppress cholesterol's ordering effect. There is also evidence for ASA molecules directly hydrogen bonding to cholesterol molecules in the bilayers. Our results are in agreement with previous observations in the literature and provide a molecular mode-of-action for aspirin's known effect on membrane cholesterol.

5. MATERIALS AND METHODS

5.1. Membrane Preparation

Highly oriented multi-lamellar stacks of 1,2-dimyristoyl-sn-glycero-3-phosphocholine (DMPC), cholesterol, and ASA were prepared on 1 cm × 1 cm, 300 μm thick, single-side polished Si wafers. The coherent scattering of the lipid hydrocarbon chains was enhanced by using tail deuterated DMPC-d54. A 20 mg/mL solution of DMPC-d54 1:1 chloroform and 2,2,2-trifluoroethanol (TFE) was prepared. Solutions of chloroform and ASA were also prepared in TFE:chloroform. DMPC, cholesterol, and ASA were then mixed to achieve the desired molecular concentrations.

The Si wafers were cleaned with 30 minute sonications in dichloromethane (DCM) at 310 K to remove all organic contamination and leave the substrates in a hydrophobic state. The wafers were then thoroughly rinsed three times using alternating ∼50 mL of ultrapure water and methanol. The cleaned wafers were placed on a heated sample preparation surface, which was kept at 40°C (313 K). This temperature is above the main phase transition of DMPC, thus the heated substrates ensured that the lipids were in the fluid phase during deposition and the self-assembly of the lipids. 80 μL of the lipid solution was deposited on each Si wafer in a titling incubator, which was set to a speed of 15 rev/min and tilt of 10 degrees, such that the lipid solution spread evenly across the wafer. The temperature was kept at 313 K and the solvent was allowed to slowly evaporate for 10 min. The wafers were kept in vacuum overnight to remove all traces of the solvent and then incubated with heavy water, D_2O, at 313 K for 48 h. Following this protocol, each wafer contained ∼3000 highly oriented membranes totally ∼10 μm in thickness.

Eighteen sample-containing Si wafers were mounted in an aluminium sample holder fabricated to be inserted into IN12's orange cryostat. A photo of the sample and the aluminum sample holder is shown in Figures 7. Hydration of the lipid membranes from the vapour phase was achieved by a D_2O reservoir in the bottom of the sample can. The samples were mounted vertically in the neutron beam such that the scattering vector ($\mathbf{Q}$) could either be placed in the plane of the membrane ($q_{||}$), or perpendicular to the membrane(q_z).

5.2. Neutron Scattering

Experiments were conducted using the cold triple-axis spectrometer IN12 at the high flux reactor at the Institut Laue-Langevin in Grenoble, France. Two instrumental setups were used: 1) A lower resolution setup with k_f = 1.5 Å^{-1} and λ = 4.2 Å resulting in an energy resolution of ∼0.3 meV; and 2) A higher resolution setup with k_f = 1.1 Å^{-1} and λ = 5.71 Å resulting in an energy resolution of ∼0.2 meV. The higher resolution setup was implemented at $q_{||}$ = 1.37 Å^{-1} to verify the presence of three phonon peaks. The three axis of the spectrometers refer to the axes of rotation of the monochromator, the sample and the analyzer. The incident and final neutron energies are defined by the Bragg reflections from py-

Sample	d_z (Å)	d_{HH} (Å)	A_T (Å^2)
Cholesterol	61.1	46.0	23.9
ASA	60.6	45	24.4

TABLE 2. Structural parameters determined from neutron diffraction.

rolytic graphite (PG) crystals. In-plane and out-of-plane structure can be measured simultaneously on a TAS by simply rotating the sample by 90°.

5.1. Elastic Scattering

Elastic neutron scattering scans were taken along q_z ($q_{||} = 0$) and $q_{||}$ ($q_z = 0$) to measure the static structure of the bilayers. Scans along q_z (Fig. 8a)) observe a series of Bragg peaks, evenly separated by Δq_z, indicating well-ordered and lamellar samples. The lamellar spacing is calculated by $d_z = \frac{2\pi}{\Delta q_z}$. We obtained $d_z = 61.1$ Å for the cholesterol sample and $d_z = 60.6$ Å for the ASA sample, which agrees with previous reports of a decrease in d_z for membrane samples with ASA [34, 36].

By integrating the lamellar peaks, the neutron scattering length densities (SLDs), $\rho_{z(n)}$. The density is calculated using:

$$\rho_{z(n)} = \sum_{n=1}^{N} \sqrt{I_n q_n} \nu_n \cos(\frac{2\pi z}{d_z}), \quad (3)$$

where I_n are the integrated peak intensities, q_n the peak positions, and ν_n the Fourier phases, which are ± 1 for the stacked membrane systems. The phases for both samples are taken from Armstrong *et al.* and are [1 −1 −1 −1 −1 1 1 −1 1] [41]. The resulting densities are shown in Fig. 8c) on a relative scale. Unlike bilayer electron density profiles, neutron densities, for bilayers with deuterated chains, show a minima in the headgroups at $|z|$ ∼20 Å. The scattering length densities are maximum in the tails at $|z|$ ∼10 Å and at the edge of the bilayer, $|z|=d_z/2$, where deuterated water and tails contribute. The position of the minima at $|z|$ ∼20 Å is used to determine the bilayer head-head spacing, d_{HH}. In the cholesterol sample, d_{HH} was determined to d_{HH} = 46 Å and reduced to 45 Å for the ASA sample.

Elastic scans along $q_{||}$ measure the in-plane lipid structure, and are displayed in Fig. 8b). For both samples, a single intense peak is observed, associated with lipid tail correlations, at $q_{||}$ ∼1.37 Å^{-1}. Additional, smaller peaks are observed at $q_{||}$ ∼1.25 Å^{-1}, $q_{||}$ ∼1.7 Å^{-1} and 1.95 Å^{-1} associated with higher-order scattering of silicon and aluminum [30].

While the area-per-lipid is not directly accessible by in-plane scattering, the area-per-tail is calculated from q_T by $A_T = \frac{8\pi^2}{\sqrt{3} q_T^2}$. $A_T = 23.9$ Å^2 for the cholesterol sample and $A_T = 24.2$ Å^2 for the ASA sample, a slight increase.

5.2. Resolution Considerations

The phonon peak width in the constant-$q_{||}$ energy scans is associated with phonon damping in the damped harmonic oscillator model. However, the width of the peak is not just a sample feature, but is convoluted with the instrumental resolution function. For a triple-axis spectrometer, this resolution function takes the form of a tilted elipsoid in the energy-momentum plane, where any excitation within the ellipsoid is recorded. A cartoon of the elipsoid on a lipid dispersion is in Fig. 9. When this ellipsoid intersects a region on the dispersion with high-slope the effect is to make peaks appear broader. Therefore, at the minima in the dispersion, where the slope is zero, a constant-$q_{||}$ scan would produce a peak width closest to the true width.

5.3. Molecular Dynamics Simulations

All simulations were run in-house on MacSim, a GPU accelerated workstation with 20 physical Intel XeonCPU cores and two GeForce GTX 1080 high power graphics cards resulting in 5120 CUDA Cores. This system produces about 180 ns of MD simulations in standard 128 lipid membrane patches in GROMACS.

A united-atom, DMPC + 30 mol% cholesterol bilayer with 142 lipid + cholesterol molecules, was obtained from Hub *et al.* [53]. Aspirin topology was obtained using the Automated Force Field Topology Builder (ATB) [61, 62]. The SPC water model was used for system solvation [63]. All MD simulations were performed using the GROMACS 5.1.2 software package [64], implementing the GROMOS 54a7 force field [65] modified with Berger lipid parameters [66]. All simulations used a 2 fs time step, a periodic boundary condition applied to all directions, the particle-mesh Ewald to solve for long-range electrostatics [67], a short-range van der Waals cutoff of 1.2 nm, and the LINCS algorithm to determine bond constraints [68]. Temperature coupling was controlled using a Nose-Hoover thermostat at 28°C ($\tau = 0.5$ ps) [69], and pressure was kept at 1.0 bar using Parrinello-Rahman semi-isotropic weak coupling ($\tau = 1$ ps) [70].

A total of two distinct simulations were conducted. First, the DMPC+cholesterol system is equilibrated with 25 waters per lipid for 200 ns. . Next, the a bilayer system with 10 mol% aspirin was prepared, in a three-step process. First, all water in the system was removed, and the aspirin added to the now empty space outside the bilayer. Second, all water (25 per lipid) was replaced in the system. Finally, the system was re-equilibrated and then simulated for 200 ns. All analyses were performed with the final 50 ns of the simulations using GROMACS algorithms and simple scripts [71]. The electron density profiles were calculated for different constituents of the system. The function used calculates the relative distance along the bilayer normal of each atom within the specified index group, assigns a weighting based upon the

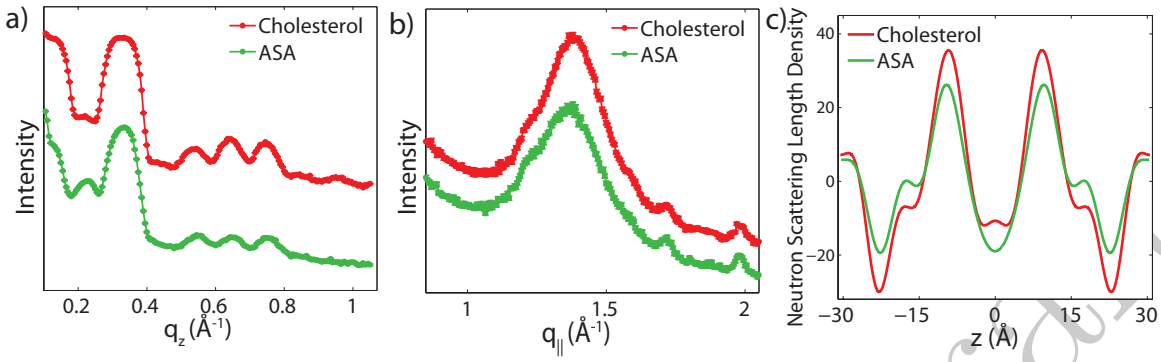

FIG. 8. Results of elastic neutron scattering. a) Out-of-plane neutron reflectivities along q_z. Both the cholesterol and ASA samples show a set of ∼7 evenly spaced Bragg peaks. b) In-plane elasic scattering along $q_{||}$. A broad feature is observed at $q_{||} \sim 1.37$ Å^{-1}. Additional reflections are associated with higher-order reflections of silicon. c) Relative neutron scattering length densities assembled by Fourier analysis of the q_z peaks.

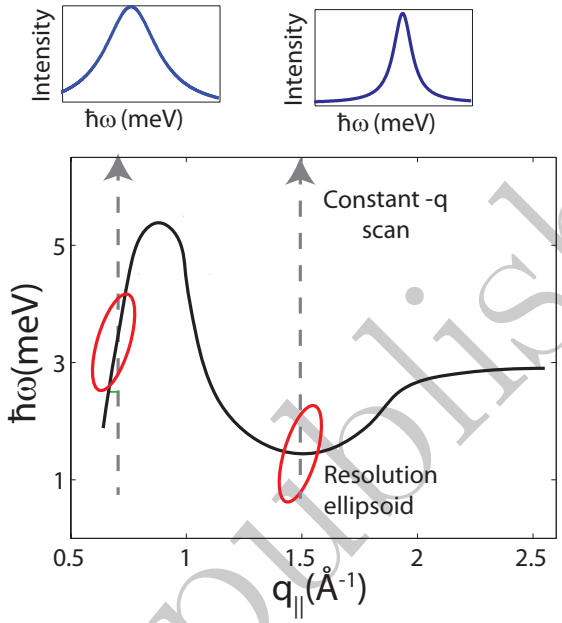

FIG. 9. Lipid dispersion and instrumental resolution. The lipid dispersion is drawn schematically. During a constant-$q_{||}$ scan, the resolution ellipsoid is moved across the dispersion to detect the corresponding excitations. The smallest peak width in the spectra is observed when the dispersion is cut perpendicular, in the minimum of the dispersion relation.

number of electrons in each atom, and delivers an electron density as averaged over the specified time range.

The proportion of gauche dihedrals within a lipid system is commonly used as a measure of bilayer fluidity [72–74]. The proportion of gauche dihedrals as a function of increasing distance from aspirin was determined using dynamic scripting and GROMACS algorithms. A script was constructed to generate an index file containing only carbon chains belonging to lipids within the specified radius from the center of mass of any aspirin molecule within the system every 50 frames. This index file specified the DMPC molecules whose carbons were to be used in calculation of the Ryckaert-Bellemans dihedral angles over that time interval. This was repeated over the final 50 ns of the simulation and averaged for each carbon position. Averaging across the SN1 and SN2 tails was then performed to generate the value shown in Fig. 5d) and h), and the script was run successively to consider each new distance from aspirin.

RESEARCH ETHICS

Does not apply

DATA AVAILABILITY

All data are included in the manuscript.

AUTHORS' CONTRIBUTIONS

RJA conceived and designed the study, prepared membrane samples for the neutron experiments, conducted the experiment, analyzed the data and conducted and analyzed the MD simulations, and wrote the manuscript; SH collected and analyzed data; KS conceived of the study, coordinated and conducted the neutron experiment and analyzed data; MCR conceived of the study, designed the study, coordinated the study, analyzed data

and wrote the manuscript. All authors gave final approval for publication.

COMPETING INTERESTS

The authors declare no competing interests

FUNDING

This research was funded by the Natural Sciences and Engineering Research Council of Canada (NSERC), the National Research Council Canada (NRC), the Canada Foundation for Innovation (CFI) and the Ontario Ministry of Economic Development and Innovation. R.J.A. is the recipient of an NSERC PGS-D scholarship. M.C.R. is the recipient of an Early Researcher Award of the Province of Ontario and a University Scholar Award from McMaster University.

[1] SJ Singer and Garth L Nicolson, "The fluid mosaic model of the structure of cell membranes," Membranes and Viruses in Immunopathology; Day, SB, Good, RA, Eds , 7–47 (1972).

[2] Andrew Callan-Jones, Benoit Sorre, and Patricia Bassereau, "Curvature-driven lipid sorting in biomembranes," Cold Spring Harbor perspectives in biology **3**, a004648 (2011).

[3] Emma Falck, Tomasz Róg, Mikko Karttunen, and Ilpo Vattulainen, "Lateral diffusion in lipid membranes through collective flows," Journal of the American Chemical Society **130**, 44–45 (2008).

[4] Maikel C Rheinstädter, Jhuma Das, Elijah J Flenner, Beate Brüning, Tilo Seydel, and Ioan Kosztin, "Motional coherence in fluid phospholipid membranes," Physical review letters **101**, 248106 (2008).

[5] Sebastian Busch, Christoph Smuda, Luis Carlos Pardo, and Tobias Unruh, "Molecular mechanism of long-range diffusion in phospholipid membranes studied by quasielastic neutron scattering," Journal of the American Chemical Society **132**, 3232–3233 (2010).

[6] CL Armstrong, M Trapp, J Peters, T Seydel, and MC Rheinstädter, "Short range ballistic motion in fluid lipid bilayers studied by quasi-elastic neutron scattering," Soft Matter **7**, 8358–8362 (2011).

[7] Clare L Armstrong, Laura Toppozini, Hannah Dies, Antonio Faraone, Michihiro Nagao, and Maikel C Rheinstädter, "Incoherent neutron spin-echo spectroscopy as an option to study long-range lipid diffusion," ISRN Biophysics **2013** (2013).

[8] Stefan Paula, AG Volkov, AN Van Hoek, TH Haines, and David W Deamer, "Permeation of protons, potassium ions, and small polar molecules through phospholipid bilayers as a function of membrane thickness," Biophysical journal **70**, 339–348 (1996).

[9] MC Rheinstädter, C Ollinger, G Fragneto, F Demmel, and T Salditt, "Collective dynamics of lipid membranes studied by inelastic neutron scattering," Physical review letters **93**, 108107 (2004).

[10] Martin D Kaye, Karin Schmalzl, Valeria Conti Nibali, Mounir Tarek, and Maikel C Rheinstädter, "Ethanol enhances collective dynamics of lipid membranes," Physical Review E **83**, 050907 (2011).

[11] Mikhail Zhernenkov, Dima Bolmatov, Dmitry Soloviov, Kirill Zhernenkov, Boris P Toperverg, Alessandro Cunsolo, Alexey Bosak, and Yong Q Cai, "Revealing the mechanism of passive transport in lipid bilayers via phonon-mediated nanometre-scale density fluctuations," Nature communications **7** (2016).

[12] Richard J Alsop and Maikel C Rheinstädter, "Lipid rafts in binary lipid/cholesterol bilayers," in *Membrane Organization and Lipid Rafts in the Cell and Artificial Membranes*, Series on Cell Biology Research Progress, edited by A. Catalá (Nova, 2016) pp. 17–42, ISBN: 978-1-63484-589-2.

[13] Daniel Lingwood and Kai Simons, "Lipid rafts as a membrane-organizing principle," Science **327**, 46–50 (2010).

[14] Kai Simons and Elina Ikonen, "Functional rafts in cell membranes," Nature **387**, 569 (1997).

[15] Kai Simons and Mathias J Gerl, "Revitalizing membrane rafts: new tools and insights," Nature reviews Molecular cell biology **11**, 688–699 (2010).

[16] Philip L Yeagle, "Lanosterol and cholesterol have different effects on phospholipid acyl chain ordering," Biochimica et Biophysica Acta (BBA)-Biomembranes **815**, 33–36 (1985).

[17] Ole G Mouritsen and Kent Jørgensen, "Dynamical order and disorder in lipid bilayers," Chemistry and physics of lipids **73**, 3–25 (1994).

[18] Ole G Mouritsen and Kent Jørgensen, "Small-scale lipid-membrane structure: simulation versus experiment," Current opinion in structural biology **7**, 518–527 (1997).

[19] Michael C Pitman, Frank Suits, Alexander D MacKerell, and Scott E Feller, "Molecular-level organization of saturated and polyunsaturated fatty acids in a phosphatidylcholine bilayer containing cholesterol," Biochemistry **43**, 15318–15328 (2004).

[20] Ole G Mouritsen and Martin J Zuckermann, "What's so special about cholesterol?" Lipids **39**, 1101–1113 (2004).

[21] Ken Jacobson, Ole G Mouritsen, and Richard GW Anderson, "Lipid rafts: at a crossroad between cell biology and physics," Nature cell biology **9**, 7–14 (2007).

[22] Tomasz Róg, Marta Pasenkiewicz-Gierula, Ilpo Vattulainen, and Mikko Karttunen, "Ordering effects of cholesterol and its analogues," Biochimica et Biophysica Acta (BBA)-Biomembranes **1788**, 97–121 (2009).

[23] Linda J Pike, "The challenge of lipid rafts," Journal of lipid research **50**, S323–S328 (2009).

[24] Christian Eggeling, Christian Ringemann, Rebecca Medda, Günter Schwarzmann, Konrad Sandhoff, Svetlana Polyakova, Vladimir N Belov, Birka Hein, Claas von Middendorff, Andreas Schönle, *et al.*, "Direct observation of the nanoscale dynamics of membrane lipids in a living

cell," Nature **457**, 1159 (2009).

[25] Ole G Mouritsen, "The liquid-ordered state comes of age," Biochimica et Biophysica Acta (BBA)-Biomembranes **1798**, 1286–1288 (2010).

[26] Maikel C Rheinstädter and Ole G Mouritsen, "Small-scale structure in fluid cholesterol–lipid bilayers," Current opinion in colloid & interface science **18**, 440–447 (2013).

[27] Laura Toppozini, Sebastian Meinhardt, Clare L Armstrong, Zahra Yamani, Norbert Kučerka, Friederike Schmid, and Maikel C Rheinstädter, "Structure of cholesterol in lipid rafts," Physical review letters **113**, 228101 (2014).

[28] Clare L Armstrong, Wolfgang Häußler, Tilo Seydel, John Katsaras, and Maikel C Rheinstädter, "Nanosecond lipid dynamics in membranes containing cholesterol," Soft matter **10**, 2600–2611 (2014).

[29] Cláudia Nunes, Gerald Brezesinski, Catarina Pereira-Leite, José LFC Lima, Salette Reis, and Marlene Lúcio, "Nsaids interactions with membranes: a biophysical approach," Langmuir **27**, 10847–10858 (2011).

[30] Richard J Alsop, Laura Toppozini, Drew Marquardt, Norbert Kučerka, Thad A Harroun, and Maikel C Rheinstädter, "Aspirin inhibits formation of cholesterol rafts in fluid lipid membranes," Biochimica et Biophysica Acta (BBA)-Biomembranes **1848**, 805–812 (2015).

[31] Hannah Dies, Bonnie Cheung, Jennifer Tang, and Maikel C Rheinstädter, "The organization of melatonin in lipid membranes," Biochimica et Biophysica Acta (BBA)-Biomembranes **1848**, 1032–1040 (2015).

[32] Axel Schmidt, Pia Lenzig, Adrienne Oslender-Bujotzek, Jana Kusch, Susana Dias Lucas, Stefan Gründer, and Dominik Wiemuth, "The bile acid-sensitive ion channel (basic) is activated by alterations of its membrane environment," PloS one **9**, e111549 (2014).

[33] Jens A Lundbæk, Roger E Koeppe, and Olaf S Andersen, "Amphiphile regulation of ion channel function by changes in the bilayer spring constant," Proceedings of the National Academy of Sciences **107**, 15427–15430 (2010).

[34] Matthew A Barrett, Songbo Zheng, Golnaz Roshankar, Richard J Alsop, Randy KR Belanger, Chris Huynh, Norbert Kučerka, and Maikel C Rheinstädter, "Interaction of aspirin (acetylsalicylic acid) with lipid membranes," PLoS One **7**, e34357 (2012).

[35] Alexandr Nasedkin, Jan Davidsson, and Mont Kumpugdee-Vollrath, "Determination of nanostructure of liposomes containing two model drugs by x-ray scattering from a synchrotron source," Journal of synchrotron radiation **20**, 721–728 (2013).

[36] Richard J Alsop, Matthew A Barrett, Songbo Zheng, Hannah Dies, and Maikel C Rheinstädter, "Acetylsalicylic acid (asa) increases the solubility of cholesterol when incorporated in lipid membranes," Soft Matter **10**, 4275–4286 (2014).

[37] Lenard M Lichtenberger, Yong Zhou, Elizabeth J Dial, and Robert M Raphael, "Nsaid injury to the gastrointestinal tract: evidence that nsaids interact with phospholipids to weaken the hydrophobic surface barrier and induce the formation of unstable pores in membranes," Journal of pharmacy and pharmacology **58**, 1421–1428 (2006).

[38] Sebastian Himbert, Richard J Alsop, Markus Rose, Laura Hertz, Alexander Dhaliwal, Jose M Moran-Mirabal, Chris P Verschoor, Dawn ME Bowdish, Lars Kaestner, Christian Wagner, *et al.*, "The molecular structure of human red blood cell membranes from highly oriented, solid supported multi-lamellar membranes," Scientific Reports **7** (2017).

[39] VK Sharma, E Mamontov, M Ohl, and M Tyagi, "Incorporation of aspirin modulates the dynamical and phase behavior of the phospholipid membrane," Physical Chemistry Chemical Physics **19**, 2514–2524 (2017).

[40] Matthew A Barrett, Songbo Zheng, Laura A Toppozini, Richard J Alsop, Hannah Dies, Aili Wang, Nicholas Jago, Michael Moore, and Maikel C Rheinstädter, "Solubility of cholesterol in lipid membranes and the formation of immiscible cholesterol plaques at high cholesterol concentrations," Soft Matter **9**, 9342–9351 (2013).

[41] Clare L Armstrong, Matthew A Barrett, Arno Hiess, Tim Salditt, John Katsaras, An-Chang Shi, and Maikel C Rheinstädter, "Effect of cholesterol on the lateral nanoscale dynamics of fluid membranes," European Biophysics Journal **41**, 901–913 (2012).

[42] Richard J Alsop, Clare L Armstrong, Amna Maqbool, Laura Toppozini, Hannah Dies, and Maikel C Rheinstädter, "Cholesterol expels ibuprofen from the hydrophobic membrane core and stabilizes lamellar phases in lipid membranes containing ibuprofen," Soft matter **11**, 4756–4767 (2015).

[43] SH Chen, CY Liao, HW Huang, TM Weiss, MC Bellisent-Funel, and F Sette, "Collective dynamics in fully hydrated phospholipid bilayers studied by inelastic x-ray scattering," Physical review letters **86**, 740 (2001).

[44] Thomas M Weiss, Poe-Jou Chen, Harald Sinn, Ercan E Alp, Sow-Hsin Chen, and Huey W Huang, "Collective chain dynamics in lipid bilayers by inelastic x-ray scattering," Biophysical journal **84**, 3767–3776 (2003).

[45] Poe-Jou Chen, Yun Liu, Thomas M Weiss, Huey W Huang, Harald Sinn, Ercan E Alp, Ahmet Alatas, Ayman Said, and Sow-Hsin Chen, "Studies of short-wavelength collective molecular motions in lipid bilayers using high resolution inelastic x-ray scattering," Biophysical Chemistry **105**, 721–741 (2003).

[46] Jochen S Hub, Tim Salditt, Maikel C Rheinstädter, and Bert L De Groot, "Short-range order and collective dynamics of dmpc bilayers: a comparison between molecular dynamics simulations, x-ray, and neutron scattering experiments," Biophysical journal **93**, 3156–3168 (2007).

[47] B Brüning, MC Rheinstädter, A Hiess, B Weinhausen, T Reusch, S Aeffner, and T Salditt, "Influence of cholesterol on the collective dynamics of the phospholipid acyl chains in model membranes," The European Physical Journal E: Soft Matter and Biological Physics **31**, 419–428 (2010).

[48] M Tarek, DJ Tobias, S-H Chen, and ML Klein, "Short wavelength collective dynamics in phospholipid bilayers: a molecular dynamics study," Physical review letters **87**, 238101 (2001).

[49] Valeria Conti Nibali, Giovanna D'Angelo, and Mounir Tarek, "Molecular dynamics simulation of short-wavelength collective dynamics of phospholipid membranes," Physical Review E **89**, 050301 (2014).

[50] Clare L Armstrong, Drew Marquardt, Hannah Dies, Norbert Kučerka, Zahra Yamani, Thad A Harroun, John Katsaras, An-Chang Shi, and Maikel C Rheinstädter, "The observation of highly ordered domains in membranes with cholesterol," PLoS One **8**, e66162 (2013).

[51] Clare L Armstrong, MA Barrett, L Toppozini, N Kučerka, Z Yamani, John Katsaras, Giovanna Fragneto, and Maikel C Rheinstädter, "Co-existence of gel and fluid lipid domains in single-component phospholipid membranes," Soft Matter **8**, 4687–4694 (2012).

[52] Adree Khondker, Alexander Dhaliwal, Richard J Alsop, Jennifer Tang, Matilda Backholm, An-Chang Shi, and Maikel C Rheinstädter, "Partitioning of caffeine in lipid bilayers reduces membrane fluidity and increases membrane thickness," Physical Chemistry Chemical Physics (2017).

[53] Christian L Wennberg, David Van Der Spoel, and Jochen S Hub, "Large influence of cholesterol on solute partitioning into lipid membranes," Journal of the American Chemical Society **134**, 5351–5361 (2012).

[54] William J Allen, Justin A Lemkul, and David R Bevan, "Gridmat-md: A grid-based membrane analysis tool for use with molecular dynamics," Journal of computational chemistry **30**, 1952–1958 (2009).

[55] Norbert Kučerka, Jana Gallová, Daniela Uhríková, Pavol Balgavỳ, Monica Bulacu, Siewert-Jan Marrink, and John Katsaras, "Areas of monounsaturated diacylphosphatidylcholines," Biophysical journal **97**, 1926–1932 (2009).

[56] Christofer Hofsäß, Erik Lindahl, and Olle Edholm, "Molecular dynamics simulations of phospholipid bilayers with cholesterol," Biophysical journal **84**, 2192–2206 (2003).

[57] Mario Suwalsky, Jessica Belmar, Fernando Villena, María José Gallardo, Malgorzata Jemiola-Rzeminska, and Kazimierz Strzalka, "Acetylsalicylic acid (aspirin) and salicylic acid interaction with the human erythrocyte membrane bilayer induce in vitro changes in the morphology of erythrocytes," Archives of biochemistry and biophysics **539**, 9–19 (2013).

[58] Yong Zhou, Kwang-Jin Cho, Sarah J Plowman, and John F Hancock, "Nonsteroidal anti-inflammatory drugs alter the spatiotemporal organization of ras proteins on the plasma membrane," Journal of Biological Chemistry **287**, 16586–16595 (2012).

[59] Charles F Majkrzak, Christopher Metting, Brian B Maranville, Joseph A Dura, Sushil Satija, Terrence Udovic, and Norman F Berk, "Determination of the effective transverse coherence of the neutron wave packet as employed in reflectivity investigations of condensed-matter structures. i. measurements," Physical Review A **89**, 033851 (2014).

[60] HELMUT Rauch, "Reality in neutron interference experiments," Foundations of physics **23**, 7–36 (1993).

[61] Katarzyna B Koziara, Martin Stroet, Alpeshkumar K Malde, and Alan E Mark, "Testing and validation of the automated topology builder (atb) version 2.0: prediction of hydration free enthalpies," Journal of computer-aided molecular design **28**, 221–233 (2014).

[62] Alpeshkumar K Malde, Le Zuo, Matthew Breeze, Martin Stroet, David Poger, Pramod C Nair, Chris Oostenbrink, and Alan E Mark, "An automated force field topology builder (ATB) and repository: version 1.0," Journal of chemical theory and computation **7**, 4026–4037 (2011).

[63] Herman JC Berendsen, James PM Postma, Wilfred F van Gunsteren, and Jan Hermans, "Interaction models for water in relation to protein hydration," in *Intermolecular forces* (Springer, 1981) pp. 331–342.

[64] Mark James Abraham, Teemu Murtola, Roland Schulz, Szilárd Páll, Jeremy C Smith, Berk Hess, and Erik Lindahl, "Gromacs: High performance molecular simulations through multi-level parallelism from laptops to supercomputers," SoftwareX **1**, 19–25 (2015).

[65] Nathan Schmid, Andreas P Eichenberger, Alexandra Choutko, Sereina Riniker, Moritz Winger, Alan E Mark, and Wilfred F van Gunsteren, "Definition and testing of the GROMOS force-field versions 54a7 and 54b7," European biophysics journal **40**, 843–856 (2011).

[66] Oliver Berger, Olle Edholm, and Fritz Jähnig, "Molecular dynamics simulations of a fluid bilayer of dipalmitoylphosphatidylcholine at full hydration, constant pressure, and constant temperature." Biophysical journal **72**, 2002 (1997).

[67] Tom Darden, Darrin York, and Lee Pedersen, "Particle mesh Ewald: An N! log (N) method for Ewald sums in large systems," The Journal of chemical physics **98**, 10089–10092 (1993).

[68] Berk Hess, Henk Bekker, Herman JC Berendsen, and Johannes GEM Fraaije, "Lincs: a linear constraint solver for molecular simulations," Journal of computational chemistry **18**, 1463–1472 (1997).

[69] Denis J Evans and Brad Lee Holian, "The nose–hoover thermostat," The Journal of chemical physics **83**, 4069–4074 (1985).

[70] Michele Parrinello and Aneesur Rahman, "Polymorphic transitions in single crystals: A new molecular dynamics method," Journal of Applied physics **52**, 7182–7190 (1981).

[71] David Van Der Spoel, Erik Lindahl, Berk Hess, Gerrit Groenhof, Alan E Mark, and Herman JC Berendsen, "Gromacs: fast, flexible, and free," Journal of computational chemistry **26**, 1701–1718 (2005).

[72] Hiroaki Saito and Wataru Shinoda, "Cholesterol effect on water permeability through DPPC and PSM lipid bilayers: a molecular dynamics study," The Journal of Physical Chemistry B **115**, 15241–15250 (2011).

[73] Christofer Hofsäß, Erik Lindahl, and Olle Edholm, "Molecular dynamics simulations of phospholipid bilayers with cholesterol," Biophysical journal **84**, 2192–2206 (2003).

[74] Richard M Venable, Bernard R Brooks, and Richard W Pastor, "Molecular dynamics simulations of gel ($L\beta I$) phase lipid bilayers in constant pressure and constant surface area ensembles," The Journal of Chemical Physics **112**, 4822–4832 (2000).

Chapter 5

Membranes Influence the Molecular Effects of Drugs: Publications IV, V, & VI

Chapter 4 illustrated, using aspirin as a case study, how a drug can influence the molecular structure and dynamics of the lipid membrane. The interaction with the membrane is based on hydrogen bonding interactions with the lipids and cholesterol. Composition, therefore, plays a role in driving the effect.

The membrane has many other relevant properties other than composition. They include membrane phase, lipid curvature, stiffness, hydration. What could happen when a drug encounters a stiff membrane vs a soft membrane? A hydrated membrane *vs* a dehydrated membrane? Some case studies exploring these topics will presented in this chapter.

In addition, can the membrane change the drug itself? The membrane is an amphiphliic, two-dimensional interface that is often useful for facilitating biochemical reactions between biomolecules. For example, the membrane is speculated to play an important role in the misfolding and aggregation of the Amyloid-β peptide in the physiology of Alzheimer's disease [79, 80]. An example of the membrane influencing drug chemistry is presented in this chapter.

Unlike Chapter 4, the studies in this chapter were not motivated by a central question. They all began as general curiosities, often introduced by junior students. However, taken together, they present a unique set of discoveries that add to the set of possible drug-membrane interactions.

5.1 Paper IV: Cholesterol Expels Ibuprofen from the Hydrophobic Membrane Core and Stabilizes Lamellar Phases in Lipid Membranes Containing Ibuprofen

Richard J. Alsop, Clare L. Armstrong, Amna Maqbool, Laura Toppozini, and Maikel C. Rheinstädter. (2015) *Cholesterol Expels Ibuprofen from the Hydrophobic Membrane Core and Stabilizes Lamellar Phases in Lipid Membranes Containing Ibuprofen.* Soft Matter. 11(24) 4756-4767

5.1.1 Preface to Paper IV

Ibuprofen is in the same class of drugs as aspirin, they are both non-steroidal anti-inflammatory drugs (NSAIDs). Much like aspirin, ibuprofen is known to inhibit the cyclo-oxygenase (COX) pathway [81]. However, it inhibits the pathway reversibly compared to the irreversible effects of aspirin. Evidence exists that ibuprofen also disrupts mucosal membrane integrity, promoting the diffusion of stomach acid and gastrointestinal discomfort or injury. The molecular structure has significant differences: it has the same ketone, hydroxyl, and aromatic groups, but with an extra carbon tail making the hydrophobic region of the molecule larger.

After the results of Paper I, and the work of Barrett *et al.*, samples were prepared and measured using X-ray diffraction. At high ibuprofen concentrations (>5 mol%), it was clear that the membranes were not in the lamellar phase. However, the observed scattering was not random but instead formed a clear pattern. The samples formed a cubic lipid phase. The cubic phase is created by lipids with negative intrinsic curvature, but can be induced by surfactants that embed in the tails and create curvature [22]. Hypothesizing that ibuprofen interacted with the tails due to its long hydrophobic tail, we performed an analysis of electron densities and determined that 55% of the ibuprofen molecules indeed enter the tails, while the rest interact in the heads as well as the water layer as part of two additional states.

We were also curious whether ibuprofen would interact with cholesterol-containing membranes in the same way. We therefore prepared membranes with 20 mol% cholesterol and increasing ibuprofen. However, diffraction experiments produced a surprise: at no ibuprofen concentration was a cubic phase observed. We again conducted an electron density analysis to find that there was no embedded state for ibuprofen in the cholesterol membranes. All the ibuprofen was either in the head group or water layer. We concluded that, as the title of the paper suggests, ibuprofen expels cholesterol from the membrane core and protects it from cubic phases.

Clearly, membrane composition and likely membrane stiffness plays a role in ibuprofen's effect. The cubic phase is indicative of pore formation, which is akin to membrane rupture. Ibuprofen could therefore have detrimental effects on membranes not stiff enough to avoid pores. Further research is needed to understand whether the pore-forming effects of ibuprofen contribute to any of its physiological side-effects.

The paper was featured on the cover of June 28, 2015 edition of Soft Matter, and featured as a

HOT article.

Author Contributions:

- *Experimental Concept:* Richard Alsop, Clare Armstrong, Maikel Rheinstädter
- *Sample Preparation:* Richard Alsop, Clare Armstrong, Amna Maqbool, Laura Toppozini
- *X-ray Experiments:* Richard Alsop, Clare Armstrong, Amna Maqbool, Laura Toppozini
- *Data Analysis:* Richard Alsop, Clare Armstrong, Amna Maqbool, Laura Toppozini, Maikel Rheinstädter
- *Manuscript Preparation:* Richard Alsop, Maikel Rheinstädter

Soft Matter

PAPER

Cholesterol expels ibuprofen from the hydrophobic membrane core and stabilizes lamellar phases in lipid membranes containing ibuprofen

Richard J. Alsop, Clare L. Armstrong, Amna Maqbool, Laura Toppozini, Hannah Dies and Maikel C. Rheinstädter*

Cite this: *Soft Matter*, 2015, **11**, 4756

Received 12th March 2015,
Accepted 20th April 2015

DOI: 10.1039/c5sm00597c

www.rsc.org/softmatter

There is increasing evidence that common drugs, such as aspirin and ibuprofen, interact with lipid membranes. Ibuprofen is one of the most common over the counter drugs in the world, and is used for relief of pain and fever. It interacts with the cyclooxygenase pathway leading to inhibition of prostaglandin synthesis. From X-ray diffraction of highly oriented model membranes containing between 0 and 20 mol% ibuprofen, 20 mol% cholesterol, and dimyristoylphosphatidylcholine (DMPC), we present evidence for a non-specific interaction between ibuprofen and cholesterol in lipid bilayers. At a low ibuprofen concentrations of 2 mol%, three different populations of ibuprofen molecules were found: two in the lipid head group region and one in the hydrophobic membrane core. At higher ibuprofen concentrations of 10 and 20 mol%, the lamellar bilayer structure is disrupted and a lamellar to cubic phase transition was observed. In the presence of 20 mol% cholesterol, ibuprofen (at 5 mol%) was found to be expelled from the membrane core and reside solely in the head group region of the bilayers. 20 mol% cholesterol was found to stabilize lamellar membrane structure and the formation of a cubic phase at 10 and 20 mol% ibuprofen was suppressed. The results demonstrate that ibuprofen interacts with lipid membranes and that the interaction is strongly dependent on the presence of cholesterol.

1 Introduction

In addition to specific interactions with biochemical targets, many drugs and pharmaceuticals are known to interact with lipid membranes through non-specific molecular interactions.[1,2] For example, physical interactions with lipid membranes can cause changes to the membrane's fluidity, thickness, or area per lipid.[3,4] As many biological processes, such as cell signalling and adhesion, are mediated by the membrane and membrane bound proteins, changes to membrane processes induced by drugs can lead to significant changes in their biological function.[5–9]

When assessing the impact of a foreign molecule (such as a drug) on membrane properties, the partitioning of the drug within the membrane is often crucial. As an example, the common analgesic aspirin has been shown to interact with the head group region of the lipid membrane leading to an increase in lipid fluidity.[10,11] Aspirin was eventually found to counteract cholesterol's condensing effect and to redissolve cholesterol plaques in lipid bilayers at high cholesterol concentrations,[12,13] and also to inhibit formation of cholesterol rafts at physiological concentrations of cholesterol.[14] In contrast, the co-surfactant hexanol partitions into the tail group region leading to profound changes in the membrane structure as it induces a lamellar to hexagonal phase transition.[15] In particular, small molecules can change partitioning of peptides in membranes. Melatonin was shown to reduce the population of the membrane-embedded state of amyloid-β_{25-35}, a peptide involved in plaque formation in Alzheimer's disease.[16]

Ibuprofen is a non-steroidal anti-inflammatory drug (NSAID) who's primary effect is related to the inhibition prostaglandin synthesis, leading to anti-inflammatory and pain killing properties.[17,18] Ibuprofen is a non-selective inhibitor of the cyclooxygenase enzyme. However, there is evidence for an interaction of ibuprofen with lipid membranes. Several studies have reported that ibuprofen leads to an increase in area per lipid[19] and membrane defects,[20] as well as a decreased membrane bending modulus, κ.[21]

Here, we determine the location of ibuprofen in saturated lipid bilayers at a concentration of 2 mol% and report experimental evidence for an indirect, non-specific interaction between ibuprofen and cholesterol in membranes containing

Department of Physics and Astronomy, McMaster University, ABB-241, 1280 Main Street West, Hamilton, Ontario L8S 4M1, Canada. E-mail: rheinstadter@mcmaster.ca; Fax: +1-(905)-546-1252; Tel: +1-(905)-525-9140-23134

5 mol% ibuprofen and 20 mol% cholesterol. Through X-ray diffraction in multi-lamellar, oriented membranes, we locate the ibuprofen molecule in the head group region and the hydrophobic core of the bilayers and observe that the presence of cholesterol expels ibuprofen from the membrane core. Cholesterol was also found to stabilize lamellar membrane structure, as the formation of an inverse cubic phase at high concentrations of 10 and 20 mol% ibuprofen was suppressed when 20 mol% cholesterol was present.

2 Results

Highly oriented, multi-lamellar membrane stacks were prepared on silicon wafers and the molecular structure was studied using high resolution X-ray diffraction imaging, as depicted in Fig. 1. By using oriented membranes, the in-plane ($q_{||}$) and out-of-plane (q_z) structure was determined separately, but simultaneously. All membranes were incubated at 30 °C in 100% humidity for 24 h before the measurements and scanned at a temperature of T = 28 °C and 50% relative humidity (RH). Similar to protein crystallography, this dehydrated state suppresses thermal fluctuations, increases the number of higher order Bragg peaks and thereby enhances structural features, allowing for a high spatial resolution.[22]

Fig. 2 shows 2-dimensional reciprocal space maps for a subset of samples in this study. Measurements are taken for -0.3 Å^{-1} $< q_{||} <$ 3 Å^{-1} and 0 Å^{-1} $< q_z <$ 1.1 Å^{-1}. Pure DMPC membranes are shown in Fig. 2(a). Some qualitative conclusions can be drawn from the scattering patterns. The observed scattering shows a number of well defined intensities along both, the out-of-plane (q_z) and in-plane ($q_{||}$) axis, indicative of lamellar bilayers with strong in-plane ordering.

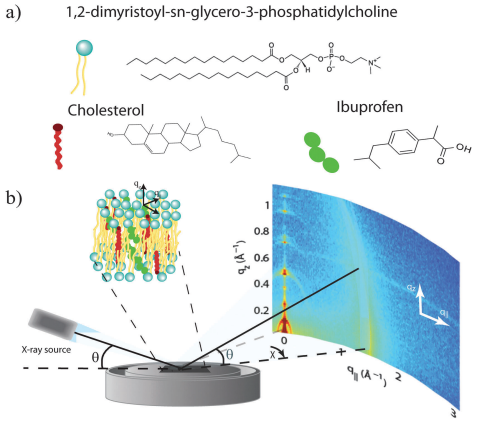

Fig. 1 (a) Schematic representations of dimyristoylphosphatidylcholine (DMPC), cholesterol, and ibuprofen molecules. (b) Diagram of the experimental setup used for X-ray diffraction measurements. Two-dimensional data was obtained to probe the structure of the oriented membrane stack parallel (in-plane) and perpendicular (out-of-plane) to the plane of the membranes.

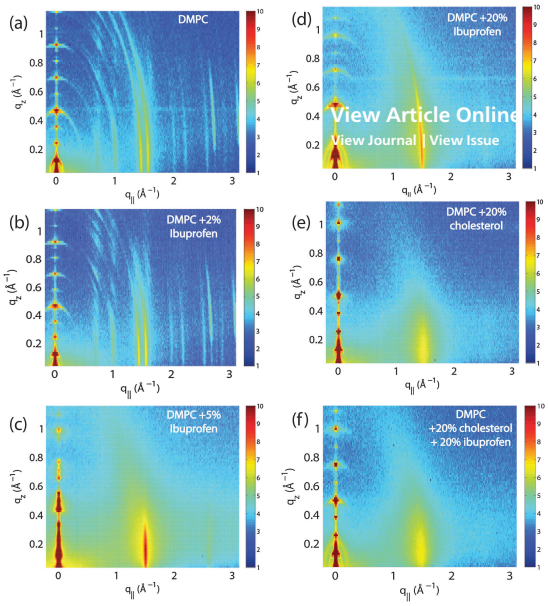

Fig. 2 Reciprocal space maps of selected samples: (a) pure DMPC bilayers; (b) DMPC + 2 mol% ibuprofen; (c) DMPC + 5 mol% ibuprofen; (d) DMPC + 20 mol% ibuprofen; (e) DMPC + 20 mol% cholesterol; (f) DMPC + 20 mol% cholesterol + 20 mol% ibuprofen. While a small concentration of ibuprofen of 2 mol% in part (b) does not alter membrane structure significantly, concentrations of more than 5 mol% induce changes in the in-plane and out-of-plane pattern (parts (c) and (d)). Lamellar membrane structure is stabilized in the presence of cholesterol (parts (e) and (f)).

The arrangement of the different molecular components in the plane of the membranes can be determined from the in-plane scattering along $q_{||}$. As suggested by Katsaras and Raghunathan,[23,24] different molecular components, such as lipid tails, lipid head groups and also ibuprofen and cholesterol molecules, can form molecular sub-lattices in the plane of the membrane leading to non-overlapping sets of Bragg peaks.

The 100% DMPC sample in Fig. 2(a) shows a number of well developed in-plane Bragg peaks. The diffracted intensity has a distinct rod-like shape, typical for a 2-dimensional system. The out-of-plane scattering along q_z shows pronounced and equally spaced Bragg intensities due to the multi lamellar structure of the membranes.

As detailed for instance in Barrett *et al.*,[10] the in-plane Bragg peaks can be assigned to two different molecular lattices, the lipid head groups and the lipid tails: an orthorhombic head group lattice (planar space group $p2$) with lattice parameters a = 8.773 Å and b = 9.311 Å (γ = 90°) and a commensurate monoclinic lattice of the lipid tails with parameters a_T = 4.966 Å, b_T = 8.247 Å and γ_S = 94.18°. The orthorhombic unit cell of the head group lattice contains two lipid molecules and has an area of $A_H = a_H b_H$ = 81.69 Å^2. The area per lipid can also be determined from the unit cell of the tails, which contains one lipid molecule, to $A_T = a_T b_T \sin\gamma_T$ = 40.84 Å^2. This area can be

View Article Online
Soft Matter Paper

compared to results published by Tristram-Nagle, Liu, Legleiter and Nagle,[25] who provided a reference for the structure of gel phase DMPC membranes. The authors find an area per lipid of ~ 47 Å^2 in fully hydrated bilayers at $T = 10$ °C. The membranes in our study were measured at $T = 28$ °C, however, de-hydrated to 50% RH to enhance structural features leading to a more closely packed gel structure.

The sample with 2 mol% ibuprofen in Fig. 2(b) shows a qualitatively similar pattern indicating that small amounts of ibuprofen do not lead to a significant change in membrane structure or topology. However, membranes prepared with 5 mol% and 20 mol% ibuprofen in Fig. 2(c) and (d) show a single in plane feature at $q_{||} = 1.5$ Å^{-1}. This peak is indicative of hexagonal packing of disordered lipid tails.[26] Additional reflections are observed along q_z, indicative of a change in membrane topology from the lamellar phase. Samples prepared with 20 mol% cholesterol also show disordered in-plane profiles (Fig. 2(e) and (f)), however, a lamellar q_z pattern.

2.1 Electronic properties of ibuprofen

Ibuprofen is an overall hydrophobic drug consisting of a large, hydrophobic body comprised of an aromatic ring and a carbon tail, and a small, hydrophilic head, where the oxygen groups are located. Ibuprofen was found to have low partitioning into water and to locate in the lipid phase,[27] preferentially in the interfacial region of the bilayer.[28]

As electromagnetic waves, X-rays mainly interact with the electronic structure of molecules. Electron distributions describing the ibuprofen molecule were calculated using the solved crystal structure of ibuprofen.[29] The corresponding structure file is deposited in the Crystallography Open Database with reference number 2006278. To take into account thermal motion of atoms and electrons, the position of each atom was modeled by a Gaussian distribution with a width (FWHM) of 1 Å (or, in the case of samples with cholesterol, 2 Å) and the corresponding electron distributions were then projected onto the z-axis. The molecule can be rotated to have any orientation with respect to the z-axis.

When the long axis of the molecule is not tilted with respect to the z-axis, three Gaussian distributions well describe the averaged profile, as shown in Fig. 3(a). The first peak is assigned to the tail region of the ibuprofen, the second to the ring structure, and the third peak to the oxygenated head region. When the ibuprofen molecule is tilted between 30° and 60° two Gaussians are required, as depicted in Fig. 3(b) and (c). When the molecule is tilted 90°, only a single Gaussian is needed to describe the distribution, as shown in Fig. 3(d).

The Gaussian distributions used to describe the ibuprofen profiles were then shifted and scaled to fit observed changes in membrane electron density with the inclusion of ibuprofen. The orientation and position of all membrane-embedded states can be determined in this fashion with high accuracy. This technique was used previously by Dies *et al.*, who used the atomic structures of amyloid-β peptides and melatonin to determine the location of peptides and enzyme in lipid membranes of different membrane compositions.[16,30]

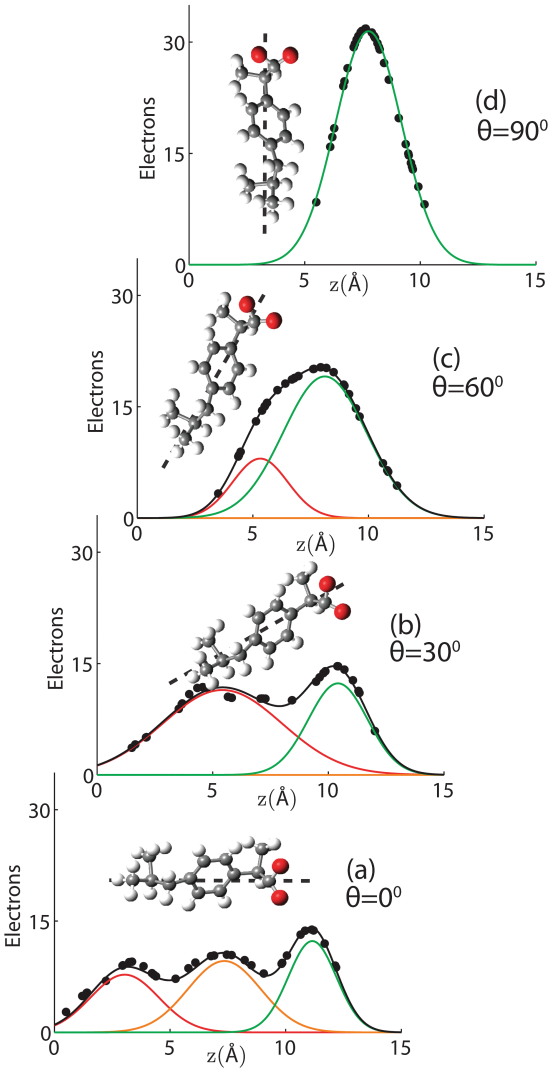

Fig. 3 Gaussian distributions used to describe the electronic distribution of the ibuprofen molecule, projected on the z-axis. Fits are presented when ibuprofen is tilted (a) 0°, (b) 30°, (c) 60°, and (d) 90°. Three Gaussians are required to describe the untilted ibuprofen, two Gaussians are needed when the molecule is tilted to 30° or 60°, and one Gaussian is needed when $\theta = 90°$. Dashed lines indicate ibuprofen's long axis. Electronic profiles were calculated by modelling the thermal motion of each atom by a distribution with FWHM of 1 Å.

2.2 The interaction of ibuprofen with DMPC membranes

For further quantitative analysis, the 2-dimensional data in Fig. 2 were cut along the q_z direction. Out-of-plane diffraction for DMPC membranes prepared with ibuprofen concentrations from 0 mol% to 20 mol% is presented in Fig. 4(a). Up to twelve evenly spaced diffraction peaks were observed for pure DMPC bilayers, indicative of a well ordered lamellar structure. The measured lamellar spacing, d_z, for the pure DMPC was determined to be 55.1 Å, in

View Article Online

Paper Soft Matter

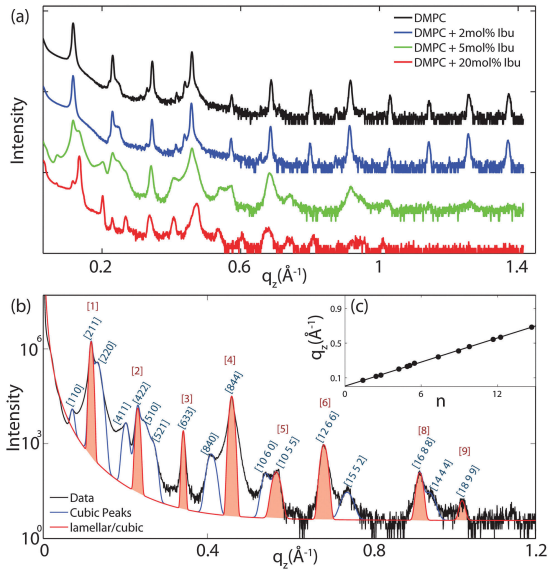

Fig. 4 (a) Out-of-plane X-ray diffraction ($q_{||}$ = 0 Å^{-1}) of oriented DMPC membranes containing ibuprofen at concentrations of 0 mol% (black), 2 mol% (blue), 5 mol% (green), and 20 mol% (red). (b) Peak indexing for a membrane with 5 mol% ibuprofen. Gaussian peaks were fit to describe the observed reflectivity curve. Peaks drawn in blue correspond to peaks, which scatter solely from cubic phases. Peaks in red agree with scattering from either a cubic phase or an epitaxially related lamellar phase. The inset (c) shows the position of the peaks along q_z *vs.* assigned peak indices $(h^2 + k^2 + l^2)^{1/2}$ for a cubic phase. The quality of the peak assignments is shown by the perfectly linear behaviour.

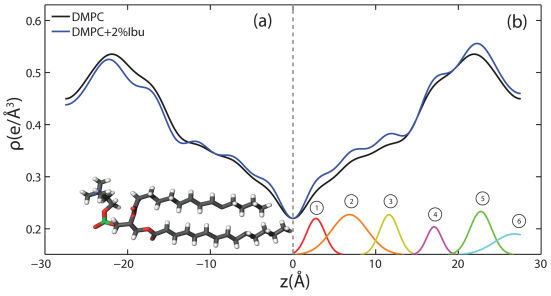

Fig. 5 Electron density profiles for membranes composed of DMPC (black) and DMPC + 2 mol% ibuprofen (blue). Curves on the left, side (a), are on an absolute scale. In (b), the curve representing the membrane prepared with ibuprofen has been scaled by a factor of 1.08 to overlap the profile with that of a pure DMPC membrane (see details in text). The difference between the scaled curve and the DMPC curve is best fit by 6 Gaussian profiles labelled by ① to ⑥.

agreement with previous reports.[10,25] A similar pattern is observed for DMPC + 2 mol% ibuprofen, which indicates that small amounts of ibuprofen do not change the structure of the bilayers significantly or alter the topology of the membranes. Additional peaks are observed at higher ibuprofen concentrations of 5 mol% and 20 mol% in Fig. 4(a). The structural changes associated with these reflections will be discussed below.

The location of the ibuprofen molecules in the saturated lipid bilayers can be determined by comparing the results for pure DMPC and DMPC + 2 mol% ibuprofen. Electron density profiles of the membranes, $\rho(z)$, were assembled by Fourier synthesis of the observed lamellar Bragg peaks, as detailed in the Materials and methods section (Section 4). Bilayer profiles for samples with 0 mol% and 2 mol% ibuprofen are plotted in Fig. 5. The profile for a pure DMPC membrane corresponds to a lipid bilayer in the gel state with both chains in an all-*trans* configuration, as reported previously.[25] The electron rich phosphorous group in the head region can be identified by the absolute maximum in the electron density profile at $z \sim 22$ Å. ρ_z monotonically decreases to the bilayer centre at $z = 0$, where CH_3 groups reside in the centre with an electron density of $\rho_z = 0.22$ e$^-$ Å^{-3}.

The electron density profiles for both samples are shown in Fig. 5(a) on an absolute scale for $\rho(z)$. There is a general decrease in electron density with the addition of electron-poor ibuprofen and the removal of electron-richer DMPC molecules. The ibuprofen-containing profile was scaled to compensate this overall loss of electron density and to to more clearly determine the profile changes induced by the drug, as shown in Fig. 5(b). The electron density profile for 98% DMPC + 2 mol% ibuprofen was scaled such that it modelled a pure DMPC (100% DMPC + 2 mol% ibuprofen). The difference curve between the scaled profile with ibuprofen and the unscaled DMPC profile shows an increase in electron density due to ibuprofen in both the head group and tail regions, which is well modelled by 6 Gaussian distributions, marked by ① to ⑥. Regions of the bilayer profile without ibuprofen molecules coincide with the pure DMPC bilayer in part (a).

The electronic distribution of an ibuprofen molecule can be fit to the difference curve to determine the position and orientation ibuprofen molecules. Three embedded states were observed. Three of the observed Gaussian distributions at z = 3 Å, 7 Å, and 11.5 Å were assigned to a single ibuprofen molecule residing in the hydrophobic membrane core, oriented parallel with the bilayer z-axis, with a tilt angle of 0° ± 5°. In addition to changes in the tail regions, two additional increases in electron density were observed in the head group region. A single peak is found at z = 17 Å, best described by a bound ibuprofen molecule, rotated by 90° ± 11° with respect to the z-axis, at the interface of the head group and tail group regions. Two peaks at z = 23 Å and z = 27 Å are best described by a molecule which is distributed between the two bilayers and aligned with the z-axis (tilt of 0° ± 5°). The peak at z = 23 Å is described by the electron distribution of both the hydroxyl group and the terminal methyl groups of an ibuprofen molecule, suggesting both portions of the molecule are observed embedded in the head groups (of opposite bilayers). The peak at z = 27 Å suggests the ring-group of ibuprofen observed between bilayers. A cartoon depicting the three membrane bound states for ibuprofen is shown in Fig. 9(a). By integrating the area under the peaks in the difference electron density curve, the relative occupation of each bound state can be determined.

View Article Online

Soft Matter Paper

Table 1 Peak position, *d*-spacing, and assigned Miller index for the reflectivity peaks measured from 5 mol% ibuprofen. All peaks are well described by a cubic phase with space group *Im3m* and a = 134 Å

q_z-Position (Å^{-1})	*d*-Spacing (Å)	Miller index
0.077	88.3	[110]
0.117	53.7	[211]
0.131	48.1	[220]
0.201	31.2	[411]
0.231	27.2	[422]
0.242	25.9	[015]
0.268	23.4	[521]
0.342	18.4	[633]
0.410	15.3	[840]
0.460	13.7	[844]
0.543	11.6	[10 6 0]
0.568	11.1	[10 5 5]
0.684	9.18	[12 6 6]
0.741	8.48	[2 5 15]
0.918	6.84	[16 8 8]
0.940	6.68	[4 14 14]
1.021	6.15	[18 9 9]

A relative occupation of 56% is observed for the upright state in the tails, 8% for the rotated state at the head–tail interface, and 36% for the state in the head groups.

Fig. 4(b) shows the out-of-plane diffraction pattern obtained from a membrane prepared with 5 mol% ibuprofen in a pure DMPC membrane. All observed peaks are fit with Gaussian peak profiles. The observed peaks cannot be indexed by a pure lamellar phase, however, may be indexed to a *Im3m* cubic structure with lattice parameter a = 134 Å. The corresponding cubic phase Miller indices are given on the figure; however, select peaks are indexed by a lamellar phase with bilayer spacing of d_z = 55.1 Å. These peaks are indicated by red Gaussian profiles in Fig. 4(b). Peaks solely indexed by the cubic phase are described by blue profiles. Note that the spacing of the [211] plane of cubic phases is often observed to be epitaxially related to the bilayer spacing of the lamellar phase. The position, *d*-spacing, and Miller indices for all peaks extracted from Fig. 4(b) are listed in Table 1.

To determine the relation between cubic and lamellar phase and the orientation of both phases, 2-dimensional X-ray maps of the region of interest were obtained for membranes with 0 mol%, 10 mol%, and 20 mol% ibuprofen, and are displayed in Fig. 6. The plots show the region $0 < q_z < 0.21$ Å^{-1} and $0 < q_{||} < 0.21$ Å^{-1} in more detail, as compared to the overview plots in Fig. 2. The pure DMPC bilayers in Fig. 6(a) show the lamellar $[100]_L$ Bragg peak and two diffuse contributions: the lamellar diffuse scattering occurring in horizontal sheets is the result of bilayer undulation dynamics. Bilayers, which are not perfectly oriented parallel to the silicon substrate lead to a faint powder ring, labeled as ''defect scattering''. The number of these defect bilayers is typically very small as evidenced by the logarithmic intensity plot.

In addition to the cubic peaks observed in the out-of-plane curves in Fig. 4, there is a drastic increase in the intensity of defect scattering with increasing ibuprofen content (DMPC + 10 mol% ibuprofen is shown in Fig. 6(b)), indicating an increase of membranes, which have a random orientation with respect to the perpendicular *z*-axis. While cubic peaks were observed in the specular out-of-plane scans, no diffuse cubic

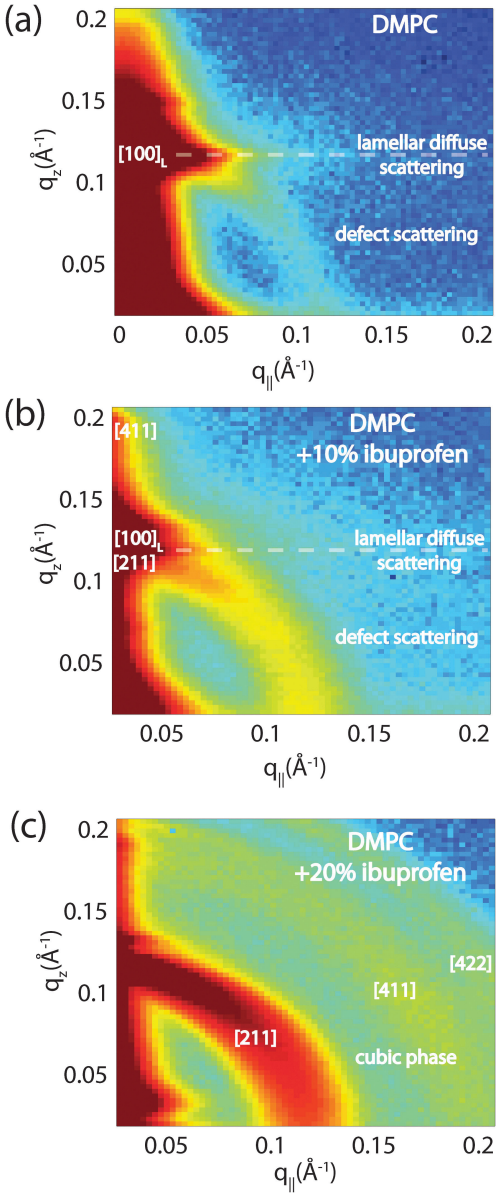

Fig. 6 High resolution reciprocal space maps show the increase in powder scattering with increased ibuprofen. Bilayers were prepared with concentrations of: (a) 0 mol%; (b) 10 mol% and (c) 20 mol% ibuprofen. Only a lamellar peak is observed for pure DMPC. The observed diffuse scattering was attributed to lamellar diffuse scattering due to fluctuations and defect scattering as the result of a small fraction of bilayers not perfectly aligned on the substrate.[31] For a membrane with 10 mol% ibuprofen, the defect scattering significantly increased indicative of a large fraction of ''misaligned'' bilayers. A cubic pattern is observed at 20 mol% ibuprofen. Intensities are shown on a logarithmic scale.

View Article Online
Paper Soft Matter

signals are visible in the 2-dimensional data at this ibuprofen concentration, most likely because the volume fraction of the cubic phase is still small. The pattern at 10 mol% ibuprofen is indicative of a coexistence of lamellar and cubic phases.

A distinct cubic peak pattern is observed at 20 mol% ibuprofen in Fig. 6(c). The positions of the broad powder-rings agree with cubic peaks observed in reflectivity measurements: the [211], [411], and [422] peaks are observed corresponding to a cubic phase (see Fig. 4(b)). The faint [110] and [220] peaks observed in out-of-plane curves could not be resolved from the more diffuse in-plane scattering.

2.3 The interaction of ibuprofen with membranes containing cholesterol

Because ibuprofen molecules were found to partition in pure lipid bilayers, DMPC membranes with cholesterol concentrations of 20 mol% and between 0 mol% to 20 mol% ibuprofen were prepared to study a potential interaction between cholesterol and ibuprofen. Out-of-plane diffraction scans for DMPC + 20 mol% cholesterol, DMPC + 20 mol% cholesterol + 5 mol% ibuprofen and DMPC + 20 mol% cholesterol + 20 mol% ibuprofen are plotted in Fig. 7. The diffraction patterns could all be indexed by lamellar phases. Electron density profiles for 0 mol% and 5 mol% ibuprofen were used to determine the position of the ibuprofen molecule in cholesterol-containing DMPC membranes and are shown in Fig. 8(a). The curve containing ibuprofen in Fig. 8(b) was scaled to represent a DMPC + 20 mol% cholesterol bilayer with 5 mol% ibuprofen embedded, as in Section 2.2. The difference between this scaled curve and the curve without ibuprofen was used to locate ibuprofen in membranes with cholesterol. Note that for membranes with cholesterol, when modelling the electronic distribution of ibuprofen for fitting to the difference curve, each atom is modelled by a Gaussian distribution with a width of 2 Å, as opposed to 1 Å for membranes without cholesterol. The need for increased Gaussian blurring is most likely a consequence of increased molecular disorder with the addition of cholesterol to gel phase membranes.[13]

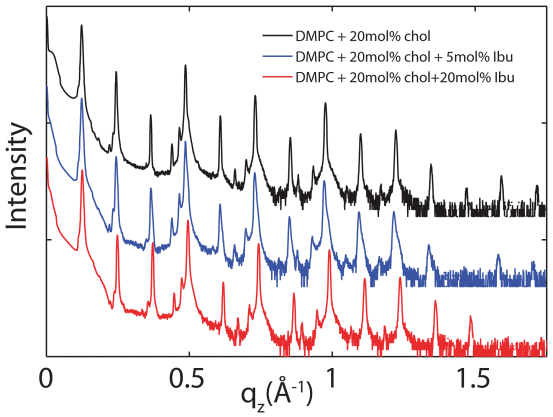

Fig. 7 Out-of-plane diffraction for bilayers prepared with 20 mol% cholesterol and ibuprofen concentrations of: (a) 0 mol%, (b) 5 mol%, (c) 20 mol%.

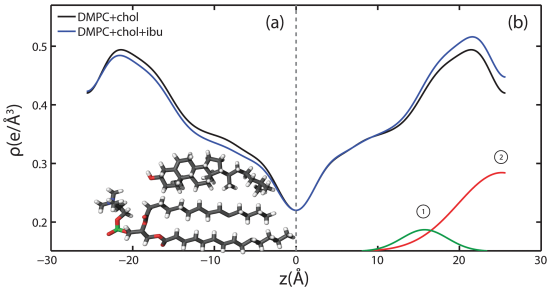

Fig. 8 Electron density profiles for DMPC membranes prepared with 20 mol% cholesterol (black) and 20 mol% cholesterol with 5 mol% ibuprofen (blue). The curves in (a) are on an absolute scale, while the ibuprofen containing curve in (b) was scaled to overlap the profile with that of a 20 mol% cholesterol-containing DMPC membrane (see details in text). The difference between the scaled curve and the black curve is best described by two Gaussian profiles, which are labelled in (b).

Two Gaussian distributions, centred at z = 15 Å and at 26 Å, were found to well describe the difference in electron density and were modelled as membrane embedded states for ibuprofen. The location of these states is in excellent agreement with the head group states observed in bilayers without ibuprofen in Section 2.2. The peak at z = 15 Å is best described by an ibuprofen molecule tilted by 90° ± 1° relative to the bilayer normal, as depicted in the electron distribution calculations in Fig. 3(b). The peak at z = 26 Å describes an ibuprofen molecule oriented parallel with the z-axis, and embedded between bilayers (tilt of 0° ± 1°), similar to the bilayer spanning state observed in membranes without cholesterol. Note that the two membrane electron density profiles in Fig. 8(b) coincide in the tail group region, suggesting that ibuprofen does not occupy this region in the presence of cholesterol. By comparing the integrated intensity of the corresponding Gaussian peaks, the relative occupations of the states at z = 15 Å and z = 26 Å are 14% and 86%, respectively.

3 Discussion and conclusions

Structural parameters, such as the lamellar spacing, d_z, the cubic spacing and the area per lipid, A_L, were determined for all samples and are listed in Table 2. Ibuprofen was found to not

Table 2 Lamellar and cubic spacings and area per lipid are provided for all samples examined. For samples with cubic symmetry, the bilayer repeat distance was calculated using peaks which fit a lamellar spacing

DMPC (mol%)	Ibuprofen (mol%)	Cholesterol (mol%)	d_z (Å)	Cubic spacing (Å)	A_L (Å^2)
1	0	0	55.1		40.84
2	2	0	55.1		40.84
3	5	0	55.3	135.7	40.5
4	10	0	56	137	40.5
5	20	0	—	135.7	40.5
6	0	20	51.3		42.5
7	5	20	51.7		42.5
8	20	20	50.9		42.5

View Article Online
Soft Matter Paper

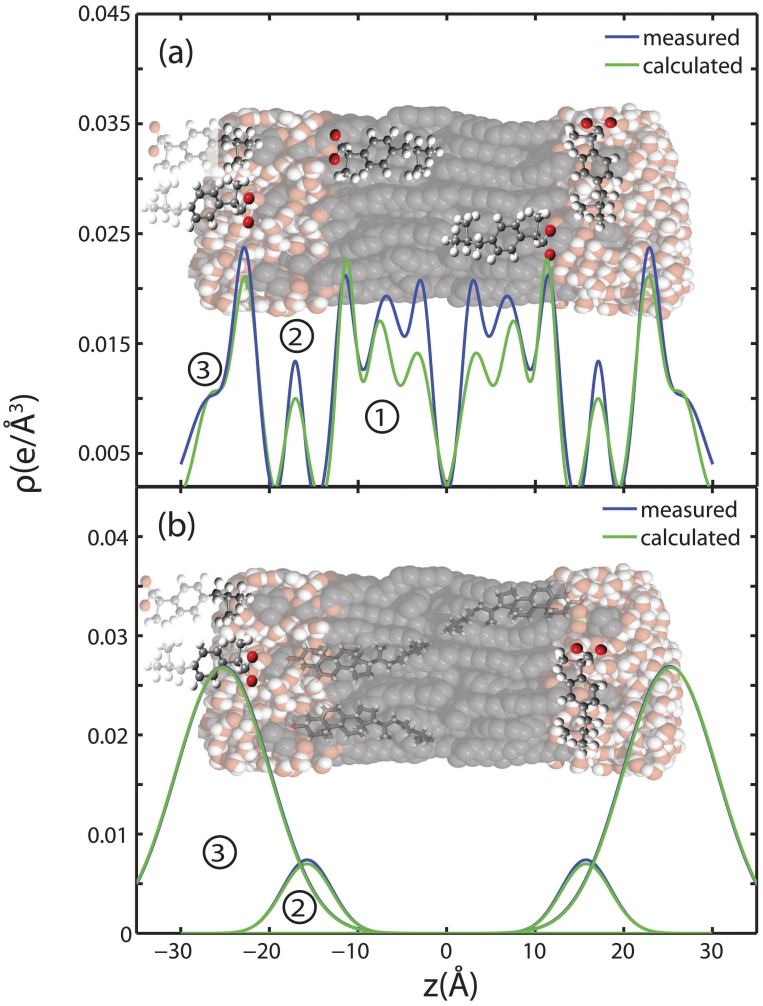

Fig. 9 Measured difference in electron density with the addition of ibuprofen to DMPC membranes and calculated electron distributions of ibuprofen molecules. (a) Three membrane bound states are fit to changes in electron density when 2 mol% ibuprofen is added to pure DMPC bilayers. The calculations take into account ibuprofen molecules, which extend into and are shared with neighbouring bilayers. (b) Two embedded states are fit to the observed changes in electron density when 5 mol% ibuprofen is added to a membrane composed of DMPC + 20 mol% cholesterol.

change d_z and A_L in gel DMPC bilayers for the concentrations used and within the resolution of this experiment. Addition of 20 mol% cholesterol led to an increase in lipid area and a decrease of lamellar spacing, as reported previously for gel phase bilayers.[13] The presence of 20 mol% cholesterol was found to suppress the formation of a cubic phases when up to 20 mol% ibuprofen was incorporated as well.

3.1 Partitioning of ibuprofen in saturated lipid membranes with and without cholesterol

The partitioning of ibuprofen in gel phase DMPC membranes was determined using a combination of X-ray diffraction and electronic structure calculations using crystallographic ibuprofen data. The result is summarized in Fig. 9. While the peak amplitudes in the calculated profiles in part (a) appear to be systematically slightly smaller than the measured differences, peak positions and peak widths show an excellent agreement. Based on the electronic properties in Section 2.1, the orientation of the ibuprofen molecules can be determined: while 3 peaks in the electron density difference indicate a parallel orientation, a single peak is consistent with a perpendicular, 90° orientation.

Three different membrane bound populations were observed when 2 mol% ibuprofen were added to the DMPC bilayers, as sketched in Fig. 9(a): ① a state in the hydrophobic membrane core, where the ibuprofen molecules align parallel to the lipid acyl chains; 56% of ibuprofen molecules were found in this state; ② 8% of ibuprofen molecules were observed at the interface between head groups-tail groups, and ③ 36% of ibuprofen

View Article Online
Paper Soft Matter

molecules were found attached to the membrane head group region, situated between the lipid head groups of two bilayers. At ibuprofen concentrations greater than 5 mol% (10 and 20 mol%), disruption of the lamellar membrane phase and the formation of a cubic lyotropic phase was observed.

Based on a fit of the molecular electronic distribution of the ibuprofen molecule to the experimental data, as depicted in Fig. 3, the ibuprofen molecules in the hydrophobic membrane core align parallel to the lipid tails, with their hydrophilic head groups located in the head group region of the bilayers (population ①). The 180° position, where the oxygen groups would locate in the bilayer centre, was found to be less favourable with a χ^2 value of 6.33×10^4, as compared to $\chi^2 = 4.28 \times 10^4$ for the 0° case. The locations of the ibuprofen molecules are consistent with previous studies, where ibuprofen was reported to associate with PC lipids.[3,27] Based on electrostatic considerations, the hydrophilic head of the ibuprofen is likely to locate in the head group region of the bilayers.[19,28] Population ③ corresponds to a state, where the ibuprofen molecule appears to be partially embedded in the head groups of two lipid bilayers, with the hydroxyl group in one bilayer and the terminal methyl groups in another. This membrane-spanning state of ibuprofen is likely a consequence of the stacked bilayers used for the diffraction experiments.

Only two populations of ibuprofen molecules were observed in the presence of cholesterol, as depicted in Fig. 9(b). 14% of the ibuprofen molecules were found to occupy a state at the head group-tail group interface (population ②), while 86% of the molecules were found in the space between two bilayers, attached to the head group region (population ③). While the two states are in agreement with states ② and ③ observed with no cholesterol, no membrane embedded ibuprofen state was observed in the cholesterol-containing lipid bilayers. The presence of cholesterol in the membrane seems to suppress partitioning of ibuprofen into the tail region. As ibuprofen and cholesterol molecules compete for the same space, cholesterol seems to have a higher affinity for the lipid acyl chains.

X-ray diffraction has been used previously to determine the position of a similar NSAID, aspirin, in DMPC membranes with and without cholesterol.[10,12] Aspirin was found to reside exclusively in the lipid head group region. However, there is a large hydrophobic component to the ibuprofen molecule, which would increase its affinity for the hydrophobic membrane core. Previous simulations of membrane systems incorporating ibuprofen locate the molecule in the tail group regions.[21,32] In addition, Langmuir isotherm experiments have also suggested that ibuprofen may partition into the head group regions of lipid monolayers.[33]

Our results agree qualitatively with other reports. Simulations by Khajeh *et al.* report that the relative position of ibuprofen shifts towards the head groups in DMPC membranes containing 25 mol% cholesterol.[32] Additional studies have suggested that drug–membrane interactions are significantly influenced by the presence of cholesterol.[34,35] Our experiments present experimental evidence that cholesterol influences the position of ibuprofen in the membrane and, as will be described below, also suppresses the cubic phase induced by ibuprofen.

3.2 The suppression of cubic phases by cholesterol

Inverse (type II) phases, such as inverse cubic or inverse-hexagonal phases, are frequently observed in amphiphile–water systems, including systems with lipids, surfactants, and block co-polymers.[36–38] A lamellar to cubic phase transition may be induced in membranes by temperature or pressure jumps in systems containing lipids with negative curvature.[39,40] Alternatively, inverse phases can be induced by the addition of a largely hydrophobic co-surfactant.[15,41,42] The fingerprint of a lamellar to cubic phase transition is the appearance of Bragg peaks in diffraction experiments, which require 3-fold symmetry to properly index.[43]

Oriented membranes with ibuprofen concentrations less than 5 mol% formed lamellar phases, while samples with concentrations greater than 5 mol% could not be indexed by a single 1-dimensional lamellar phase and required a 3-dimensional cubic phase to index all peaks. The observed Bragg peaks for all samples in the cubic phase are consistent with either *Im3m* or *Pn3m* space groups, which are frequently observed in membrane systems.[36,43,44] The [111] peak, which we did not observe, is systematically absent for *Im3m* but not *Pn3m*, suggesting *Im3m* is the best candidate. Another frequently observed cubic phase, with space group *Ia3d*, did not describe the peaks as the [110] reflection (absent for *Ia3d*) was observed.[44,45]

In membranes prepared on a solid substrate, where the lamellar phase is oriented, Bragg scattering from the membrane stack is observed solely along the out-of-plane axis, q_z. However, the formation of 3-dimensional cubic phases leads to the appearance of off-specular scattering. Typically, cubic phases form as grains with random orientation, resulting in powder scattering, although oriented cubic phases have been prepared.[46] Two-dimensional measurements of reciprocal space were collected to observe off-specular scattering in the presence of ibuprofen and are depicted in Fig. 6. The maps highlight the monotonic increase in powder scattering with increasing ibuprofen concentration. This suggests that increasing ibuprofen leads to cubic phases with grains at random orientation.

While specular peaks can unambiguously be indexed by cubic phases for ibuprofen concentrations greater than 5 mol%, we note that a subset of those peaks may be indexed by a lamellar phase with bilayer spacing in close agreement with samples displaying a pure lamellar phase. The [211] plane of cubic phases is often observed to be epitaxially related to a bilayer spacing in systems with a lamellar to cubic transition.[39,44,47] Fig. 4(b) demonstrates how the observed peaks are indexed by either a cubic phase, or a cubic phase and a lamellar phase. The experiments, therefore, do not rule out the possibility of a lamellar phase coexisting with the cubic phase. From the 2-dimensional diffraction data in Fig. 6 it seems that the formation of cubic phases is accompanied by the a distortion of the lipid bilayers phase and the occurrence of bilayers not parallel to the *z*-axis.

There is evidence that the impact of certain drugs on the lipid membrane is dependent on membrane composition. For example, negatively charged lipids have been shown to accelerate

View Article Online
Soft Matter Paper

the binding of the antimicrobial peptide Lacticin Q.[48] In addition, the anti-cancer drug Taxol has a different impact on saturated model membranes and unsaturated membranes.[49] In a recent paper by Khajeh *et al.*, molecular dynamics (MD) simulations were performed on membranes with cholesterol and ibuprofen[32] to report that the permeation of ibuprofen across the membrane is decreased by an increased stiffness of the membrane caused by cholesterol.

An increase in chain rigidity and decrease in permeability with the inclusion of cholesterol could explain the reduced penetration depth of Ibuprofen into the membrane.[32,50] In addition, a change in the position of ibuprofen could explain why cholesterol suppresses cubic phase formation. Cholesterol itself has not been shown to suppress cubic phases in membranes with inherently negative curvature.[51] However, by causing ibuprofen to partition in the head groups as opposed to the tail groups, cholesterol may prevent the negative curvature or decrease in bending modulus induced by ibuprofen. Our results demonstrate how a membrane constituent, such as cholesterol, can influence the membrane impact of a drug, such as ibuprofen, by changing the partitioning of the drug. Cholesterol can, therefore, act as a protective agent, by inhibiting cubic phases even when ibuprofen is present in high concentration.

4 Materials and methods

4.1 Preparation of the multi-lamellar membranes

Highly oriented, multi-lamellar membranes were prepared on polished 2 × 2 cm^2 silicon wafers. The wafers were first pretreated by sonication in dichloromethane (DCM) at 310 K for 25 minutes to remove all organic contamination and create a hydrophobic substrate. After removal from the DCM post-sonication, each wafer was thoroughly rinsed three times by alternating with ~50 mL of ultra pure water and methanol.

1,2-Dimysteroyl-*sn*-glycero-3-phosphocholine (DMPC) and cholesterol were obtained from Avanti Polar Lipids and individually dissolved in 1 : 1 mixtures of chloroform and tri-fluoroethanol (TFE). Ibuprofen (Sigma-Aldrich) was also dissolved in a mixture of 1 : 1 chloroform and TFE. The DMPC, cholesterol and ibuprofen solutions were then mixed in the appropriate ratios to achieve the desired membrane compositions for the experiment. All samples prepared for this study are listed in Table 2. Molecular representations of the components are depicted in Fig. 1(a).

A tilting incubator was heated to 313 K and the lipid solutions placed inside to equilibrate. 200 μL of lipid solution was deposited on each wafer and the solvent was then allowed to slowly evaporate for ~10 minutes while being gently rocked, such that the lipid solution spread evenly on the wafers. After drying, the samples were placed in vacuum at 313 K for 12 hours to remove all traces of solvent. Samples were then placed in a sealed container containing an open vial of pure water and allowed to equilibrate to 293 K. The temperature was then slowly increased to 303 K over a period of 24 hours. This procedure results in highly oriented, multi-lamellar membrane stacks an a uniform coverage of the silicon substrates. About 3000 highly oriented stacked membranes with a total thickness of ~10 μm are produced using this protocol. The high sample quality and high degree of order is a prerequisite to determine in-plane and out-of-plane structure of the membranes separately, but simultaneously.

4.2 X-Ray scattering experiment

Out-of-plane and in-plane X-ray scattering data was obtained using the Biological Large Angle Diffraction Experiment (BLADE) in the Laboratory for Membrane and Protein Dynamics at McMaster University. BLADE uses a 9 kW (45 kV, 200 mA) CuK-α Rigaku Smartlab rotating anode at a wavelength of 1.5418 Å. Both source and detector are mounted on moveable arms such that the membranes stay horizontal during measurements. Focussing, multi layer optics provide a high intensity parallel beam with monochromatic X-ray intensities up to 10^{10} counts per (s mm^2). This beam geometry provides optimal illumination of the membrane samples to maximize the scattered signal. By using highly-oriented stacks, the in-plane ($q_{||}$) and out-of-plane (q_z) structure of the membranes could be determined independently. A sketch of the scattering geometry is depicted in Fig. 1(b). Full 2-dimensional reciprocal space maps are shown in Fig. 2.

The X-ray scattering experiments determine three pieces of information relevant to molecular structure of the membranes. Firstly, out-of-plane diffraction scans allow for the identification of the phase of the membranes (lamellar or cubic) and also permit the reconstruction of electron density profiles (for lamellar samples). Electron density profiles were used to determine the position of the molecular constituents. Secondly, in-plane scattering measurements at high $q_{||}$ allow for the organization of the lipid molecules in the plane of the membrane to be determined. The area per lipid may be determined from the in-plane structure, as detailed in Barrett *et al.*[10] Thirdly, scans performed at low $q_{||}$ and low q_z can be used to measure the degree of orientation within the samples.

The 2-dimensional X-ray data in Fig. 2 show well-defined peaks along the $q_{||}$-axis, which allow the determination of the lateral membrane structure. Several correlation peaks were observed in the in-plane data for ibuprofen concentrations of less than 2 mol%, and were well fit by Lorentzian peak profiles. The intensity has a distinct rod-like shape, typical for a 2-dimensional system. Membranes containing more than 2 mol% ibuprofen showed one broad Lorentzian peak, centered at ~1.5 $Å^{-1}$ due to the organization of the lipid tails in the hydrophobic membrane core. The area per lipid molecule can be determined from the in-plane diffraction data, when assuming that the lipid tails form a densely packed structure with hexagonal symmetry (planar group *p*6), as reported from, *e.g.*, neutron diffraction.[26] In the absence of fluctuations (in gel state lipid bilayers), the area per lipid molecule can be determined from the position of the in-plane Bragg peak at q_T to $A_L = 16\pi^2/(\sqrt{3}q_T^2)$.[10,13,52] The distance between two acyl tails is determined to be $a_T = 4\pi/(\sqrt{3}q_T)$, with the area per

View Article Online
Paper Soft Matter

lipid simplified to $A_L = \sqrt{3}a_T{}^2$, as listed in Table 2. The area per lipid for the pure DMPC and DMPC + 2 mol% ibuprofen samples, which show a highly organized lateral membrane structure with additional in-plane Bragg peaks in Fig. 2, were determined from the lattice parameters of the corresponding orthogonal tail lattice.

Structural parameters measured using the diffraction measurements, such as d_z spacing and A_L, for all samples are provided in Table 2.

4.3 Out-of-plane structure and electron densities

The out-of-plane structure of the membranes was determined using out-of-plane X-ray diffraction. The membrane electron density, $\rho(z)$, is approximated by a 1-dimensional Fourier analysis:

$$\rho(z) = \rho_W + \frac{F(0)}{d_z} + \frac{2}{d_z}\sum_{n=1}^{N} F(q_n)\nu_n \cos(q_n z) = \rho_W + \frac{F(0)}{d_z} + \frac{2}{d_z}\sum_{n=1}^{N} \sqrt{I_n q_n}\nu_n \cos\left(\frac{2\pi n z}{d_z}\right). \quad (1)$$

N is the highest order of the Bragg peaks observed in the experiment and ρ_W is the electron density of bulk water. The integrated peak intensities, I_n, are multiplied by q_n to generate the form factors, $F(q_n)$. The bilayer form factor which is in general a complex quantity, is real-valued when the structure is centro-symmetric. The phase problem of crystallography, therefore, simplifies to the sign problem $F(q_z) = \pm|F(q_z)|$ and the phases, ν_n, can only take the values ± 1. The phases, ν_n are needed to reconstruct the electron density profile from the scattering data following eqn (1). When the membrane form factor $F(q_z)$ is measured at several q_z values in a continuous fashion, $T(q_z)$, which is proportional to $F(q_z)$, can be fit to the data:

$$T(q_z) = \sum_n \sqrt{I_n q_n}\,\mathrm{sinc}\left(\frac{1}{2}d_z q_z - \pi n\right). \quad (2)$$

In order to determine the phases quantitatively, the form factor has to be measured at different q_z-values using the so-called swelling technique or by measuring the bilayer at different contrast conditions when using neutron diffraction. In this paper, by fitting the experimental peak intensities and comparing them to the analytical expression for $T(q_z)$ in eqn (2), the phases, ν_n, could be assessed. Good agreement was obtained, and the results shown in Fig. 10.

The calculated electron densities, $\rho(z)$, which are initially on an arbitrary scale, were then transformed to an absolute scale. The curves were vertically shifted to fulfil the condition $\rho(0) = 0.22\ e^-/Å^{-3}$ (the electron density of a CH_3 group) in the centre of a bilayer. The curves were then scaled until the total number of electrons $e^- = AL\int_0^{dz/2}\rho(z)dz$ across a membrane leaflet agrees with the total number of electrons expected based on the sample composition, with the addition of 7 hydration water molecules, in agreement with.[16,53]

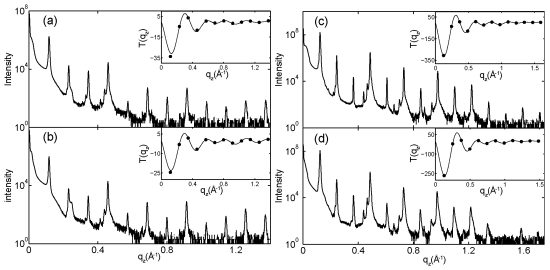

Fig. 10 Out-of-plane diffraction data for all samples for which Fourier analysis was performed. $T(q_z)$, which is proportional to the membrane form factor, is shown in each inset and was used to determine the phases ν_n. (a) pure DMPC; (b) 2 mol% ibuprofen; (c) 20 mol% cholesterol; (d) 20 mol% cholesterol and 20 mol% ibuprofen.

The d_z-spacing between two neighbouring membranes in the stack was determined from the distance between the Bragg reflections ($d_z = 2\pi/\Delta q_z$) along the out-of-plane axis, q_z. Up to a peak order of 12 was observed from DMPC membranes, and up to 14 for DMPC membranes with cholesterol. Note that not all diffraction orders are necessarily observed for the different samples as the scattering intensity depends on the form factor of the bilayers.

Acknowledgements

This research was funded by the Natural Sciences and Engineering Research Council (NSERC) of Canada, the National Research Council (NRC), the Canada Foundation for Innovation (CFI), and the Ontario Ministry of Economic Development and Innovation. R.J.A. is the recipient of an Ontario Graduate Scholarship, L.T. is the recipient of a Canada Graduate Scholarship, M.C.R. is the recipient of an Early Researcher Award from the Province of Ontario.

References

1 C. Pereira-Leite, C. Nunes and S. Reis, Interaction of non-steroidal anti-inflammatory drugs with membranes: *In vitro* assessment and relevance for their biological actions, *Prog. Lipid Res.*, 2013, **52**, 571–584.
2 J. Seydel and M. Wiese, *Drug-Membrane Interactions*, Wiley-VCH, Germany, 2002.
3 L. M. Lichtenberger, Y. Zhou, V. Jayaraman, J. R. Doyen and R. G. O'Neil, *et al.*, Insight into nsaid-induced membrane alterations, pathogenesis and therapeutics: characterization of interaction of nsaids with phosphatidylcholine, *BBA-MOL CELL BIOL L*, 2012, **1821**, 994–1002.
4 D. Goldstein, The effects of drugs on membrane fluidity, *Annu. Rev. Pharmacol. Toxicol*, 1984, **24**, 43–64.
5 J. N. G. Frydman, A. S. Fonseca, V. C. Rocha, M. O. Benarroz and G. S. Rocha, *et al.*, Acetylsalicylic acid and morphology of red blood cells, *Braz. Arch. Biol. Technol.*, 2010, **53**, 575–582.

6 Y. Zhou, K. J. Cho, S. J. Plowman and J. F. Hancock, Nonsteroidal anti-inflammatory drugs alter the spatiotemporal organization of ras proteins on the plasma membrane, *J. Biol. Chem.*, 2012, **287**, 16586–16595.

7 Y. Zhou, S. J. Plowman, L. M. Lichtenberger and J. F. Hancock, The anti-inflammatory drug indomethacin alters nanoclustering in synthetic and cell plasma membranes, *J. Biol. Chem.*, 2010, **285**, 35188–35195.

8 M. C. Rheinstädter, K. Schmalzl, K. Wood and D. Strauch, Protein-protein interaction in purple membrane, *Phys. Rev. Lett.*, 2009, **103**, 128104.

9 C. L. Armstrong, E. Sandqvist and M. C. Rheinstädter, Protein-protein interactions in membranes, *Protein Pept. Lett.*, 2011, **18**, 344–353.

10 M. Barrett, S. Zheng, G. Roshankar, R. Alsop and R. Belanger, *et al.*, Interaction of aspirin (acetylsalicylic acid) with lipid membranes, *PLoS One*, 2012, **7**, e34357.

11 M. Suwalsky, J. Belmar, F. Villena, M. J. Gallardo and M. Jemiola-Rzeminska, *et al.*, Acetylsalicylic acid (aspirin) and salicylic acid interaction with the human erythrocyte membrane bilayer induce *in vitro* changes in the morphology of erythrocytes, *Arch. Biochem. Biophys.*, 2013, **539**, 9–19.

12 R. J. Alsop, M. A. Barrett, S. Zheng, H. Dies and M. C. Rheinstädter, Acetylsalicylic acid (asa) increases the solubility of cholesterol when incorporated in lipid membranes, *Soft Matter*, 2014, **10**, 4275–4286.

13 M. Barrett, S. Zheng, L. Toppozini, R. Alsop and H. Dies, *et al.*, Solubility of cholesterol in lipid membranes and the formation of immiscible cholesterol plaques at high cholesterol concentrations, *Soft Matter*, 2013, **9**, 9342–9351.

14 R. J. Alsop, L. Toppozini, D. Marquardt, N. Kučerka, T. A. Harroun and M. C. Rheinstädter, Aspirin inhibits formation of cholesterol rafts in fluid lipid membranes, *Biochim. Biophys. Acta, Biomembr.*, 2015, **1848**, 805–812.

15 I. Koltover, T. Salditt, J. O. Rädler and C. R. Safinya, An inverted hexagonal phase of cationic liposome-dna complexes related to dna release and delivery, *Science*, 1998, **281**, 78–81.

16 H. Dies, L. Toppozini and M. C. Rheinstädter, The interaction between amyloid-β peptides and anionic lipid membranes containing cholesterol and melatonin, *PLoS One*, 2014, **9**, e99124.

17 N. M. Davies, Clinical pharmacokinetics of ibuprofen, *Clin. Pharmacokinet.*, 1998, **34**, 101–154.

18 L. H. Rome and W. Lands, Structural requirements for time-dependent inhibition of prostaglandin biosynthesis by anti-inflammatory drugs, *Proc. Natl. Acad. Sci. U. S. A.*, 1975, **72**, 4863–4865.

19 M. B. Boggara and R. Krishnamoorti, Small-angle neutron scattering studies of phospholipid- nsaid adducts, *Langmuir*, 2009, **26**, 5734–5745.

20 L. Du, X. Liu, W. Huang and E. Wang, A study on the interaction between ibuprofen and bilayer lipid membrane, *Electrochim. Acta*, 2006, **51**, 5754–5760.

21 M. B. Boggara, A. Faraone and R. Krishnamoorti, Effect of ph and ibuprofen on the phospholipid bilayer bending modulus, *J. Phys. Chem. B*, 2010, **114**, 8061–8066.

22 K. Hristova and S. H. White, Determination of the hydrocarbon core structure of fluid dioleoylphosphocholine (dopc) bilayers by x-ray diffraction using specific bromination of the double-bonds, *Effect of hydration, Biophysical Journal*, 1998, **74**, 2419–2433.

23 J. Katsaras, V. A. Raghunathan, E. J. Dufourc and J. Dufourcq, Evidence for a two-dimensional molecular lattice in subgel phase dppc bilayers, *Biochemistry (Moscow)*, 1995, **34**, 4684–4688.

24 V. A. Raghunathan and J. Katsaras, Structure of the l_c' phase in a hydrated lipid multilamellar system, *Phys. Rev. Lett.*, 1995, **74**, 4456–4459.

25 S. Tristram-Nagle, Y. Liu, J. Legleiter and J. F. Nagle, Structure of gel phase dmpc determined by x-ray diffraction, *Biophys. J.*, 2002, **83**, 3324–3335.

26 C. L. Armstrong, D. Marquardt, H. Dies, N. Kučerka, Z. Yamani, T. A. Harroun, J. Katsaras, A.-C. Shi and M. C. Rheinstädter, *et al.*, The observation of highly ordered domains in membranes with cholesterol, *PLoS One*, 2013, **8**, e66162.

27 F. Barbato, M. I. La Rotonda and F. Quaglia, Interactions of nonsteroidal antiinflammatory drugs with phospholipids: comparison between octanol/buffer partition coefficients and chromatographic indexes on immobilized artificial membranes, *J. Pharm. Sci.*, 1997, **86**, 225–229.

28 H. C. Gaede and K. Gawrisch, Lateral diffusion rates of lipid, water, and a hydrophobic drug in a multilamellar liposome, *Biophys. J.*, 2003, **85**, 1734–1740.

29 N. Shankland, C. Wilson, A. Florence and P. Cox, Refinement of ibuprofen at 100k by single-crystal pulsed neutron diffraction, *Acta Crystallogr., Sect. C: Cryst. Struct. Commun.*, 1997, **53**, 951–954.

30 H. Dies, B. Cheung, J. Tang and M. C. Rheinstädter, The organization of melatonin in lipid membranes, *Biochim. Biophys. Acta, Biomembr.*, 2015, **1848**, 1032–1040.

31 C. L. Armstrong, W. Häußler, T. Seydel, J. Katsaras and M. C. Rheinstädter, Nanosecond lipid dynamics in membranes containing cholesterol, *Soft Matter*, 2014, **10**, 2600–2611.

32 A. Khajeh and H. Modarress, The influence of cholesterol on interactions and dynamics of ibuprofen in a lipid bilayer, *Biochim. Biophy. Acta, Biomembr.*, 2014, **1838**, 2431–2438.

33 V. P. Geraldo, F. J. Pavinatto, T. M. Nobre, L. Caseli and O. N. Oliveira, Langmuir films containing ibuprofen and phospholipids, *Chem. Phys. Lett.*, 2013, **559**, 99–106.

34 W. Kopeć, J. Telenius and H. Khandelia, Molecular dynamics simulations of the interactions of medicinal plant extracts and drugs with lipid bilayer membranes, *FEBS J.*, 2013, **280**, 2785–2805.

35 A. H. Hansen, K. T. Sørensen, R. Mathieu, A. Serer, L. Duelund, H. Khandelia, P. L. Hansen and A. C. Simonsen, *et al.*, Propofol modulates the lipid phase transition and localizes near the headgroup of membranes, *Chem. Phys. Lipids*, 2013, **175**, 84–91.

36 G. Lindblom and L. Rilfors, Cubic phases and isotropic structures formed by membrane lipids–possible biological relevance, *Biochim. Biophys. Acta, Biomembr.*, 1989, **988**, 221–256.

37 G. Shearman, A. Tyler, N. Brooks, R. Templer, O. Ces, R. Law and J. Seddon, Ordered micellar and inverse micellar lyotropic phases, *Liq. Cryst.*, 2010, **37**, 679–694.

38 M. Morris, Directed self-assembly of block copolymers for nanocircuitry fabrication, *Microelectron. Eng.*, 2015, **132**, 207–217.

39 A. M. Squires, R. Templer, J. Seddon, J. Woenckhaus, R. Winter, S. Finet and N. Theyencheri, *et al.*, Kinetics and mechanism of the lamellar to gyroid inverse bicontinuous cubic phase transition, *Langmuir*, 2002, **18**, 7384–7392.

40 C. E. Conn, O. Ces, X. Mulet, S. Finet, R. Winter, J. M. Seddon and R. H. Templer, *et al.*, Dynamics of structural transformations between lamellar and inverse bicontinuous cubic lyotropic phases, *Phys. Rev. Lett.*, 2006, **96**, 108102.

41 G. Montalvo, R. Pons, G. Zhang, M. Dáz and M. Valiente, Structure and phase equilibria of the soybean lecithin/peg 40 monostearate/water system, *Langmuir*, 2013, **29**, 14369–14379.

42 R. J. Gillams, T. Nylander, T. S. Plivelic, M. K. Dymond and G. S. Attard, Formation of inverse topology lyotropic phases in dioleoylphosphatidylcholine/oleic acid and dioleoylphosphatidylethanolamine/oleic acid binary mixtures, *Langmuir*, 2014, **30**, 3337–3344.

43 N. W. Schmidt and G. C. Wong, Antimicrobial peptides and induced membrane curvature: Geometry, coordination chemistry, and molecular engineering, *Curr. Opin. Solid State Mater. Sci.*, 2013, **17**, 151–163.

44 C. V. Kulkarni, Nanostructural studies on monoelaidin–water systems at low temperatures, *Langmuir*, 2011, **27**, 11790–11800.

45 Y. Rançon and J. Charvolin, Epitaxial relationships during phase transformations in a lyotropic liquid crystal, *J. Phys. Chem.*, 1988, **92**, 2646–2651.

46 A. M. Squires, J. E. Hallett, C. M. Beddoes, T. S. Plivelic and A. M. Seddon, Preparation of films of a highly aligned lipid cubic phase, *Langmuir*, 2013, **29**, 1726–1731.

47 B. Angelov, A. Angelova, U. Vainio, V. M. Garamus, S. Lesieur, R. Willumeit and P. Couvreur, *et al.*, Long-living intermediates during a lamellar to a diamond-cubic lipid phase transition: a small-angle x-ray scattering investigation, *Langmuir*, 2009, **25**, 3734–3742.

48 F. Yoneyama, K. Shioya, T. Zendo, J. Nakayama and K. Sonomoto, Effect of a negatively charged lipid on membrane-lacticin q interaction and resulting pore formation, *Biosci., Biotechnol., Biochem.*, 2010, **74**, 218–221.

49 C. Bernsdorff, R. Reszka and R. Winter, Interaction of the anticancer agent taxol™ (paclitaxel) with phospholipid bilayers, *J. Biomed. Mater. Res.*, 1999, **46**, 141–149.

50 K. E. Bloch, Sterol, structure and membrane function, *Crit. Rev. Biochem. Mol. Biol.*, 1983, **14**, 47–92.

51 B. G. Tenchov, R. C. MacDonald and D. P. Siegel, Cubic phases in phosphatidylcholine-cholesterol mixtures: cholesterol as membrane ''fusogen'', *Biophys. J.*, 2006, **91**, 2508–2516.

52 T. T. Mills, G. E. S. Toombes, S. Tristram-Nagle, D.-M. Smilgies, G. W. Feigenson and J. F. Nagle, *et al.*, Order parameters and areas in fluid-phase oriented lipid membranes using wide angle X-ray scattering, *Biophys. J.*, 2008, **95**, 669–681.

53 E. Nováková, K. Giewekemeyer and T. Salditt, Structure of two-component lipid membranes on solid support: An x-ray reflectivity study, *Phys. Rev. E*, 2006, **74**, 051911.

5.2 Paper V: The Lipid Bilayer Provides a Site for Cortisone Crystallization at High Cortisone Concentrations

Richard J. Alsop, Adree Khondker, Jochen S. Hub, Maikel C. Rheinstädter. (2016). *The Lipid Bilayer Provides a Site for Cortisone Crystallization at High Cortisone Concentrations.* Scientific Reports. 6, 22425

5.2.1 Preface to Paper V

Whereas aspirin and ibuprofen are *non*-steroidal anti-inflammatory drugs, cortisone is considered a steroidal drug [82]. It is naturally produced, but also used as a treatment for sore joints. Cortisone is given as an injection into a joint, and therefore exists at high concentration in a membrane joint. In ∼5% of cases, the cortisone actually causes pain, due to a side-effect known as a "flare" [83]. While it has a known receptor in the cell nucleus [84], the exact mechanism of the flares is unknown.

Adree Khondker, then a high school student looking for a science fair project, brought the molecule to our attention. We initially hypothesized that increased lipid fluidity and perhaps decreasing membrane integrity. We prepared POPC membranes with cortisone included, and measured them by X-ray diffraction in their hydrated fluid phase. POPC was chosen for this experiment as we wanted to measure whether cortisone could decrease the integrity of fluid membranes. From electron density analysis of X-ray diffraction experiments, we could locate cortisone in the head group / tail group interface, ∼17 Å from the bilayer centre. Most interestingly, we saw extra diffraction signals at high (>30 mol%) cortisone concentrations, and these signals were indicative of crystallized cortisone. Most importantly they signals were oriented with the lipid bilayer, suggesting the crystals sit in the bilayer. The cortisone was crystallizing in the bilayer

To better understand how cortisone might have been interacting with the bilayer to create crystals, we collaborated with Jochen Hub of the University of Göttingen to perform MD simulations. The results confirmed that cortisone embeds into the interface. At high concentrations, we saw that cortisone actually embedded deeper in the membrane, such that it became trans-membrane, and started to aggregate. The simulations were too slow to produce crystals, but they illustrated how the membrane can nucleate crystal formation.

Crystallized cortisone is actually believed to be the main source for flares [83]. The cortisone does not typically crystallize in free solution, so our results highlight the potential for membranes as a nucleating surface. This is an example of the membrane changing the chemistry of a drug. The results do not highlight why some people get flares while others do not. It would be interesting to test different membrane concentrations to assess the lipid conditions most amenable to crystallization.

Author Contributions:

- *Experimental Concept:* Richard Alsop, Adree Khondker, Maikel Rheinstädter
- *Sample Preparation:* Richard Alsop, Adree Khondker
- *X-ray Experiments:* Richard Alsop, Adree Khondker
- *MD Simulations:* Jochen Hub
- *Data Analysis:* Richard Alsop, Adree Khondker, Jochen Hub, Maikel Rheinstädter
- *Manuscript Preparation:* Richard Alsop, Adree Khondker, Jochen Hub, Maikel Rheinstädter

www.nature.com/scientificreports

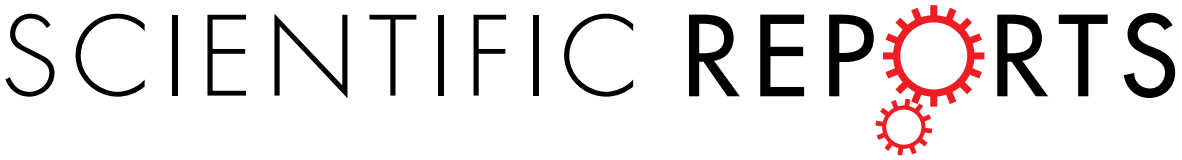

OPEN

The Lipid Bilayer Provides a Site for Cortisone Crystallization at High Cortisone Concentrations

Received: 16 November 2015
Accepted: 15 February 2016
Published: 03 March 2016

Richard J. Alsop[1], Adree Khondker[1], Jochen S. Hub[2] & Maikel C. Rheinstädter[1]

Cortisone is an injected anti-inflammatory drug that can cause painful side effects known as "steroid flares" which are caused by cortisone crystallizing at the injection site. We used molecular dynamics simulations and X-ray diffraction to study the interaction of cortisone with model lipid membranes made of 1-palmitoyl-2-oleoyl-sn-glycero-3-phosphocholine (POPC) at drug concentrations from 0 mol% to 50 mol%. Cortisone was found to partition in the lipid bilayer and locate in the hydrophilic to hydrophobic interface of the membranes. Cortisone strongly affects the integrity of the membrane, as quantified by a decreased membrane thickness, increased area per lipid, and decreased lipid tail order parameters. At cortisone concentrations of more than 20 mol%, signals from crystallized cortisone were observed. These crystallites are embedded in the bilayers and orient with the membranes. While the cortisone molecules align parallel to the bilayers at low concentrations, they start to penetrate the hydrophobic core at higher concentrations. Trans-membrane crystallites start to nucleate when the membrane thickness has decreased such that cortisone molecules in the different leaflets can find partners from the opposite leaflet resulting in a non-zero density of cortisone molecules in the bilayer center. We suggest that the lipid bilayer provides a site for cortisone crystallization.

In the pharmaceutical industry, drugs are typically developed to interact directly with molecular targets, such as protein receptors, and these targets (or receptors) may be embedded in cell membranes[1,2]. However, a drug molecule, such as cortisone, can also directly influence the lipid membrane via physical interactions, thereby changing the properties and functioning of the membrane[3–5]. These non-specific interactions are believed to often be responsible for drug side effects, as changes to the membrane's properties can influence the function of membrane-embedded proteins[4,5].

Cortisone (17-hydroxy-11-dehydrocorticosterone) is a synthetic glucocorticoid used globally and listed under the World Health Organization's Essential Medicines[6]. Glucocorticoids are a subcategory of steroids, which have anti-inflammatory properties[7,8].

Cortisone can be taken orally to treat general inflammation, although it is more commonly used to treat local joint inflammation by direct injection to the active site. Cortisone primarily acts by specifically binding to an intracytoplasmic nuclear receptor, forming a complex, which enters the nuclear membrane and interacts with basic transcription factors[9,10]. This causes the release of lipocortins, thereby inhibiting the production of prostaglandins, and leukotrienes, which reduce inflammation[11–14].

However, there are several severe side-effects of cortisone, which include muscle wasting, hyperglycemia, and steroid psychosis[15–17]. These side-effects have partially been explained by non-specific interactions with lipid membranes[18]. In addition, corticosteroid injections can cause so-called "steroid flares", which are characterized by pain at the site of injection and typically occur within 1–2 days of injection[19,20]. Insoluble, μm sized cortisone crystals forming on the synovial membrane cause macrophages to collect at the cite of crystallization. The immune response, known as a flare, leads to the release of synovial fluid, swelling, and pain at the site of injection[21–23].

X-ray diffraction experiments have shown cortisol, the antiderivative of cortisone, which differs from cortisone only by a hydroxyl group in place of a ketone group, to localize within the bilayer at z-values of $10\,\text{Å} < z < 19\,\text{Å}$[24] ($z = 0$ marks the bilayer center). In addition, MD simulations of cortisone show that it is able to localize in the head group-tail group interface of bilayer; however, dependent upon initial position[25]. The

[1]Department of Physics and Astronomy, McMaster University, Hamilton, Ontario, Canada. [2]Institute for Microbiology and Genetics, Georg-August-University Göttingen, Göttingen, Germany. Correspondence and requests for materials should be addressed to J.S.H. (email: jhub@gwdg.de) or M.C.R. (email: rheinstadter@mcmaster.ca)

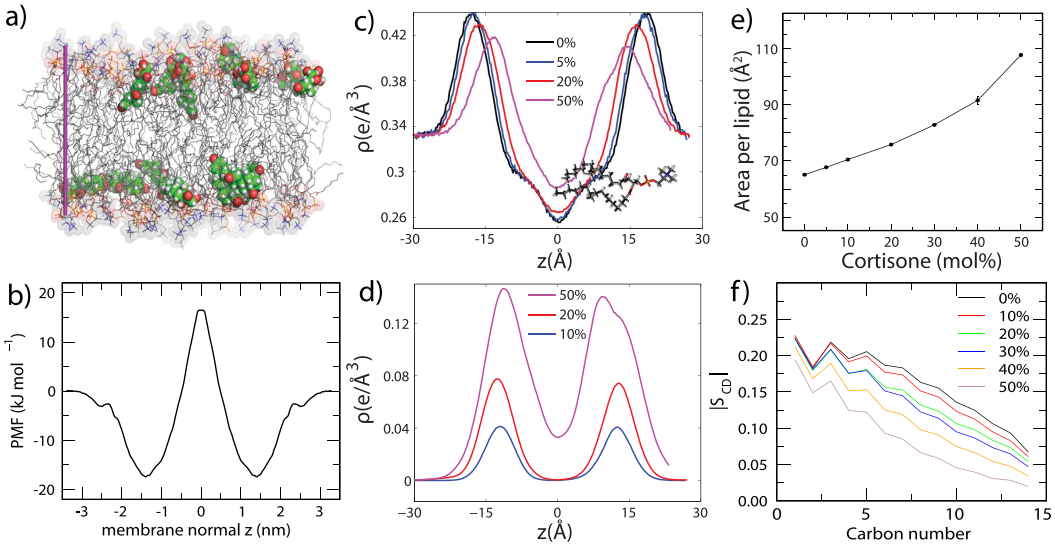

Figure 1. (**a**) A simulation snapshot of a POPC membrane containing 10 mol% cortisone; POPC is show as sticks, cortisone as solid spheres. Water is not shown for clarity. (**b**) Potential of mean force (PMF) for cortisone across along the membrane normal z. $z = 0$ corresponds to the membrane center. (**c**) Electron density profiles calculated from simulations. (**d**) electron density of cortisone. (**e**) Area per phospholipid molecule as a function of cortisone content. (**f**) Deuterium order parameter of the saturated POPC tail as calculated from the simulations.

simulations suggest the polar groups on the cortisone molecule interact with the choline, glycerol, and phosphate groups of the lipid molecules.

By combining MD simulations and high resolution X-ray diffraction we show that cortisone crystallizes inside of lipid membranes at high cortisone concentrations. Unsaturated 1-palmitoyl-2-oleoyl-sn-glycero-3-phosphocholine (POPC) membranes were studied at cortisone concentrations between 0 and 50 mol%. Cortisone was found to partition in the lipid bilayers and to locate between the hydrophilic and hydrophobic regions, orienting parallel to the membranes. The presence of cortisone leads to a continuous thinning of the bilayers and an increase of the lipid area at concentrations of up to 20 mol%. At higher concentrations, cortisone was found to strongly penetrate the hydrophobic core and eventually nucleate in 2-dimensional crystallites inside the membranes. This mechanism may be related to the formation of steroid flares in cortisone therapy in biological tissue.

Results

Molecular Dynamics Simulations. We used MD simulations to identify the energetics and conformations of cortisone in the membranes, as well as the effects of cortisone on the structure of the lipid bilayer. A typical simulation snapshot for a concentration of 10 mol% cortisone is shown in Fig. 1a.

First, we computed the potential of mean force (PMF) for a single cortisone molecule across the pure POPC membrane (Fig. 1b). The PMF suggests an average membrane/water partition coefficient of 220, demonstrating a strong preference of cortisone for the membrane over bulk water. In line with a previous simulation study[25], the PMF exhibits pronounced minima at a distance of $|z| \sim 14$ Å from the bilayer center. Thus, at low cortisone concentrations, the molecule preferentially binds at the head group-tail interfaces of the membrane. Visual inspection of the simulations showed that, at this position, cortisone predominantly binds with the hydrophobic edge of the sterol groups oriented towards the hydrophobic tails, thereby minimizing any hydrophobic/hydrophilic mismatch.

In order to compare the simulations to our X-ray scattering data (see below), we further computed electron density profiles from equilibrium simulations at various cortisone concentrations. Figure 1c presents the overall density profiles, representing POPC, cortisone and water. The electron density at the edge of the bilayers is found to be 0.33 e$^-$/Å^3 corresponding to bulk water. The maximum in density at $|z| \sim 22$ Å is caused by the electron rich phospholipid head group region. Upon the addition of cortisone, the density peaks continuously shifts towards the center of the membranes, indicative of a decrease in bilayer thickness.

Further insight into cortisone conformations is given by the density purely from cortisone molecules in Fig. 1d. At low cortisone content, all cortisone molecules are localized at the head-group tail-group interface (near the glycerol moiety) as suggested by the single-cortisone PMF. At high local cortisone concentration, however, the molecules begin to span the entire membrane, as indicated by a non-zero cortisone density at $z = 0$.

To quantify the effect of cortisone on the structure of membrane, we computed the area per phospholipid (A_L) as well as the the deuterium order parameter ($|S_{CD}|$) of the saturated POPC tail as a function of cortisone content,

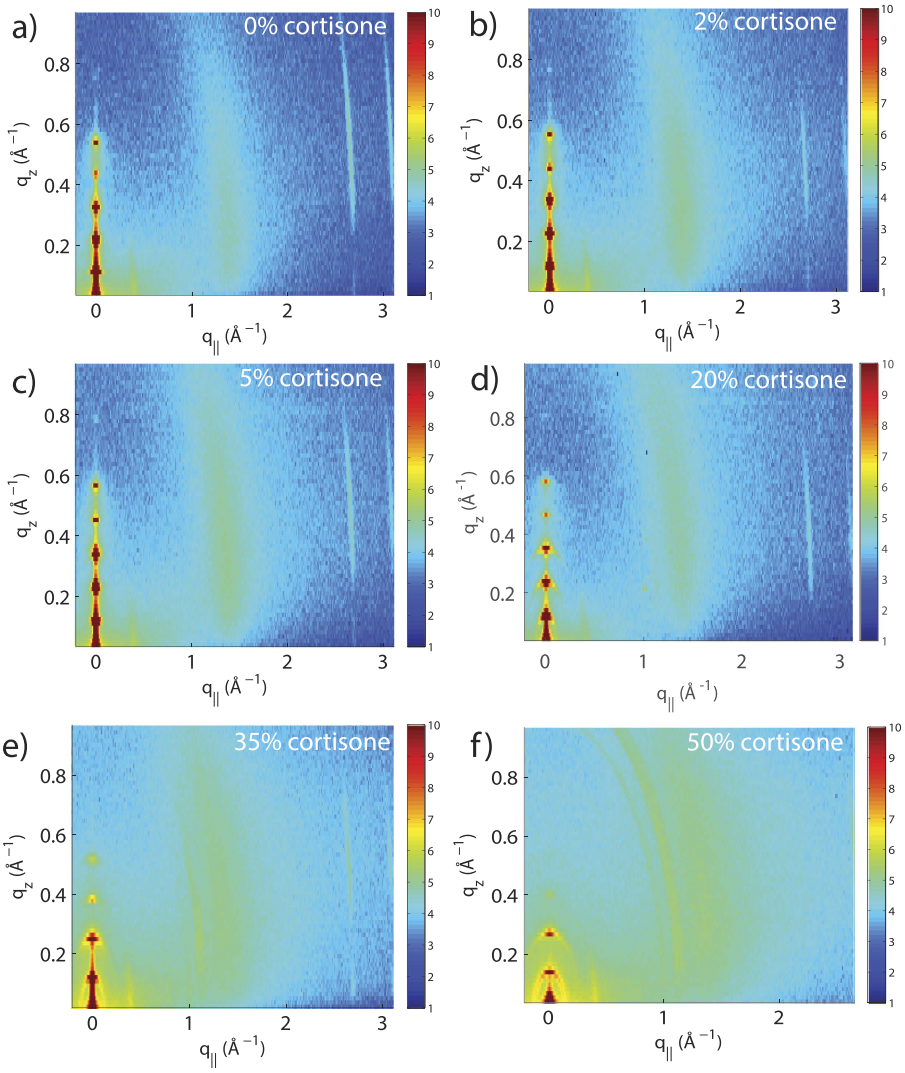

Figure 2. Two-dimensional X-ray intensity maps of bilayers with increasing cortisone concentration . (**a**) 0 mol%, (**b**) 2 mol%, (**c**) 5 mol%, (**d**) 20 mol%, (**e**) 35 mol% and (**f**) 50 mol% cortisone. All samples exhibit well-spaced Bragg peaks along q_z, and a broad peak at $q_{||}$, indicative of oriented fluid-phase membranes. At >20 mol%, additional peaks are observed in-plane indicating crystallization of cortisone.

as shown in Fig. 1e,f. We observed a large increase in A_L from 65 Å^2 at 0% cortisone up 105 Å^2 at 50% cortisone. The lipid area for the pure POPC bilayer is in good agreement with the experimental value of 68.3 Å^2[26]. Simultaneously, the order of the lipid tails strongly decreases with increasing cortisone content. Taken together, the simulations highlight that the membrane does not merely provide a passive solvent for the accumulation of cortisone. Instead, cortisone has drastic effects on the integrity of the membrane, leading to a decreased bilayer thickness, increased area per lipid, and increased tail disorder.

X-ray Diffraction of POPC Membranes with Cortisone. Highly oriented, multi-lamellar membrane stacks were prepared on silicon wafers and the molecular structure was studied using high resolution X-ray diffraction imaging. By using oriented membranes, the in-plane structure ($q_{||}$) and the out-of-plane structure (q_z) were determined independently, however, simultaneously. All membranes were scanned at T = 28 °C and 97% relative humidity (RH), in the fluid state of the POPC bilayers.

Two-dimensional X-ray intensity maps for cortisone concentrations of 0, 2, 5, 10, 35 and 50 mol% cortisone are shown in Fig. 2. The pure POPC sample in Fig. 2a shows five well-developed Bragg peaks along the q_z axis,

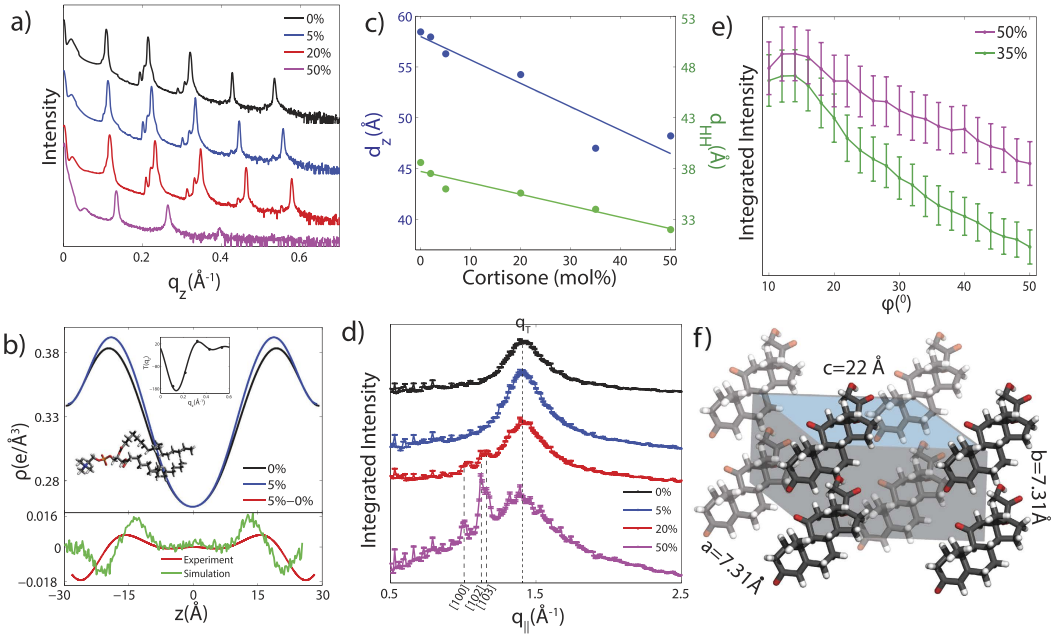

Figure 3. (**a**) Out-of plane X-ray diffraction of oriented POPC membranes containing cortisone. (**b**) Top: scaled electron densities across the axis perpendicular to the bilayer for 0 mol% and 5 mol% cortisone. Bottom: the difference of these curves shows a positive peak at $|z| \sim 15$ Å, indicating the position of cortisone, and a negative peak at $|z| \sim 25$ Å due to the thinning of the membrane. The difference curve from the MD simulations at 5 mol% is included for comparison. The slight disagreement in peak position and width between experiment in simulation is likely due to bilayer undulations[28]. An example of $T(q_z)$ is shown as an inset. (**c**) The lamellar spacing, d_z, and the head-head distance, d_{HH}, as a function of cortisone concentration as determined from diffraction experiments. (**d**) Scattering along $q_{||}$ for the oriented membrane samples. Additional peaks, which appear for cortisone concentrations >20 mol%, can be indexed by crystalline cortisone. (**e**) The integrated intensities for the crystalline cortisone peak observed at $q_{||} = 1.1$ Å^{-1} as a function of azimuthal angle ϕ. (**f**) Unit cell of the observed cortisone crystallites, as determined from the in-plane Bragg peaks.

indicative of well organized lamellar bilayers. A single, broad in-plane peak at $q_{||} = 1.4$ Å^{-1} is the result of the hexagonal packing of the lipid tails in the membrane core and the tell-tale of a fluid, disordered structure[27]. In line with scattering intensities computed from the simulations (Figure S1), this tail correlation peak is smeared out with increasing cortisone content, indicative for increasing disorder of the lipid tails. Additional in-plane reflections are observed for cortisone concentrations of 20 and 35 mol%, indicative of the formation of cortisone crystallites. 20 mol% was, therefore, defined as the experimental solubility limit of cortisone in POPC bilayers.

Electron density profiles $\rho(z)$ of the bilayers were determined through Fourier analysis of the out-of-plane Bragg peaks shown in Fig. 3a. $\rho(z)$ for the pure POPC bilayer and POPC + 5 mol% cortisone are shown in Fig. 3b (top). In addition, Fig. 3b (bottom) presents change in electron density upon the addition of 5% cortisone, computed from the Bragg peaks (red curve) and from the MD simulations (green curve). We find that, upon the addition of cortisone, the electron density increases at $|z| \sim 15$ Å, which corresponds to the position of cortisone molecules, and the density decreases at $|z| \sim 23$ Å due to thinning of the membrane. The difference between experimental and simulation peak positions (2–3 Å) and width likely arise due to bilayer undulations present in the bilayer stack[28]. The experiments thus locate cortisone inside the bilayers, between the head group and tail group region, in agreement with the MD simulations.

The lamellar spacing, d_z, and head group to head group spacing, d_{HH}, are depicted in Fig. 3c. Both spacings significantly decrease with increasing cortisone concentrations. The width of the head group region can be estimated from the width of the corresponding peak in the electron densities from MD simulations and experiment to be ~7 Å. The lamellar spacing at a cortisone concentration of 50 mol% is determined to be $d_z = 48$ Å, the head group distance to $d_{HH} = 32$ Å and the thickness of the hydrophobic core to ~25 Å. The fact that the lamellar spacing decreased slightly faster than the membrane thickness with increasing cortisone content is strong evidence that the cortisone molecules partition in the bilayers and cortisone crystallites do not form outside of the membranes.

In-plane diffraction is shown in Fig. 3d. While 0, 2 and 5 mol% cortisone membranes show the lipid acyl chain correlation peak, only, additional peaks are observed at 20 mol% and 50 mol% whose intensities increase with increasing cortisone. The peaks at $q_{||} = 1$ Å^{-1}, 1.12 Å^{-1}, and 1.17 Å^{-1} agree well with the [100], [102], [103] reflec-

tions observed from crystallized cortisone[29], respectively, with lattice constants of $a = 7.31$ Å and $c = 22$ Å. The presence of these peaks suggests the formation of crystallized cortisone at high concentrations.

To determine the orientation of the cortisone structures with respect to the bilayers, the peaks at $q_{\parallel} = 1.12\,\text{Å}^{-1}$ and $1.17\,\text{Å}^{-1}$ were integrated along the azimuthal angle ϕ from $10° < \phi < 60°$ ($\phi < 10$ was not included due to the effect of absorption). The results for 35 mol% and 50 mol% cortisone are presented in Fig. 3e. Herman's orientation function, $f = \frac{3}{2} < \cos^2(\phi) > -\frac{1}{2}$, was used to quantify the orientation of the crystals with the membrane stack. Crystals observed in the 35 mol% sample result in $f = 0.96$ and crystals from the 50 mol% sample show $f = 0.64$. While a perfect orientation has $f = 1$, randomly oriented crystallites would result in $f = 0.25$. The cortisone crystals, therefore, have a preferred orientation along $q_{\parallel}$. The organization of the cortisone molecules and the corresponding unit cell is depicted in Fig. 3f.

Discussion

The interaction of cortisone with model POPC bilayers was studied using MD simulations and X-ray diffraction. In both, experiment and simulation, cortisone was found to strongly interact with the lipid bilayer. X-ray and neutron diffraction experiments have previously reported conformational changes in lipid bilayers with the introduction of drugs and hormones[30–33]. Amphiphilic drugs, such as aspirin or ibuprofen were shown to partition into the interfacial region[31–33,34].

A membrane bound state for cortisone was found in MD simulations and X-ray diffraction experiments at low cortisone concentrations. The simulations observed a minima in the PMF for cortisone across the bilayer, with a strong preference to avoid entering the bilayer center. Simulations and experiments observe cortisone in the hydrophilic to hydrophobic interface with the hydrophobic face in contact with the lipid tails. By positioning into the interfacial region of the bilayer, cortisone causes a decrease in the bilayer thickness and an increase in the area per lipid molecule.

Additional scattering features were observed at 20 mol% cortisone, indicating the presence of crystallized cortisone within the membranes. These cortisone crystals are oriented with the membrane; the corresponding crystal lattices are forming perpendicular to the membrane plane. During the simulations, however, no evidence for cortisone crystallization was observed, neither from visual inspection of the trajectories nor from computed X-ray intensity maps (Figure S1), suggesting that crystallization occurs on time scales beyond the accessible simulation times. The lipids provide a viscous environment for cortisone, which leads to slow conformational sampling of cortisone-cortisone contacts, which would be required for crystallization. Alternatively, we cannot exclude the possibility that the applied force fields do not reproduce the free-energy difference between crystallized and solubilized cortisone.

The process of cortisone crystallite formation is illustrated in Fig. 4. Parts a) to d) show simulation snapshots for cortisone concentrations of 0, 10, 40 and 50 mol%. At low cortisone concentrations of 10 mol%, the cortisone molecules partition in the hydrophilic/hydrophobic bilayer interface and align parallel to the bilayers. The presence of cortisone increases the area per lipid molecule and decreases the membrane width. With increasing cortisone content, the cortisone molecules start to penetrate the hydrophobic core. At cortisone concentrations of 50 mol% in the simulations (in part d), the membrane's thickness has decreased such that cortisone molecules in the different leaflets can find partners from the opposite leaflet when they penetrate the hydrophobic core. We propose that these structures are the pre-cursors for the formation of cortisone crystallites. Although the experimental threshold for detecting crystals is 20 mol%, we cannot exclude the possibility that crystals also exist at concentrations below 20 mol% and that the corresponding signals are too small to be detected by diffraction in the present study.

The corresponding structure of a membrane with embedded crystallite is shown in Fig. 4e. The thickness of the hydrophobic core at 50 mol% cortisone of ~25 Å corresponds to about 4 layers of cortisone. The decrease in the lamellar spacing d_z is mainly caused by the decrease in membrane thickness; the small value of d_z of 48 Å excludes that the cortisone crystallites form outside of the bilayers.

Cortisone is often used to treat inflammation of the joints to function as inflammation reducing agents, which in turn reduces pain in the joints. It is used in the treatment of bursitis, tendonitis, and arthritis in the form of local injections in the knee, shoulder, elbow or back, or systemic injections for inflammation all over the body. Up to 100 mg of cortisone are commonly injected during an anti-inflammatory treatment[35]. From a simple coarse calculation, if we assume that a cell is ~50 μm in diameter, and the average lipid has an area of 65 Å^2, and a membrane/water partition coefficient of 200, then 100 mg of cortisone could result in up to 10^9 cells obtaining cortisone/plasma membrane lipid concentrations of ~20 mol%. Therefore, cortisone is likely present in the elevated concentrations studied here. A cortisone flare is a reaction of the body to a cortisone injection, typically 24–48 hours after the injection has been administered. In about 5% of the cases, cortisone is found to crystallize and cause pain around the soft tissue along with the joint lining, in conjunction with strong pain. A flare is typically treated by resting the inflamed area.

In our simulations and experiments, the lipid bilayer was found to serve as a 2-dimensional substrate for cortisone accumulation and crystallization As cortisone is believed to cross the membrane by free diffusion or membrane mediated endocytosis, the steroid can bind to both the inner and outer leaflet of the plasma membrane, thereby initiating crystallization in the manner outlined in Fig. 4[36]. As crystals were found to nucleate inside the bilayers, the composition of the membranes, such as cholesterol content and ratio between saturated and unsaturated fatty acids is likely an important parameter. The present study adds to the increasing evidence that drug-membrane interactions are important for modeling drug side-effects.

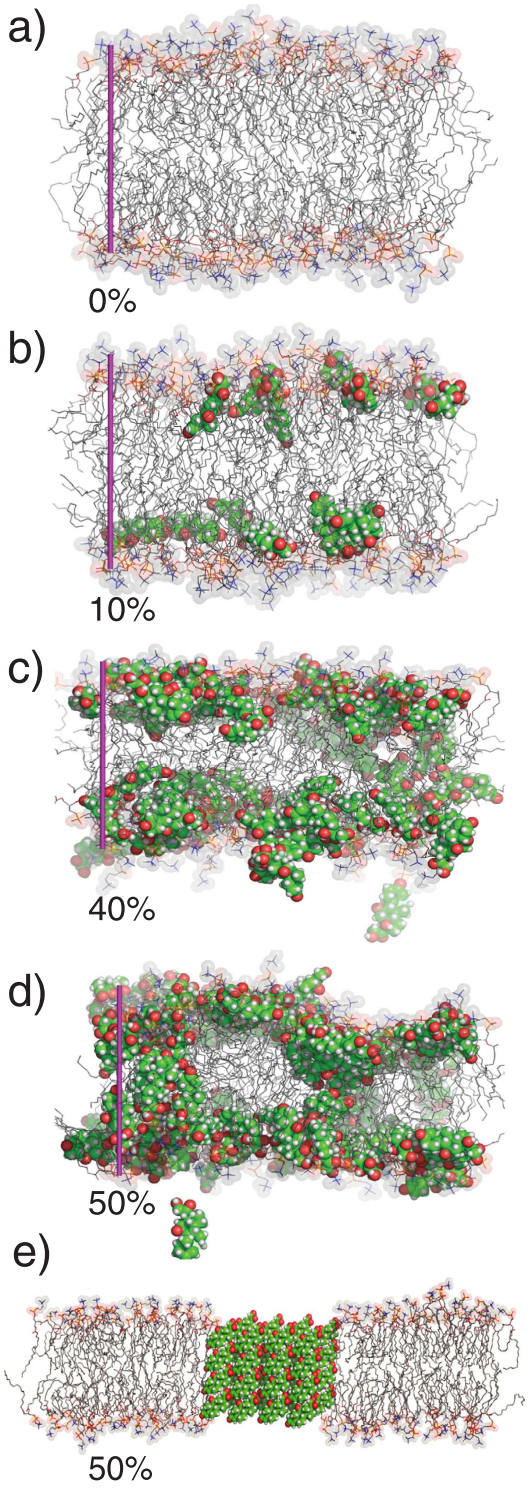

Figure 4. Simulation snapshots for POPC membranes at 0, 10, 40 and 50 mol% (**a**–**d**). The purple bar indicates a 40 Å ruler. The structural model of the cortisone crystals based on X-ray experiments is shown in (**e**).

Conclusions

Steroid flares, commonly observed after cortisone injection, have been attributed to the formation of microcrystalline corticosteroid. In this study, we show that crystallized cortisone is observed in POPC model membranes at high cortisone concentration. By combining molecular dynamics simulations and X-ray diffraction, we present a potential mechanism for the nucleation of cortisone flares, where the steroid crystals nucleate within the 2-dimensional plane of the lipid membrane.

Cortisone partitions into the head group-tail group interfacial region of the bilayers at low cortisone concentrations, aligning parallel to the membranes. Increasing cortisone concentration results in an increased area per lipid, a decreasing membrane width, and more disordered lipid tails. At concentrations of more than 20 mol% cortisone, the formation of crystalized cortisone inside the hydrophobic membrane core was observed. These crystals form when the membrane thickness has decreased such that cortisone molecules in the different leaflets can find partners from the opposite leaflet, resulting in a non-zero density of cortisone molecules in the bilayer center. The corresponding crystallites orient with the membranes.

Materials and Methods

Experimental Details. *Preparation of Multi-Lamellar Membrane Samples.* Highly-oriented multi lamellar membranes were prepared on single-side polished silicon wafers ($1 \times 1\,cm^2$). 1-palmitoyl-2-oleoyl-sn-glycero-3-phosphocholine, (POPC, Avanti Polar Lipids) and Cortisone (17-hydroxy-11-dehydrocorticosterone, Sigma) were mixed at the desired molecular ratio and dissolved in a 1:1 mixture of chloroform (Caledon)/2,2,2-trifluoroethanol (TFE) (Sigma). The final solution concentration was 16 mg/mL.

The wafers were placed in 1,2-dichloromethane (Caledon) within a closed Pyrex dish. Wafers were cleaned by sonication for 30 minutes, which resulted in a hydrophobic silicon surface. The wafers were then removed and rinsed three times thoroughly with alternating methanol and 18.2 MΩ·cm water. The wafers were then dried with pressurized nitrogen gas (N_2) and placed on a tilting incubator set to 310 K. A syringe was used to deposit ~65 μL of the POPC-cortisone solution on the wafer while the tilt (speed 15, tile angle 1°) provided circular flow and even distribution. The samples was allowed to dry for 20 minutes on the tilting incubator.

The samples were then placed in a vacuum for ~24 hours at 298 K to allow for the evaporation of trace solvent. Wafers were stored in a glove box (8% H_2O) to prevent lipid peroxidation, prior to the X-ray scattering experiments[37,38].

X-ray Diffraction Experiment. Out-of-plane and in-plane X-ray scattering data was obtained using the Biological Large Angle Diffraction Experiment (BLADE) in the Laboratory for Membrane and Protein Dynamics at McMaster University. BLADE uses a 9 kW (45 kV, 200 mA) CuKα Rigaku Smartlab rotating anode at a wavelength of 1.5418 Å. Both source and detector are mounted on moveable arms such that the membranes stay horizontal during measurements. Focussing, multi layer optics provide a high intensity parallel beam with monochromatic X-ray intensities up to 10^{10} counts/(s × mm^2). This beam geometry provides optimal illumination of the membrane samples to maximize the scattered signal. By using highly-oriented stacks, the in-plane ($q_\parallel$) and out-of-plane (q_z) structure of the membranes could be determined independently. Full 2-dimensional reciprocal space maps are shown in Fig. 2. All scans were measured at 301 K and 97% hydration, in the fluid phase of bilayers.

As in-plane features are usually orders of magnitude weaker than the pronounced out-of-plane features, slices $0.03\,Å^{-1} < q_z < 0.3\,Å^{-1}$ were integrated to enhance the data quality.

Calculation of Electron Densities. The out-of-plane structure of the membrane was determined using specular reflectivity. The relative electron density, ρ(z), is approximated by a 1-dimensional Fourier analysis[31,39].

$$\rho(z) = \frac{2}{d_z}\sum_{n=1}^{N}\sqrt{I_n q_n}\,\nu_n\,\cos\left(\frac{2\pi n z}{d_z}\right). \tag{1}$$

N is the highest order of the Bragg peaks observed in the experiment. The integrated peak intensities, I_n, are multiplied by q_n to receive the form factors, $F(q_n)$[31,39]. The bilayer form factor $F(q_z)$, which is in general a complex quantity, is real-valued in the case of centro-symmetry. The phase problem of crystallography, therefore, simplifies to the sign problem $F(q_z) = \pm\left|F(q_z)\right|$ and the phases, ν_n, can only take the values ± 1. The phases ν_n are needed to reconstruct the electron density profile from the scattering data following Equation 1. When the membrane form factor $F(q_z)$ is measured at several q_z values, a continuous function, $T(q_z)$, which is proportional to $F(q_z)$, can be fitted to the data[31,39].

$$T(q_z) = \sum_n \sqrt{I_n q_n}\,\mathrm{sinc}\left(\frac{1}{2}d_z q_z - \pi n\right). \tag{2}$$

Once an analytical expression for $T(q_z)$ has been determined from fitting the experimental peak intensities, the phases ν_n can be assessed from $T(q_z)$. The phase array $\nu_n = [-1\ -1\ 1\ -1\ 1]$ was used for all samples. A sample $T(q_z)$ is shown in Fig. 3b.

For POPC and POPC + 5 mol% cortisone, the calculated electron densities, $\rho(z)$, which are initially on an arbitrary scale, were then scaled using the following protocol: The curves were vertically shifted, such that the density at the center of the bilayer was equal to the electron density value determined in the simulations of

$\rho(z) = 0.26\,e^-/Å^3$. The curves were then scaled until the total number of electrons within the lipid unit cell across a membrane leaflet, $e^- = A_L \int_0^{dz/2} \rho(z)\,dz$ agrees with the total number of electrons expected based on the sample composition. The area per lipid obtained from simulation were used for the calculation.

The total number of electrons includes contributions from POPC, cortisone, and water molecules. The number of water molecules per lipid was calculated by calculating the approximate volume of water, $V_w = A_L(d_z - d_{HH})/2$, and $\rho_w = 0.33\,e^-/Å^3$. For pure POPC and POPC with 5 mol% cortisone, 20 and 21 water molecules per POPC were calculated, respectively. Therefore, for the POPC sample, the integral over the lipid unit cell is assumed to contain one POPC molecule and 20 water molecules. For the 5 mol% cortisone sample, the integral number of electrons over a lipid unit cell in the bilayer is assumed to contain a full lipid molecule, 21 water molecules, and 5% of a cortisone molecule. The procedure follows that outlined by Alsop *et al.*[33].

Molecular Dynamics Simulations. *Simulation setup and parameters.* Parameters for POPC were taken from the SLipids force fields[40], and water was described by the TIP3P model[41]. Cortisone was described by the General Amber Force Field[42]. The cortisone topology was generated by ACPYPE, which builds upon the Antechamber software[43,44]. Following the default Antechamber protocol, partial charges were computed on the Hartree-Fock level using the 6-31G* basis set, with the Gaussian 09 software package[45]. The charges were fitted to reproduce the electrostatic potential produced by the quantum chemical calculations with the RESP method[46]. The topology file is available from the author (JSH) upon request.

The lipid membrane simulation systems were generated with the web server MemGen (http://memgen.uni-goettingen.de)[47]. The patches corresponding to cortisone concentrations between 0 and 50% contained between 128 and 100 POPC, between 0 and 100 cortisone, and between 4480 and 6300 water molecules (Supporting Table S1). After energy minimization, each system was simulated for 200 ns. The first 40 ns of all simulations was removed for equilibration. To validate the convergence of the simulations, three independent 200 ns repetitions of the system with 40% cortisone were simulated (Figure S2).

All simulations were carried out using the Gromacs simulation software, version 4.6[48]. During equilibrium simulations, the temperature was controlled at 300 K through velocity rescaling[49] ($\tau = 0.5$ ps), and the pressure was kept at 1 bar using a semi-isotropic weak coupling scheme[50] ($\tau = 1$ ps). The SETTLE[51] algorithm was applied to constrain bond lengths and angles of water molecules, and LINCS[52] was used to constrain all other bond lengths, allowing a time step of 2 fs. Electrostatic interactions were calculated using the particle-mesh Ewald method[53,54], and dispersive interactions were described by a Lennard-Jones potential with a cut-off at 10 Å. To exclude that the cut-off has a major on the results, three additional 200 ns simulations of the system with 40% cortisone were conducted, but simulating instead with a cut-off at 12 Å. The results from these simulations were very similar, suggesting that a 10 Å is acceptable for the present study.

Umbrella sampling simulations. The simulation protocol was chosen similar to previous studies[55,56]. Accordingly, starting structures for the umbrella simulations were taken from randomly chosen snapshots of the last 10 ns of an 20-nanosecond equilibrium simulation of 98 POPC and 5390 water molecules. The membrane normal, z, was chosen as reaction coordinate for solute permeation, where $z = 0$ Å is defined by the center of mass (COM) of the lipid molecules. Adjacent umbrella windows were separated by 1 Å, and the umbrella windows spanned the complete space between one bulk water region across the membrane and into the other bulk water region.

Solutes were inserted at the center of the respective umbrella windows. To save computational resources, two or three different umbrella windows were sampled within each simulation, keeping a distance of 35 Å along z between cortisone molecules. Water molecules, which overlapped with the solute were removed. Overlaps between the solute and lipid atoms were removed by gradually switching on Lennard-Jones interactions between the solute and the rest of the system within 5000 simulation steps, using soft-core Lennard-Jones potentials and a stochastic dynamics integration scheme. During these insertion simulations only, a large virtual site atom was added to the center of every aromatic ring. That procedure ensured that lipid tails were fully repelled from the aromatic rings of the solutes. Subsequently, the energy of each structure was minimized.

A harmonic umbrella potential acting on the center of mass of the solute was applied (force constant 2000 kJ $mol^{-1}nm^{-2}$). Each umbrella simulation was carried out for 80 ns. The temperature was set to 300 K through a stochastic dynamics integrator ($\tau = 0.1$ ps). The pressure was controlled at 1 bar using a semi-isotropic weak coupling scheme[50], scaling the box in the x-y plane only, but keeping the box dimension in z-direction fixed. After removing the first 10 ns for equilibration, the PMFs were computed with the weighted histogram analysis method (WHAM)[57], as implemented in the g_wham software[58]. First, non-periodic and non-symmetrized PMFs were computed. These PMFs were reasonably symmetric with respect to the membrane center and exhibited only a small offset between the two bulk water regimes, suggesting that the PMFs were converged. Subsequently, a periodic PMF was computed and symmetrized with respect to the membrane center ($z = 0$). Because the PMF $G(z)$ was defined to zero in bulk water, the membrane/water partition coefficient could be computed via $K = L^{-1}\int_{-L/2}^{L/2} \exp(-G(z)/k_BT)\,dz$, where k_B denotes the Boltzmann constant and T the temperature.

References

1. Seydel, J. *et al.* The importance of drug-membrane interaction in drug research and development. *Quant. Struct.-Act. Rel.* **11,** 205–210 (1992).
2. Overington, J. P., Al-Lazikani, B. & Hopkins, A. L. How many drug targets are there? *Nat. Rev. Drug Discov.* **5,** 993–996 (2006).
3. Zhou, Y., Plowman, S. J., Lichtenberger, L. M. & Hancock, J. F. The anti-inflammatory drug indomethacin alters nanoclustering in synthetic and cell plasma membranes. *J. Biol. Chem.* **285,** 35188–35195 (2010).
4. Zhou, Y., Cho, K.-J., Plowman, S. J. & Hancock, J. F. Nonsteroidal anti-inflammatory drugs alter the spatiotemporal organization of ras proteins on the plasma membrane. *J. Biol. Chem.* **287,** 16586–16595 (2012).

5. Rheinstädter, M. C., Schmalzl, K., Wood, K. & Strauch, D. Protein-protein interaction in purple membrane. *Phys. Rev. Lett.* **103,** 128104–1 (2009).
6. World Health Organization. *World Health Organization 19th List of Essential Medicines*.
7. Fadale, P. D. & Wiggins, M. E. Corticosteroid injections: their use and abuse. *J. Am. Acad. Orthop. Surg.* **2,** 133–140 (1994).
8. Cole, B. J. & Schumacher, H. R. Injectable corticosteroids in modern practice. *J. Am. Acad. Orthop. Surg.* **13,** 37–46 (2005).
9. Lu, N. Z. *et al.* International union of pharmacology. lxv. the pharmacology and classification of the nuclear receptor superfamily: glucocorticoid, mineralocorticoid, progesterone, and androgen receptors. *Pharmacol. Rev.* **58,** 782–797 (2006).
10. Rousseau, G. G., Baxter, J. D. & Tomkins, G. M. Glucocorticoid receptors: relations between steroid binding and biological effects. *J. Mol. Biol.* **67,** 99–115 (1972).
11. Beato, M., Herrlich, P. & Schütz, G. Steroid hormone receptors: many actors in search of a plot. *Cell* **83,** 851–857 (1995).
12. Vane, J. & Botting, R. Inflammation and the mechanism of action of anti-inflammatory drugs. *FASEB J.* **1,** 89–96 (1987).
13. Thompson, E. B. & Lippman, M. E. Mechanism of action of glucocorticoids. *Metabolism* **23,** 159–202 (1974).
14. Flower, R. Lipocortin and the mechanism of action of the glucocorticoids. *Br. J. Pharmacol.* **94,** 987–1015 (1988).
15. Ling, M. H., Perry, P. J. & Tsuang, M. T. Side effects of corticosteroid therapy: psychiatric aspects. *Archives Gen. Psychiatry* **38,** 471–477 (1981).
16. Buchman, A. L. Side effects of corticosteroid therapy: Inflammatory bowel disease. *J. Clin. Gastroenterol.* **33,** 289–294 (2001).
17. Sirois, F. Steroid psychosis: a review. *Gen. Hosp. Psychiatry*. **25,** 27–33 (2003).
18. Schäcke, H., Döcke, W.-D. & Asadullah, K. Mechanisms involved in the side effects of glucocorticoids. *Pharmacol. Ther.* **96,** 23–43 (2002).
19. Berthelot, J.-M., Le Goff, B. & Maugars, Y. Side effects of corticosteroid injections: What's new? *Joint Bone Spine* **80,** 363–367 (2013).
20. Goldfarb, C. A., Gelberman, R. H., McKeon, K., Chia, B. & Boyer, M. I. Extra-articular steroid injection: early patient response and the incidence of flare reaction. *J. Hand Surg.* **32,** 1513–1520 (2007).
21. McCarty, D. J. & Hogan, J. M. Inflammatory reaction after intrasynovial injection of microcrystalline adrenocorticosteroid esters. *Arthritis Rheum.* **7,** 359–367 (1964).
22. Kahn, C. B., Hollander, J. L. & Schumacher, H. R. Corticosteroid crystals in synovial fluid. *JAMA* **211,** 807–809 (1970).
23. Rull, M., Clayburne, G., Sieck, M. & Schumacher, H. R. Intra-articular corticosteroid preparations: different characteristics and their effect during inflammation induced by monosodium urate crystals in the rat subcutaneous air pouch *Rheumatology* **42,** 1093–1100 (2003)
24. Golden, G., Rubin, R. & Mason, R. Steroid hormones partition to distinct sites in a model membrane bilayer: direct demonstration by small-angle x-ray diffraction. *BBA-Biomembranes* **1368,** 161–166 (1998).
25. Vijayan, R. & Biggin, P. C. A steroid in a lipid bilayer: localization, orientation, and energetics. *Biophys. J.* **95,** L45–L47 (2008).
26. Kučerka, N., Tristram-Nagle, S. & Nagle, J. F. Structure of fully hydrated fluid phase lipid bilayers with monounsaturated chains. *J. Membr. Biol.* **208,** 193–202 (2006).
27. Armstrong, C. L. *et al.* The observation of highly ordered domains in membranes with cholesterol. *PLOS ONE* **8,** e66162 (2013).
28. Braun, A. R. *et al.* Determination of electron density profiles and area from simulations of undulating membranes. *Biophys. J.* **100,** 2112–2120 (2011).
29. Dey, R., Langer, V., Roychowdhury, P., Roychowdhury, S. & Drew, M. 21-deoxycortisone (17α-hydroxy-4-pregnene-3, 11, 20-trione). *Acta Crystallogr. Sect. C* **61,** 201–203 (2005).
30. Pabst, G., Kučerka, N., Nieh, M.-P., Rheinstädter, M. & Katsaras, J. Applications of neutron and x-ray scattering to the study of biologically relevant model membranes. *Chem. Phys. Lipids* **163,** 460–479 (2010).
31. Barrett, M. A. *et al.* Interaction of aspirin (acetylsalicylic acid) with lipid membranes. *PLOS ONE* **7,** e34357 (2012).
32. Dies, H., Cheung, B., Tang, J. & Rheinstädter, M. C. The organization of melatonin in lipid membranes. *BBA-Biomembranes* **1848,** 1032–1040 (2015).
33. Alsop, R. J. *et al.* Cholesterol expels ibuprofen from the hydrophobic membrane core and stabilizes lamellar phases in lipid membranes containing ibuprofen. *Soft Matter* **11,** 4756–4767 (2015).
34. Alsop, R. J., Barrett, M. A., Zheng, S., Dies, H. & Rheinstädter, M. C. Acetylsalicylic acid (asa) increases the solubility of cholesterol when incorporated in lipid membranes. *Soft Matter* **10,** 4275–4286 (2014).
35. Hollander, J. L., Brown, E. M., Jessar, R. A. & Brown, C. Y. Hydrocortisone and cortisone injected into arthritic joints: comparative effects of and use of hydrocortisone as a local antiarthritic agent. *JAMA* **147,** 1629–1635 (1951).
36. Chen, Hubert C., Farese & Robert, V. Steroid hormones: interactions with membrane-bound receptors *Curr. Biol.* **9,** R478–R481 (1999).
37. Porter, N. A., Caldwell, S. E. & Mills, K. A. Mechanisms of free radical oxidation of unsaturated lipids. *Lipids* **30,** 277–290 (1995).
38. Yin, H., Xu, L. & Porter, N. A. Free radical lipid peroxidation: mechanisms and analysis. *Chem. Rev.* **111,** 5944–5972 (2011).
39. Nagle, J. & Wiener, M. Relations for lipid bilayers. connection of electron density profiles to other structural quantities. *Biophys. J.* **55,** 309 (1989).
40. Jämbeck, J. P. M. & Lyubartsev, A. P. An extension and further validation of an all-atomistic force field for biological membranes. *J. Chem. Theory Comput.* **8,** 2938–2948 (2012).
41. Jorgensen, W. L., Chandrasekhar, J., Madura, J. D., Impey, R. W. & Klein, M. L. Comparison of simple potential functions for simulating liquid water. *J. Chem. Phys.* **79,** 926–935 (1983).
42. Wang, J., Wolf, R. M., Caldwell, J. W., Kollman, P. A. & Case, D. A. Development and testing of a general amber force field. *J. Comput. Chem.* **25,** 1157–1174, doi: 10.1002/jcc.20035 (2004).
43. Wang, J., Wang, W., Kollman, P. & Case, D. Automatic atom type and bond type perception in molecular mechanical calculations. *Mol. Graphics Modell.* **26,** 247260 (2006).
44. Da Silva, A. W. S. & Vranken, W. F. ACPYPE-Antechamber python parser interface. *BMC. Res. Notes* **5,** 367 (2012).
45. Frisch, M. J. *et al. Gaussian 09 Revision D.01*. Gaussian Inc. Wallingford CT (2009).
46. Bayly, C. I., Cieplak, P., Cornell, W. & Kollman, P. A. A well-behaved electrostatic potential based method using charge restraints for deriving atomic charges: the resp model. *J. Phys. Chem.* **97,** 10269–10280 (1993).
47. Knight, C. J. & Hub, J. S. MemGen: A general web server for the setup of lipid membrane simulation systems. *Bioinformatics* btv292 (2015).
48. Pronk, S. *et al.* GROMACS 4.5: a high-throughput and highly parallel open source molecular simulation toolkit. *Bioinformatics* **29,** 845–854 (2013).
49. Bussi, G., Donadio, D. & Parrinello, M. Canonical sampling through velocity rescaling. *J. Chem. Phys.* **126,** 014101 (2007).
50. Berendsen, H. J. C., Postma, J. P. M., DiNola, A. & Haak, J. R. Molecular dynamics with coupling to an external bath. *J. Chem. Phys.* **81,** 3684–3690 (1984).
51. Miyamoto, S. & Kollman, P. A. SETTLE: An analytical version of the SHAKE and RATTLE algorithms for rigid water models. *J. Comp. Chem.* **13,** 952–962 (1992).
52. Hess, B. P-LINCS: A parallel linear constraint solver for molecular simulation. *J. Chem. Theory Comput.* **4,** 116–122 (2008).
53. Darden, T., York, D. & Pedersen, L. Particle mesh Ewald: an N·log(N) method for Ewald sums in large systems. *J. Chem. Phys.* **98,** 10089–10092 (1993).
54. Essmann, U. *et al.* A smooth particle mesh ewald potential. *J. Chem. Phys.* **103,** 8577–8592 (1995).

55. Wennberg, C., van der Spoel, D. & Hub, J. S. Large influence of cholesterol on solute partitioning into lipid membranes. *J. Am. Chem. Soc.* **134,** 5351–5361 (2012).
56. Zocher, F., Wennberg, C., van der Spoel, D., Pohl, P. & Hub, J. S. Local micro-partition coefficients govern solute permeability of cholesterol-containing membranes. *Biophys. J.* **105,** 2760–2770 (2013).
57. Kumar, S., Bouzida, D., Swendsen, R. H., Kollman, P. A. & Rosenberg, J. M. The weighted histogram analysis method for free-energy calculations on biomolecules. I. The method. *J. Comp. Chem.* **13,** 1011–1021 (1992).
58. Hub, J. S., de Groot, B. L. & van der Spoel, D. g_wham-A free weighted histogram analysis implementation including robust error and autocorrelation estimates. *J. Chem. Theory Comput.* **6,** 3713–3720 (2010).

Acknowledgements
We thank Kalina Atkovska for generating the GAFF topology of cortisone. This research was funded by the Natural Sciences and Engineering Research Council (NSERC) of Canada, the National Research Council (NRC), the Canada Foundation for Innovation (CFI), and the Ontario Ministry of Economic Development and Innovation. R.J.A. is the recipient of an NSERC PGS-D, M.C.R. is the recipient of an Early Researcher Award from the Province of Ontario. J.S.H. was supported by the Deutsche Forschungsgemeinschaft (HU 1971/1-1 and SFB 803/A12).

Author Contributions
R.J.A., A.K. and M.C.R. designed, performed, and analyzed the experiments. J.S.H. designed, performed, and analyzed the simulations. R.J.A., A.K., J.S.H. and M.C.R. wrote and edited the manuscript.

Additional Information
Supplementary information accompanies this paper at http://www.nature.com/srep

Competing financial interests: The authors declare no competing financial interests.

How to cite this article: Alsop, R. J. *et al.* The Lipid Bilayer Provides a Site for Cortisone Crystallization at High Cortisone Concentrations. *Sci. Rep.* **6**, 22425; doi: 10.1038/srep22425 (2016).

The Lipid Bilayer Provides a Site for Cortisone Crystallization at High Cortisone Concentrations

Richard J. Alsop,[1] Adree Khondker,[1] Jochen S. Hub,[2,*] and Maikel C. Rheinstädter[1,†]

[1] *Department of Physics and Astronomy, McMaster University, Hamilton, Ontario, Canada*

[2] *Georg-August-University Göttingen, Institute for Microbiology and Genetics, Göttingen, Germany*

[*] jhub@gwdg.de; Institute for Microbiology and Genetics, Georg-August-University Göttingen, Justus-von-Liebig-Weg 11, 37077 Göttingen, Germany; Phone: +49-(0)551-39-14189

[†] rheinstadter@mcmaster.ca; Department of Physics and Astronomy, McMaster University, ABB-241, 1280 Main Street West, Hamilton, Ontario L8S 4M1, Canada; Phone: +1-(905)-525-9140-23134, Fax: +1-(905)-546-1252

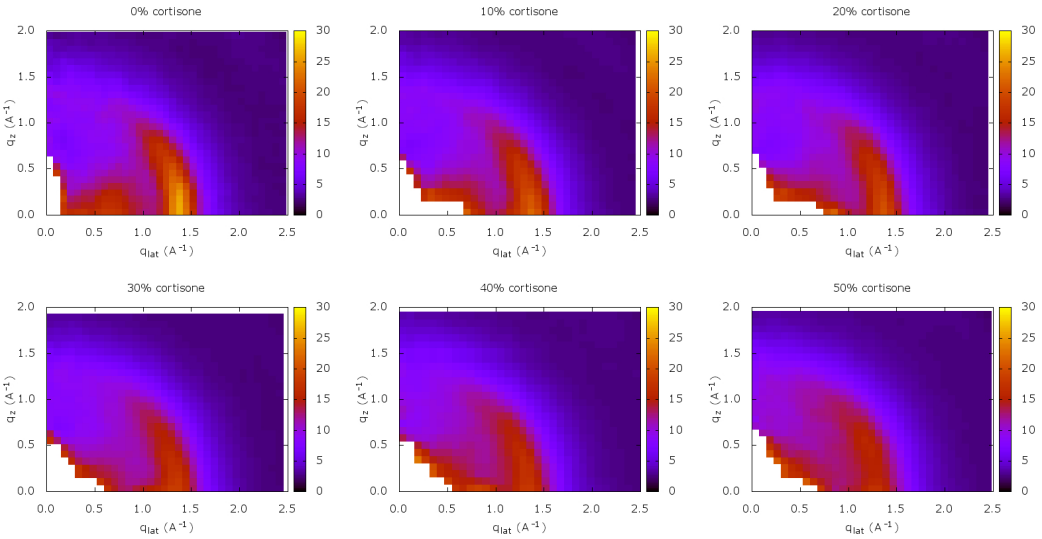

FIG. S1. Two-dimensional X-ray intensities $S(q_{\mathrm{lat}}, q_z)$ computed from molecular dynamics simulations, at cortisone concentrations between 0 and 50% (see figure titles). $S(q_{\mathrm{lat}}, q_z)$ was computed from POPC and cortisone atoms. $S(q_{\mathrm{lat}}, q_z)$ is plotted as a function of momentum transfer q_{lat} in the membrane plane and q_z perpendicular to the membrane plane. In agreement with the experimental data, the chain correlation peak at $q = \sqrt{q_{\mathrm{lat}}^2 + q_z^2} \approx 1.4\,\mathrm{\AA}^{-1}$ is reduced and smeared out upon increasing cortisone content. In contrast to the experimental data, no additional peaks due to cortisone crystals appear because crystals did not form within the accessible simulation time.

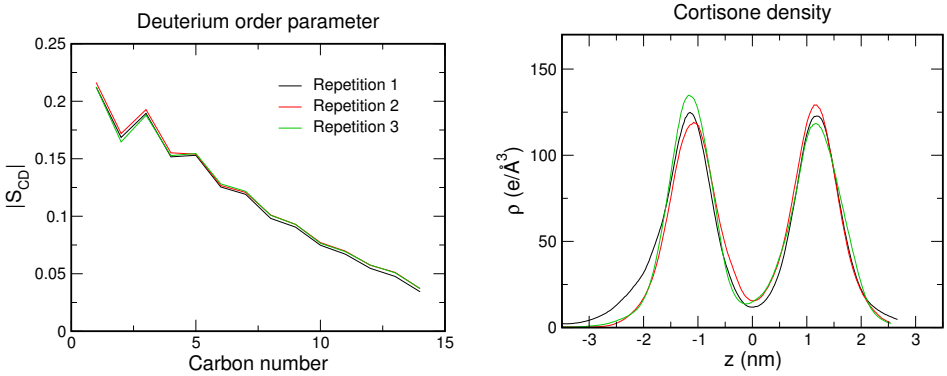

FIG. S2. Deuterium order parameter (left) and cortisone density (right) computed from three independent 200 ns simulations of the simulation system with 40% cortisone (after removing the first 40 ns for equilibration). The agreement suggests that the conformational sampling accessible on this time scale is converged. However, the analysis does not exclude the possibility of the formation of cortisone crystals on longer time scales.

TABLE 1. Summary of equilibrium MD simulations: approximate cortisone content, number of POPC N_L, coritsone N_c, and water molecules N_w, simulation time, number of repetitions.

cortisone content	N_L / N_c / N_w	t_{sim} (ns)	repetitions
0%	128 / 0 / 4480	100	1
5%	132 / 8 / 4900	200	1
10%	122 / 14 / 4760	200	1
20%	120 / 30 / 5250	200	1
30%	126 / 54 / 6300	200	1
40%	108 / 72 / 5400	200	3
50%	100 / 100 / 6000	200	1

5.3 Paper VI: Curcumin Protects Membranes Through Carpet or Insertion Model Depending on Hydration

Richard J. Alsop, Alexander Dhaliwal, Maikel C. Rheinstädter. *Curcumin Protects Membranes Through Carpet or Insertion Model Depending on Hydration.* Accepted to Langmuir

5.3.1 Preface to Paper VI

Curcumin is the main ingredient in the Indian spice Turmeric. It is used as an anti-inflammatory and anti-oxidant in traditional medicine. In addition, recent studies have suggested it could help in fighting Alzhemer's and cancer [85, 86]. The breadth and diversity of curcumin's supposed benefits, and lack of common receptor, has led to speculation that it has a general mechanism of membrane protection. However, there is debate for how curcumin could effect lipid membranes [87]. Two interactions have been observed:

1. Curcumin is a planar molecule with three rings. In one model, curcumin lies flat on membranes, hydrogen bonding with the head groups and protecting against rogue peptide insertion. We refer to this model as the "carpet" model [88].

2. Curcumin embeds within the bilayer in an upright position and orders lipid tails, much like cholesterol. By stiffening tails, it prevents insertion of problematic peptides. This is hereby referred to as the "embedded model" [89].

In this paper, we sought to understand how curcumin actually bonded to lipid membranes. We prepared oriented DMPC membranes, and studied the structure using MD simulations and X-ray diffraction. Whereas many of the other papers used only dry or hydrated membranes, we chose to study the curcumin-containing membranes in both their hydrated and dehydrated states.

This turned out to be important. In dehydrated membranes, both MD simulations and experiments demonstrated that curcumin lay flat on the bilayer, in agreement with the carpet model. In hydrated membranes, the embedded model was observed. However, curcumin in the embedded state we observed was not like cholesterol: it was tilted rather than upright, and it did not increase lipid tail order.

An interplay between hydrophobic and hydrophilic interactions likely explains why both states are observed. Curcumin is a hydrophobic molecule that does not dissolve in water. At the same time, it has hydroxyl groups that encourage hydrogen bonding with the head groups. Therefore, the molecule chooses a deeper state when more hydration is present.

In a physiological system, bilayers are generally thought of as fully hydrated. However, membranes also experience osmotic pressure. Bilayers at physiological salt concentrations actually may be in a dehydrated state [90, 19]. Therefore, curcumin may protect the membrane by a carpet or embedded state, depending on the osmotic pressure. Also, it is unclear how curcumin would protect

the membrane in the embedded state, as no stiffening effect is observed. The experiment therefore presents a case study of membrane hydration/osmotic pressure influencing the drug's effect.

Author Contributions:

- *Experimental Concept:* Richard Alsop
- *Sample Preparation:* Richard Alsop
- *X-ray Experiments:* Richard Alsop
- *MD Simulations:* Richard Alsop, Alexander Dhaliwal
- *Data Analysis:* Richard Alsop
- *Manuscript Preparation:* Richard Alsop, Maikel Rheinstädter

Curcumin Protects Membranes Through Carpet or Insertion Model Depending on Hydration

Richard J. Alsop,[1] Alexander Dhaliwal,[1] and Maikel C. Rheinstädter[1,*]

[1] *Department of Physics and Astronomy, McMaster University, Hamilton, Ontario, Canada*

(Dated: May 9, 2017)

Curcumin is the main ingredient of tumeric, a common indian spice. Curcumin shows a broad spectrum of effects, including anti-Alzheimer's and anti-oxidant properties. An interaction between curcumin and lipid membranes has been speculated as the root-cause, and the molecule is often proposed to 'protect' the bilayer. However, the detailed molecular mechanism of this protection is disputed. There is evidence that curcumin either a) lies flat on the bilayer and provides a 'carpet' for protection by forming a steric barrier, or b) inserts into the membrane and stiffens tails, thereby protecting against peptide insertion. We studied the interaction between curcumin and 1,2-dimyristoyl-sn-glycero-3-phosphocholine (DMPC) bilayers at different concentrations using high-resolution X-ray diffraction and Molecular Dynamics (MD) computer simulations. We observed curcumin molecules forming a carpet in dehydrated bilayers, while in hydrated membranes, the curcumin molecules were found to insert in the bilayers. From calculations of the potential of mean force (PMF) we find two minima, a metastable state in the head group region, at $|z| \sim$22 Å, and a global minimum in the hydrophobic membrane core, at $|z| \sim$9 Å. Population of the two states depends on membrane hydration. Experiments may thus observe curcumin in carpet or inserted, depending on osmotic pressure conditions created for instance by salts, buffer solutions, substrates or macromolecular solutes. In the carpet model, curcumin dehydrates lipid bilayers and decreases fluidity. When inserted, curcumin leads to a further fluidification of the membranes and an increase in tail fluctuations, contrary to cholesterol's condensing effect.

Keywords: curcumin, membrane interaction, carpet model, insertion model, X-ray diffraction, Molecular Dynamics simulations, Alzheimer's disease, anti-oxidant

1. INTRODUCTION

Curcumin is the active ingredient in the Indian spice Turmuric. In addition to being a food additive and preservative, it is used as an anti-inflammatory agent in traditional Chinese and Indian medicine. More recently, there is evidence for curcumin as an anti-Alzheimers, antioxidant, anti-cancer, and anti-inflammatory agent [1–3].

There is intense interest in identifying the general mechanism of curcumin. Curcumin seems to influence a number of structurally unrelated proteins and processes. For example, there is evidence that curcumin affects the cross-β structure of aggregated amyloid-β peptides [3] and inhibits formation of amyloid-β oligomers and binds to plaques [4]. It also reduces lipid peroxidation by oxidizing Fe^{3+} free radicals [2]. The breadth of curcumin's interactions has led to speculation that it may alter the membrane environment and indirectly leads to the observed effects [5].

Curcumin is a highly hydrophobic molecule (see Fig. 1a), and has indeed been observed partitioning into lipid membranes. The molecule was reported to cause membrane thinning, influence the bilayers' mechanical properties, and change lipid domain behaviour [5–7]. Curcumin partitioning was found to stiffen the membrane, which indirectly influences the diffusion of the epidermal growth factor receptor, affecting protein behaviour, and potentially revealing anti-cancer properties [8]. A novel mechanism for the anti-oxidant properties of curcumin (and other flavenoids) was proposed, whereby curcumin stiffens the membrane and slows lipid and ion diffusion, thereby decreasing the oxidation rates [9]. Curcumin was also shown to protect the membrane against disruption by Aβ by acting as a physical barrier and preventing insertion of the peptide [10, 11].

Two models have been proposed to explain how curcumin protects lipid membranes on a molecular level. Some results suggest that curcumin lies flat on the lipid head groups, where it forms hydrogen bonds with the lipid molecules. In this position, curcumin can act as a physical barrier, a so-called carpet, preventing peptide or oxidant penetration [6, 8, 12]. In contrast, curcumin can also embed deep in the membrane and intercalate with the lipid tails [5, 9, 13–15]. Similar to cholesterol, in this position curcumin is proposed to increase lipid chain order and stiffen membranes, thereby slowing lipid kinetics and increasing the energetic barrier to ion or peptide embedding. The two models are pictured in Fig. 1b).

In this study, we investigated the interaction between curcumin and lipid bilayers using high-resolution X-ray diffraction and Molecular Dynamics (MD) computer simulations at different levels of membrane hydration to mimic different osmotic pressure conditions. In the experiments, we used a novel assay of synthetic oriented lipid bilayers, that has become relevant for measuring

* rheinstadter@mcmaster.ca; Department of Physics and Astronomy, McMaster University, ABB-241, 1280 Main Street West, Hamilton, Ontario L8S 4M1, Canada; Phone: +1-(905)-525-9140-23134, Fax: +1-(905)-546-1252

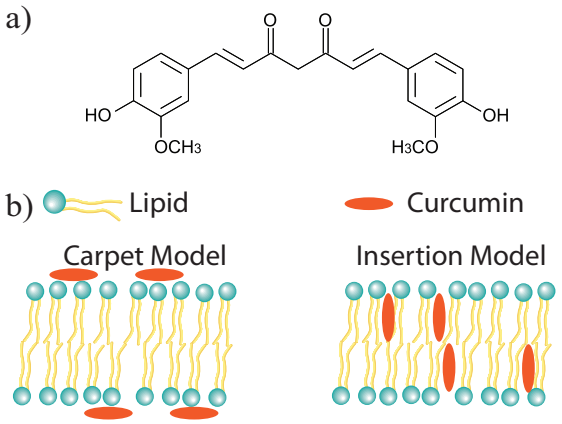

FIG. 1. a) Curcumin molecule. b) Cartoons of the two models proposed to explain curcumin's protective membrane effects: the 'carpet' and the 'insertion' model.

Curcumin (mol%)	n_w	A_L (Å^2)	d_z (Å)	d_{HH} (Å)	d_w (Å)
X-ray diffraction					
0	7	40.6	54.6	41.4	13.2
2	5.2	40.6	53.9	41.5	12.4
10	–	40.6	53.1	42.7	10.4
20	–	41.1	52.8	42.8	10.0
0	25.6	59.9[a]	61.2	35.8	25.4
5	23.0	59.9[a]	57.8	34.8	23
MD simulations					
0	7	49	51	39	12
2	5.2	48.4	51.4	39	12
0	27	59.5	58.7	32.4	26.3
2	25	60.8	58.6	32.2	26.4

TABLE 1. Structural parameters from X-ray diffraction and MD simulations. Membranes were studied in a dry (∼7 hydration water molecules at 50% RH) and a hydrated, fluid state (∼27 hydration water molecules at 100% RH). Lamellar spacing, d_z, membrane thickness, d_{HH}, and hydration water layer thickness, d_w, were determined from out-of-plane diffraction and electron density calculations. Area per lipid (A_L) was experimentally determined for dry membranes, only. [a]Fluid areas were taken from [25]

drug-membrane and peptide-membrane interactions on a nanometer scale [16–24]. In experiments and simulations, curcumin was found in both its suggested locations and population of the two states was found to dependent on membrane hydration.

2. RESULTS

Highly oriented, multi-lamellar membrane stacks of fully saturated 1,2-dimyristoyl-sn-glycero-3-phosphocholine (DMPC) were prepared for the X-ray diffraction experiments and similar systems were constructed for MD simulations, such that the results between experiments and simulations can be compared. Details are provided in the Materials and Methods Section. All membranes were scanned at a temperature of T = 28°C. Fluid membranes were simulated at T=28°C, while 17°C was required for the gel phase simulations. Curcumin was added to the membranes at concentration between 0 and 20mol%. To investigate the role of membrane hydration, two sets of membranes were constructed in experiment and simulation: dehydrated bilayers with ∼7 hydration water molecules per lipid molecules, and fully hydrated bilayers including ∼27 water molecules per lipid. In the experiment, membrane stacks were exposed to 50% and 100% relative humidity.

2.1. X-ray Diffraction Experiments

Dehydrated Membranes

Out-of-plane diffraction data for a pure DMPC membrane and curcumin concentrations of 2, 10 and 20mol% is shown in Fig. 2a). Ten well-developed and equally-spaced Bragg peaks were observed indicating well-ordered lamellar structures. The lamellar spacing of the bilayers, d_z, is calculated using $d_z = 2\pi/\Delta q_z$. d_z for a pure DMPC membrane was determined to 54.7 Å, in good agreement with previous reports on DMPC at low hydrations [26, 27].

Membranes with curcumin also formed well-ordered, lamellar membrane stacks. However, the lamellar spacing monotonically decreased with increasing curcumin concentration to 52.8 Å at 20mol% curcumin. This is in agreement with Hung *et al*, who reported a decrease in lamellar width with curcumin [7] from X-ray diffraction of multi-lamellar vesicles.

To determine the position of curcumin in the bilayer and to model changes to the atomic-level bilayer structure, electron density profiles were constructed for the pure DMPC membranes, as well as membranes with 2mol% curcumin. $\rho(z)$ for the pure DMPC membrane is shown in Fig. 2b). The maximum in the electron density at z values of $|z|$ ∼20 Å represents the position of the electron rich head groups. The bilayer density decreases to a minimum at the center of the bilayer at z=0, between the tails, where CH_3 groups reside. The distance between the maxima is assigned to the bilayer head-to-head spacing, d_{HH}, and the thickness of the water layer was determined using $d_w = d_z$ - d_{HH}. d_{HH} was determined to be 41 Å, and slightly increased at 20mol% curcumin to 42.8 Å. At the same time, the water layer was found to significantly decrease in width from d_w = 13.2 Å for DMPC to d_w=10.0 Å. Values for d_{HH} and d_z for all membranes are given in Table 1. The area per lipid, A_L was determined from in-plane diffraction (complete 2-dimensional data are shown in Fig. S1 in the Supplementary Material).

A component group model was fit to the electron densities [26, 28]. The model decomposes the bilayer into five

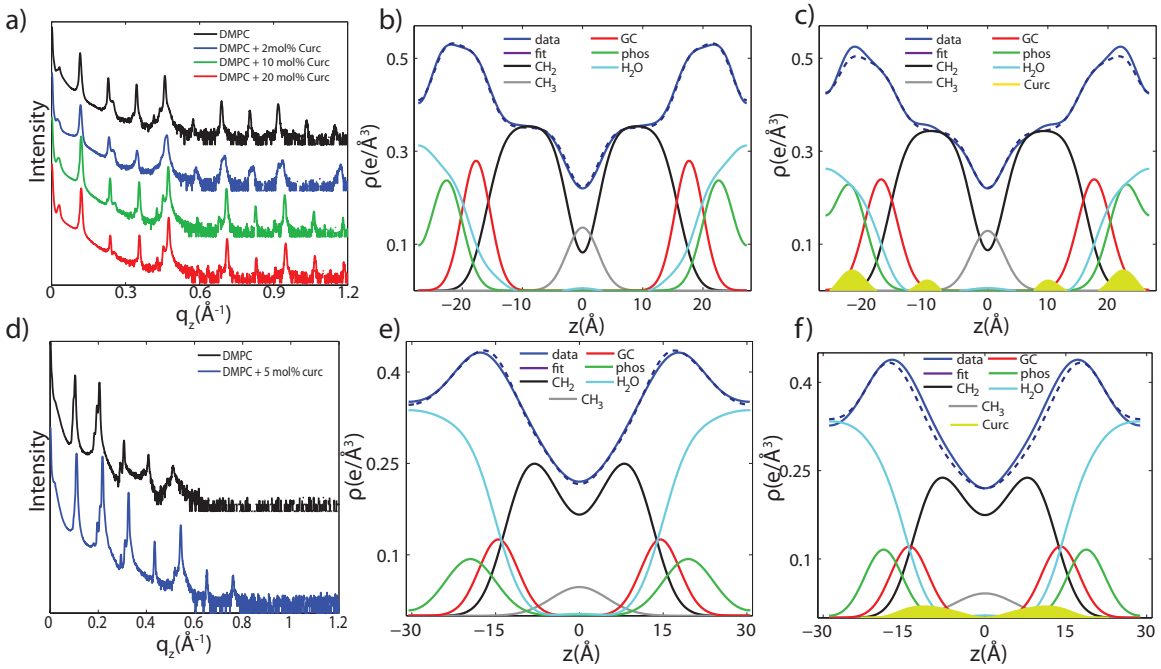

FIG. 2. X-ray diffraction of dehydrated membranes with curcumin. a) Out-of-plane diffraction; b) Pure DMPC bilayer fit with a component group model. c) DMPC + 2mol% curcumin, fit with a component group model. The highlighted areas indicate residual density associated with the curcumin molecules. Curcumin molecules were found at $|z|$ ∼21 Å and $|z|$ ∼10 Å. Results of the X-ray experiments on fluid membranes. d) q_z plots; e) DMPC membranes fit to the component group model; f) Membranes + 5mol% curcumin fit to the component group model. The highlighted residual density at $|z|$ ∼8 Å was assigned to curcumin molecules.

components: The CH_3 groups in the center of the bilayer ($\rho_{CH3}(z)$); a function for the lipid tails in each leaflet ($\rho_{CH2}(z)$); a profile for the glycerol chemical group in the heads ($\rho_{GC}(z)$); a profile for the phosphate group ($\rho_p(z)$); and a profile for the combined water and choline group ($\rho_{BC}(z)$). The results for DMPC (shown in Fig. 2b) agree well with past observations [26, 28]. All fitting parameters are given in Table 2.

The component group analysis was then applied to the electron density of DMPC/2mol% curcumin in Fig. 2c). In the fitting process, the width of the individual component groups were fixed to the values determined from pure DMPC. The positions of the groups, z_p, z_{GC}, and d_c were adjusted to accommodate the d_{HH} observed in the experimental density. The model assumes that the structure of the bilayer is not altered significantly by 2 mol% curcumin, such that an excess of electron density can be attributed to the presence of curcumin in the bilayers. This analysis suggests multiple binding sites for curcumin in the dehydrated bilayers: at $|z|$ ∼21 Å in the lipid head groups, and at $|z|$ ∼10 Å, in the hydrophobic membrane core. From the integrated intensities, the population of the head group state is estimated at 2.5:1 *vs.* the tail group state.

Hydrated Membranes

Out-of-plane scans for pure DMPC membranes, and membranes with 5 mol% curcumin measured at 100% RH are shown in Fig. 2d). The out-of-plane scattering for the hydrated DMPC membranes produced five Bragg peaks, only, as compared to 10 in the dehydrated state. The absence of higher order Bragg peaks and the lamellar spacing of $d_z = 61.3$ Å are consistent with a highly fluid structure [29].

Electron density profiles were generated (Figs. 2e)&f) and the component group model applied. The different groups become considerably broader in fluid membranes. Fitted parameters are given in Table 2, structural parameters in Table 1. The excess electron density in Fig. 2f) suggests that in fluid bilayers, the curcumin molecules reside entirely in the membrane tail-group region, with an average position of $|z|$ ∼8 Å.

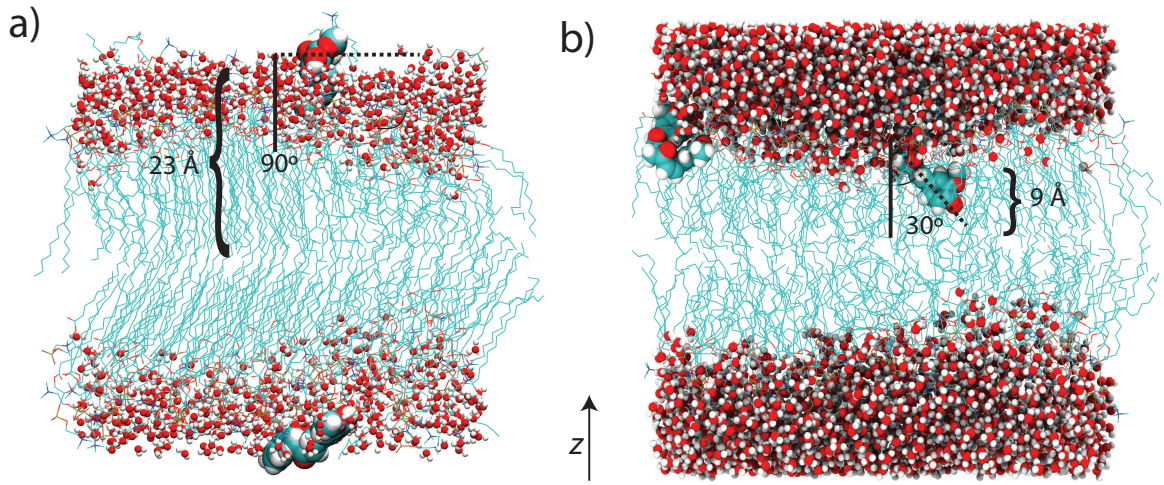

FIG. 3. a) In dehydrated membranes, curcumin was found to lie flat on the bilayer surface (90°) at $|z|$ ∼23 Å, and hydrogen-bond with the lipid head groups, compatible with the carpet model. Experiments and PMF calculations show a second, embedded state of the molecule at $|z|$ ∼9 Å, which was not populated during the timescales of the simulations. b) In hydrated bilayers, the curcumin molecule was found to embed within the tails at $|z|$ ∼9 Å at a tilted angle, compatible with the insertion model. Molecules were fluctuating between 20° and 90° with an average tilt angle of 65° (∼30° in this snapshot).

2.2. Molecular Dynamic Simulations

Dehydrated Membranes

United-atom MD simulations were performed with curcumin in a 128-lipid DMPC membrane. Simulations were performed with 7 water molecules per lipid molecule in order to mimic experimental conditions. To create a bilayer in its gel phase, the carbon bonds along the lipid chains were forced into an all-trans configuration for 100 ns. Next, the bonds were released and the system then simulated for 200 ns. After this procedure, the system equilibrated with $A_L = 49$ Å^2 and $d_z = 51$ Å. Temperature was kept at 17°C; higher temperatures made the system transition into a fluid state in the simulations. Two curcumin molecules were introduced into the pure bilayer system and simulated for a further 200 ns, corresponding to ∼2mol%. A snapshot is shown in Fig. 3a). The curcumin molecules were initially placed at the edge of the thin water layer, and spontaneously entered the head groups within ∼10 ns.

The final 50 ns of each simulation were used for the analysis. Electron density profiles of the various system components were generated via number density calculations along along the z-coordinate, and scaled using the appropriate weighting based upon the number of electrons within each component. The component analysis is shown in Fig. 4a). The yellow areas highlight the positions of the curcumin molecules in the region of the phosphate group at z ∼23 Å, in good agreement with the experiments. At this position, each curcumin molecule forms multiple hydrogen bonds with the lipid head groups. The bilayers equilibrated to an area-per-lipid of 48.4 Å^2 and $d_z = 51.4$ Å. Structural parameters for all simulations are summarized in Table 1.

Umbrella simulations were performed to calculate the potential of mean force (PMF). The results are displayed in Fig. 4b). The PMF reveals a local minima at $|z|$ ∼9 Å but the absolute minima in the profile occurs at the edge of the bilayer system. These two states agree well with the observed positions of curcumin in the X-ray experiments. We did not observe a curcumin molecule in the 9 Å position in the simulations, likely because the insertion process takes significantly longer than 200 ns.

In addition to the PMF, in every umbrella window, the change in number of water molecules per lipid molecule near a curcumin molecule was calculated. The number of water molecules per lipid in a radius of 5 Å around the curcumin molecule was caculated, and compared to the value of the bulk membrane. As shown in Fig. 4c), when the curcumin molecule is fixed in the water layer or the head groups, there is a decrease in the number of water molecules in the surrounding area.

Hydrated Membranes

Membrane simulations were performed with curcumin in fully hydrated bilayers, at 28°C and 27 water molecules per lipid molecule. Two curcumin molecules were introduced and found to partition spontaneously into the tail group region within 50 ns. The system was simulated

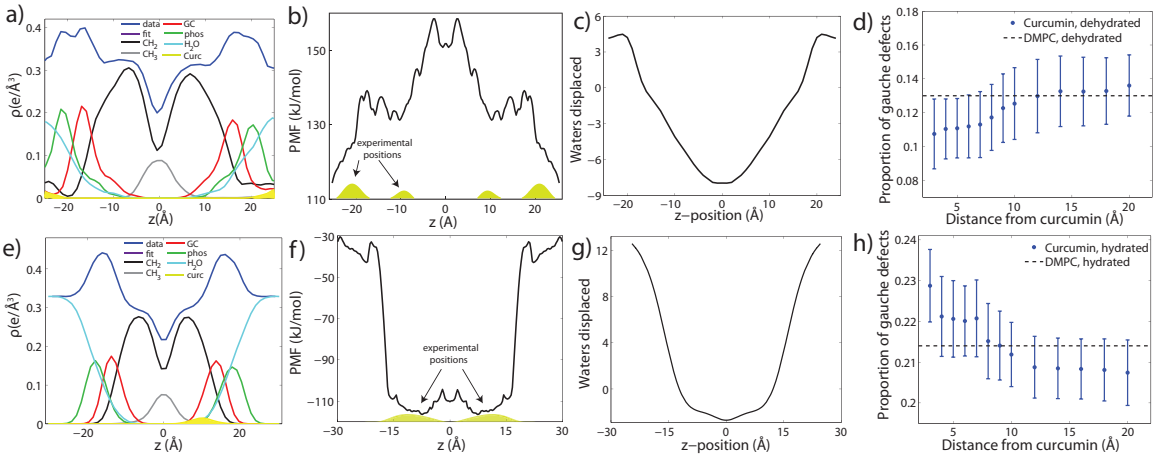

FIG. 4. Analysis of the MD simulations in the dry (a)-d)) and hydrated membranes (e)-g)). a) A component group density model, showing the position of the curcumin densities in the dehydrated membrane. b) The results of the umbrella simulations: the potential of mean force (PMF) for the curcumin in each umbrella window. c) The number of water molecules displaced from a 5 Å radius around a curcumin molecule, calculated at each umbrella window and smoothed by 1 Å. e) Component group density model showing curcumin density in the fluid membrane. f) PMF for curcumin in the hydrated bilayer. Experimentally determined positions are marked. g) The number of water molecules displaced from a 5 Å radius around a curcumin molecule, in hydrated membrane. d) Proportion of gauche defects as a function of distance from the curcumin molecule, compared to pure DMPC. h) Gauche defects for the hydrated membrane.

for 200 ns. A snapshot is shown in Fig. 3b). An area-per-lipid of 61 Å^2 was achieved with d_z = 60.5 Å, in good agreement with the experimental value for d_z and the fully hydrated area of 60.8 Å^2 reported for the GROMOS54a7 force field [30] and the experimentally determined value of 59.9 Å^2 [25] (both determined at 30°C).

The component analysis is shown in Fig. 4e) and demonstrates that the curcumin molecules partition deep into the tail region, at z ∼10 Å, in agreement with previous reports [13] and our experimental findings. At this position, each curcumin molecule still participates in hydrogen bonding with the lipid head groups, forming one bond each. The tilt of the curcumin was also measured as the angle between the long-axis of the molecule projected on the z-axis of the bilayer. The tilt was measured every 1 ns and averaged over the final 50 ns. While the tilt is a dynamic quantity which fluctuated between 20° and 90°, the curcumin molecules were on average tilted by ∼65°.

The results from umbrella simulations are displayed in Fig. 4f). The minima in the PMF at $|z|$ = 9 Å are in excellent agreement with the simulated densities and the experimental results. The number of water molecules per lipid in an area of 5 Å around the curcumin molecule is shown in Fig. 4g). Following that, curcumin increases the number of water molecules in the membranes when inserted.

In addition to structural parameters, the number of gauche defects in the lipid tails, *i.e.*, kinks in the lipid alkyl chains, was calculated as a function of the lateral distance from the curcumin molecules. This quantity is often used to directly indicate fluidity [31–33]. The proportion of gauche dihedrals was analyzed using a dynamic selection of lipid molecules located within a specified radius around the curcumin molecules. The results are shown in Figs. 4d)&h). There was a decrease in the proportion of gauche defects near curcumin in the gel phase, however, an increase in the fluid phase.

3. DISCUSSION

Different models for where curcumin embeds in the membranes propose different mechanisms for its supposed protective effects. The carpet model suggests curcumin lies flat on lipid heads, and provides a steric barrier against molecular binding. Models which suggest curcumin embeds in the membrane core propose that curcumin has a mechanism similar to cholesterol: by increasing lipid chain-order, the molecule stiffens tails and increases energetic barriers against insertion.

Care was taken to prepare comparable systems for experiments and simulations and there is a strong agreement of the structural properties between the experimental and simulated systems. In fully hydrated bilayers, differences between experimental and simulated curcumin positions can be the result of bilayer undulations present in the bilayer stacks that are not accurately replicated using the short timescale and small patch size of the simulations. The undulation fluctuations in membranes were

previously measured using the neutron spin-echo technique [34, 35]. The corresponding undulation amplitudes can be estimated from the underlying theory of a solid supported stack of membranes by Romanov and Ul'yanov [36] to about 3 Å, which well account for the observed deviations between experiments and simulations. A similar effect has been observed before when comparing diffraction experiment and MD simulations in the case of the interaction between cortisone and membranes [23].

In dehydrated lipid membranes, the curcumin molecule was found to reside in the head group region, at z-values of $|z| \sim 22$ Å (21 Å in experiment, 23 Å in the simulation). In these locations, the molecule interacts with the carbonyl moieties in the heads, as well as the hydrophobic tails. The curcumin molecule lies flat on the bilayer, and quickly forms hydrogen bonds with the lipid head groups, in good agreement with the proposed carpet model [6, 8, 12]. A small population of curcumin molecules was found to embed at $|z| \sim 10$ Å in experiments.

Simulation and experiment also agree that in fully hydrated bilayers, curcumin prefers to embed deeper in the membrane, at $|z| \sim 9$ Å (8 Å in experiment, 10 Å in the simulation). Simulations indicate that in this position curcumin is still forming hydrogen bonds with the head groups. The long-axis of curcumin is tilted to an average angle of $\sim 65°$ with respect to the membrane normal. This is in contrast to studies which suggest that curcumin positions up-right with the bilayer when embedding in the tails [5, 9, 13–15], similar to cholesterol.

The MD simulations give insight into the corresponding energy landscape. According to the PMF calculations, curcumin has two preferred locations in lipid bilayers. The position in the head-group region was found to be metastable in both hydrated and dehydrated bilayers. Locating into the lipid tail region becomes more favorable with increasing hydration of the membranes: the PMF significantly decreases from ~10 kJ/mol to values of ~110 kJ/mol from dry to fully hydrated bilayers.

We note that, to achieve low hydration in our experiments and simulations, water must be removed and the reduced hydration water layer thickness may increase inter-bilayer interactions given the periodicity of both systems. The increased head group - head groups interaction may have the potential to influence the position of curcumin by increasing the potential for hydrogen bonding. However, based on the PMF in Fig. 4c), the embedded state is significantly less favorable than in hydrated bilayers, suggesting that head group interactions due to periodicity do likely not influence the result.

In experiments presented here, reduced membrane hydration was achieved through exposure of the membranes to a reduced relative humidity. A relative humidity p/p_0 creates an osmotic pressure $\Pi_{osm} = (k_B T/v_w) \ln(p_0/p)$, where v_w is the partial molar volume of a water molecule [37]. In membranes, this osmotic pressure leads to an attractive potential, which is proportional to the thickness of the hydration water later, $V(d_w) = \Pi_{osm} d_w$. Membrane swelling, *i.e.*, the absorption of hydration water molecules from the surrounding water vapor, is the result of water molecules migrating into the membrane stack and leading to an increase in hydration water layer thickness against the attractive forces between neighboring bilayers in the stack. As the chemical potential of water molecules in relative humidities is reduced by $\Delta\mu_w = k_B T \ln(p/p_0)$, this process can be inhibited at reduced humidity levels.

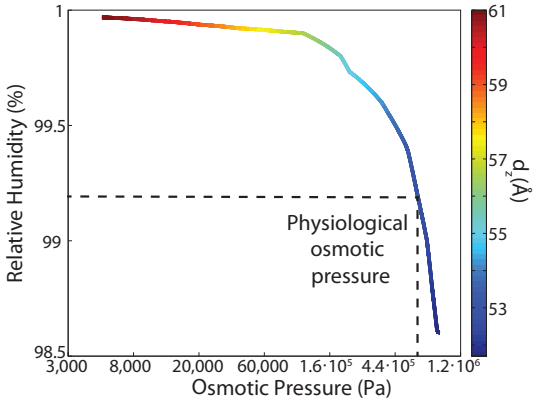

FIG. 5. Relation between osmotic pressure, relative humidity, RH, and lamellar spacing, d_z of DMPC bilayers. Data for bilayer swelling as function of RH were taken from Chu *et al.* [29]. d_z as function of osmotic pressure was determined by Petrache *et al.* [38] and Mennicke, Constantin and Salditt [39].

Changes in osmotic pressure can directly be related to swelling of the membranes and the thickness of the hydration water layer in the experimental system. Petrache *et al.* [38] and Mennicke, Constantin and Salditt [39] measured the lamellar spacing of DMPC bilayers for different osmotic pressures by varying concentrations of polyethyleneglycol (PEG). A d_z spacing of 53 Å was, for instance, observed at an osmotic presssure of $\Pi \sim 7 \cdot 10^6$ Pa. Also protein solutions can cause osmotic stress [40], depending on their concentration. The osmotic pressure of a physiological saline solution with a density of 1.005 g/mol at 37°C is calculated to 760,000 Pa. Osmotic pressure of a 10 mM Hepes buffer solution typically used corresponds to ~26,000 Pa. The physiological saline and Hepes buffer solutions would thus reduce the lamellar d_z-spacing in DMPC from 61 Å to ~53 Å, respective, ~59 Å. By using swelling data from the Nagle group [29], these d_z spacings correspond to relative humidity levels of ~99% and close to 100%. The relation between osmotic pressure, relative humidity and lamellar spacing is plotted in Fig. 5.

These results can help to unify the different models that have been suggested for curcumin's position and effects. As different biological environments, such as salts,

buffer solutions, the presence of substrates or macromolecular solutes, may lead to an effective dehydration of lipid bilayers, it is plausible that they can shift the population of the two preferred curcumin locations in the membranes. Some experiments may thus observe curcumin in carpet or inserted depending on experimental conditions. Curcumin's effect on lipid membranes strongly depends on its location.

In the carpet model, the presence of curcumin molecules in the lipid head groups led to a decrease in fluidity and dehydration of the bilayers, as reported previously. We do not find evidence for a cholesterol-like chain ordering effect of curcumin in the insertion model. For one, the molecule does not insert into our bilayers with an up-right orientation. Secondly, d_{HH} does not increase when curcumin is added to fluid-phase bilayers, but in fact slightly decreases, by $\sim$1 Å in experiments and 0.2 Å in simulations. The protective effect of curcumin in the insertion model is thus not similar to cholesterol's stiffening and condensation effect. Instead, curcumin was found to increase the number of water molecules in the bilayers and the number of gauche defects, making the bilayers more fluid. This finding is inconsistent with the current literature hypothesis, as described in the introduction, which involves curcumin increasing lipid chain order, similarly to cholesterol, Future work including curcumin and peptides is needed to unveil the exact mechanism how curcumin can inhibit peptide insertion in the insertion model under these circumstances.

4. CONCLUSION

Curcumin was added to phospholipid bilayers made of DMPC and partitioning of the molecule was studied using high-resolution X-ray diffraction and MD simulations. Curcumin was found in two locations in the membranes: in the lipid head groups, at z values of $|z| \sim$20 Å lying flat on the bilayer edge, and inside the hydrophobic membrane core, tilted with respect to the bilayer normal, at $|z| \sim$9 Å. Population of the two states was found to depend on membrane hydration. While the head group position is metastable, the core position becomes significantly more attractive with increasing hydration.

The two observed positions correspond to the two models for curcumin's protective properties: in the carpet model it lies flat on the bilayer and provides a 'carpet' for protection by forming a steric barrier, while in the insertion model, it protects against peptide insertion. We suggest that curcumin can be observed in carpet or inserted depending on osmotic pressure conditions created by salts, buffer solutions, substrates or macromolecular solutes.

It was suggested that curcumin stiffens membranes and decreases lipid diffusion and increases the energy barrier to molecule binding, similar to the effect of cholesterol. In the carpet model, the presence of curcumin molecules in the lipid head groups led to a decrease in fluidity and dehydration of the bilayers. With the insertion models, we find that curcumin leads to a further fluidification of lipid membranes at high hydration levels, in contradiction to cholesterol's condensing effect.

5. MATERIALS AND METHODS

5.1. Preparation of the highly-oriented multi-lamellar membrane complexes

Highly oriented, multi-lamellar membranes were prepared on polished 1$\times$ 1 cm^2 silicon wafers. The wafers were first pre-treated by sonication in dichloromethane (DCM) at 310 K for 25 minutes to remove all organic contamination and create a hydrophobic substrate. After removal from the DCM post-sonication, each wafer was thoroughly rinsed three times by alternating with $\sim$ 50 mL of ultra pure water (18.2 MΩ·cm) and methanol. This treatment renders the surface of the wafers hydrophobic.

1,2-Dimysteroyl-*sn*-glycero-3-phosphocholine (DMPC) is initially dissolved in a chloroform solution. Curcumin (Sigma, SAS 458-37-7) is also dissolved in chloroform and then mixed with the lipid solution. The chloroform was then evaporated, and the lipid-curcumin precipitate re-dissolved in either pure water or a 1:1 solution of trifluoroethanol and chloroform. Water solutions were point sonicated, TFE/chloroform solution vortexed and heated to 313 K.

A tilting incubator was heated to 313 K and the solutions placed inside to equilibrate. 80 μL of lipid solution was deposited on each wafer. The solvent was then allowed to slowly evaporate for while gently rocked, such that the lipid solution spread evenly on the wafers. Samples were then placed in a sealed container containing an open vial of ultra pure water and incubated for 24 hours at 100% RH at 303 K. This procedure results in highly oriented, multi-lamellar membrane stacks and a uniform coverage of the silicon wafers. About 3000 highly oriented stacked membranes with a total thickness of $\sim$ 10 μm are produced using this protocol.

5.2. X-ray diffraction experiment and construction of electron densities

Out-of-plane X-ray diffraction measurements were obtained using the Biological Large Angle Diffraction Experiment (BLADE) in the Laboratory for Membrane and Protein Dynamics at McMaster University. BLADE uses a 9 kW (45 kV, 200 mA) CuK-α Rigaku Smartlab rotating anode at a wavelength of 1.5418 Å. Both source and detector are mounted on moveable arms such that the membranes stay horizontal during measurements. Focussing, multi layer optics provide a high intensity parallel beam with monochromatic X-ray intensities up to 10^{10} counts/(s $\times$ mm^2). This beam geometry provides optimal illumination of the membrane samples to maximize

the scattered signal. By using highly-oriented stacks, the out-of-plane (q_z) structure of the membranes could be determined independently from the in-plane ($q_{||}$) structure.

Electron densities, $\rho(z)$, were calculated through Fourier transform of the integrated intensities of the reflectivity Bragg peaks. $\rho(z)$, can be approximated by a 1-dimensional Fourier analysis:

$$\rho(z) = \frac{2}{d_z}\sum_{n=1}^{N}\sqrt{I_n q_n}\nu_n \cos\left(\frac{2\pi n z}{d_z}\right), \quad (1)$$

where N is the highest order of the Bragg peaks observed in the experiment. The integrated reflectivity Bragg peak intensities, I_n, are multiplied by q_n to generate the form factors, $F(q_n)$. The bilayer form factor, which is in general a complex quantity, is real-valued when the structure is centro-symmetric. The phase problem of crystallography, therefore, simplifies to the sign problem $F(q_z) = \pm|F(q_z)|$ and the phases, ν_n, can only take the values ± 1.

The phases, ν_n, were assessed by fitting the experimental peak intensities, as detailed in Fig. S1 in the Supplementary Material. In order to transform the $\rho(z)$ to an absolute scale, the curves were vertically shifted to fulfil the condition $\rho(0) = 0.22\ e^-/\text{Å}^3$ (the electron density of a CH_3 group) in the center of a bilayer. The curves were then scaled until the total number of electrons $e^- = A_L \int_0^{dz/2}\rho(z)dz$ across a membrane leaflet agrees with the total number of electrons of a DMPC molecule with n_w water molecules and the contribution from curcumin.

To determine the number of water molecules per lipid, n_w, the following relation was used:

$$\frac{1}{2}A_L d_z = V_L + n_w V_w, \quad (2)$$

where A_L is the area-per-lipid, V_L the volume-per-lipid, and V_w the volume per water molecule, known to be 30 Å^3. For DMPC in the gel phase at low hydrations the volume-per-lipid was calculated previously to V_L=891 Å^3 [26], while the fluid volume of V_L=1101 Å^3 was taken from [41]. We note that V_L for the dehydrated gel phase is lower than the value of 1041 Å^3 reported by Tristram-Nagle *et al.* for hydrated gel membranes [27]. The discrepancy is mainly the effect of reduced hydration resulting in a reduced area per lipid, A_L. We measure A_L ∼41 Å^2, in good agreement with previous reports for dehydrated gel phases [42, 43], while Tristram-Nagle *et al.* report 47 Å^2 in the hydrated gel phase.

5.3. Real-space modelling of electron density profiles

To model the bilayer structure and determine the position of the curcumin molecule, electron density profiles were decomposed using a composite model. The specific models used for the lipid component groups are those used by Klauda *et al.* and Alsop *et al* [28]. Atoms from the DMPC molecules were distributed between five component groups representing distinct portions of the bilayer. These regions are 1) The terminal CH_3 groups at the end of the lipid chains, for both lipids in the bilayer, found at the center of the bilayer (CH3); 2) The CH_2 groups composing the hydrocarbon core of the lipid molecule (CH2); 3) The glycerol moiety in the head group (GC); 4) The phosphate group in the head group (P). An additional function is added to describe the hydration water layer and the choline group of the lipid (BC). The functions describe a full bilayer, *i.e.*, two leaflets. For a detailed description of the model, please see *e.g.*[26, 28].

Curcumin (mol%)	n_w	σ_{CH3} (Å)	σ_{CH2} (Å)	d_c (Å)	σ_{GC} (Å)	z_{GC} (Å)	σ_p (Å)	z_p (Å)
0	7	2.6	2.4	15.9	2.4	17.6	2.65	22.6
2	5.2	2.7	2.4	16.2	2.4	17.9	2.65	22.95
0	27.6	5	3.5	13	3.6	14.5	3.5	18.5
5	25.0	5	3.5	13	3.5	14	3.5	18.5

TABLE 2. Fitting parameters of the component group analysis.

In total, there are 7-9 free parameters in the fitting: the width of the CH_3 peak, σ_{CH3}, the width of the tail CH_2 interface, σ_{CH2}, the thickness of the hydrocarbon region, d_C; and the positions and widths of the glycerol and phosphate groups, z_{GC}, σ_{GC}, z_P, σ_P. As the phosphate and glycerol groups are coupled by chemical bonds, σ_{GC}, σ_p, and σ_{CH2} are softly constrained to covary.

To determine the position of the curcumin molecule, the component group model is first applied to the pure DMPC membrane in the appropriate hydration state. Next, the same fitting parameters are applied to the electron density for membranes with curcumin. Adjustments are made to z_p, z_{GC}. and d_c so that the fitting d_{HH} matches the experimental value. The density that remains after the lipids are subtracted from the measured density is attributed to the curcumin molecule.

5.4. Molecular Dynamics Simulations

All simulations were run in-house on MacSim, a GPU accelerated workstation with 20 physical Intel XeonCPU cores and two GeForce GTX 1080 high power graphics cards resulting in 5120 CUDA Cores. This system produces about 180 ns of MD simulations in standard 128 lipid membrane patches in GROMACS.

A system of 128 DMPC lipids (64 per leaflet) was taken from Tieleman *et al.* [44]. Curcumin topology was obtained using the Automated Force Field Topology Builder (ATB) [45, 46]. The SPC water model was used for system solvation [47]. All MD simulations were performed using the GROMACS 5.1.2 software package [48], implementing the GROMOS 54a7 force field [49] modified with Berger lipid parameters [50]. All simula-

tions used a 2 fs time step, a periodic boundary condition applied to all directions, the particle-mesh Ewald to solve for long-range electrostatics [51], a short-range van der Waals cutoff of 1.2 nm, and the LINCS algorithm to determine bond constraints [52]. Temperature coupling was controlled using a Nose-Hoover thermostat at 28°C (τ = 0.5 ps) [53], and pressure was kept at 1.0 bar using Parrinello-Rahman semi-isotropic weak coupling (τ = 1 ps) [54].

A total of four distinct simulations were conducted. First, two pure DMPC membranes with 7 and 27 waters per lipid were simulated for 200 ns, each, to mimic the dehydrated and hydrated membranes, respectively. Next, two curcumin are introduced into the pure membranes and the system simulated for another 200 ns. All analyses were performed with the final 50 ns of the simulations using GROMACS algorithms and simple scripts [55]. The electron density profiles were calculated for different constituents of the system, similar to other studies using lipid bilayers [22, 56]. The function used calculates the relative distance along the bilayer normal of each atom within the specified index group, assigns a weighting based upon the number of electrons in each atom, and delivers an electron density as averaged over the specified time range.

Umbrella simulations were also performed, with the protocol based on previous studies [23, 57, 58]. The initial condition of a curcumin molecule placed at the membrane edge. Umbrella simulations are obtained by pulling the molecule through the bilayer, along the z direction with a force constant of 3000 kJ/mol, and umbrella windows are obtained with $\Delta z = 1$ Å. Each window is then simulated for 15 ns. Potentials of mean force (PMFs) are then calculated using the Weighted Histogram Analysis Method in Gromacs [59], using the final 5 ns of each umbrella window and the center of the bilayer as the reference point.

The proportion of gauche dihedrals within a lipid system is commonly used as a measure of bilayer fluidity [31–33]. The proportion of gauche dihedrals as a function of increasing distance from curcumin was determined using dynamic scripting and GROMACS algorithms. A script was constructed to generate an index file containing only carbon chains belonging to lipids within the specified radius from the center of mass of any curcumin molecule within the system every 50 frames. This index file specified the DMPC molecules whose carbons were to be used in calculation of the Ryckaert-Bellemans dihedral angles over that time interval [60]. This was repeated over the final 50 ns of the simulation and averaged for each carbon position. Averaging across the SN1 and SN2 tails was then performed to generate the value shown in Fig. 4 d) and h), and the script was run successively to consider each new distance from curcumin. Testing with the script showed that windows shorter than 50 frames did not produce statistically different results, so this frame length was used to decrease computational time.

Supporting Information A single PDF is provided with additional analysis of X-ray diffraction data.

ACKNOWLEDGMENTS

This research was funded by the Natural Sciences and Engineering Research Council of Canada (NSERC), the National Research Council Canada (NRC), the Canada Foundation for Innovation (CFI) and the Ontario Ministry of Economic Development and Innovation. R.J.A. is the recipient of an NSERC PGS-D scholarship. A.D. is the recipient of an NSERC USRA, M.C.R. is the recipient of an Early Researcher Award of the Province of Ontario and a University Scholar Award from McMaster University.

[1] Hu S, Maiti P, Ma Q, Zuo X, Jones MR, Cole GM, Frautschy SA. Clinical development of curcumin in neurodegenerative disease. Expert review of neurotherapeutics. 2015;15(6):629–637.

[2] Hamaguchi T, Ono K, Yamada M. REVIEW: Curcumin and Alzheimer's disease. CNS neuroscience & therapeutics. 2010;16(5):285–297.

[3] Ak T, Gülçin İ. Antioxidant and radical scavenging properties of curcumin. Chemico-biological interactions. 2008;174(1):27–37.

[4] Yang F, Lim GP, Begum AN, Ubeda OJ, Simmons MR, Ambegaokar SS, Chen PP, Kayed R, Glabe CG, Frautschy SA, Cole GM. Curcumin inhibits formation of amyloid β oligomers and fibrils, binds plaques, and reduces amyloid in vivo. Journal of Biological Chemistry. 2005;280(7):5892–5901.

[5] Ingolfsson HI, Koeppe RE, Andersen OS. Curcumin is a modulator of bilayer material properties. Biochemistry. 2007;46(36):10384–10391.

[6] Varshney GK, Kintali SR, Gupta PK, Das K. Effect of Bilayer Partitioning of Curcumin on the Adsorption and Transport of a Cationic Dye Across POPG Liposomes Probed by Second-Harmonic Spectroscopy. Langmuir. 2016;32(40):10415–10421.

[7] Hung WC, Chen FY, Lee CC, Sun Y, Lee MT, Huang HW. Membrane-thinning effect of curcumin. Biophysical journal. 2008;94(11):4331–4338.

[8] Starok M, Preira P, Vayssade M, Haupt K, Salome? L, Rossi C. EGFR Inhibition by Curcumin in Cancer Cells: A Dual Mode of Action. Biomacromolecules. 2015;16(5):1634–1642.

[9] Arora A, Byrem TM, Nair MG, Strasburg GM. Modulation of liposomal membrane fluidity by flavonoids and isoflavonoids. Archives of Biochemistry and Biophysics. 2000;373(1):102–109.

[10] Lim GP, Chu T, Yang F, Beech W, Frautschy SA, Cole GM. The curry spice curcumin reduces oxidative damage and amyloid pathology in an Alzheimer transgenic

mouse. Journal of Neuroscience. 2001;21(21):8370–8377.
[11] Mishra S, Palanivelu K. The effect of curcumin (turmeric) on Alzheimer's disease: An overview. Annals of Indian Academy of Neurology. 2008;11(1):13.
[12] Thapa A, Vernon BC, De la Pena K, Soliz G, Moreno HA, Lopez GP, Chi EY. Membrane-mediated neuroprotection by curcumin from amyloid-β-peptide-induced toxicity. Langmuir. 2013;29(37):11713–11723.
[13] Kopeć W, Telenius J, Khandelia H. Molecular dynamics simulations of the interactions of medicinal plant extracts and drugs with lipid bilayer membranes. Febs Journal. 2013;280(12):2785–2805.
[14] Barry J, Fritz M, Brender JR, Smith PE, Lee DK, Ramamoorthy A. Determining the effects of lipophilic drugs on membrane structure by solid-state NMR spectroscopy: the case of the antioxidant curcumin. Journal of the American Chemical Society. 2009;131(12):4490–4498.
[15] Erlejman A, Verstraeten S, Fraga C, Oteiza PI. The interaction of flavonoids with membranes: potential determinant of flavonoid antioxidant effects. Free radical research. 2004;38(12):1311–1320.
[16] Balali-Mood K, Ashley RH, Hauß T, Bradshaw JP. Neutron diffraction reveals sequence-specific membrane insertion of pre-fibrillar islet amyloid polypeptide and inhibition by rifampicin. FEBS letters. 2005;579(5):1143–1148.
[17] Barrett MA, Zheng S, Roshankar G, Alsop RJ, Belanger RKR, Huynh C, Kučerka N, Rheinstädter MC. Interaction of Aspirin (Acetylsalicylic Acid) with Lipid Membranes. PLoS ONE. 2012 04;7(4):e34357.
[18] Drolle E, Kučerka N, Hoopes M, Choi Y, Katsaras J, Karttunen M, Leonenko Z. Effect of melatonin and cholesterol on the structure of DOPC and DPPC membranes. Biochimica et Biophysica Acta (BBA)-Biomembranes. 2013;1828(9):2247–2254.
[19] Dies H, Toppozini L, Rheinstädter MC. The interaction between amyloid-β peptides and anionic lipid membranes containing cholesterol and melatonin. PLoS One. 2014;9(6):e99124.
[20] Alsop RJ, Barrett MA, Zheng S, Dies H, Rheinstädter MC. Acetylsalicylic acid (ASA) increases the solubility of cholesterol when incorporated in lipid membranes. Soft Matter. 2014;10(24):4275–4286.
[21] Tang J, Alsop RJ, Backholm M, Dies H, Shi AC, Rheinstädter MC. Amyloid-β 25–35 peptides aggregate into cross-β sheets in unsaturated anionic lipid membranes at high peptide concentrations. Soft matter. 2016;12(13):3165–3176.
[22] Alsop RJ, Armstrong CL, Maqbool A, Toppozini L, Dies H, Rheinstädter MC. Cholesterol expels ibuprofen from the hydrophobic membrane core and stabilizes lamellar phases in lipid membranes containing ibuprofen. Soft matter. 2015;11(24):4756–4767.
[23] Alsop RJ, Khondker A, Hub JS, Rheinstädter MC. The Lipid Bilayer Provides a Site for Cortisone Crystallization at High Cortisone Concentrations. Scientific reports. 2016;6.
[24] Schmidt A, Löhrer D, Alsop RJ, Lenzig P, Oslender-Bujotzek A, Wirtz M, Rheinstädter MC, Gründer S, Wiemuth D. A Cytosolic Amphiphilic α-Helix Controls the Activity of the Bile Acid-sensitive Ion Channel (BASIC). Journal of Biological Chemistry. 2016;291(47):24551–24565.
[25] Kučerka N, Nieh MP, Katsaras J. Fluid phase lipid areas and bilayer thicknesses of commonly used phosphatidylcholines as a function of temperature. Biochimica et Biophysica Acta (BBA)-Biomembranes. 2011;1808(11):2761–2771.
[26] Alsop RJ, Schober RM, Rheinstädter MC. Swelling of phospholipid membranes by divalent metal ions depends on the location of the ions in the bilayers. Soft Matter. 2016;12(32):6737–6748.
[27] Tristram-Nagle S, Liu Y, Legleiter J, Nagle JF. Structure of Gel Phase DMPC Determined by X-Ray Diffraction. Biophysical Journal. 2002;83:3324–3335.
[28] Klauda JB, Kučerka N, Brooks BR, Pastor RW, Nagle JF. Simulation-Based Methods for Interpreting X-Ray Data from Lipid Bilayers. Biophys J. 2006;90:2796–2807.
[29] Chu N, Kučerka N, Liu Y, Tristram-Nagle S, Nagle JF. Anomalous swelling of lipid bilayer stacks is caused by softening of the bending modulus. Physical review E. 2005;71(4):041904.
[30] Pluhackova K, Kirsch SA, Han J, Sun L, Jiang Z, Unruh T, Bockmann RA. A critical comparison of biomembrane force fields: structure and dynamics of model DMPC, POPC, and POPE bilayers. The Journal of Physical Chemistry B. 2016;120(16):3888–3903.
[31] Saito H, Shinoda W. Cholesterol effect on water permeability through DPPC and PSM lipid bilayers: a molecular dynamics study. The Journal of Physical Chemistry B. 2011;115(51):15241–15250.
[32] Hofsäß C, Lindahl E, Edholm O. Molecular dynamics simulations of phospholipid bilayers with cholesterol. Biophysical journal. 2003;84(4):2192–2206.
[33] Venable RM, Brooks BR, Pastor RW. Molecular dynamics simulations of gel (LβI) phase lipid bilayers in constant pressure and constant surface area ensembles. The Journal of Chemical Physics. 2000;112(10):4822–4832.
[34] Rheinstädter MC, Häußler W, Salditt T. Dispersion relation of lipid membrane shape fluctuations by neutron spin-echo spectrometry. Physical review letters. 2006;97(4):048103.
[35] Armstrong CL, Häußler W, Seydel T, Katsaras J, Rheinstädter MC. Nanosecond lipid dynamics in membranes containing cholesterol. Soft matter. 2014;10(15):2600–2611.
[36] Romanov V, Ulyanov S. Dynamic and correlation properties of solid supported smectic-a films. Physical Review E. 2002;66(6):061701.
[37] Parsegian V, Rand R. Interaction in membrane assemblies. Structure and Dynamics of Membranes. 1995;1:643–690.
[38] Petrache HI, Gouliaev N, Tristram-Nagle S, Zhang R, Suter RM, Nagle JF. Interbilayer interactions from high-resolution x-ray scattering. Physical Review E. 1998;57(6):7014.
[39] Mennicke U, Constantin D, Salditt T. Structure and interaction potentials in solid-supported lipid membranes studied by x-ray reflectivity at varied osmotic pressure. The European Physical Journal E. 2006;20(2):221–230.
[40] Licata VJ, Allewell NM. Measuring hydration changes of proteins in solution: applications of osmotic stress and structure-based calculations. Methods in enzymology. 1997;295:42–62.
[41] Nagle JF, Wilkinson DA. Lecithin bilayers. Density measurement and molecular interactions. Biophysical journal. 1978;23(2):159–175.

[42] Church S, Griffiths D, Lewis R, McElhaney R, Wickman H. X-ray structure study of thermotropic phases in isoacylphosphatidylcholine multibilayers. Biophysical journal. 1986;49(3):597–605.

[43] Raghunathan V, Katsaras J. Structure of the l c? phase in a hydrated lipid multilamellar system. Physical review letters. 1995;74(22):4456.

[44] Tieleman DP, Sansom MS, Berendsen HJ. Alamethicin helices in a bilayer and in solution: molecular dynamics simulations. Biophysical journal. 1999;76(1):40–49.

[45] Koziara KB, Stroet M, Malde AK, Mark AE. Testing and validation of the Automated Topology Builder (ATB) version 2.0: prediction of hydration free enthalpies. Journal of computer-aided molecular design. 2014;28(3):221–233.

[46] Malde AK, Zuo L, Breeze M, Stroet M, Poger D, Nair PC, Oostenbrink C, Mark AE. An automated force field topology builder (ATB) and repository: version 1.0. Journal of chemical theory and computation. 2011;7(12):4026–4037.

[47] Berendsen HJ, Postma JP, van Gunsteren WF, Hermans J. Interaction models for water in relation to protein hydration. In: Intermolecular forces. Springer; 1981. p. 331–342.

[48] Abraham MJ, Murtola T, Schulz R, Páll S, Smith JC, Hess B, Lindahl E. GROMACS: High performance molecular simulations through multi-level parallelism from laptops to supercomputers. SoftwareX. 2015;1:19–25.

[49] Schmid N, Eichenberger AP, Choutko A, Riniker S, Winger M, Mark AE, van Gunsteren WF. Definition and testing of the GROMOS force-field versions 54A7 and 54B7. European biophysics journal. 2011;40(7):843–856.

[50] Berger O, Edholm O, Jähnig F. Molecular dynamics simulations of a fluid bilayer of dipalmitoylphosphatidylcholine at full hydration, constant pressure, and constant temperature. Biophysical journal. 1997;72(5):2002.

[51] Darden T, York D, Pedersen L. Particle mesh Ewald: An $N\log(N)$ method for Ewald sums in large systems. The Journal of chemical physics. 1993;98(12):10089–10092.

[52] Hess B, Bekker H, Berendsen HJ, Fraaije JG. LINCS: a linear constraint solver for molecular simulations. Journal of computational chemistry. 1997;18(12):1463–1472.

[53] Evans DJ, Holian BL. The nose–hoover thermostat. The Journal of chemical physics. 1985;83(8):4069–4074.

[54] Parrinello M, Rahman A. Polymorphic transitions in single crystals: A new molecular dynamics method. Journal of Applied physics. 1981;52(12):7182–7190.

[55] Van Der Spoel D, Lindahl E, Hess B, Groenhof G, Mark AE, Berendsen HJ. GROMACS: fast, flexible, and free. Journal of computational chemistry. 2005;26(16):1701–1718.

[56] Boggara MB, Krishnamoorti R. Partitioning of nonsteroidal antiinflammatory drugs in lipid membranes: a molecular dynamics simulation study. Biophysical journal. 2010;98(4):586–595.

[57] Wennberg CL, Van Der Spoel D, Hub JS. Large influence of cholesterol on solute partitioning into lipid membranes. Journal of the American Chemical Society. 2012;134(11):5351–5361.

[58] Zocher F, Wennberg CL, Pohl P, Hub J. Local micro-partition coefficients govern solute permeability of cholesterol-containing membranes. Biophysical Journal. 2013;104(2):82a.

[59] Hub JS, De Groot BL, Van Der Spoel D. g_wham A Free Weighted Histogram Analysis Implementation Including Robust Error and Autocorrelation Estimates. Journal of Chemical Theory and Computation. 2010;6(12):3713–3720.

[60] Ryckaert JP, Bellemans A. Molecular dynamics of liquid alkanes. Faraday Discussions of the Chemical Society. 1978;66:95–106.

Curcumin Protects Membranes Through Carpet or Insertion Model Depending on Hydration

Richard J. Alsop,[1] Alexander Dhaliwal,[1] and Maikel C. Rheinstädter[1,*]

[1]*Department of Physics and Astronomy, McMaster University, Hamilton, Ontario, Canada*

(Dated: May 9, 2017)

* rheinstadter@mcmaster.ca; Department of Physics and Astronomy, McMaster University, ABB-241, 1280 Main Street West, Hamilton, Ontario L8S 4M1, Canada; Phone: +1-(905)-525-9140-23134, Fax: +1-(905)-546-1252

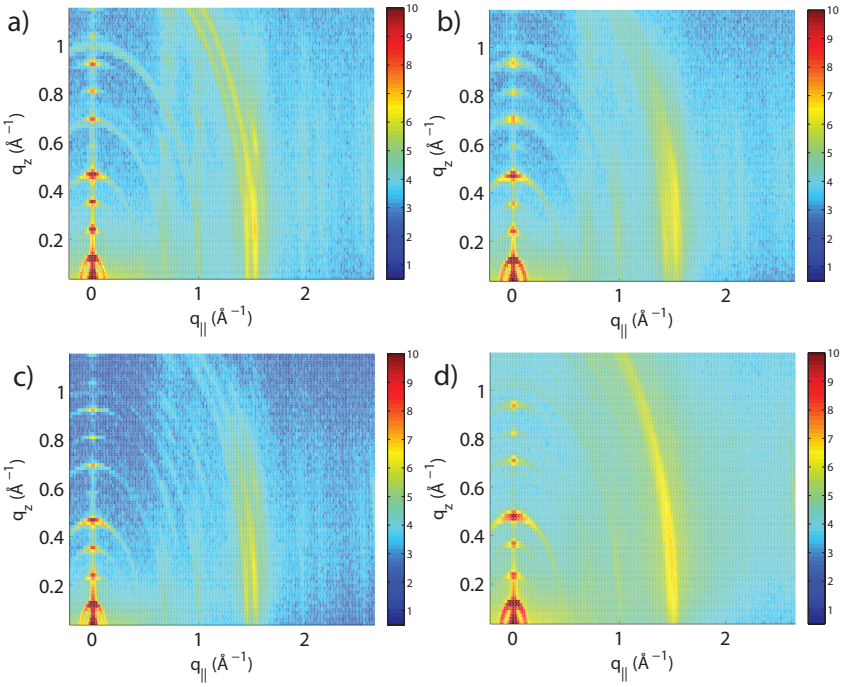

FIG. S1. Two-dimensional X-ray intensity maps measured for all gel samples in this study. a) Pure DMPC; b) DMPC + 2mol% curcumin; c) DMPC + 10mol% curcumin; d) DMPC + 20mol% curcumin.

1. DETERMINATION OF AREA PER LIPID IN DEHYDRATED MEMBRANES FROM X-RAY DIFFRACTION

The 2-dimensional X-ray data, taken for the dehydrated data in this study, in Figure S1 show well-defined peaks along the $q_{||}$-axis, which allow the determination of the lateral membrane structure. Several correlation peaks were observed in the in-plane data for all curcumin concentrations and were well fit by Lorentzian peak profiles. The intensity has a distinct rod-like shape, typical for a 2-dimensional system.

For all dehydrated scans in Figure S1, peaks are observed at $q_{||} \sim 0.67$ Å^{-1}, 0.73 Å^{-1}, 1.0 Å^{-1}, and 1.44 Å^{-1}. These peaks have been observed previously, and correspond to lipid head groups ordered in an orthogonal lattice [1, 2]. The observed peaks correspond, respectively, to the [1 0 0], [0 1 0], [1 1 0], and [2 0 0] reflections. From these reflections, the

Curcumin (mol%)	Peak positions (Å^{-1})	Lattice parameters	A_L (Å^2)
0	0.67, 0.73, 0.99, 1.45	a_H = 9.38 Å, b_H=8.63 Å, γ=90°	40.6
2	0.675, 0.73, 1.00, 1.44	a_H = 9.38 Å, b_H=8.63 Å, γ=90°	40.6
10	0.675, 0.73, 0.99, 1.44	a_H = 9.38 Å, b_H=8.63 Å, γ=90°	40.6
20	0.67, 1.0	a_H = 9.38 Å, b_H=8.63 Å, γ=90°	40.6

TABLE 1. In plane ($q_{||}$) peaks observed for all dehydrated scans, as well as the corresponding lattice parameters and A_L

head group lattice parameters, a_H, b_H, and γ are determined, as well as the area per lipid by $A_L = \frac{1}{2} a_H b_H \sin\gamma$. The peak positions and parameters are shown in Table 1. Note that only the [1 0 0] and [1 1 0] peaks are observed for the 20 mol% curcumin sample, so γ=90° is assumed.

2. DETERMINING PHASES FOR FOURIER TRANSFORM

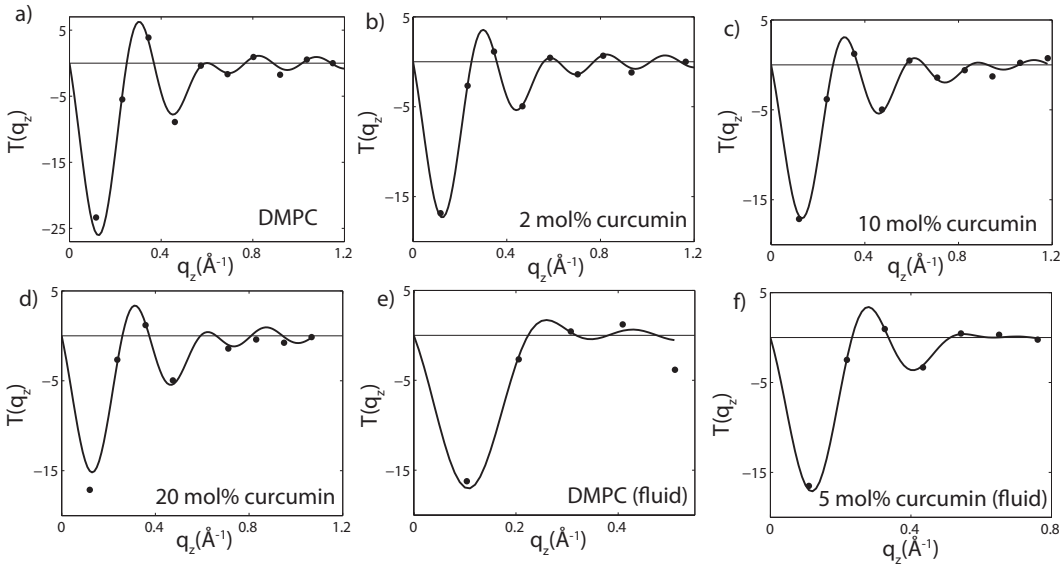

FIG. S2. Function $T(q_z)$ for all membrane complexes. The Fourier phases ν_n were assessed from these figures.

The phases, ν_n are needed to reconstruct the electron density profile from the scattering data accoring to Eq. (1) in the main text. $T(q_z)$, which is proportional to the membrane form factor $F(q_z)$, was fit to the experimentally determined integrated peak intensities [1, 3]:

$$T(q_z) = \sum_n \sqrt{I_n q_n} \mathrm{sinc}\left(\frac{1}{2} d_z q_z - \pi n\right). \quad (1)$$

The results are depicted in Figure S2. See the Materials and Methods Section in the main article for full details.

---

[1] Matthew A. Barrett, Songbo Zheng, Golnaz Roshankar, Richard J. Alsop, Randy K.R. Belanger, Chris Huynh, Norbert Kučerka, and Maikel C. Rheinstädter, "Interaction of aspirin (acetylsalicylic acid) with lipid membranes," PLoS ONE **7**, e34357 (2012).

[2] Richard J Alsop, Rafaëla Maria Schober, and Maikel C Rheinstädter, "Swelling of phospholipid membranes by divalent metal ions depends on the location of the ions in the bilayers," Soft Matter **12**, 6737–6748 (2016).

[3] Tomohiro Adachi, "A new method for determining the phase in the x-ray diffraction structure analysis of phosphatidylcholine:alcohol," Chemistry and Physics of Lipids **107**, 93–97 (2000).

Chapter 6

Outlook & Conclusions

The major findings of this thesis are grouped into two chapters. Chapter 4 discussed several studies on the effect of aspirin on cholesterol-driven ordering in model membranes. The major conclusion was that aspirin preferentially effects the ℓ_o phase and locally disrupts lipid order. Chapter 5, in contrast, demonstrates how several drug molecules are themselves impacted by the membrane.

The papers typically employed multiple techniques to arrive at their conclusions, including Molecular Dynamics simulations and differential scanning calorimetry. However, the hero of the thesis was the use of X-ray and neutron scattering techniques. In particular, these techniques are most effective when applied to oriented lipid membranes. Angstrom-level information on the structural impacts of drugs, both in-plane and out-of-plane, was obtained.

It is important at this stage in the thesis to discuss the limitations of the results and the tools used. First of all, there are potential artefacts introduced in the use of oriented membrane systems. The presence of a solid support has the effect of limiting dynamical motions near the substrate. However, samples were prepared with >3000 bilayers per wafer, and the X-rays probed only the top bilayers, which have more mobility. In addition, interpretation of the scattering results relied on the use of molecular models. While the papers leveraged additional techniques to support the models used in scattering experiments, as with all models, we cannot verify unambiguously the validity of every model using scattering.

Secondly, simplifications were made to the systems by reducing the number of lipids relative to a native biological membrane. Typically, the systems only used 1-3 lipids, and generally these lipids were either exclusively saturated (all DMPC or DPPC), or exclusively unsaturated (POPC). In addition, only PC lipids were used. Reducing complexity is necessary to achieve any reasonable resolution. However, this means we are unable to comment on the impact of complexities such as saturated/unsaturated interactions, or perhaps different chemical interactions arising from different headgroups.

Lastly, in trying to understand fundamental drug-membrane interactions, we took a wholly lipid-centric view. A biological membrane interacts with proteins, sugars, salts, etc., and in general, these elements were not explored. For example, as mentioned in the Section 2.4, drugs may influence

proteins by interacting with the membrane. These knock-on effects were not explored. In general, variables such as the salt concentration or pH were not systematically explored. These exclusions have the potential for being highly relevant to understanding drug-membrane interactions [2].

The major innovations of the thesis are in the adaptation of scattering tools to unveil the drug-membrane interactions on atomic and molecular length scales. With these tools now at our disposal, there are a number of ways for drug-membrane interactions to be studied more significantly.

In principle, any drug can be tested against various membranes. Therefore, future experiments should evolve the technique towards a decision-useful platform for testing drug-membrane interactions. Studies should be designed where interactions are measured and then used to predict physiological effect. A study could identify an aspirin derivative that does not have the same effect on cholesterol rafts, and also test whether the derivative also impacts low-dose-aspirin therapy. In addition, NSAID's could be tested for their ability to produce cubic phases, and the results correlated with the toxicity of the NSAID's *in-vitro*.

In addition, native membrane systems should be developed and used in parallel with model membranes. Model membranes eliminate complexity which allow fine details to emerge. However, the complexity of real membranes is often an important element of the structure. To truly verify the relevance of drug membrane interactions, they should be measured in model membranes, verified in native membranes, and then confirmed in an *in-vitro system*.

Our group has recently developed a method for extracting and oriented red-blood-cell (RBC) membranes onto silicon wafers. The technique was developed by Sebastian Himbert. Human blood is extracted and placed in a hypotonic solution, which causes the cells to rupture and spill their contents. The empty cells then close and form "ghosts". The ghosts are transformed into small unilamellar vesicles and deposited on the wafers, where they then form multi-lamellar, oriented membranes [91].

The system was studied by X-ray diffraction and found to be heterogenous. RBC's contain cholesterol at >30 mol% and are believed to contain rafts. We indeed found ordered domains among less ordered domains. Naturally, aspirin was then added and, in agreement with Chapter 4, we saw that it preferentially impacted and fluidified the ordered phase.

Artificial membranes should also be evolved to more closely mimic human tissues and disease pathologies. This will allow the measured drug-membrane interactions to be more closely associated with an observed physiological effect. For example, our lab is developing a synthetic membrane system designed to recreate the key pathologies of Alzheimer's. The leading theory for Alzheimer's is the amyloid cascade hypothesis: misfolded amyloid-beta peptides aggregate and cause oxidative stress and cell death [79]. The lipid bilayer is believed to be a key player in this process [92]. The membrane tissues in our lab produce amyloid aggregates, and the aggregates depend on membrane properties [93, 94]. The next step would be to introduce drug molecules in an attempt to eliminate the fingerprint of the aggregates. The synthetic membrane system could play a major role in determining the mode-of-action of future Alzheimer's drug candidates.

Appendix A

Copyright Information for Publications

A.1 Soft Matter Publications

As stated in http://www.rsc.org/journals-books-databases/journal-authors-reviewers/licences-copyright-permissions/, authors may use the version of record for "use in submissions of grant applications, or academic requirements such as theses or dissertations".

A.2 BBA-Biomembranes Publication

Quoted from https://www.elsevier.com/about/our-business/policies/sharing: "Theses and dissertations which contain embedded PJAs as part of the formal submission can be posted publicly by the awarding institution with DOI links back to the formal publications on ScienceDirect". In line with this policy, the link to the formal Paper II is: http://www.sciencedirect.com/science/article/pii/S0005273614004222

A.3 Scientific Reports

Quoted from https://www.nature.com/srep/journal-policies/editorial-policies "Scientific Reports does not require authors to assign copyright of their published original research papers to the journal. Articles are published under a CC BY license (Creative Commons Attribution 4.0 International License). The CC BY license allows for maximum dissemination and re-use of open access materials and is preferred by many research funding bodies. Under this license users are free to share (copy, distribute and transmit) and remix (adapt) the contribution including for commercial purposes, providing they attribute the contribution in the manner specified by the author or licensor."

A.4 Langmuir

Quoted from the American Chemical Society Journal Publishing Agreement (*http : //pubs.acs.org/page/copyright/permissio*
"Authors may reuse all or part of the Submitted, Accepted or Published Work in a thesis or dissertation that the Author writes and is required to submit to satisfy the criteria of degree-granting institutions."

Bibliography

[1] Kai Simons and Julio L Sampaio. Membrane organization and lipid rafts. *Cold Spring Harbor perspectives in biology*, 3(10):a004697, 2011.

[2] Joachim K Seydel and Michael Wiese. *Drug-membrane interactions: analysis, drug distribution, modeling*, volume 15. John Wiley & Sons, 2009.

[3] A. Jan Fijalkowski. Lipid raft organisation scheme. Wikimedia Commons, December 2006. Image credit.

[4] David W Deamer. Role of amphiphilic compounds in the evolution of membrane structure on the early earth. *Origins of Life and Evolution of Biospheres*, 17(1):3–25, 1986.

[5] Markus S Almén, Karl JV Nordström, Robert Fredriksson, and Helgi B Schiöth. Mapping the human membrane proteome: a majority of the human membrane proteins can be classified according to function and evolutionary origin. *BMC biology*, 7(1):50, 2009.

[6] SJ Singer and Garth L Nicolson. The fluid mosaic model of the structure of cell membranes. *Day and Good Membranes and viruses in immunopathology*, pages 7–47, 1972.

[7] Kai Simons, Elina Ikonen, et al. Functional rafts in cell membranes. *Nature*, 387(6633):569–572, 1997.

[8] Daniel Lingwood and Kai Simons. Lipid rafts as a membrane-organizing principle. *science*, 327(5961):46–50, 2010.

[9] Kai Simons, Robert Ehehalt, et al. Cholesterol, lipid rafts, and disease. *The Journal of clinical investigation*, 110(110 (5)):597–603, 2002.

[10] Kai Simons and Gerrit Van Meer. Lipid sorting in epithelial cells. *Biochemistry*, 27(17):6197–6202, 1988.

[11] Mark S Bretscher and Sean Munro. Cholesterol and the golgi apparatus. *Science*, 261(5126):1280–1281, 1993.

[12] Eoin Fahy, Shankar Subramaniam, H Alex Brown, Christopher K Glass, Alfred H Merrill, Robert C Murphy, Christian RH Raetz, David W Russell, Yousuke Seyama, Walter Shaw, et al. A comprehensive classification system for lipids. *Journal of lipid research*, 46(5):839–862, 2005.

[13] Norbert Kučerka, Stephanie Tristram-Nagle, and John F Nagle. Structure of fully hydrated fluid phase lipid bilayers with monounsaturated chains. *The Journal of membrane biology*, 208(3):193–202, 2006.

[14] Norbert Kučerka, Mu-Ping Nieh, and John Katsaras. Fluid phase lipid areas and bilayer thicknesses of commonly used phosphatidylcholines as a function of temperature. *Biochimica et Biophysica Acta (BBA)-Biomembranes*, 1808(11):2761–2771, 2011.

[15] Juliette Jouhet. Importance of the hexagonal lipid phase in biological membrane organization. *Frontiers in plant science*, 4:494, 2013.

[16] Vitor Teixeira, Maria J Feio, and Margarida Bastos. Role of lipids in the interaction of antimicrobial peptides with membranes. *Progress in lipid research*, 51(2):149–177, 2012.

[17] Thomas Heimburg. *Thermal biophysics of membranes*. John Wiley & Sons, 2008.

[18] RP Rand and VA Parsegian. Hydration forces between phospholipid bilayers. *Biochimica et Biophysica Acta (BBA)-Reviews on Biomembranes*, 988(3):351–376, 1989.

[19] Ulrike Mennicke, Doru Constantin, and Tim Salditt. Structure and interaction potentials in solid-supported lipid membranes studied by x-ray reflectivity at varied osmotic pressure. *The European Physical Journal E: Soft Matter and Biological Physics*, 20(2):221–230, 2006.

[20] Ilya Koltover, Tim Salditt, Joachim O Rädler, and Cyrus R Safinya. An inverted hexagonal phase of cationic liposome-dna complexes related to dna release and delivery. *Science*, 281(5373):78–81, 1998.

[21] GC Shearman, AII Tyler, NJ Brooks, RH Templer, O Ces, RV Law, and JM Seddon. Ordered micellar and inverse micellar lyotropic phases. *Liquid Crystals*, 37(6-7):679–694, 2010.

[22] Chandrashekhar V Kulkarni. Nanostructural studies on monoelaidin–water systems at low temperatures. *Langmuir*, 27(19):11790–11800, 2011.

[23] Elijah Flenner, Jhuma Das, Maikel C Rheinstädter, and Ioan Kosztin. Subdiffusion and lateral diffusion coefficient of lipid atoms and molecules in phospholipid bilayers. *Physical Review E*, 79(1):011907, 2009.

[24] J Antoinette Killian. Hydrophobic mismatch between proteins and lipids in membranes. *Biochimica et Biophysica Acta (BBA)-Reviews on Biomembranes*, 1376(3):401–416, 1998.

[25] Jannik Bruun Larsen, Martin Borch Jensen, Vikram K Bhatia, Søren L Pedersen, Thomas Bjørnholm, Lars Iversen, Mark Uline, Igal Szleifer, Knud J Jensen, Nikos S Hatzakis, et al. Membrane curvature enables n-ras lipid anchor sorting to liquid-ordered membrane phases. *Nature chemical biology*, 11(3):192–194, 2015.

[26] Frédérick de Meyer and Berend Smit. Effect of cholesterol on the structure of a phospholipid bilayer. *Proceedings of the National Academy of Sciences*, 106(10):3654–3658, 2009.

[27] Emma Falck, Michael Patra, Mikko Karttunen, Marja T Hyvönen, and Ilpo Vattulainen. Lessons of slicing membranes: interplay of packing, free area, and lateral diffusion in phospholipid/cholesterol bilayers. *Biophysical journal*, 87(2):1076–1091, 2004.

[28] Maikel C Rheinstädter and Ole G Mouritsen. Small-scale structure in fluid cholesterol–lipid bilayers. *Current opinion in colloid & interface science*, 18(5):440–447, 2013.

[29] Jianjun Pan, Thalia T Mills, Stephanie Tristram-Nagle, and John F Nagle. Cholesterol perturbs lipid bilayers nonuniversally. *Physical review letters*, 100(19):198103, 2008.

[30] Norbert Kucerka, Drew Marquardt, Thad A Harroun, Mu-Ping Nieh, Stephen R Wassall, Djurre H de Jong, Lars V Schfer, Siewert J Marrink, and John Katsaras. Cholesterol in bilayers with pufa chains: doping with dmpc or popc results in sterol reorientation and membrane-domain formation. *Biochemistry*, 49(35):7485–7493, 2010.

[31] Clare L Armstrong, Wolfgang Häußler, Tilo Seydel, John Katsaras, and Maikel C Rheinstädter. Nanosecond lipid dynamics in membranes containing cholesterol. *Soft matter*, 10(15):2600–2611, 2014.

[32] Sean Munro. Lipid rafts: elusive or illusive? *Cell*, 115(4):377–388, 2003.

[33] Anna M Fra, Edward Williamson, Kai Simons, and Robert G Parton. Detergent-insoluble glycolipid microdomains in lymphocytes in the absence of caveolae. *Journal of Biological Chemistry*, 269(49):30745–30748, 1994.

[34] Christian Eggeling, Christian Ringemann, Rebecca Medda, Günter Schwarzmann, Konrad Sandhoff, Svetlana Polyakova, Vladimir N Belov, Birka Hein, Claas von Middendorff, Andreas Schönle, et al. Direct observation of the nanoscale dynamics of membrane lipids in a living cell. *Nature*, 457(7233):1159–1162, 2009.

[35] Frederick A Heberle and Gerald W Feigenson. Phase separation in lipid membranes. *Cold Spring Harbor perspectives in biology*, 3(4):a004630, 2011.

[36] Frederick A Heberle, Robin S Petruzielo, Jianjun Pan, Paul Drazba, Norbert Kuc?erka, Robert F Standaert, Gerald W Feigenson, and John Katsaras. Bilayer thickness mismatch controls domain size in model membranes. *Journal of the American Chemical Society*, 135(18):6853–6859, 2013.

[37] Sebastian Meinhardt, Richard LC Vink, and Friederike Schmid. Monolayer curvature stabilizes nanoscale raft domains in mixed lipid bilayers. *Proceedings of the National Academy of Sciences*, 110(12):4476–4481, 2013.

[38] Richard J Alsop and Maikel C Rheinstädter. Lipid rafts in binary lipid/cholesterol bilayers. Nova, 2016.

[39] Aurelia R Honerkamp-Smith, Benjamin B Machta, and Sarah L Keller. Experimental observations of dynamic critical phenomena in a lipid membrane. *Physical review letters*, 108(26):265702, 2012.

[40] Aurelia R Honerkamp-Smith, Pietro Cicuta, Marcus D Collins, Sarah L Veatch, Marcel den Nijs, M Schick, and Sarah L Keller. Line tensions, correlation lengths, and critical exponents in lipid membranes near critical points. *Biophysical journal*, 95(1):236–246, 2008.

[41] Ha Giang, Roie Shlomovitz, and Michael Schick. Microemulsions, modulated phases and macroscopic phase separation: a unified picture of rafts. *Essays in biochemistry*, 57:21–32, 2015.

[42] Roy Ziblat, Iael Fargion, Leslie Leiserowitz, and Lia Addadi. Spontaneous formation of two-dimensional and three-dimensional cholesterol crystals in single hydrated lipid bilayers. *Biophysical journal*, 103(2):255–264, 2012.

[43] Matthew A Barrett, Songbo Zheng, Laura A Toppozini, Richard J Alsop, Hannah Dies, Aili Wang, Nicholas Jago, Michael Moore, and Maikel C Rheinstädter. Solubility of cholesterol in lipid membranes and the formation of immiscible cholesterol plaques at high cholesterol concentrations. *Soft Matter*, 9(39):9342–9351, 2013.

[44] Neta Varsano, Iael Fargion, Sharon G Wolf, Leslie Leiserowitz, and Lia Addadi. Formation of 3d cholesterol crystals from 2d nucleation sites in lipid bilayer membranes: Implications for atherosclerosis. *Journal of the American Chemical Society*, 137(4):1601–1607, 2015.

[45] Matthew A Barrett, Songbo Zheng, Golnaz Roshankar, Richard J Alsop, RK Belanger, Chris Huynh, Norbert Kučerka, and Maikel C Rheinstädter. Interaction of aspirin (acetylsalicylic acid) with lipid membranes. *PLoS One*, 7(4):e34357, 2012.

[46] Varley F Sears. Neutron scattering lengths and cross sections. *Neutron news*, 3(3):26–37, 1992.

[47] Gen Shirane, Stephen M Shapiro, and John M Tranquada. *Neutron scattering with a triple-axis spectrometer: basic techniques*. Cambridge University Press, 2002.

[48] Gordon Leslie Squires. *Introduction to the theory of thermal neutron scattering*. Cambridge university press, 2012.

[49] Mark James Abraham, Teemu Murtola, Roland Schulz, Szilárd Páll, Jeremy C Smith, Berk Hess, and Erik Lindahl. Gromacs: High performance molecular simulations through multi-level parallelism from laptops to supercomputers. *SoftwareX*, 1:19–25, 2015.

[50] Alpeshkumar K Malde, Le Zuo, Matthew Breeze, Martin Stroet, David Poger, Pramod C Nair, Chris Oostenbrink, and Alan E Mark. An automated force field topology builder (ATB) and repository: version 1.0. *Journal of chemical theory and computation*, 7(12):4026–4037, 2011.

[51] Scott E Feller. Molecular dynamics simulations of lipid bilayers. *Current opinion in colloid & interface science*, 5(3):217–223, 2000.

[52] Luca Monticelli and D Peter Tieleman. Force fields for classical molecular dynamics. *Biomolecular simulations: Methods and protocols*, pages 197–213, 2013.

[53] D Peter Tieleman, Justin L MacCallum, Walter L Ash, Christian Kandt, Zhitao Xu, and Luca Monticelli. Membrane protein simulations with a united-atom lipid and all-atom protein model: lipid–protein interactions, side chain transfer free energies and model proteins. *Journal of Physics: Condensed Matter*, 18(28):S1221, 2006.

[54] Robert D Kaufman. Biophysical mechanisms of anesthetic action: historical perspective and review of current concepts. *Anesthesiology*, 46(1):49–62, 1977.

[55] Keith W Miller. The nature of the site of general anesthesia. *International review of neurobiology*, 27:1–61, 1985.

[56] Cameron J Weir. The molecular mechanisms of general anaesthesia: dissecting the gabaa receptor. *Continuing Education in Anaesthesia, Critical Care & Pain*, 6(2):49–53, 2006.

[57] Robert S Cantor. The lateral pressure profile in membranes: a physical mechanism of general anesthesia. *Biochemistry*, 36(9):2339–2344, 1997.

[58] M Suwalsky, F Martinez, H Cardenas, J Grzyb, and K Strzałka. Iron affects the structure of cell membrane molecular models. *Chemistry and physics of lipids*, 134(1):69–77, 2005.

[59] Mario Suwalsky, Jessica Belmar, Fernando Villena, María José Gallardo, Malgorzata Jemiola-Rzeminska, and Kazimierz Strzalka. Acetylsalicylic acid (aspirin) and salicylic acid interaction with the human erythrocyte membrane bilayer induce in vitro changes in the morphology of erythrocytes. *Archives of biochemistry and biophysics*, 539(1):9–19, 2013.

[60] Marcela Manrique-Moreno, Mario Suwalsky, Fernando Villena, and Patrick Garidel. Effects of the nonsteroidal anti-inflammatory drug naproxen on human erythrocytes and on cell membrane molecular models. *Biophysical chemistry*, 147(1):53–58, 2010.

[61] Wojciech Kopeć, Jelena Telenius, and Himanshu Khandelia. Molecular dynamics simulations of the interactions of medicinal plant extracts and drugs with lipid bilayer membranes. *Febs Journal*, 280(12):2785–2805, 2013.

[62] Rigaku Corporation. Powder diffraction optics for smartlab x-ray diffractometer. *The Rigaku Journal*, 26:29–30, 2010.

[63] Tomohiro Adachi. A new method for determining the phase in the x-ray diffraction structure analysis of phosphatidylcholine:alcohol. *Chemistry and Physics of Lipids*, 107:93–97, 2000.

[64] Joakim PM Jmbeck and Alexander P Lyubartsev. Another piece of the membrane puzzle: extending slipids further. *Journal of chemical theory and computation*, 9(1):774–784, 2012.

[65] Nathan Schmid, Andreas P Eichenberger, Alexandra Choutko, Sereina Riniker, Moritz Winger, Alan E Mark, and Wilfred F van Gunsteren. Definition and testing of the gromos force-field versions 54a7 and 54b7. *European biophysics journal*, 40(7):843, 2011.

[66] Walter Sneader. The discovery of aspirin: a reappraisal. *Bmj*, 321(7276):1591–1594, 2000.

[67] Gerald J Roth, Nancy Stanford, and Philip W Majerus. Acetylation of prostaglandin synthase by aspirin. *Proceedings of the National Academy of Sciences*, 72(8):3073–3076, 1975.

[68] Steven M Weisman and David Y Graham. Evaluation of the benefits and risks of low-dose aspirin in the secondary prevention of cardiovascular and cerebrovascular events. *Archives of Internal Medicine*, 162(19):2197–2202, 2002.

[69] Carlo Patrono, Luis A García Rodríguez, Raffaele Landolfi, and Colin Baigent. Low-dose aspirin for the prevention of atherothrombosis. *New England Journal of Medicine*, 353(22):2373–2383, 2005.

[70] Hironori Tsuchiya and Shuichi Ohmoto. Comparative effects of β-carbolines on platelet aggregation and lipid membranes. *Pharmacological Reports*, 62(4):689–695, 2010.

[71] Charles F Majkrzak, Christopher Metting, Brian B Maranville, Joseph A Dura, Sushil Satija, Terrence Udovic, and Norman F Berk. Determination of the effective transverse coherence of the neutron wave packet as employed in reflectivity investigations of condensed-matter structures. i. measurements. *Physical Review A*, 89(3):033851, 2014.

[72] Clare L. Armstrong, Drew Marquardt, Hannah Dies, Norbert Kuerka, Zahra Yamani, Thad A. Harroun, John Katsaras, An-Chang Shi, and Maikel C. Rheinstdter. The observation of highly ordered domains in membranes with cholesterol. *PLoS ONE*, 8(6):e66162, 06 2013.

[73] Laura Toppozini, Sebastian Meinhardt, Clare L Armstrong, Zahra Yamani, Norbert Kučerka, Friederike Schmid, and Maikel C Rheinstädter. Structure of cholesterol in lipid rafts. *Physical review letters*, 113(22):228101, 2014.

[74] Maikel C Rheinstädter, Jhuma Das, Elijah J Flenner, Beate Brüning, Tilo Seydel, and Ioan Kosztin. Motional coherence in fluid phospholipid membranes. *Physical review letters*, 101(24):248106, 2008.

[75] Maikel C Rheinstädter, Karin Schmalzl, Kathleen Wood, and Dieter Strauch. Protein-protein interaction in purple membrane. *Physical review letters*, 103(12):128104, 2009.

[76] Clare L Armstrong, MA Barrett, L Toppozini, N Kučerka, Z Yamani, John Katsaras, Giovanna Fragneto, and Maikel C Rheinstädter. Co-existence of gel and fluid lipid domains in single-component phospholipid membranes. *Soft Matter*, 8(17):4687–4694, 2012.

[77] Clare L Armstrong, Matthew A Barrett, Arno Hiess, Tim Salditt, John Katsaras, An-Chang Shi, and Maikel C Rheinstädter. Effect of cholesterol on the lateral nanoscale dynamics of fluid membranes. *European Biophysics Journal*, 41(10):901–913, 2012.

[78] MC Rheinstädter, C Ollinger, G Fragneto, F Demmel, and T Salditt. Collective dynamics of lipid membranes studied by inelastic neutron scattering. *Physical review letters*, 93(10):108107, 2004.

[79] Marcel M Verbeek, Dirk J Ruiter, RMW De Waal, et al. The role of amyloid in the pathogenesis of alzheimers's disease. *Biological chemistry*, 378:937–950, 1997.

[80] Hui-Hsu Gavin Tsai, Jian-Bin Lee, Sheng-Shiuan Tseng, Xiao-An Pan, and Yuan-Ci Shih. Folding and membrane insertion of amyloid-beta (25–35) peptide and its mutants: Implications for aggregation and neurotoxicity. *Proteins: Structure, Function, and Bioinformatics*, 78(8):1909–1925, 2010.

[81] Neal M Davies. Clinical pharmacokinetics of ibuprofen. *Clinical pharmacokinetics*, 34(2):101–154, 1998.

[82] Paul D Fadale and Michael E Wiggins. Corticosteroid injections: their use and abuse. *Journal of the American Academy of Orthopaedic Surgeons*, 2(3):133–140, 1994.

[83] Jean-Marie Berthelot, Benoît Le Goff, and Yves Maugars. Side effects of corticosteroid injections: What's new? *Joint Bone Spine*, 80(4):363–367, 2013.

[84] Miguel Beato, Peter Herrlich, and Günther Schütz. Steroid hormone receptors: many actors in search of a plot. *Cell*, 83(6):851–857, 1995.

[85] Shuxin Hu, Panchanan Maiti, Qiulan Ma, Xiaohong Zuo, Mychica R Jones, Greg M Cole, and Sally A Frautschy. Clinical development of curcumin in neurodegenerative disease. *Expert review of neurotherapeutics*, 15(6):629–637, 2015.

[86] Tsuyoshi Hamaguchi, Kenjiro Ono, and Masahito Yamada. Review: Curcumin and alzheimer's disease. *CNS neuroscience & therapeutics*, 16(5):285–297, 2010.

[87] Helgi I Ingolfsson, Roger E Koeppe, and Olaf S Andersen. Curcumin is a modulator of bilayer material properties. *Biochemistry*, 46(36):10384–10391, 2007.

[88] Marcelina Starok, Pascal Preira, Muriel Vayssade, Karsten Haupt, Laurence Salom, and Claire Rossi. Egfr inhibition by curcumin in cancer cells: A dual mode of action. *Biomacromolecules*, 16(5):1634–1642, 2015.

[89] Arti Arora, Todd M Byrem, Muraleedharan G Nair, and Gale M Strasburg. Modulation of liposomal membrane fluidity by flavonoids and isoflavonoids. *Archives of Biochemistry and Biophysics*, 373(1):102–109, 2000.

[90] Horia I Petrache, Nikolai Gouliaev, Stephanie Tristram-Nagle, Ruitian Zhang, Robert M Suter, and John F Nagle. Interbilayer interactions from high-resolution x-ray scattering. *Physical Review E*, 57(6):7014, 1998.

[91] Sebastian Himbert, Richard J Alsop, Markus Rose, Laura Hertz, Alexander Dhaliwal, Jose M Moran-Mirabal, Chris P Verschoor, Dawn ME Bowdish, Lars Kaestner, Christian Wagner, et al. The molecular structure of human red blood cell membranes from highly oriented, solid supported multi-lamellar membranes. *Scientific Reports*, 7, 2017.

[92] W Gibson Wood, Friedhelm Schroeder, Urule Igbavboa, Nicolai A Avdulov, and Svetlana V Chochina. Brain membrane cholesterol domains, aging and amyloid beta-peptides. *Neurobiology of aging*, 23(5):685–694, 2002.

[93] Hannah Dies, Laura Toppozini, and Maikel C Rheinstädter. The interaction between amyloid-β peptides and anionic lipid membranes containing cholesterol and melatonin. *PLoS One*, 9(6):e99124, 2014.

[94] Jennifer Tang, Richard J Alsop, Matilda Backholm, Hannah Dies, An-Chang Shi, and Maikel C Rheinstädter. Amyloid-β 25–35 peptides aggregate into cross-β sheets in unsaturated anionic lipid membranes at high peptide concentrations. *Soft matter*, 12(13):3165–3176, 2016.